

**Sites involved in ligand binding and  
translocation in the Na<sup>+</sup>/proline symporter  
*PutP of Escherichia coli***

---

Dissertation  
der Fakultät für Biologie  
der Ludwig-Maximilians-Universität München

vorgelegt von  
Michael Konstantin Raba  
aus München

München  
23. April 2012



Gutachter:

1. Prof. Dr. Heinrich Jung
2. Prof. Dr. Thorsten Mascher

Datum der mündlichen Prüfung: 26. Juni 2012

## **EIDESSTATTLICHE ERKLÄRUNG**

Ich versichere hiermit an Eides statt, dass die vorgelegte Dissertation von mir selbstständig und ohne unerlaubte Hilfe angefertigt ist. Des Weiteren erkläre ich, dass ich nicht anderweitig ohne Erfolg versucht habe, eine Dissertation einzureichen oder mich der Doktorprüfung zu unterziehen. Die folgende Dissertation liegt weder ganz, noch in wesentlichen Teilen einer anderen Prüfungskommission vor.

München, 23.4.12

# PUBLICATIONS AND MANUSCRIPTS ORIGINATING FROM THIS THESIS

## CHAPTER 2

Raba, M., Baumgartner, T., Hilger, D., Klempahn, K., Hartel, T., Jung, K., and Jung, H. (2008). Function of transmembrane domain IX in the Na<sup>+</sup>/proline transporter PutP. *Journal of Molecular Biology* 382(4): 884-893.

## CHAPTER 3

Olkhova, E.\* , Raba, M.\*, Bracher, S., Hilger, D., and Jung, H. (2010). Homology Model of the Na(+)/Proline Transporter PutP of Escherichia coli and Its Functional Implications. *Journal of Molecular Biology* 406(1):59-74

## CHAPTER 4

Raba, M., Dunkel, S., Lipiszko, K., Hilger, D., Klare, J., Polyhach, Y., Jeschke, G., Steinhoff, H.-J., and Jung, H. Ligand-dependent structural dynamics of extracellular loop eL4 of PutP, a member of the LeuT structural family. *Manuscript*

## CHAPTER 5

Jung, H., Hilger, D., and Raba, M. (2012). The Na<sup>+</sup>/L-proline transporter PutP. *Frontiers in bioscience : a journal and virtual library* 17: 745-759.

---

\* these authors contributed equally to this work

# CONTRIBUTIONS TO PUBLICATIONS AND MANUSCRIPTS PRESENTED IN THIS THESIS

## CHAPTER 2

M. Raba, T. Baumgartner, and K. Klempahn constructed the mutants. M. Raba, T. Baumgartner, K. Klempahn, and T. Härtel performed the transport measurements. M. Raba and T. Baumgartner analyzed the expression of the mutants, determined the kinetic parameters of the PutP derivatives, and performed the accessibility analyses. D. Hilger analyzed the influence of ligands on MTSET labeling. He conducted the experiments performed by M. Raba, T. Baumgartner, T. Härtel, and K. Klempahn. H. Jung wrote the manuscript and discussed the results with D. Hilger and M. Raba.

## CHAPTER 3

E. Olkhova computed and *in silico* validated the PutP homology model. E. Olkhova performed proline docking analyses and predicted proline binding residues. M. Raba constructed the mutants, analyzed the expression of the mutants, performed transport measurements, and *in vivo* and *in vitro* Cys accessibility analyses. M. Raba tested the influence of ligands on Cys labeling. M. Raba conducted the work of S. Bracher. M. Raba and S. Bracher determined the kinetic parameters of the PutP derivatives. H. Jung and E. Olkhova wrote the manuscript and discussed the results with M. Raba and D. Hilger.

## CHAPTER 4

M. Raba constructed the mutants and performed *in vivo* transport measurements. M. Quick<sup>1</sup> determined binding activities of spin labeled PutP derivatives. M. Raba<sup>2</sup> prepared the samples and performed ligand-dependent cw EPR measurements at room temperature and analyzed data together with D. Hilger<sup>2</sup>. S. Dunkel<sup>3</sup> performed ligand-dependent cw EPR measurements at 160 K and analyzed data together with J. Klare<sup>3</sup>. K. Lipiszko<sup>4</sup> performed DEER measurements and analyzed data together with Y. Polyhach<sup>4</sup>. H. Jung<sup>2</sup>, H.-J. Steinhoff<sup>3</sup>, and G. Jeschke<sup>4</sup> designed research. M. Raba wrote the manuscript.

<sup>1</sup> Columbia University College of Physicians & Surgeons, Center of Molecular Recognition, New York (USA)

<sup>2</sup> LMU Munich, Biocentre, Department of Microbiology, Martinsried (Germany)

<sup>3</sup> Universität Osnabrück, Fachbereich Physik, Experimentalphysik/Makromolekülstruktur, Osnabrück (Germany)

<sup>4</sup> ETH Zürich, Laboratory of Physical Chemistry, Zürich (Switzerland)

## **CHAPTER 5**

H. Jung wrote sections 1 to 4. M. Raba wrote sections 5 and 6. D. Hilger wrote sections 7 and 8.

I hereby confirm the above statements:

Michael Raba

Prof. Dr. Heinrich Jung

## Table of Contents

<b>Eidesstattliche Erklärung .....</b>	<b>III</b>
<b>Publications and Manuscripts originating from this Thesis .....</b>	<b>IV</b>
<b>Contributions to Publications and Manuscripts presented in this Thesis .....</b>	<b>V</b>
<b>Table of Contents .....</b>	<b>VII</b>
<b>Nomenclature .....</b>	<b>IX</b>
<b>Abbreviations .....</b>	<b>X</b>
<b>SUMMARY .....</b>	<b>1</b>
<b>ZUSAMMENFASSUNG .....</b>	<b>3</b>
<b>1 INTRODUCTION .....</b>	<b>5</b>
<b>1.1 Diversity of membrane transport systems .....</b>	<b>5</b>
1.1.1 Diffusion/channels .....	5
1.1.2 Primary transporter .....	5
1.1.3 Secondary transporter .....	6
1.1.4 Phosphoenolpyruvate:carbohydrate phosphotransferase system (PTS) .....	6
<b>1.2 Physiological significance of secondary transport systems .....</b>	<b>7</b>
<b>1.3 Bioenergetics of secondary transport .....</b>	<b>8</b>
<b>1.4 Symporters work according to an alternating access mechanism .....</b>	<b>10</b>
<b>1.5 Structural diversity of secondary active transporters .....</b>	<b>12</b>
<b>1.6 LeuT-structural fold .....</b>	<b>13</b>
1.6.1 LeuT-structural family .....	13
1.6.2 Global fold and internal symmetry .....	14
1.6.3 Na <sup>+</sup> binding sites .....	15
1.6.4 Substrate binding sites .....	16
1.6.5 From structure to function: Rigid body movements as key element for secondary active transport .....	17
<b>1.7 PutP – a member of the LeuT structural family .....</b>	<b>18</b>
<b>1.8 Scope of this work .....</b>	<b>23</b>
<b>1.9 References .....</b>	<b>24</b>
<b>2 FUNCTION OF TRANSMEMBRANE DOMAIN IX IN THE NA<sup>+</sup>/PROLINE TRANSPORTER PUTP .....</b>	<b>33</b>
<b>3 HOMOLOGY MODEL OF THE NA<sup>+</sup>/PROLINE TRANSPORTER PUTP OF <i>ESCHERICHIA COLI</i> AND ITS FUNCTIONAL IMPLICATIONS .....</b>	<b>44</b>

---

<b>4</b>	<b>LIGAND-DEPENDENT STRUCTURAL DYNAMICS OF EXTRACELLULAR LOOP 4 OF PUTP, A MEMBER OF THE LEUT STRUCTURAL FAMILY</b> .....	<b>61</b>
4.1	Abstract .....	61
4.2	Introduction .....	61
4.3	Materials and Methods .....	64
4.3.1	<i>In vivo</i> proline transport assay .....	64
4.3.2	Scintillation proximity assay (SPA) .....	64
4.3.3	Determination of Na <sup>+</sup> .....	65
4.3.4	Site-directed spin labeling .....	65
4.3.5	Continuous-wave EPR (cw EPR) measurements .....	66
4.3.6	DEER measurements .....	67
4.4	Results .....	67
4.4.1	Activity and binding properties of spin-labeled PutPΔCys derivatives .....	67
4.4.2	Analysis of the mobility of spin labels attached to Cys placed into eL4 of PutP .....	69
4.4.3	Analysis of the polarity of the microenvironment of nitroxide spin labels attached to single-Cys derivatives .....	71
4.4.4	Ligand influence on spin label mobility and on the microenvironment .....	73
4.4.5	Intramolecular distances and ligand influence on the distance distribution .....	74
4.5	Discussion .....	77
4.6	References .....	84
4.7	Supplementary Material .....	90
<b>5</b>	<b>THE NA<sup>+</sup>/L-PROLINE TRANSPORTER PUTP</b> .....	<b>94</b>
<b>6</b>	<b>CONCLUDING DISCUSSION</b> .....	<b>110</b>
6.1	A homology model based on vSGLT gives insights into the three-dimensional architecture of PutP .....	110
6.2	Sites of Na <sup>+</sup> and proline binding and release in PutP .....	112
6.3	Substrate translocation pathway and structural dynamics of PutP .....	117
6.4	References .....	122
	<b>Acknowledgements</b> .....	<b>125</b>
	<b>Curriculum Vitae</b> .....	<b>127</b>

## NOMENCLATURE

In the course of this thesis an unexpected structural similarity of PutP to the LeuT structural family became evident. All members of this class of proteins share a common core composed of 10 transmembrane domains (TMs). In LeuT, this core is formed by the first 10 TMs which are numbered from 1-10. In PutP, the 10 TM core domain is preceded by a peripheral N-terminal TM. In order to avoid confusion the 10 TM core domain of PutP is numbered according to LeuT from 1'-10'. The preceding TM is numbered -1', succeeding C-terminal TMs are numbered 11' and 12'. This nomenclature is used in Chapter 1, 4, and 6.

In Chapter 2 and 3, TMs of PutP are numbered from 1-13, according to the secondary-structure model, using Roman numerals in Chapter 2 and Arabic numerals in Chapter 3. Therefore, TM IX in Chapter 2 or TM 9 in Chapter 3 corresponds to TM 8' in Chapter 1,4, and 6.

**ABBREVIATIONS**

ABC	ATP-binding cassette
AU	arbitrary units
BP	high affinity periplasmic binding protein
BSA	bovine serum albumin
cw	continuous-wave
Cys	cysteine
DEER	double electron-electron resonance
eL4	extracellular loop domain 4
EPR	electron paramagnetic resonance
FM	fluorescein-5-maleimide
HRP	horseradish peroxidase
MD	molecular dynamics
MES	2-[ <i>N</i> -morpholino]ethanesulfonic acid
MTSET	methanethiosulfonate ethyltrimethylammonium
MTSSL	(1-oxyl-2,2,5,5,-tetramethylpyrroline-3-methyl)-methanethiosulfonate
m.w.	microwave
NEM	<i>N</i> -ethylmaleimide
NBD	nucleotide binding domain
Ni <sup>2+</sup> -NTA	Ni <sup>2+</sup> -nitrilotriacetic acid
NSS	neurotransmitter/sodium symporter
PELDOR	pulsed electron-electron double resonance
PEP	phosphoenolpyruvate
<i>pmf</i>	proton motive force
PutP( $\Delta$ Cys)	engineered PutP devoid of all five native cysteine residues
RMSD	root mean-square deviation
SD	standard deviations
SDSL	site-directed spin labeling
<i>smf</i>	sodium motive force
smFRET	single molecule fluorescence resonance energy transfer
SPA	scintillation proximity assay
SSSF	sodium solute symporter family
TM	transmembrane domain
TRIS	Tris(hydroxymethyl)aminomethan
TSU	transmembrane subunit

## SUMMARY

Due to its hydrophobicity, the cellular membrane serves as natural permeability barrier between the cytoplasm of living cells and the surrounding environment. A prerequisite for the viability of bacteria is the controlled exchange of solutes between the interior and exterior compartment. Membrane integrated Na<sup>+</sup>/solute symporters utilize energy stored in an electrochemical Na<sup>+</sup> gradient to catalyze the import of a wide array of substrates such as amino acids, vitamins, ions, or sugars. The main objective of this thesis was to elucidate the molecular mechanism of function of transporters belonging to the sodium/solute symporter family (SSSF) using the Na<sup>+</sup>/proline symporter PutP of *Escherichia coli* as model system. By applying a combination of biochemical, biophysical, and bioinformatic approaches, new insights into structure-function relationships of PutP were gained.

The first part of this thesis addressed the functional significance of transmembrane domain (TM) 8' for the transport mechanism. Previous studies revealed that conserved residues in this domain are involved in Na<sup>+</sup> binding. A Cys scanning mutagenesis and subsequent *in vivo* proline uptake assays identified G328, S332, A337, Q345, and L346 as crucial for transport. Subsequent Cys accessibility studies using various membrane-permeant and -impermeant thiol-specific compounds indicated that TM 8' is involved in the alternating formation of an inward- and an outward-facing cavity. Proline in the presence of Na<sup>+</sup> reduced the accessibility on the cytoplasmic half of TM 8', whereas on the periplasmic half Na<sup>+</sup> alone had a similar effect. Considering all results, the data suggest that TM 8' is crucial for ion and substrate binding and lines two aqueous vestibules conveying access to the ligand binding sites from the periplasm and ligand release to the cytoplasm.

Using the crystal structure of the Na<sup>+</sup>/galactose symporter vSGLT of *V. parahaemolyticus*, in the second part of this work a first three-dimensional structural model of PutP was generated, showing the permease in an inward-facing conformation. A LeuT-like 10-helix core domain became discernable, that was composed of symmetrically related TMs 1-5 and 6-10. The resulting homology model was in good agreement with available experimental data and was used for the identification of the Na<sup>+</sup> and proline binding site by docking analyses. Remarkably, the predicted residues W59 (TM 1'), Y140 (TM 3'), W244 (TM 6'), and Y248 (TM 6') were found to be important for transporter function by kinetic analyses and Cys accessibility studies. Besides the characterization of Na<sup>+</sup> and proline binding residues, this study gave, for the first time, insights into the gating mechanism of Na<sup>+</sup>-coupled proline transport.

Finally, an electron paramagnetic resonance (EPR) based approach was chosen to analyze the structure and dynamic of extracellular loop 4 (eL4) of PutP. In the course of a complete Cys scanning mutagenesis and *in vivo* uptake assays conserved E311 was shown

to be crucial for function. After covalently linking a nitroxide probe to the Cys residues (spin-labeling), EPR measurements were performed. Based on the spin-label mobility and polarity of the microenvironment two  $\alpha$ -helical domains (298-308; 310-318) could be identified. The presence of  $\text{Na}^+$  or  $\text{Na}^+$  and proline specifically induced changes in the EPR spectra hinting at rigid body movements of eL4. Ligand-dependent intramolecular distance measurements using double electron-electron resonance spectroscopy were used to integrate the dynamics of eL4 into the context of the transport cycle implicating eL4 as key element in regulating access to the  $\text{Na}^+$  and/or proline binding site(s) from the periplasm.

## ZUSAMMENFASSUNG

Aufgrund ihrer Hydrophobizität dient die Zellmembran als Permeabilitätsbarriere zwischen dem Zytoplasma und dem umgebenden Milieu. Eine Grundvoraussetzung für das Überleben von Bakterien ist der kontrollierte Austausch von Stoffen zwischen dem Zellinneren und der Umwelt. Membran-integrierte Na<sup>+</sup>-abhängige Symporter nutzen die Energie eines elektrochemischen Na<sup>+</sup>-Gradienten um die Aufnahme eines Spektrums diverser chemischer Substrate, wie zum Beispiel Aminosäuren, Vitamine, Ionen oder Zucker, in die Zelle zu katalysieren. Der Schwerpunkt dieser Dissertation lag auf der Analyse des molekularen Funktionsmechanismus von Transportern der Na<sup>+</sup>/Substrat-Symporter Familie (SSSF). Hierfür wurde der Na<sup>+</sup>/Prolin-Transporter PutP aus *Escherichia coli* als Modellsystem verwendet. Durch eine Kombination biochemischer, biophysikalischer und bioinformatischer Methoden wurden neuartige Einblicke in die Struktur-Funktionsbeziehungen von PutP erhalten.

Der erste Teil dieser Arbeit befasste sich mit der funktionellen Bedeutung der Transmembrandomäne (TM) 8' für den Transportmechanismus von PutP. In vorhergehenden Arbeiten wurde gezeigt, dass konservierte Reste dieser Domäne an der Na<sup>+</sup>-Bindung beteiligt sind. Um darauf aufbauend die Rolle von TM 8' weiter zu charakterisieren, wurde jede Aminosäure individuell durch Cystein ausgetauscht. In darauf folgenden *in vivo* Aufnahmestudien erwiesen sich die Aminosäuren G328, S332, A337, Q345 und L346 als besonders wichtig für den Transportprozess. Anschließende Cystein-Zugänglichkeitsuntersuchungen mittels Membran-permeablen und -impermeablen Substanzen wiesen darauf hin, dass TM 8' an der alternierenden Ausbildung einer nach außen beziehungsweise einer nach innen orientierten Kavität beteiligt ist. Bei Anwesenheit von Na<sup>+</sup> und Prolin wurde auf der zytoplasmatischen Seite von TM 8' die Zugänglichkeit aus der wässrigen Phase drastisch reduziert. Auf der periplasmatischen Seite hatte Na<sup>+</sup> allein einen vergleichbaren Effekt. Unter Berücksichtigung aller Versuchsergebnisse konnte gezeigt werden, dass TM 8' eine zentrale Rolle in der Ionen- und Substratbindung spielt. Des Weiteren konnte nachgewiesen werden, dass TM 8' an der Ausbildung zweier wasserzugänglicher Spalten innerhalb von PutP beteiligt ist, die vermutlich den Zugang des Substrats zur Bindestelle von außen und die Entlassung des Substrats in das Zellinnere gewährleisten.

Im zweiten Teil dieser Arbeit konnte durch Zuhilfenahme der Kristallstruktur des Na<sup>+</sup>/Galactose Symporters vSGLT aus *Vibrio parahaemolyticus* ein erstes dreidimensionales Strukturmodell von PutP generiert werden, das in bemerkenswerter Weise mit bisherigen experimentellen Analysen übereinstimmt. Demnach beinhaltet der Transporter eine zentrale Domäne, bestehend aus 10 TMs, in der die Helices 1-5 symmetrisch zu den Helices 6-10

orientiert sind. Diese Architektur der TMs ist für Proteine der LeuT-Strukturfamilie charakteristisch. In der Tertiärstruktur ist zudem eine zum Zytoplasma geöffnete Kavität zu erkennen. Anhand von *in silico* Vorhersagen wurde die mutmaßliche Na<sup>+</sup>- und Prolin-Bindestelle identifiziert. In anschließenden kinetischen Analysen und Zugänglichkeitsstudien konnte den vorgeschlagenen Resten W59 (TM 1'), Y140 (TM 3'), W244 (TM 6') und Y248 (TM 6') eine wichtige Rolle im Transportmechanismus zugeordnet werden. Zusätzlich zu der Charakterisierung der Liganden-Bindestellen wurden erstmalig Einblicke in den *gating*-Mechanismus des Na<sup>+</sup>-gekoppelten Prolintransports erlangt.

Im dritten und letzten Teil dieser Dissertation wurde mittels Elektronenparamagnetischer Resonanz (EPR) die Struktur und Dynamik der extrazellulären Schleife 4 (eL4) von PutP untersucht. Jede einzelne Aminosäure dieser Domäne wurde gezielt gegen Cystein ausgetauscht. Mit Hilfe anschließender *in vivo* Prolinaufnahmestudien wurde die für die Transporteraktivität essentielle Aminosäure E311 identifiziert. Nach erfolgter Reaktion der Cysteinreste mit einem Nitroxidderivat (Spinmarkierung) wurden die Mobilität und die Polarität der Umgebung der Spinmarkierung mittels EPR bestimmt. Dabei konnten zwei  $\alpha$ -helikale Bereiche nachgewiesen werden, welche die Aminosäurepositionen 298-308 und 310-318 umfassen. Durch die Zugabe von Na<sup>+</sup> beziehungsweise Na<sup>+</sup> und Prolin wurden spezifische Änderungen der EPR-Spektren beobachtet, die auf eine Bewegung von eL4 als Ganzes relativ zu anderen Domänen in PutP hinweisen. Des Weiteren wurden Liganden-abhängige intramolekulare Abstandsänderungen gemessen, um die Dynamik von eL4 in den Transportzyklus einzuordnen. Zusammenfassend weist diese biophysikalische Analyse darauf hin, dass eL4 eine zentrale Rolle in der Regulation der Zugänglichkeit der Na<sup>+</sup> und/oder Prolinbindestelle(n) aus dem Periplasma spielt.

# 1 INTRODUCTION

## 1.1 Diversity of membrane transport systems

The cytoplasmic membrane functions as a permeability barrier thereby separating the cytosol from the surrounding medium. Occluding the internal compartment from the outside world facilitates cellular processes, which otherwise would not be possible because of, e.g. an unfavorable pH, low concentrations of educts or enzymes, presence of toxic compounds, protein instability, or the lack of macromolecular crowding effects (Lengeler *et al.*, 1999). However, in order to maintain cell homeostasis a controlled exchange of ions and molecules with the surrounding environment is indispensable.

Apolar as well as small and uncharged molecules such as water, ammonia, and oxygen can pass the lipid bilayer by diffusion in significant amounts. In contrast polar and charged molecules cannot cross the membrane freely. Import of compounds that feed catabolic or anabolic pathways and the export of metabolic end products or toxic substances with low membrane permeability are mediated by membrane-integrated transport proteins. Based on the applied driving force, these carriers can be divided into four different classes: channels, primary transporters, secondary transporters, and phosphoenolpyruvate:carbohydrate phosphotransferase system (PTS) (Fig. 1.1):

### 1.1.1 Diffusion/channels

Contrary to apolar and small and uncharged molecules, large and charged solutes cannot pass the membrane freely. Channels in the cytoplasmic membrane or porins in the outer membrane of bacteria facilitate the flux of ions and other molecules across the membrane in a thermodynamically favorable direction. Directed opening and closing of channels can be triggered by voltage changes (K<sub>v</sub>AP), ligands (GLIC), or mechanical forces (MscL) (Kung *et al.*, 2010, Catterall, 2010, Corringer *et al.*, 2010).

### 1.1.2 Primary transporter

Primary transporters couple transport across the membrane to chemical or photochemical reactions. Electron transport chains involved in respiratory and photosynthetic processes utilize energy that is released by the transfer of electrons from a donor molecule (reduced organic or inorganic substrates, H<sub>2</sub>O, or H<sub>2</sub>S) to an electron acceptor (O<sub>2</sub>, SO<sub>4</sub><sup>2-</sup>, or NADP). In the case of respiration, the yielded energy is converted into ATP by the F<sub>1</sub>F<sub>0</sub>-ATPase. Photosynthetically synthesized NADPH is used for the fixation of CO<sub>2</sub> and biomass production (Schultz & Chan, 2001, Boyer, 1997). ATP-binding cassette (ABC) transporters are a large superfamily of transporters which drive the import of a broad range of substrates by energy gained from ATP hydrolysis catalyzed in a highly conserved nucleotide binding

domain (NBD). Depending on the direction of transport, ABC transporters can be divided into two classes. Firstly, there are ABC importers that are involved in nutrient uptake and are exclusively found in prokaryotes. These transporters require a periplasmic high affinity binding protein (BP) that captures a free substrate and delivers it to a transmembrane subunit (TSU) that facilitates its translocation. Secondly, there are ABC exporters that are found in all three kingdoms of life. In this case, the TSU recruits the substrate directly from either the cytoplasm or the lipid bilayer (Hollenstein *et al.*, 2007). Members of the second class are involved in drug resistance of bacterial pathogens or cancer cells (Gottesman & Ambudkar, 2001). Beside the above-mentioned systems, also primary transporters are known that use energy derived from decarboxylation reactions or methyl-group transfer to pump ions across the membrane (Dimroth, 1980, Gottschalk & Thauer, 2001)

### **1.1.3 Secondary transporter**

Secondary transporters exploit preexisting (electro)chemical gradients to drive the movement of substrates across the lipid bilayer against their own concentration gradients. This family of permeases is ubiquitously distributed and can be found in prokaryotes as well as in eukaryotes. According to the mode of transport, secondary transporters can be divided into three different groups: symporters, antiporters, and uniporters (Fig. 1.1). Symporters catalyze the translocation of two compounds across the lipid bilayer in the same direction. Well-characterized model systems are the H<sup>+</sup>/lactose permease LacY (Abramson *et al.*, 2003), the Na<sup>+</sup>/proline symporter PutP of *Escherichia coli* (Jung *et al.*, 1998b), and the human Na<sup>+</sup>/glucose cotransporter SGLT1 (Wright *et al.*, 1992). In contrast to symporters, antiporters mediate the transport of two ions or molecules in opposite directions. Recent structural data for the arginine/agmatine (AdiC) (Fang *et al.*, 2009), the carnitine/butyrobetaine (CaiT) (Schulze *et al.*, 2010), and the Na<sup>+</sup>/H<sup>+</sup> antiporter (NhaA) (Hunte *et al.*, 2005) gave insights into the molecular mechanism of function at atomic resolution. Due to similar structural and functional properties, uniporters are also added to the class of secondary transporters. The driving force for the translocation of the substrate is its own concentration gradient. Import is not coupled to other compounds and therefore this class of secondary transporters only facilitates transport without accumulation of the substrate as shown for the sugar transporter Gif of *Zymomonas mobilis* (Weisser *et al.*, 1995).

### **1.1.4 Phosphoenolpyruvate:carbohydrate phosphotransferase system (PTS)**

The PTSs are multi-component transport systems which are, as known so far, unique to (Gram-positive and -negative) bacteria (Saier *et al.*, 2005). A striking feature of this mode of transport is that during the translocation process a phosphorylgroup is transferred from phosphoenolpyruvate (PEP) to the transported substrate, which is in most cases a

carbohydrate. Two general, sugar-unspecific cytoplasmic proteins mediate transfer of the phosphoryl group. Enzyme I receives the phosphoryl group from PEP which subsequently hands it over to a second acceptor in the cascade, the heat stable protein HPr. Substrate specificity is conferred by the next phospho-acceptor, the enzyme II complex (EII) that consists of two soluble proteins EIIA and EIIB where substrate phosphorylation finally comes to pass and the membrane integrated permease EIIC.

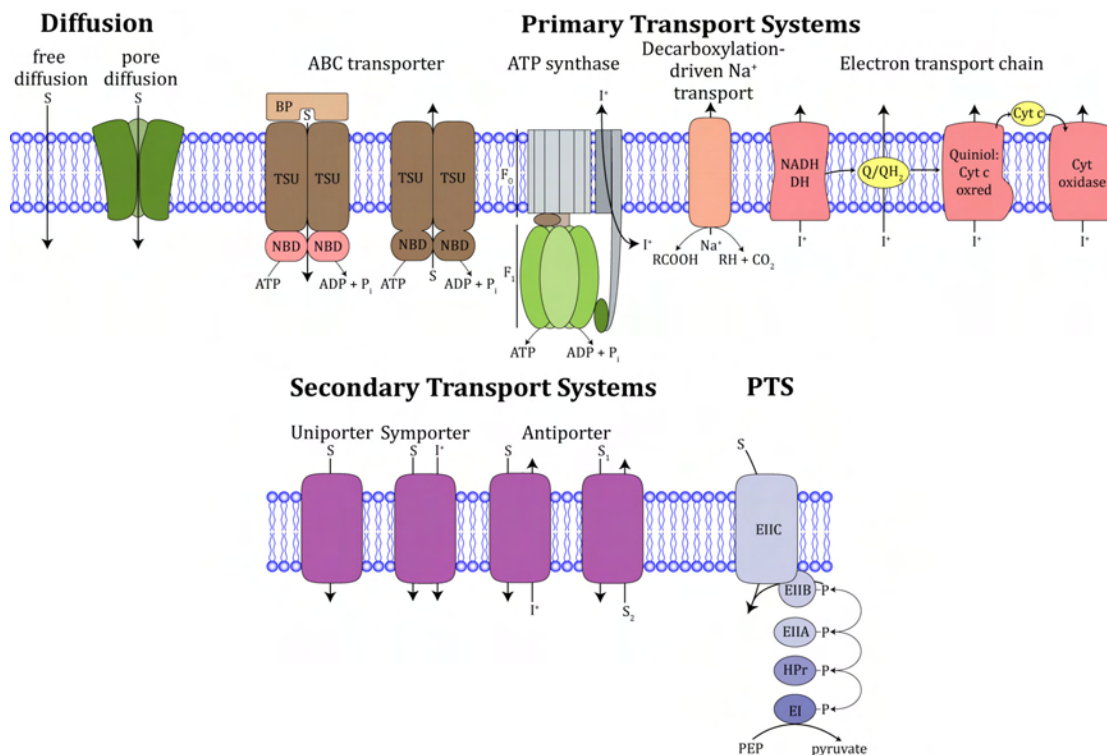


**Fig. 1.1 Diversity of transport systems.** On the one hand solutes can cross the membrane passively by diffusion (free diffusion or mediated by channel-type proteins). On the other hand they can be actively transported by carrier-mediated processes. According to the utilized energy source three classes can be discriminated: primary transport systems, secondary transport systems, and the phosphoenolpyruvate:carbohydrate phosphotransferase system. Based on (Konings, 2006). (BP: periplasmic binding protein, TSU: transmembrane subunit, NBD: nucleotide binding domain, DH: dehydrogenase, oxred: oxidoreductase, EI: enzyme I, HPr: heat stable protein, EII: enzyme II, PEP: phosphoenolpyruvate)

## 1.2 Physiological significance of secondary transport systems

In prokaryotes secondary transporters account for up to 68% of all encoded transport proteins (Paulsen *et al.*, 2000). The most prominent function of these carriers is the uptake of N- and C-sources for anabolic and catabolic purposes. In this way these transporters contribute in aerobic bacteria indirectly to the energization of the cytoplasmic membrane. In lactic acid bacteria secondary transporters are also able to create a *pmf* directly by coupling the extrusion of lactate to the export of two protons (Konings, 2006). In addition to this metabolic role, secondary transporters are key elements in bacterial stress response systems. Under hyperosmotic conditions e.g. the Na<sup>+</sup>-dependent symporter BetP is

upregulated and imports the compatible solute glycine betaine in order to restore normal hydration levels within the cell (Ressler *et al.*, 2009). Beside BetP, the  $\text{Na}^+/\text{H}^+$  antiporter NhaA is not only switched on under osmotic stress, but it is also involved in pH homeostasis (Padan *et al.*, 2005). Furthermore the lysine permease LysP, which regulates the transcriptional activator CadC by direct interaction, and the lysine/cadaverine antiporter CadB are involved in the acid stress response of *E. coli* (Tetsch *et al.*, 2008). Secondary transporters can also function as multidrug efflux pumps and can convey resistance to a chemical diverse array of toxic compounds such as antibiotics, bile salts, or dyes (Eicher *et al.*, 2009).

Comparative genomic analysis revealed that many bacterial transport systems have identifiable homologues in eukaryotes. In humans, there are 50 solute carrier (SLC) families described. Transport proteins of these families are involved in the uptake of nutrients and solutes such as sugars, peptides, amino acids, ions, vitamins, or fatty acids. Acquisition of these substrates in kidney and intestine is needed to feed anabolic and metabolic pathways. In addition, carriers like SERT (Rudnick, 2006) and GAT-1 (Eulenburg & Gomez, 2010) play a role in terminating neurotransmission by extruding neurotransmitters from the synaptic space into presynaptic neurons. Furthermore, transporters such as NIS (Dohan *et al.*, 2003) are synthesized specifically in thyroid follicular cells to drive the accumulation of  $\text{I}^-$ , which is an essential cofactor for thyroid hormones. It was also shown that solute carriers, together with other uptake systems determine the permeability properties of the blood-brain barrier (Pardridge, 2005). Due to the central role of secondary active transporters in human physiology, defects of respective genes are frequently associated with human diseases such as hypertension, deafness, diabetes, Parkinson's disease, depression, or renal glycosuria (Wright *et al.*, 2011, Yamashita *et al.*, 2005, Hediger *et al.*, 2004). Owing to this physiological significance, transporters are of great pharmaceutical importance. They are either utilized as primary drug targets like neurotransmitter transporters or they are alternatively used to deliver drugs into respective tissue, for example the  $\text{Na}^+/\text{I}^-$  symporter NIS is used for the radioiodine treatment of thyroid cancer.

### 1.3 Bioenergetics of secondary transport

Secondary transporters exploit energy stored in electrochemical gradients to drive the uphill transport of substrates. The most commonly used energy source in bacteria is the electrochemical proton gradient  $\Delta\mu_{\text{H}^+}$ . The biophysical properties of the bacterial cytoplasmic membrane are a major prerequisite to establish a membrane potential. Due to the low ion-permeability of the lipid bilayer, membrane integrated proton pumps which are involved in respiration, photosynthesis, and pyrophosphate hydrolysis, or ATPases in anaerobic bacteria are able to translocate protons into the periplasm (Simon *et al.*, 2008, Skulachev, 1991,

Baltscheffsky *et al.*, 1999, Feniouk *et al.*, 2007). As a result of this vectorial ion transport, a proton motive force *pmf* is generated that is composed of a pH gradient ( $\Delta\text{pH}$ ), outside acidic versus inside, and an electrical potential ( $\Delta\psi$ ) due to the concomitant charge translocation (Mitchell, 1966).

$$\Delta\mu_{H^+} = F\Delta\psi + RT \ln[H^+]_{in} / \ln[H^+]_{out} \quad (1.1)$$

$$pmf = \frac{\Delta\mu_{H^+}}{F} = -\frac{2.3RT}{F} \Delta\text{pH} + \Delta\psi \quad (1.2)$$

As a result of the low permeability of the lipid bilayer for ions, influx of protons is mediated by membrane-integrated proteins. These proteins couple the energy stored in the inwardly oriented electrochemical gradient to drive other membrane-associated endergonic processes such as ATP synthesis by the  $F_0F_1$ -ATPase or the rotation of bacterial flagella (Boyer, 1993, Mitsui & Ohshima, 2005). In addition, the *pmf* is also the driving force for symporters and antiporters that catalyze the translocation of solutes and ions across the cytoplasmic membrane. Imported substrates can subsequently feed catabolic and anabolic pathways. Antiporter mediated exchange of  $H^+$  and  $Na^+$  can convert the *pmf* into a sodium motive force (*smf*), an alternative energy source for secondary transporters (Winkelmann, 2001, Padan *et al.*, 2005).

In addition to  $Na^+/H^+$  antiporters several classes of primary  $Na^+$  pumps are involved in maintaining a  $Na^+$  gradient. The oxalacetate decarboxylase of *Klebsiella pneumoniae* is a well characterized representative of a group of membrane proteins that couples the efflux of  $Na^+$  to the decarboxylation of organic compounds (Dimroth, 1980). Another class, which is so far unique to methanogenic archaea, catalyzes the methyl transfer from N(5)-methyltetrahydromethanopterin to coenzyme M by a  $Na^+$ -translocating enzyme (Gottschalk & Thauer, 2001). Furthermore, electrogenic  $Na^+$  extrusion can also be mediated by P-type ATPases or ABC transporters (Cheng *et al.*, 1997, Suzuki *et al.*, 2005). Recently, within the group of pyrophosphatases, which were thought to exclusively pump  $H^+$  out of the cytoplasm, also  $Na^+$  exporting representatives were identified (Luoto *et al.*, 2011).

In principle, the created *smf* provides energy to similar cellular processes as the *pmf*, such as secondary transport, ATP synthesis or the rotation of the flagellar motor. Even though there are *smf*-dependent membrane proteins present in mesophilic prokaryotes, these organisms predominantly couple their energy-consuming membrane-bound processes to the proton gradient. Originally it was believed that the exclusive use of the *smf* is an adaptive response of organisms that live under extreme environmental conditions like alkaline pH (low proton availability) or high temperatures (increased proton leakage of the membrane). Due to its pH independence and because the membrane permeability of protons is several orders of magnitude higher compared to  $Na^+$ , the *smf* is under these conditions the preferred energy source (Skulachev, 1988, van de Vossenberg *et al.*, 1995). The major disadvantage of using the *smf* is that primary  $Na^+$  pumps within electron transport chains use

a much smaller redox gap compared to primary redox-driven H<sup>+</sup>-translocators. Therefore the energy yield during electron transport coupled phosphorylation is lower (Mulkidjanian *et al.*, 2008a).

Genomic analysis of various hyperthermophilic and alkaliphilic organisms revealed that other criteria also play a role in the discrimination between Na<sup>+</sup> or H<sup>+</sup> 'users' (Takami *et al.*, 2000, Deckert *et al.*, 1998). Hyperthermophilic bacteria, archaea that live under oxic or microoxic conditions, or anaerobes which are using high potential alternative electron acceptors cope with the problem of proton leakage by using high potential energy sources. If the energy status of microorganisms is tightly calculated for example in *Caloramator fervidus* (former *Clostridium fervidus*) these organisms utilize the less membrane-permeable Na<sup>+</sup> as energy source in order to avoid energy losses due to proton leakage (Speelmans *et al.*, 1993).

Recent findings support the idea that the *smf* is not only an adaptation mechanism of extremophilic microorganisms, but during evolution the *smf* may preceded the *pmf*. This theory is strongly supported by evolutionary analysis of V- and F-type ATPases and by the fact that H<sup>+</sup>-tight membranes show a much higher complexity compared to Na<sup>+</sup>-tight membranes, which therefore might have evolved in several distinct evolutionary steps (Mulkidjanian *et al.*, 2008b, Konings *et al.*, 2002).

#### 1.4 Symporters work according to an alternating access mechanism

More than 50 years ago Peter Mitchell discussed the involvement of 'translocases' in the uptake of solutes into bacterial cells. The first general theory derived from these results was refined by Oleg Jardetzky who proposed that secondary transporters work according to an alternating access mechanism (Jardetzky, 1966, Mitchell, 1957). This assumption suggests that transport proteins isomerize between two major conformations. In these two states ligand binding sites, which are located approximately halfway across the membrane, are either accessible from the extracellular space or from the cytoplasm via cavities in the interior of the protein. In contrast to channels, during the transport cycle only alternatively opening and closing intra- and extracellular cavities are observed, but no membrane-spanning pores.

Recent biochemical, biophysical, and structural analyses gave rise to a more detailed picture of the transport cycle. In the course of the transition between the two major conformations, the transporter adopts a number of other transient states that can be merged to a 10-step transport mechanism (Fig. 1.2).

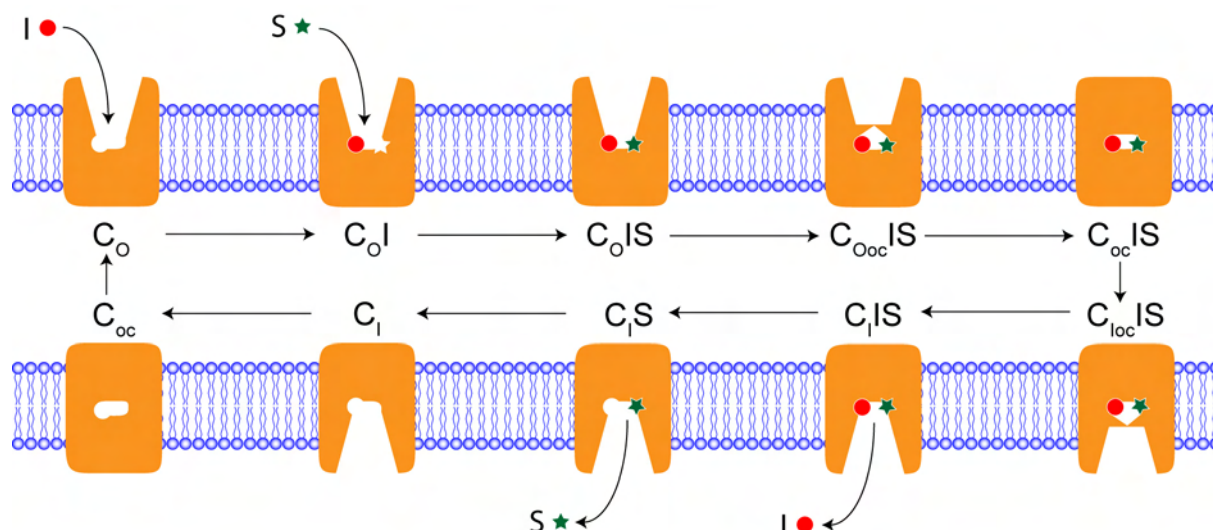


**Fig. 1.2 Transport cycle of secondary active symporters based on the alternating-access mechanism.** Schematic presentation of ion-coupled solute symport and proposed conformational alterations during the translocation process. Based on (Forrest *et al.*, 2011). I: coupling ion; S: substrate;  $C_O$ : outward-facing open conformation of the transporter;  $C_{OI}$ : binary complex of the transporter in the outward-facing open conformation in complex with the respective coupling ion;  $C_{OIS}$ : ternary complex of the transporter in the outward-facing open conformation in complex with the respective substrate and coupling ion;  $C_{OocIS}$ : ternary complex of the transporter in the outward-facing occluded conformation;  $C_{ocIS}$ : ternary complex of the transporter in an occluded conformation;  $C_{locIS}$ : ternary complex of the transporter in the inward-facing occluded conformation;  $C_{IIS}$ : ternary complex of the transporter in the inward-facing open conformation in complex with the respective substrate and coupling ion;  $C_I$ : binary complex of the transporter in the inward-facing open conformation in complex with the respective coupling ion;  $C_I$ : inward-facing open conformation of the transporter;  $C_{oc}$ : Apo-state of the transporter in an occluded conformation;

As it was shown for several secondary transporters such as LacY, GltS, or PutP of *E. coli*, symporters work according to an ordered binding mechanism, suggesting that substrate and coupling ion binding or release are two separate, but interdependent events (Guan & Kaback, 2006, Yamato, 1992, Zhou *et al.*, 2004). In the Apo-state, in the absence of ligands, the transporter occupies an outward-facing open conformation ( $C_O$ ). In the first step of the transport cycle, the coupling ion (I) accesses the ion binding site via an extracellular vestibule and binds to the vacant transporter. The formation of this binary complex ( $C_{OI}$ ) leads to structural rearrangements, which result in an increase of the affinity of the transporter for its actual substrate (S), followed by subsequent binding of the co-transported solute. Subsequently, the occupied binding sites in the ion/substrate/carrier ternary complex ( $C_{OIS}$ ) are shielded from the outside of the cell by protein domains called gates, leaving the transporter in an outward-facing occluded conformation ( $C_{OocIS}$ ). In the course of the transition from the outward-facing to the inward-facing conformation the symporter undergoes major conformational changes. The extracellular cavity is closed and the protein adopts a transient occluded state ( $C_{ocIS}$ ). In the next step the intracellular cavity opens, but the intracellular gate, which restricts access to site of substrate and ion binding from the cytoplasm, remains closed ( $C_{locIS}$ ). Opening of the gates ( $C_{IIS}$ ) is followed by a sequential release of the coupling ion ( $C_{IS}$ ) and the substrate, resulting in a transporter molecule in the inward-facing open Apo-state ( $C_I$ ). In order to start the next transport cycle, the carrier

isomerizes from the inward-facing back to the outward-facing conformation, passing through a substrate-free occluded state ( $C_{oc}$ ).

## 1.5 Structural diversity of secondary active transporters

Elucidation of three-dimensional protein structures is indispensable for understanding the molecular mechanism of function of secondary active transport. Despite the recent advances in the structure determination of membrane proteins, these amphipathic molecules are still underrepresented in databases of protein structures. While typically approximately 30% of the proteome of an organism are membrane proteins, only 1462 out of 76041 (1.9%) structures in the protein database represent membrane proteins (Wallin & von Heijne, 1998, Tusnady *et al.*, 2004).

At the moment 97 high-resolution structures of 28 different secondary transporters are available, which describe 11 unique folds (Fig. 1.3) (White, 2011). As described above, secondary transporters are supposed to work according to a multi-step alternating access mechanism and in order to draw a detailed picture of the transport cycle a crystal structure of every single intermediate conformation would be necessary. So far only a few of the crystallized symporters and antiporters such as AcrB, Glt<sub>Ph</sub>, LeuT, Mhp1, AdiC, or vSGLT were caught in different conformations. But for none of these proteins structures of every single proposed conformational state were solved. Therefore, there is still a need for other biochemical or biophysical approaches to gain deeper and more precise insights into the mechanism of secondary active transport.

A common feature, which can be found in almost all secondary transporters, are internal symmetry-related structural repeats. This term describes protein domains, which are built by consecutive loop and transmembrane domains (TMs) that can be superimposed by symmetry operations on other domains within the protein that adopt a similar three-dimensional structure. It is assumed that these structural repeats arose from gene duplication and subsequent fusion events (Lolkema *et al.*, 2008). Recent structural modeling approaches support the idea that the structural repeats are the molecular basis for the alternating access mechanism. Based on the available crystal structures of the Na<sup>+</sup>/leucine transporter LeuT (outward-facing occluded), the Na<sup>+</sup>/glutamate transporter Glt<sub>Ph</sub> (outward-facing occluded), and the H<sup>+</sup>/lactose permease (inward-facing open) the identified internal repeats were used to calculate the respective inverted conformations (Crisman *et al.*, 2009, Forrest *et al.*, 2008, Radestock & Forrest, 2011). The structural relevance of these models was either tested and confirmed by biochemical or biophysical approaches or directly shown by adequate crystal structures (Reyes *et al.*, 2009).

In contrast to carriers in which the structural repeats are found within the protein core, the zinc transporter YiiP and the multidrug resistance protein EmrE are functional

homodimers (Lu & Fu, 2007, Steiner-Mordoch *et al.*, 2008). These permeases may represent ancient forms, which arose prior to the gene duplication and fusion events.

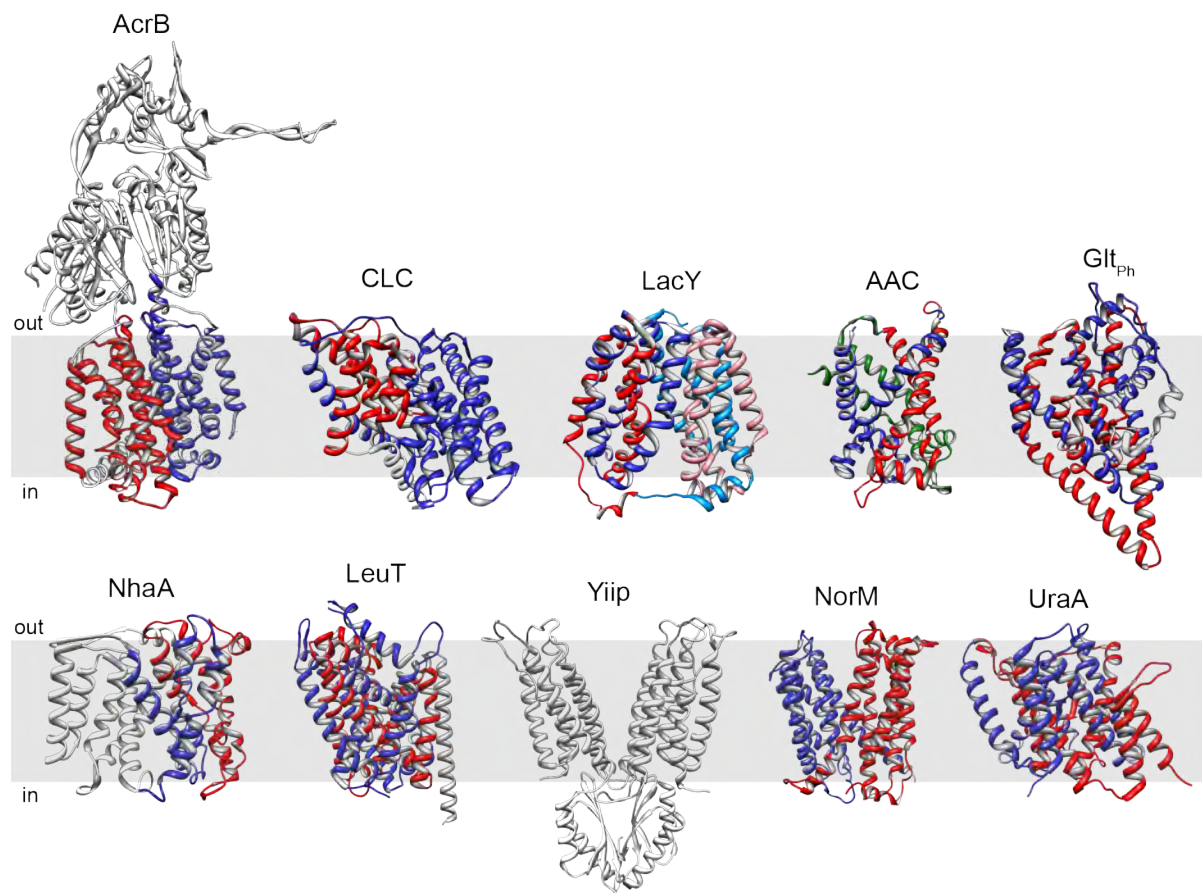


**Fig. 1.3 Architecture of secondary active transporters.** Ribbon representation of X-ray structures of secondary transporters, which represent a unique fold, viewed in the plane of the membrane. Internal structural repeats are colored in blue, red, and green. Transmembrane and soluble domains not belonging to the structural repeats are colored in gray. For the generation of the ribbon models the following PDB accession codes were used: AcrB (1IWG), CLC (1KPL), LacY (1PV7), AAC (1OKC), Glt<sub>Ph</sub> (1XFH), NhaA (1ZCD), LeuT (2A65), YiiP (2QFI), NorM (3MKT), and UraA (3QE7). Out: extracellular side, in: cytoplasmic side. This figure was prepared using UCSF chimera (Pettersen *et al.*, 2004).

## 1.6 LeuT-structural fold

### 1.6.1 *LeuT*-structural family

The transporter classification database (TCDB) applies a functional/phylogenetic approach to divide transport proteins into different families (Saier *et al.*, 2006). Since the protein fold is the major determinant for the molecular mechanism of function, in addition to the sequence based categorization, Lolkema and Slotboom used another approach, which not exclusively relies on sequence alignments. By utilizing hydropathy profile alignments, they proposed that phylogenetically unrelated transporter families together form structural classes (Lolkema & Slotboom, 1998). With the increasing number of available crystal structures, these predicted structural similarities of evolutionary unrelated transporter gene families were verified.

With the crystallization of the Na<sup>+</sup>/leucine symporter LeuT of *Aquifex aeolicus* in 2005, a member of the neurotransmitter/sodium symporter (NSS) family, a new transporter fold was described that was not known so far (Yamashita *et al.*, 2005). In the following years this protein architecture was detected in six other transport proteins of four different transporter gene families: vSGLT of *Vibrio parahaemolyticus* (sodium/solute symporter (SSS) family) (Faham *et al.*, 2008), Mhp1 of *Microbacterium liquefaciens* (nucleobase-cation symporter-1 (NCS1) family) (Weyand *et al.*, 2008), AdiC of *E. coli* (amino acid/polyamine/organocation (APC) superfamily) (Gao *et al.*, 2009), ApcT of *Methanococcus jannaschii* (APC) (Shaffer *et al.*, 2009), BetP of *Corynebacterium glutamicum* (betaine/choline/carnitine transporter (BCCT) family) (Ressl *et al.*, 2009), and CaiT of *E. coli* (BCCT) (Schulze *et al.*, 2010). Due to the lacking sequence similarity, surprisingly these diverse secondary transporters share the same core structure. Despite the common helix packing, different modes of transport are observed in the LeuT structural family. LeuT, vSGLT, Mhp1, BetP, and ApcT work as symporters, AdiC and CaiT as antiporters (Forrest *et al.*, 2011). Also differences in the utilized energy sources were observed. Except ApcT, which is using the *pmf* as driving force, all other symporters are Na<sup>+</sup>-dependent. In contrast to the symporters, AdiC and CaiT function in an ion-independent way. Despite these functional differences, there are conserved features found in the crystal structures of the respective transport proteins that can be used to draw general conclusions about the molecular mechanism of function of LeuT-like transporters.

### **1.6.2 Global fold and internal symmetry**

Even though the total number of TMs differs between the members of the LeuT structural family, all transporters share a conserved structural motif, which consists of 10 membrane-spanning helices (to avoid confusion, the TMs of the core domain of all discussed LeuT-like transporters are numbered as in LeuT from 1-10; in the case of CaiT, BetP, and PutP the 10-helix core domain is numbered from 1'-10' because the 10 TM core is preceded by 1 (PutP) or 2 (CaiT, BetP) peripheral helices at the N-terminal part; therefore numbering starts from -2 (CaiT, BetP) or from -1 (PutP) respectively; peripheral C-terminal TMs are numbered 11' and 12'). Within the core domain, TMs 1-5 are related to TMs 6-10 by an internal pseudo two-fold symmetry axis. The fact that carriers, which do not share significant sequence similarities harbor comparable core domains, suggests that this domain might be the functional unit of the transport mechanism. This idea is also supported by the observation that the helices of both repeats are intertwined and that both, the ion and the substrate binding site, are located within the domain-domain interface.

One key feature of this protein fold is that the symmetry related TMs 1 and 6 are formed by two helical domains that are connected by an unwound stretch approximately halfway across the membrane (Krishnamurthy *et al.*, 2009). Disruption of the H-bonding

pattern of an  $\alpha$ -helix exposes backbone carbonyl oxygen and nitrogen atoms as interaction partners. In addition, the dipole moments at the end of the helices create a polar microenvironment in the otherwise low dielectric core of the membrane (Screpanti & Hunte, 2007). Together with residues located in the symmetry related TMs 3 and 8, these four helices built up the ion and substrate binding site not only in LeuT, but also in Mhp1 and AdiC. Interestingly, the last two TMs of each inverted repeat form the so-called 'V-motifs', which can be superimposed by pseudo-two-fold symmetry operations. Considering the available crystal structures, these two domains seem to function as a static scaffold and swapping from one conformation to the next is achieved by a movement of the remaining 6 TMs relative to the rigid framework, build up by the two intertwined 'V-motifs' (Boudker & Verdon, 2010).

### 1.6.3 $\text{Na}^+$ binding sites

Except for the antiporters AdiC and CaiT, all other members of the LeuT structural family couple the translocation of the substrate to either the flux of  $\text{Na}^+$  or  $\text{H}^+$ . Compared to the determined crystal structures of other members of the LeuT structural family, the structure of LeuT was solved at the highest resolution (1.65 Å). Therefore up to now the collected LeuT data set is the only one in which occupied  $\text{Na}^+$  binding sites were directly observed. In total two electron densities representing bound coupling ions were identified. Interestingly, both ions are predominantly coordinated by partial charges. In the first binding site ( $\text{Na}_1$ ), which is in close contact with the substrate, the two carbonyl oxygen of A22 (TM 1) and T254 (TM 6), the side chain carbonyl oxygen of N27 (TM 1) and N286 (TM 7), the hydroxyl oxygen of T254 (TM 6), and the carboxyl oxygen of the substrate leucine coordinate the ion in an octahedral manner. The second binding site ( $\text{Na}_2$ ), which is  $\sim 7$  Å away from the leucine binding site, is composed of five binding partners, the carbonyl oxygens of G20, V23 (both TM1), A351 (TM 8) and, the side chain hydroxyl oxygen of T354 and S355 (both TM8) (Yamashita et al., 2005). To address the role of both ion binding sites of LeuT, energy perturbation molecular dynamics (FEP/MD) simulations were applied. These *in silico* analysis indicate, that  $\text{Na}_2$  is of structural importance. It stabilizes  $\text{Na}_1$  and also mediates selectivity for the second ion binding site. In contrast, the close vicinity of  $\text{Na}_1$  to the leucine binding site and the direct interaction of the bound ion with the carboxylate oxygen of the substrate already provided clear evidence for the role of this ion in substrate binding. In good accordance, molecular dynamics (MD) simulations showed that removing  $\text{Na}^+$  from  $\text{Na}_1$  results in a decreased leucine affinity (Caplan et al., 2008).

Structural alignments combined with site-directed mutagenesis and subsequent functional characterization revealed that  $\text{Na}_2$  is highly conserved in  $\text{Na}^+$ -dependent transporters of the LeuT structural family. The finding that the occupied  $\text{Na}_2$  is mimicked in the  $\text{Na}^+$ -independent secondary transporters ApcT (Shaffer et al., 2009) and CaiT (Schulze

et al., 2010) by basic amino acids, K158 and R262, further emphasizes the importance of the positive charge exactly at this very position for transporter function.

#### **1.6.4 Substrate binding sites**

Comparison of crystal structures of LeuT-like transporters in complex with bound substrates reveal similar positions of the respective substrate binding sites, approximately halfway across the membrane bilayer, at the interface between the two inverted repeat domains. LeuT, Mhp1, and AdiC were observed in either an outward-facing open or an outward-facing occluded conformation. It was shown that positions located in TMs 1, 3, 6, and 8 in all three transporters are involved in substrate coordination. In AdiC, an additional helix (TM 10) is involved in substrate binding (Abramson & Wright, 2009). In contrast to the former mentioned transporters, vSGLT, CaiT, and BetP are not described in the outward-facing but in an inward-facing occluded, inward-facing open, or intermediate occluded state. Even though the substrates are also located at similar positions within the protein core, the TMs involved in shaping the binding sites differ slightly. In BetP and CaiT, both members of the BCCT family, the substrate is sandwiched in an aromatic box, composed by tryptophan residues located in TM 2' and 6' (Ressl et al., 2009, Schulze et al., 2010). The substrate in vSGLT is located between TMs 1', 2', 6', 7', and 10' (Faham et al., 2008).

Taking all the different binding pockets into consideration, some conclusions can be drawn regarding the general properties of substrate binding sites in transporters of the LeuT structural family. The 10-helix core domain provides a scaffold for the formation of different pockets that are able to bind a diverse array of chemically different compounds. Substrates are located at similar positions in the core domain and are coordinated by H-bonds with polar side chains or by main chain nitrogen or carbonyl oxygen atoms in unwound regions. Formal charges of the ligand are either compensated by partial charges, helix dipoles, cation- $\pi$ -interactions, or coupling ions. Hydrophobic substrate moieties can be docked in hydrophobic binding pockets created by side-chain atoms (Krishnamurthy et al., 2009, Forrest et al., 2011, Abramson & Wright, 2009).

In addition to the central binding site (S1) described above, for some members of the LeuT structural family, a second allosteric binding site (S2) is proposed. Direct evidence for the presence of S2 in the LeuT structural family gave the crystal structure of CaiT (Schulze et al., 2010). In addition to a substrate in the S1 site, a second  $\gamma$ -butyrobetaine molecule is bound in an extracellular cavity. Mutations in the S2 site led to drastically reduced uptake rates and the determined Hill coefficient suggested a regulatory function of S2. The authors propose a crosstalk between both sites and thereby bound substrate in S2 triggers conformational changes in the transporter and subsequent substrate release from S1 into the cytoplasm. For LeuT, the second transporter in this group of carriers for which a second binding site is proposed, the presence and function of this site is discussed more

controversially. On the one hand, until now all available crystal structures of LeuT did not provide any evidence of a substrate located in S2 (Singh *et al.*, 2008, Singh *et al.*, 2007, Yamashita *et al.*, 2005). On the other hand, based on molecular dynamics (MD) simulations in combination with substrate binding assays and single molecule fluorescence resonance energy transfer (smFRET) measurements, also an allosteric transport mechanism was proposed, similar as described for CaiT (Shi *et al.*, 2008, Zhao *et al.*, 2011, Zhao *et al.*, 2010). So far no final consensus about a general functional role of a second binding site has been reached and in order to elucidate the importance of S2 for the transport cycle more experiments need to be done.

### **1.6.5 From structure to function: Rigid body movements as key element for secondary active transport**

The comparison of various transport protein structures in different conformational states gives insights into a putative molecular mechanism of function of members of the LeuT structural family. As described above, all members of this group share a conserved protein core consisting of 10 TMs, in which the first 5 TMs are related to the second 5 TMs by a pseudo two-fold axis along the membrane plane. Forrest and co-workers proposed that a 4-helix bundle, composed of TMs 1, 2, 6, and 7, is the major determinant for the alternating access mechanism (Forrest *et al.*, 2008). A rigid body movement ('rocking') of this bundle relative to the remaining 6 helices, the so-called scaffold, is proposed to lead to an alternative opening and closing of inward- and outward-facing cavities. In LeuT, these four helices are tilted with respect to the rest of the 10-helix core domain by 25° and inverting this tilt angle led to a model of LeuT in an inward-facing conformation, which is in good agreement with biochemical data and the subsequently published crystal structure of vSGLT in the inward-facing conformation (Faham *et al.*, 2008).

Since Mhp1 is the only transporter in the LeuT structural family that is crystallized in three different states ( $C_O$ ,  $C_{Ooc}$ |S, and  $C_I$ ), this system can be used to validate the mechanism postulated by Forrest and colleagues. The observed structural reorientations in Mhp1 during the transition from the outward- to the inward-facing conformation are in good agreement with the rocking bundle motion proposed for LeuT (Yamashita *et al.*, 2005, Shimamura *et al.*, 2010). The authors discriminate more precisely between the 4-helix bundle and the so-called 'hash' motif, composed by TMs 3, 4, 8, and 9. Both domains rotate relative to each other by 30° and this intramolecular motion is proposed to be the molecular basis for the alternating access to the centrally located S1 binding site via an extracellular or an intracellular water-filled cavity (Shimamura *et al.*, 2010). Interestingly, a recent crystal structure of BetP caught the transporter in an occluded state (Ressl *et al.*, 2009). Compared to the outward and the inward-facing conformation of Mhp1, BetP adopts an intermediate state. As described above, the proposed molecular basis for reciprocal opening and closing of cavities are structural

differences between the symmetry related repeat domains (Forrest et al., 2008). Remarkably, in the observed intermediate state of BetP the inverted repeats are clearly symmetric, what is in good concordance with the suggested transport mechanism.

By comparing the available crystal structures also structural variations within the LeuT structural family become obvious. As described above, during the transport cycle so-called gates regulate access to the substrate and ion binding sites. On the one hand, the binding pockets can be occluded from the surrounding by bulk protein (thick gates). This is observed in all structures of LeuT-like transporters. On the other hand, a small number of distinct residues can be sufficient to control access to the binding pockets (thin gates). These thin gates differ in their configuration and biochemical nature within the LeuT structural family. In the case of LeuT, the sites of Na<sup>+</sup> and leucine binding are occluded from the extracellular space by a pair of aromatic residues (Y108 and F253) and in addition by the charged pair composed of R30 and D404 (Yamashita et al., 2005). In vSGLT three hydrophobic amino acid residues (Y262, Y263, and W264) are involved in preventing substrate release from the central binding pocket (Faham et al., 2008). In contrast to the situation in LeuT and vSGLT, where a distinct and small number of residues is involved in gating, the situation in Mhp1 is different. In the transition from the outward-facing open to the outward-facing occluded conformation the N-terminal half of TM 10 bends into the water filled extracellular cavity and as a result the substrate binding site is no longer accessible from the water phase (Weyand et al., 2008). Interestingly, electron paramagnetic resonance (EPR) spectroscopic analysis added some details to the gating mechanism in LeuT. It was shown that in addition to the above-mentioned gating residues, TM 10 and extracellular loop (eL) 4 are undergoing conformational alterations upon ligand binding (Claxton *et al.*, 2010). These movements might play an important role in the gating mechanism and are in good agreement with information derived from other crystal structures e.g. Mhp1 (Shimamura et al., 2010).

## 1.7 PutP – a member of the LeuT structural family

PutP is a Na<sup>+</sup> dependent L-proline transporter, which belongs to the sodium/solute symporter family (SSSF; TC 2A.21, SLC5). This group comprises more than 1000 members that can be found in all three kingdoms of life (Jung, 2002, Wright & Turk, 2004). In the enteric bacterium *Escherichia coli*, *putP* is localized together with *putA* in the *put* operon (Wood, 1981). PutA is a multifunctional cytoplasmic flavoprotein that mediates the degradation of proline to glutamate in a two-step oxidation reaction. In the absence of substrate, PutA in its oxidized form functions as a transcriptional repressor of the *put* operon (Ostrovsky de Spicer & Maloy, 1993, Brown & Wood, 1992). In contrast to genes encoding for the proline uptake systems *proP* and *proU*, *putP* expression is not osmotically regulated (Dattananda & Gowrishankar, 1989, Culham *et al.*, 1993). Therefore, the main purpose of

PutP mediated proline uptake is rather to feed metabolic and anabolic pathways than to respond to osmotic stress. Remarkably, it was shown by transposon mutagenesis that PutP in *Helicobacter pylori* and *Staphylococcus aureus* is an essential virulence factor. Functional inactivation of the respective genes prevents stomach colonization by *H. pylori* (Kavermann *et al.*, 2003) and in *S. aureus* the proline permease is indispensable for *in vivo* survival (Bayer *et al.*, 1999). Furthermore, dysfunction of human homologues of PutP such as NIS and SGLT1 cause diseases such as iodide transport defect and glucose-galactose malabsorption (Dohan *et al.*, 2003, Wright *et al.*, 2007).

The *putp*-gene was cloned and sequenced (Nakao *et al.*, 1987). According to the DNA sequence, a primary sequence containing 502 amino acids was proposed resulting in a molecular weight of 54.343 kDa. The protein was solubilized, purified, and reconstituted. Proline uptake in proteoliposomes was traced back to PutP and a Na<sup>+</sup> to proline stoichiometry of 1:1 was determined (Jung *et al.*, 1998b, Chen & Wilson, 1986, Hanada *et al.*, 1988). In addition, *in vivo* uptake assays revealed an apparent affinity ( $K_{m(\text{pro})}$ ;  $K_{0,5(\text{Na})}$ ) of PutP for proline of 2 and for Na<sup>+</sup> of 30  $\mu\text{M}$  (Yamato & Anraku, 1993). In the transport process Li<sup>+</sup> may substitute Na<sup>+</sup> as coupling ion, but with a much lower affinity ( $K_{0,5(\text{Li})} \sim 125 \mu\text{M}$ ). As already described above as a general mechanistic principle in secondary transporters, kinetic analysis suggested that PutP works according to an ordered binding mechanism (Yamato, 1992).

Despite a lacking three-dimensional high-resolution structure, decent biochemical and biophysical analyses gave detailed insights into structure-function relationships of PutP of *E. coli*. A combination of gene fusion analyses, site-directed mutagenesis combined with Cys accessibility studies, site-specific proteolysis, and spectroscopic approaches revealed a topology model of PutP containing 13 TMs, with the N-terminus facing the periplasm and the C-terminus facing the cytoplasm (Fig. 1.4) (Jung, 1998, Jung *et al.*, 1998a, Wegener *et al.*, 2000).

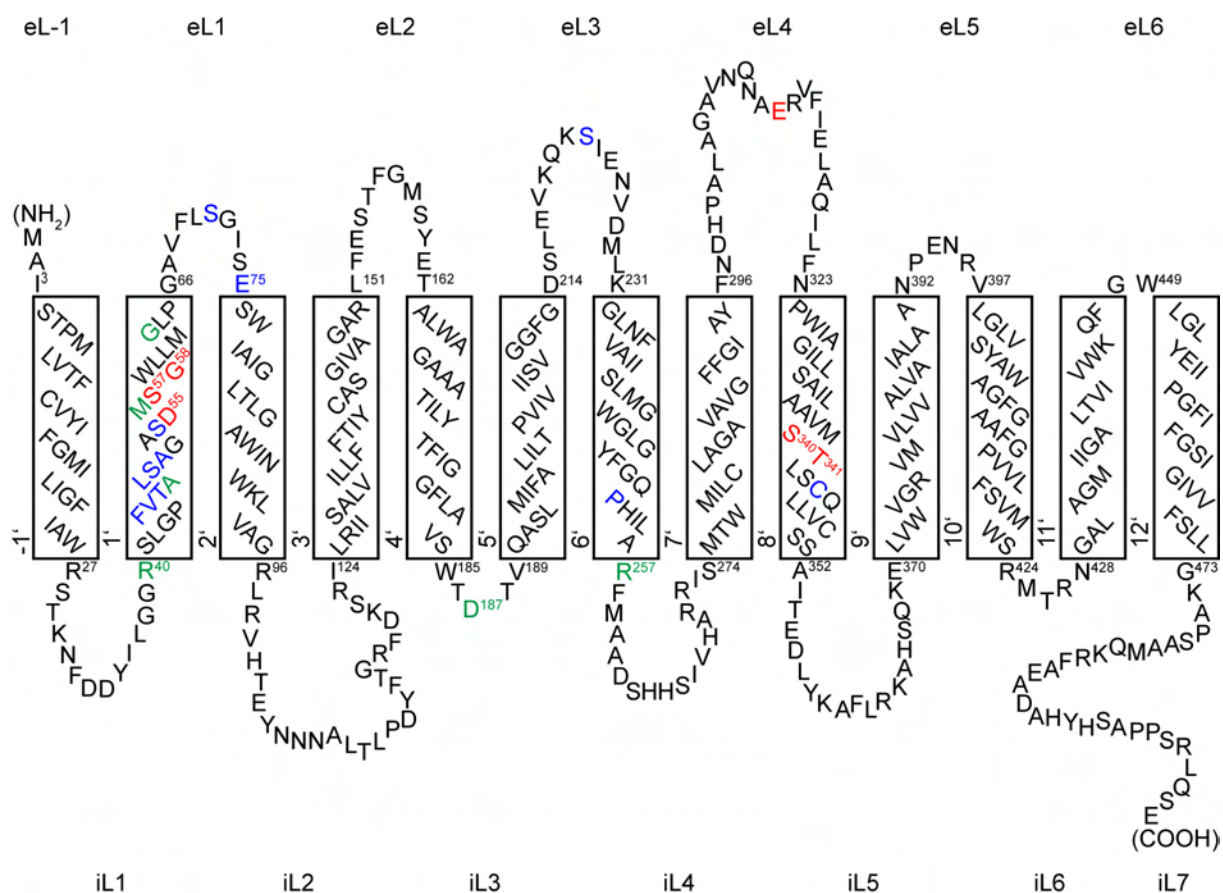


**Fig. 1.4 Secondary-structure model of the Na<sup>+</sup>/proline symporter PutP.** The predicted topology is based on a combination of EPR spectroscopic measurements, gene fusion- and accessibility analyses, and limited proteolysis (Wegener *et al.*, 2000, Jung, 1998). TMs are represented as rectangles. For clarity, TMs of the 10-helix core domain, shared by all members of the LeuT structural family, are numbered from 1' to 10', the additional N-terminal TM of PutP is numbered -1' and additional C-terminal TMs 11' and 12'. Extracellular loops (eL) are numbered from -1 to 6, intracellular loops (iL) from 1-7. For the primary sequence the one letter amino acid code is used. Residues involved in ligand binding are highlighted in red, positions involved in ligand-dependent conformational dynamics are colored in blue and other amino acids of structural/or functional importance are depicted in green.

The topology of PutP is in good agreement with the proposed general structural motif of 13 TMs of members of the SSSF. Biochemical and spectroscopic analyses gave more detailed insights into the tertiary structure of PutP. With TM 1' and 8' two helices were identified that are involved in the formation of a hydrophilic inward-facing cavity (Pirch *et al.*, 2003, Hilger *et al.*, 2008). Na<sup>+</sup> and proline dependent Cys labeling experiments of TM 1' gave first hints at ligand dependent opening and closing of the cytoplasmic vestibule. Remarkably, several conserved amino acid residues are clustering in both helices and it was shown that both TMs are at least temporarily in close proximity. Another interesting feature of TM 8' is its backbone structure, which was determined by double electron-electron resonance measurements of intrahelical distances and subsequent *in silico* modeling (Hilger *et al.*, 2009). The structural model revealed a kink near functionally important residue T341. On the one hand this kink interrupts the  $\alpha$ -helical H-bonding network and therefore backbone carbonyl oxygen and nitrogen atoms in this region might be involved in substrate and/or

coupling ion coordination. On the other hand this bended TM may function as a hinge, which is involved in reciprocal opening and closing of cavities within the transporter.

In order to gain information on the role of single amino acids for transporter function site-directed mutagenesis and additional *in vitro* and *in vivo* transport analyses of the respective protein derivatives were performed. It was shown that several positions in TM 1' are crucial for transporter function. Substitution of D55 by Cys or Asn abolished PutP mediated proline uptake completely, whereas a PutP-D55E derivative showed basal activity albeit at a highly reduced initial rate. Kinetic analysis of the latter construct suggested that D55 is either directly located in the Na<sup>+</sup> binding site or at least in close proximity (Quick & Jung, 1997). For the adjacent residue M56, which was shown not to be essential for transport, also a direct or indirect role in coupling ion coordination was proposed (Pirch *et al.*, 2002). In addition to D55 and M56 two further residues, which showed significantly altered transport kinetics upon substitution, were identified. Replacing S57 by Ala, Cys, Gly, or Thr changed the  $K_{m(\text{pro})}$  up to 400 fold, and the apparent Na<sup>+</sup> affinity approximately 100 fold. Similar but less pronounced effects were also detected by substitution of G58 by Cys (Pirch *et al.*, 2002, Quick *et al.*, 1996). In the course of a complete Cys scanning mutagenesis of TM 1', two additional amino acid residues A48 and G63 were identified to be pivotal for transporter function (Pirch *et al.*, 2003).

The characterization of the two highly conserved adjacent residues S340 and T341 gave insights into Na<sup>+</sup> binding (Hilger *et al.*, 2008). Substitution of S340 by Ala, Cys, or Thr resulted in significantly reduced transport activity. Kinetic analysis revealed that the apparent Na<sup>+</sup> affinity decreased by two to three orders of magnitude.  $K_{m(\text{pro})}$  was also affected but to a much lesser extent. This finding supports the idea of an interdependence of the sites of substrate and the coupling ion binding as it was shown in previous studies (Jung *et al.*, 1998b, Zhou *et al.*, 2004). Furthermore, the side chain size had a bigger influence on the  $K_{(0,5)\text{Na}^+}$  than the polarity. Hence, it is proposed that S340 is involved in coupling ion coordination, rather via backbone carbonyl oxygen than by the hydroxyl side chain. For T341 a clear dependence of Na<sup>+</sup> coupled proline transport on the presence of the hydroxyl group was found and a H-bond interaction between the ion and the side chain was proposed (Hilger *et al.*, 2008). Similar results were obtained for homologous residues in NIS. It was shown that S353 and T354 are crucial for Na<sup>+</sup> dependent iodide uptake and an involvement of the side chain hydroxyl groups in Na<sup>+</sup> binding is proposed (De la Vieja *et al.*, 2007). The proposed role of S340 and T341 in PutP is also confirmed by the crystal structure of LeuT. Here the corresponding residues T354 and S355 are in H-bonding distance to Na<sub>2</sub> (Yamashita *et al.*, 2005).

Remarkably, Cys placed at position 340 and 341, which was proposed to be located halfway across the membrane according to the topology model, is accessible by sulfhydryl

specific compounds from the water phase. Summarizing the kinetic and accessibility analyses of the investigated residues in TM 1' and 8', the results suggest that both TMs participate in the formation of the substrate and/or ion translocation pathway towards the cytoplasm. In addition, residues that are presumably located halfway across the membrane were shown to be crucial for transporter function, and a possible involvement in shaping the proline and/or Na<sup>+</sup> binding pocket was suggested.

In the course of further site directed mutagenesis studies additional functionally important residues were identified that are, according to the topology model, localized in hydrophilic loop domains. Three charged and functionally important residues (R40, R187, and, E311) were found that are conserved in the SSSF (Quick *et al.*, 1999, Quick & Jung, 1998; Bracher and Jung, unpublished data). In the case of R40, the removal of the positive charge led to a drastic decrease of  $V_{\max}$  and to a 10 fold decrease of the apparent Na<sup>+</sup> affinity. The authors drew the conclusion that R40 is in close proximity to the ion binding site and that this residue is important for coupling Na<sup>+</sup> to proline transport (Quick *et al.*, 1999). In contrast replacement of D187 by Cys increased the affinity of PutP approximately 10 fold and further analyses suggested that this residue might be located within or next to the ion translocation pathway and controls Na<sup>+</sup> release into the cytoplasm (Quick & Jung, 1998). A second important negatively charged residue (E311) was identified in eL4, which precedes functionally important TM 8'. Substitution of E311 by Gln or Arg abolished transport completely. Replacement by Cys and Asp resulted in 1% and 10% initial rate compared to wild type PutP. Kinetic studies revealed neither an impact on the proline nor on the Na<sup>+</sup> affinity. Instead  $V_{\max}$  was reduced by one to two orders of magnitude. These data suggest that E311 is rather involved in transporter dynamics than in ligand binding (Bracher and Jung, unpublished information).

A series of spectroscopic and biochemical analyses were performed in order to investigate the structural dynamics of PutP (Wegener *et al.*, 2000, Jeschke *et al.*, 2004, Pirch *et al.*, 2003, Pirch *et al.*, 2002). Site directed spin labeling (SDSL) of the single-Cys derivatives PutP $\Delta$ Cys-L37C and PutP $\Delta$ Cys-F45C revealed Na<sup>+</sup> and/or proline dependent mobility changes of the nitroxide group of the spin label. This could be explained by ligand induced conformational alteration of TM 1' and the preceding loop (Wegener *et al.*, 2000). These observations were additionally supported by intramolecular distance measurements using DEER. An increase in the distance between positions 37 and 187 upon Na<sup>+</sup> binding independently proved structural alterations on the cytoplasmic side of the transporter (Jeschke *et al.*, 2004). This initial characterization of the dynamics of PutP was complemented by Cys accessibility analyses. In good agreement with the spectroscopic data, Cys placed at positions 57 and 58 showed increased accessibility in the presence of Na<sup>+</sup>. Subsequent addition of proline reversed this effect (Pirch *et al.*, 2002). Interestingly, for

two positions in the consecutive loop also a  $\text{Na}^+$  mediated increase in the accessibility was observed (Pirch and Jung, unpublished information). In contrast, at several positions on the cytoplasmic half of TM 1' (F45, V46, T47, L49, S50, A51, S54, G63, and, L64) the accessibility was reduced by proline in the presence of  $\text{Na}^+$  (Pirch et al., 2003). Since these protective effects were observed across several helical turns and the initial rate of transport of the respective single-Cys derivatives was only slightly reduced, these changes in the accessibility can most likely be attributed to structural rearrangements. Effects of  $\text{Na}^+$  and proline on the labeling efficiency were also observed in TM 6' (P252), iL4 (R257), eL4 (D298, I315, L317), and TM 8' (C344) (Pirch and Jung, unpublished information; Imrich and Jung, unpublished information). Taken together the biochemical and biophysical analyses suggest that PutP is a highly dynamic protein in which various domains are involved in major conformational alterations. These findings are in good agreement with the postulated alternating access mechanism and the ordered binding model of ligand transport.

## 1.8 Scope of this work

The main objective of this thesis was to obtain insights into the structure, function, and dynamics of the  $\text{Na}^+$ /proline symporter PutP of *E. coli*. In order to address these tasks, a biochemical analysis of functionally important TM 8' of PutP was performed. Furthermore, a combination of bioinformatic and biochemical approaches was used to generate a first structural model of PutP, and to identify sites of  $\text{Na}^+$  and proline binding. Finally, the mechanistic role of eL4 in the transport cycle was analyzed by electron paramagnetic resonance (EPR) spectroscopy.

In a previous investigation, S340 and T341 of TM 8' of PutP were proposed to be involved in  $\text{Na}^+$  binding. Moreover, it was shown by intramolecular cross-linking that TMs 8' and 1' are at least temporarily in close proximity during the transport cycle. The latter TM harbors highly conserved amino acid residues that are involved in ion and substrate binding. Furthermore, TM 1' is also of structural importance as it was shown to participate in shaping an inward-facing cavity, which is opened and closed in a ligand-dependent manner. In order to identify additional functionally important residues in TM 8', in the first part of this work, a complete Cys scanning mutagenesis was performed and the transport properties of the respective PutP derivatives were characterized. To elucidate a putative role of TM 8' in the formation of a water-filled cytoplasmic and/or periplasmic cavity, the accessibility of the constructed single-Cys PutP variants to various thiol-specific compounds was tested. Finally, conformational alterations in TM 8' were tracked by analyzing the influence of ligands on the accessibility pattern.

In the second part of this thesis a homology model of PutP was computed, to obtain first insights into the three-dimensional architecture of the transporter. For this purpose, the

X-ray crystal structure of the Na<sup>+</sup>/galactose symporter vSGLT of *V. parahaemolyticus* was used as template, which is the only available high-resolution structure of a member of the sodium solute symporter family. The resulting model guided the identification of the Na<sup>+</sup> and proline binding site by docking analyses. To evaluate the relevance of the model and of the proposed substrate binding site, site-directed mutagenesis of predicted proline coordinating residues was performed in combination with a subsequent analysis of the transport kinetics of the respective PutP variants. Additional insights into substrate binding and ligand-induced local conformational alterations were gained by Cys accessibility experiments of functionally important residues.

Despite the increasing number of high-resolution structures of transport proteins, information on conformational dynamics in the course of the translocation cycle is limited. In the third part of this dissertation a complete Cys scanning mutagenesis of eL4 of PutP was performed. The transport activity and binding properties of the respective PutP derivatives were investigated. The secondary structure of the loop domain was assessed by cw EPR measurements. To address the dynamics of this domain during the alternating access mechanism of PutP, ligand-dependent changes in the mobility and polarity of the microenvironment of the spin label were determined. In order to integrate the observed ligand effects on the loop domain into the transport cycle the cw EPR analysis of eL4 was complemented with intramolecular distance measurements using four-pulse double electron-electron resonance spectroscopy.

## 1.9 References

- Abramson, J., I. Smirnova, V. Kasho, G. Verner, H. R. Kaback & S. Iwata, (2003) Structure and mechanism of the lactose permease of *Escherichia coli*. *Science* **301**: 610-615.
- Abramson, J. & E. M. Wright, (2009) Structure and function of Na(+)-symporters with inverted repeats. *Curr Opin Struct Biol* **19**: 425-432.
- Baltscheffsky, M., A. Schultz & H. Baltscheffsky, (1999) H<sup>+</sup>-proton-pumping inorganic pyrophosphatase: a tightly membrane-bound family. *FEBS Lett* **452**: 121-127.
- Bayer, A. S., S. N. Coulter, C. K. Stover & W. R. Schwan, (1999) Impact of the high-affinity proline permease gene (*putP*) on the virulence of *Staphylococcus aureus* in experimental endocarditis. *Infect Immun* **67**: 740-744.
- Boudker, O. & G. Verdon, (2010) Structural perspectives on secondary active transporters. *Trends Pharmacol Sci* **31**: 418-426.
- Boyer, P. D., (1993) The binding change mechanism for ATP synthase--some probabilities and possibilities. *Biochim Biophys Acta* **1140**: 215-250.

- Boyer, P. D., (1997) The ATP synthase--a splendid molecular machine. *Annu Rev Biochem* **66**: 717-749.
- Brown, E. D. & J. M. Wood, (1992) Redesigned purification yields a fully functional PutA protein dimer from *Escherichia coli*. *The Journal of biological chemistry* **267**: 13086-13092.
- Caplan, D. A., J. O. Subbotina & S. Y. Noskov, (2008) Molecular mechanism of ion-ion and ion-substrate coupling in the Na<sup>+</sup>-dependent leucine transporter LeuT. *Biophys J* **95**: 4613-4621.
- Catterall, W. A., (2010) Ion channel voltage sensors: structure, function, and pathophysiology. *Neuron* **67**: 915-928.
- Chen, C. C. & T. H. Wilson, (1986) Solubilization and functional reconstitution of the proline transport system of *Escherichia coli*. *The Journal of biological chemistry* **261**: 2599-2604.
- Cheng, J., A. A. Guffanti & T. A. Krulwich, (1997) A two-gene ABC-type transport system that extrudes Na<sup>+</sup> in *Bacillus subtilis* is induced by ethanol or protonophore. *Mol Microbiol* **23**: 1107-1120.
- Claxton, D. P., M. Quick, L. Shi, F. D. de Carvalho, H. Weinstein, J. A. Javitch & H. S. McHaourab, (2010) Ion/substrate-dependent conformational dynamics of a bacterial homolog of neurotransmitter:sodium symporters. *Nat Struct Mol Biol* **17**: 822-829.
- Corringer, P. J., M. Baaden, N. Bocquet, M. Delarue, V. Dufresne, H. Nury, M. Prevost & C. Van Renterghem, (2010) Atomic structure and dynamics of pentameric ligand-gated ion channels: new insight from bacterial homologues. *J Physiol* **588**: 565-572.
- Crisman, T. J., S. Qu, B. I. Kanner & L. R. Forrest, (2009) Inward-facing conformation of glutamate transporters as revealed by their inverted-topology structural repeats. *Proceedings of the National Academy of Sciences of the United States of America* **106**: 20752-20757.
- Culham, D. E., B. Lasby, A. G. Marangoni, J. L. Milner, B. A. Steer, R. W. van Nues & J. M. Wood, (1993) Isolation and sequencing of *Escherichia coli* gene proP reveals unusual structural features of the osmoregulatory proline/betaine transporter, ProP. *Journal of molecular biology* **229**: 268-276.
- Dattananda, C. S. & J. Gowrishankar, (1989) Osmoregulation in *Escherichia coli*: complementation analysis and gene-protein relationships in the proU locus. *Journal of bacteriology* **171**: 1915-1922.
- De la Vieja, A., M. D. Reed, C. S. Ginter & N. Carrasco, (2007) Amino acid residues in transmembrane segment IX of the Na<sup>+</sup>/I<sup>-</sup> symporter play a role in its Na<sup>+</sup> dependence and are critical for transport activity. *The Journal of biological chemistry* **282**: 25290-25298.

- Deckert, G., P. V. Warren, T. Gaasterland, W. G. Young, A. L. Lenox, D. E. Graham, R. Overbeek, M. A. Snead, M. Keller, M. Aujay, R. Huber, R. A. Feldman, J. M. Short, G. J. Olsen & R. V. Swanson, (1998) The complete genome of the hyperthermophilic bacterium *Aquifex aeolicus*. *Nature* **392**: 353-358.
- Dimroth, P., (1980) A new sodium-transport system energized by the decarboxylation of oxaloacetate. *FEBS Lett* **122**: 234-236.
- Dohan, O., A. De la Vieja, V. Paroder, C. Riedel, M. Artani, M. Reed, C. S. Ginter & N. Carrasco, (2003) The sodium/iodide Symporter (NIS): characterization, regulation, and medical significance. *Endocr Rev* **24**: 48-77.
- Eicher, T., L. Brandstatter & K. M. Pos, (2009) Structural and functional aspects of the multidrug efflux pump AcrB. *Biol Chem* **390**: 693-699.
- Eulenburg, V. & J. Gomeza, (2010) Neurotransmitter transporters expressed in glial cells as regulators of synapse function. *Brain Res Rev* **63**: 103-112.
- Faham, S., A. Watanabe, G. M. Besserer, D. Cascio, A. Specht, B. A. Hirayama, E. M. Wright & J. Abramson, (2008) The crystal structure of a sodium galactose transporter reveals mechanistic insights into Na<sup>+</sup>/sugar symport. *Science* **321**: 810-814.
- Fang, Y., H. Jayaram, T. Shane, L. Kolmakova-Partensky, F. Wu, C. Williams, Y. Xiong & C. Miller, (2009) Structure of a prokaryotic virtual proton pump at 3.2 Å resolution. *Nature* **460**: 1040-1043.
- Feniouk, B. A., T. Suzuki & M. Yoshida, (2007) Regulatory interplay between proton motive force, ADP, phosphate, and subunit epsilon in bacterial ATP synthase. *J Biol Chem* **282**: 764-772.
- Forrest, L. R., R. Kramer & C. Ziegler, (2011) The structural basis of secondary active transport mechanisms. *Biochim Biophys Acta* **1807**: 167-188.
- Forrest, L. R., Y. W. Zhang, M. T. Jacobs, J. Gesmonde, L. Xie, B. H. Honig & G. Rudnick, (2008) Mechanism for alternating access in neurotransmitter transporters. *Proceedings of the National Academy of Sciences of the United States of America* **105**: 10338-10343.
- Gao, X., F. Lu, L. Zhou, S. Dang, L. Sun, X. Li, J. Wang & Y. Shi, (2009) Structure and mechanism of an amino acid antiporter. *Science* **324**: 1565-1568.
- Gottesman, M. M. & S. V. Ambudkar, (2001) Overview: ABC transporters and human disease. *J Bioenerg Biomembr* **33**: 453-458.
- Gottschalk, G. & R. K. Thauer, (2001) The Na<sup>(+)</sup>-translocating methyltransferase complex from methanogenic archaea. *Biochim Biophys Acta* **1505**: 28-36.
- Guan, L. & H. R. Kaback, (2006) Lessons from lactose permease. *Annual review of biophysics and biomolecular structure* **35**: 67-91.

- Hanada, K., I. Yamato & Y. Anraku, (1988) Purification and reconstitution of Escherichia coli proline carrier using a site specifically cleavable fusion protein. *The Journal of biological chemistry* **263**: 7181-7185.
- Hediger, M. A., M. F. Romero, J. B. Peng, A. Rolfs, H. Takanaga & E. A. Bruford, (2004) The ABCs of solute carriers: physiological, pathological and therapeutic implications of human membrane transport proteins Introduction. *Pflugers Arch* **447**: 465-468.
- Hilger, D., M. Bohm, A. Hackmann & H. Jung, (2008) Role of Ser-340 and Thr-341 in transmembrane domain IX of the Na<sup>+</sup>/proline transporter PutP of Escherichia coli in ligand binding and transport. *J Biol Chem* **283**: 4921-4929.
- Hilger, D., Y. Polyhach, H. Jung & G. Jeschke, (2009) Backbone structure of transmembrane domain IX of the Na<sup>+</sup>/proline transporter PutP of Escherichia coli. *Biophys J* **96**: 217-225.
- Hollenstein, K., R. J. Dawson & K. P. Locher, (2007) Structure and mechanism of ABC transporter proteins. *Curr Opin Struct Biol* **17**: 412-418.
- Hunte, C., E. Screpanti, M. Venturi, A. Rimon, E. Padan & H. Michel, (2005) Structure of a Na<sup>+</sup>/H<sup>+</sup> antiporter and insights into mechanism of action and regulation by pH. *Nature* **435**: 1197-1202.
- Jardetzky, O., (1966) Simple allosteric model for membrane pumps. *Nature* **211**: 969-970.
- Jeschke, G., C. Wegener, M. Nietschke, H. Jung & H. J. Steinhoff, (2004) Interresidual distance determination by four-pulse double electron-electron resonance in an integral membrane protein: the Na<sup>+</sup>/proline transporter PutP of Escherichia coli. *Biophys J* **86**: 2551-2557.
- Jung, H., (1998) Topology and function of the Na<sup>+</sup>/proline transporter of Escherichia coli, a member of the Na<sup>+</sup>/solute cotransporter family. *Biochim Biophys Acta* **1365**: 60-64.
- Jung, H., (2002) The sodium/substrate symporter family: structural and functional features. *FEBS letters* **529**: 73-77.
- Jung, H., R. Rubenhagen, S. Tebbe, K. Leifker, N. Tholema, M. Quick & R. Schmid, (1998a) Topology of the Na<sup>+</sup>/proline transporter of Escherichia coli. *J Biol Chem* **273**: 26400-26407.
- Jung, H., S. Tebbe, R. Schmid & K. Jung, (1998b) Unidirectional reconstitution and characterization of purified Na<sup>+</sup>/proline transporter of Escherichia coli. *Biochemistry* **37**: 11083-11088.
- Kavermann, H., B. P. Burns, K. Angermuller, S. Odenbreit, W. Fischer, K. Melchers & R. Haas, (2003) Identification and characterization of Helicobacter pylori genes essential for gastric colonization. *J Exp Med* **197**: 813-822.
- Konings, W. N., (2006) Microbial transport: adaptations to natural environments. *Antonie Van Leeuwenhoek* **90**: 325-342.

- Konings, W. N., S. V. Albers, S. Koning & A. J. Driessen, (2002) The cell membrane plays a crucial role in survival of bacteria and archaea in extreme environments. *Antonie Van Leeuwenhoek* **81**: 61-72.
- Krishnamurthy, H., C. L. Piscitelli & E. Gouaux, (2009) Unlocking the molecular secrets of sodium-coupled transporters. *Nature* **459**: 347-355.
- Kung, C., B. Martinac & S. Sukharev, (2010) Mechanosensitive channels in microbes. *Annu Rev Microbiol* **64**: 313-329.
- Lengeler, J. W., G. Drews & H. G. Schlegel, (1999) *Biology of the Prokaryotes*, p. 984. Thieme, Stuttgart.
- Lolkema, J. S., A. Dobrowolski & D. J. Slotboom, (2008) Evolution of antiparallel two-domain membrane proteins: tracing multiple gene duplication events in the DUF606 family. *Journal of molecular biology* **378**: 596-606.
- Lolkema, J. S. & D. J. Slotboom, (1998) Estimation of structural similarity of membrane proteins by hydropathy profile alignment. *Molecular membrane biology* **15**: 33-42.
- Lu, M. & D. Fu, (2007) Structure of the zinc transporter YjiP. *Science* **317**: 1746-1748.
- Luoto, H. H., G. A. Belogurov, A. A. Baykov, R. Lahti & A. M. Malinen, (2011) Na<sup>+</sup>-translocating Membrane Pyrophosphatases Are Widespread in the Microbial World and Evolutionarily Precede H<sup>+</sup>-translocating Pyrophosphatases. *J Biol Chem* **286**: 21633-21642.
- Mitchell, P., (1957) A general theory of membrane transport from studies of bacteria. *Nature* **180**: 134-136.
- Mitchell, P., (1966) Chemiosmotic coupling in oxidative and photosynthetic phosphorylation. *Biol Rev Camb Philos Soc* **41**: 445-502.
- Mitsui, T. & H. Ohshima, (2005) Proposed model for the flagellar rotary motor. *Colloids Surf B Biointerfaces* **46**: 32-44.
- Mulkidjanian, A. Y., P. Dibrov & M. Y. Galperin, (2008a) The past and present of sodium energetics: may the sodium-motive force be with you. *Biochim Biophys Acta* **1777**: 985-992.
- Mulkidjanian, A. Y., M. Y. Galperin, K. S. Makarova, Y. I. Wolf & E. V. Koonin, (2008b) Evolutionary primacy of sodium bioenergetics. *Biol Direct* **3**: 13.
- Nakao, T., I. Yamato & Y. Anraku, (1987) Nucleotide sequence of putP, the proline carrier gene of Escherichia coli K12. *Mol Gen Genet* **208**: 70-75.
- Ostrovsky de Spicer, P. & S. Maloy, (1993) PutA protein, a membrane-associated flavin dehydrogenase, acts as a redox-dependent transcriptional regulator. *Proceedings of the National Academy of Sciences of the United States of America* **90**: 4295-4298.

- Padan, E., E. Bibi, M. Ito & T. A. Krulwich, (2005) Alkaline pH homeostasis in bacteria: new insights. *Biochim Biophys Acta* **1717**: 67-88.
- Pardridge, W. M., (2005) Molecular biology of the blood-brain barrier. *Mol Biotechnol* **30**: 57-70.
- Paulsen, I. T., L. Nguyen, M. K. Sliwinski, R. Rabus & M. H. Saier, Jr., (2000) Microbial genome analyses: comparative transport capabilities in eighteen prokaryotes. *J Mol Biol* **301**: 75-100.
- Pettersen, E. F., T. D. Goddard, C. C. Huang, G. S. Couch, D. M. Greenblatt, E. C. Meng & T. E. Ferrin, (2004) UCSF Chimera--a visualization system for exploratory research and analysis. *J Comput Chem* **25**: 1605-1612.
- Pirch, T., S. Landmeier & H. Jung, (2003) Transmembrane domain II of the Na<sup>+</sup>/proline transporter PutP of Escherichia coli forms part of a conformationally flexible, cytoplasmic exposed aqueous cavity within the membrane. *J Biol Chem* **278**: 42942-42949.
- Pirch, T., M. Quick, M. Nietschke, M. Langkamp & H. Jung, (2002) Sites important for Na<sup>+</sup> and substrate binding in the Na<sup>+</sup>/proline transporter of Escherichia coli, a member of the Na<sup>+</sup>/solute symporter family. *J Biol Chem* **277**: 8790-8796.
- Quick, M. & H. Jung, (1997) Aspartate 55 in the Na<sup>+</sup>/proline permease of Escherichia coli is essential for Na<sup>+</sup>-coupled proline uptake. *Biochemistry* **36**: 4631-4636.
- Quick, M. & H. Jung, (1998) A conserved aspartate residue, Asp187, is important for Na<sup>+</sup>-dependent proline binding and transport by the Na<sup>+</sup>/proline transporter of Escherichia coli. *Biochemistry* **37**: 13800-13806.
- Quick, M., S. Stolting & H. Jung, (1999) Role of conserved Arg40 and Arg117 in the Na<sup>+</sup>/proline transporter of Escherichia coli. *Biochemistry* **38**: 13523-13529.
- Quick, M., S. Tebbe & H. Jung, (1996) Ser57 in the Na<sup>+</sup>/proline permease of Escherichia coli is critical for high-affinity proline uptake. *Eur J Biochem* **239**: 732-736.
- Radestock, S. & L. R. Forrest, (2011) The alternating-access mechanism of MFS transporters arises from inverted-topology repeats. *Journal of molecular biology* **407**: 698-715.
- Ressl, S., A. C. Terwisscha van Scheltinga, C. Vonrhein, V. Ott & C. Ziegler, (2009) Molecular basis of transport and regulation in the Na<sup>(+)</sup>/betaine symporter BetP. *Nature* **458**: 47-52.
- Reyes, N., C. Ginter & O. Boudker, (2009) Transport mechanism of a bacterial homologue of glutamate transporters. *Nature* **462**: 880-885.
- Rudnick, G., (2006) Serotonin transporters--structure and function. *The Journal of membrane biology* **213**: 101-110.

- Saier, M. H., R. N. Hvorup & R. D. Barabote, (2005) Evolution of the bacterial phosphotransferase system: from carriers and enzymes to group translocators. *Biochem Soc Trans* **33**: 220-224.
- Saier, M. H., Jr., C. V. Tran & R. D. Barabote, (2006) TCDB: the Transporter Classification Database for membrane transport protein analyses and information. *Nucleic acids research* **34**: D181-186.
- Schultz, B. E. & S. I. Chan, (2001) Structures and proton-pumping strategies of mitochondrial respiratory enzymes. *Annu Rev Biophys Biomol Struct* **30**: 23-65.
- Schulze, S., S. Koster, U. Geldmacher, A. C. Terwisscha van Scheltinga & W. Kuhlbrandt, (2010) Structural basis of Na(+)-independent and cooperative substrate/product antiport in CaiT. *Nature* **467**: 233-236.
- Screpanti, E. & C. Hunte, (2007) Discontinuous membrane helices in transport proteins and their correlation with function. *J Struct Biol* **159**: 261-267.
- Shaffer, P. L., A. Goehring, A. Shankaranarayanan & E. Gouaux, (2009) Structure and mechanism of a Na<sup>+</sup>-independent amino acid transporter. *Science* **325**: 1010-1014.
- Shi, L., M. Quick, Y. Zhao, H. Weinstein & J. A. Javitch, (2008) The mechanism of a neurotransmitter:sodium symporter--inward release of Na<sup>+</sup> and substrate is triggered by substrate in a second binding site. *Mol Cell* **30**: 667-677.
- Shimamura, T., S. Weyand, O. Beckstein, N. G. Rutherford, J. M. Hadden, D. Sharples, M. S. Sansom, S. Iwata, P. J. Henderson & A. D. Cameron, (2010) Molecular basis of alternating access membrane transport by the sodium-hydantoin transporter Mhp1. *Science* **328**: 470-473.
- Simon, J., R. J. van Spanning & D. J. Richardson, (2008) The organisation of proton motive and non-proton motive redox loops in prokaryotic respiratory systems. *Biochim Biophys Acta* **1777**: 1480-1490.
- Singh, S. K., C. L. Piscitelli, A. Yamashita & E. Gouaux, (2008) A competitive inhibitor traps LeuT in an open-to-out conformation. *Science* **322**: 1655-1661.
- Singh, S. K., A. Yamashita & E. Gouaux, (2007) Antidepressant binding site in a bacterial homologue of neurotransmitter transporters. *Nature* **448**: 952-956.
- Skulachev, V. P., (1988) *Membrane Bioenergetics*, p. 442. Springer-Verlag, Berlin.
- Skulachev, V. P., (1991) Chemiosmotic systems in bioenergetics: H(+)-cycles and Na(+)-cycles. *Biosci Rep* **11**: 387-441; discussion 441-384.
- Speelmans, G., B. Poolman & W. N. Konings, (1993) Amino acid transport in the thermophilic anaerobe *Clostridium fervidus* is driven by an electrochemical sodium gradient. *J Bacteriol* **175**: 2060-2066.

- Steiner-Mordoch, S., M. Soskine, D. Solomon, D. Rotem, A. Gold, M. Yechieli, Y. Adam & S. Schuldiner, (2008) Parallel topology of genetically fused EmrE homodimers. *The EMBO journal* **27**: 17-26.
- Suzuki, Y., S. Ueno, R. Ohnuma & N. Koyama, (2005) Cloning, sequencing and functional expression in *Escherichia coli* of the gene for a P-type Na(+)-ATPase of a facultatively anaerobic alkaliphile, *Exiguobacterium aurantiacum*. *Biochim Biophys Acta* **1727**: 162-168.
- Takami, H., K. Nakasone, Y. Takaki, G. Maeno, R. Sasaki, N. Masui, F. Fuji, C. Hirama, Y. Nakamura, N. Ogasawara, S. Kuhara & K. Horikoshi, (2000) Complete genome sequence of the alkaliphilic bacterium *Bacillus halodurans* and genomic sequence comparison with *Bacillus subtilis*. *Nucleic Acids Res* **28**: 4317-4331.
- Tetsch, L., C. Koller, I. Haneburger & K. Jung, (2008) The membrane-integrated transcriptional activator CadC of *Escherichia coli* senses lysine indirectly via the interaction with the lysine permease LysP. *Mol Microbiol* **67**: 570-583.
- Tusnady, G. E., Z. Dosztanyi & I. Simon, (2004) Transmembrane proteins in the Protein Data Bank: identification and classification. *Bioinformatics* **20**: 2964-2972.
- van de Vossenberg, J. L., T. Ubbink-Kok, M. G. Elferink, A. J. Driessen & W. N. Konings, (1995) Ion permeability of the cytoplasmic membrane limits the maximum growth temperature of bacteria and archaea. *Mol Microbiol* **18**: 925-932.
- Wallin, E. & G. von Heijne, (1998) Genome-wide analysis of integral membrane proteins from eubacterial, archaean, and eukaryotic organisms. *Protein science : a publication of the Protein Society* **7**: 1029-1038.
- Wegener, C., S. Tebbe, H. J. Steinhoff & H. Jung, (2000) Spin labeling analysis of structure and dynamics of the Na(+)/proline transporter of *Escherichia coli*. *Biochemistry* **39**: 4831-4837.
- Weisser, P., R. Kramer, H. Sahm & G. A. Sprenger, (1995) Functional expression of the glucose transporter of *Zymomonas mobilis* leads to restoration of glucose and fructose uptake in *Escherichia coli* mutants and provides evidence for its facilitator action. *J Bacteriol* **177**: 3351-3354.
- Weyand, S., T. Shimamura, S. Yajima, S. Suzuki, O. Mirza, K. Krusong, E. P. Carpenter, N. G. Rutherford, J. M. Hadden, J. O'Reilly, P. Ma, M. Saidijam, S. G. Patching, R. J. Hope, H. T. Norbertczak, P. C. Roach, S. Iwata, P. J. Henderson & A. D. Cameron, (2008) Structure and molecular mechanism of a nucleobase-cation-symport-1 family transporter. *Science* **322**: 709-713.
- White, S., (2011) Membrane Proteins of Known Structure. In. Irvine, USA, pp.
- Winkelmann, G., (2001) Microbial Transport Systems. In. Weinheim: Wiley-VCH Verlag GmbH, pp. 300.
- Wood, J. M., (1981) Genetics of L-proline utilization in *Escherichia coli*. *Journal of bacteriology* **146**: 895-901.

- Wright, E. M., B. A. Hirayama & D. F. Loo, (2007) Active sugar transport in health and disease. *J Intern Med* **261**: 32-43.
- Wright, E. M., D. D. Loo & B. A. Hirayama, (2011) Biology of human sodium glucose transporters. *Physiol Rev* **91**: 733-794.
- Wright, E. M. & E. Turk, (2004) The sodium/glucose cotransport family SLC5. *Pflugers Arch* **447**: 510-518.
- Wright, E. M., E. Turk, K. Hager, L. Lescale-Matys, B. Hirayama, S. Supplisson & D. D. Loo, (1992) The Na<sup>+</sup>/glucose cotransporter (SGLT1). *Acta Physiol Scand Suppl* **607**: 201-207.
- Yamashita, A., S. K. Singh, T. Kawate, Y. Jin & E. Gouaux, (2005) Crystal structure of a bacterial homologue of Na<sup>+</sup>/Cl<sup>-</sup>-dependent neurotransmitter transporters. *Nature* **437**: 215-223.
- Yamato, I., (1992) Ordered binding model as a general mechanistic mechanism for secondary active transport systems. *FEBS letters* **298**: 1-5.
- Yamato, I. & Y. Anraku, (1993) Alkali Cation Transport Systems in Prokaryotes. In: Alkali Cation Transport Systems in Prokaryotes. E. P. Bakker (ed). Boca Raton, FL: CRC-Press, pp. 464.
- Zhao, Y., D. Terry, L. Shi, H. Weinstein, S. C. Blanchard & J. A. Javitch, (2010) Single-molecule dynamics of gating in a neurotransmitter transporter homologue. *Nature* **465**: 188-193.
- Zhao, Y., D. S. Terry, L. Shi, M. Quick, H. Weinstein, S. C. Blanchard & J. A. Javitch, (2011) Substrate-modulated gating dynamics in a Na<sup>+</sup>-coupled neurotransmitter transporter homologue. *Nature* **474**: 109-113.
- Zhou, A., A. Wozniak, K. Meyer-Lipp, M. Nietschke, H. Jung & K. Fendler, (2004) Charge translocation during cosubstrate binding in the Na<sup>+</sup>/proline transporter of E.coli. *J Mol Biol* **343**: 931-942.

## **2 FUNCTION OF TRANSMEMBRANE DOMAIN IX IN THE NA<sup>+</sup>/PROLINE TRANSPORTER PUTP**

## Function of Transmembrane Domain IX in the Na<sup>+</sup>/Proline Transporter PutP

Michael Raba<sup>1</sup>, Tobias Baumgartner<sup>1</sup>, Daniel Hilger<sup>1,2</sup>,  
Katrin Klempahn<sup>3</sup>, Tobias Härtel<sup>1</sup>, Kirsten Jung<sup>1,2</sup>  
and Heinrich Jung<sup>1,3\*</sup>

<sup>1</sup>LMU Munich, Department  
Biology I, Microbiology,  
Grosshaderner Strasse 2-4,  
D-82152 Planegg-Martinsried,  
Germany

<sup>2</sup>Munich Center for Integrated  
Protein Science (CiPS<sup>M</sup>),  
Munich, Germany

<sup>3</sup>Department of Microbiology,  
University of Osnabrück,  
D-49069 Osnabrück, Germany

Received 25 June 2008;  
received in revised form  
23 July 2008;  
accepted 24 July 2008  
Available online  
30 July 2008

Selected residues of transmembrane domain (TM) IX were previously shown to play key roles in ligand binding and transport in members of the Na<sup>+</sup>/solute symporter family. Using the Na<sup>+</sup>/proline transporter PutP as a model, a complete Cys scanning mutagenesis of TM IX (positions 324 to 351) was performed here to further investigate the functional significance of the domain. G328, S332, Q345, and L346 were newly identified as important for Na<sup>+</sup>-coupled proline uptake. Placement of Cys at one of these positions altered  $K_{m(\text{pro})}$  (S332C and L346C, 3- and 21-fold decreased, respectively; Q345C, 38-fold increased),  $K_{0.5(\text{Na}^+)}$  (S332C, 13-fold decreased; Q345C, 19-fold increased), and/or  $V_{\text{max}}$  [G328C, S332C, Q345C, and L346C, 3-, 22-, 2-, and 8-fold decreased compared to PutP(wild type), respectively]. Membrane-permeant *N*-ethylmaleimide inhibited proline uptake into cells containing PutP with Cys at distinct positions in the middle (T341C) and cytoplasmic half of TM IX (C344, L347C, V348C, and S351C) and had little or no effect on all other single Cys PutP variants. The inhibition pattern was in agreement with the pattern of labeling with fluorescein-5-maleimide. In addition, Cys placed into the cytoplasmic half of TM IX (C344, L347C, V348C, and S351C) was protected from fluorescein-5-maleimide labeling by proline while Na<sup>+</sup> alone had no effect. Membrane-impermeant methanethiosulfonate ethyltrimethylammonium modified Cys in the middle (A337C and T341C) and periplasmic half (L331C) but not in the cytoplasmic half of TM IX in intact cells. Furthermore, Cys at the latter positions was partially protected by Na<sup>+</sup> but not by proline. Based on these results, a model is discussed according to which residues of TM IX participate in the formation of ligand-sensitive, hydrophilic cavities in the protein that may reconstitute part of the Na<sup>+</sup> and/or proline translocation pathway of PutP.

© 2008 Elsevier Ltd. All rights reserved.

**Keywords:** secondary transport; PutP; SSSF; sodium-coupled symport; membrane transport

**Edited by I. B. Holland**

\*Corresponding author. LMU Munich, Department Biology I, Microbiology, Grosshaderner Strasse 2-4, D-82152 Planegg-Martinsried, Germany. E-mail address: [hjung@lmu.de](mailto:hjung@lmu.de).

Present addresses: K. Klempahn, Department of Neurobiology, University of Osnabrück, D-49069 Osnabrück, Germany; T. Härtel, Max von Pettenkofer Institute for Hygiene and Medical Microbiology, 80336 Munich, Germany.

Abbreviations used: AU, arbitrary units; BSA, bovine serum albumin; FM, fluorescein-5-maleimide; MalNET, *N*-ethylmaleimide; MTSET, methanethiosulfonate ethyltri-methylammonium; Mes, 4-morpholineethanesulfonic acid; PutP( $\Delta$ Cys), engineered transporter devoid of all five native cysteine residues; smf, sodium motive force; SSSF, Na<sup>+</sup>/solute symporter family; TM, transmembrane domain.

## Introduction

The Na<sup>+</sup>/solute symporter family (SSSF) (TC 2A.21, SLC5) is an evolutionary related collection of secondary transporters found in all three kingdoms of life.<sup>1-3</sup> Prokaryotic members of the family utilize a sodium motive force (smf) to specifically accumulate, for example, proline (PutP, OpuE), galactose and glucose (SGLT), pantothenate (PanF), or phenylacetate (Ppa) in cells.<sup>4</sup> Most of these transporters (PutP, SGLT, and Ppa) feed catabolic pathways or play a role in cell adaptation to osmotic stress conditions (OpuE). PanF scavenges extracellular pantothenate for coenzyme A biosynthesis in the cells.<sup>5</sup> In eukaryotes, SSSF members are responsible for the transport of, for example, monosaccharides (SGLT), myoinositol (SMIT), vitamins (SMVT), iodide (NIS), and urea (DUR).<sup>6-8</sup> So far, missing information on the three-dimensional structure of SSSF members limits access to the molecular mechanism of Na<sup>+</sup>-coupled substrate transport.

We use PutP of *Escherichia coli* as a model to obtain insights into structure and molecular mechanisms of function of SSSF members. Genetic, protein chemical, and spectroscopic analyses suggest a secondary-structure model according to which PutP contains 13 transmembrane domains (TMs) with the N terminus located on the periplasmic side of the membrane and the C terminus facing the cytoplasm (Fig. 1).<sup>9,10</sup> Furthermore, Cys accessibility experiments propose a participation of TM II in the formation of a hydrophilic cavity in the transporter and implicate the TM in ligand-induced conformational alterations.<sup>15</sup> In addition, D55 in TM II is essential for function and proposed to participate in binding of the coupling ion.<sup>11</sup> S57 and G58 of the

same TM are important for Na<sup>+</sup> and proline binding, suggesting partly overlapping binding sites for both ligands.<sup>12,13</sup> More recent Cys cross-linking data propose that TM II is close to TM IX in the tertiary structure of the protein. In fact, also, the latter TM contains residues (S340 and T341) that are required for high-affinity Na<sup>+</sup> and proline binding.<sup>14</sup> Beside PutP, polar residues of TM IX were shown to be particularly crucial also for function of human NIS,<sup>17</sup> suggesting that this domain is of general significance for members of the SSSF.

To gain further insights into the role of TM IX, all amino acids of the domain of our model system PutP (P324 to S351) were individually replaced with Cys and the functional consequences were analyzed. Furthermore, accessibilities of Cys placed throughout TM IX to sulfhydryl reagents of various sizes and polarities were determined. Finally, the influence of ligands (Na<sup>+</sup>, proline) on the labeling reactions was investigated. The results led to a model according to which TM IX contributes to the formation of hydrophilic cavities in PutP, which may reconstitute part of a ligand translocation pathway of PutP.

## Results

### Cys scanning mutagenesis of TM IX

TM IX of PutP was subjected to Cys scanning mutagenesis in order to identify residues of particular structural and/or functional significance. For this purpose, each amino acid of TM IX (P324 to S351) was individually replaced with Cys in a functional PutP molecule devoid of all five native Cys residues [PutP( $\Delta$ Cys)]. A Western blot analysis revealed that

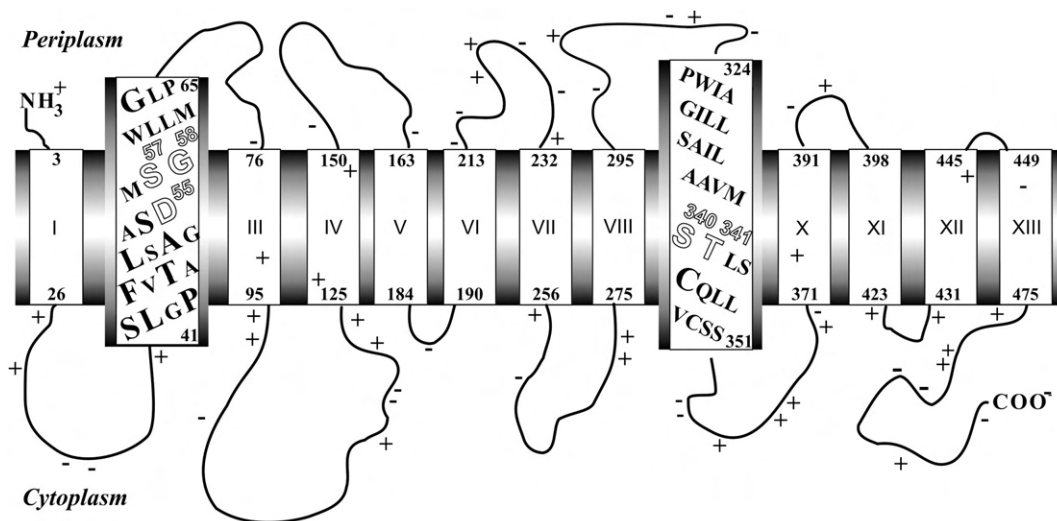


**Fig. 1.** Secondary-structure model of PutP of *E. coli* highlighting functional important residues. The model is based on a gene fusion approach, Cys accessibility analyses, site-directed spin labeling, and site-specific proteolysis.<sup>9,10</sup> Putative TMs are represented as rectangles and numbered with Roman numerals. Amino acid residues of TMs II and IX previously shown to be crucial for Na<sup>+</sup> and/or proline binding are indicated by open letters.<sup>11-14</sup> Residues of TM II proposed to line a ligand-sensitive hydrophilic cavity in the transporter are highlighted (enlarged letters).<sup>15</sup> In TM IX, only Cys344 (enlarged letter) is known so far to react with sulfhydryl reagents and is protected by substrate.<sup>16</sup> TMs II and IX are adjacent in the tertiary structure of the protein as shown by Cys cross-linking.<sup>14</sup>

these replacements resulted in amounts of transporter molecules in the membrane similar as observed for PutP( $\Delta$ Cys), indicating that possible differences in proline uptake kinetics cannot be attributed to different amounts of transporter molecules in the membrane (Fig. 2). Active transport was then measured under standard test conditions (70 mM Na<sup>+</sup>, 10  $\mu$ M proline) by using *E. coli* WG170 complemented with plasmid-encoded PutP variants. Under these conditions, PutP( $\Delta$ Cys) exhibited an initial rate of  $23 \pm 5$  nmol/min·mg [50% of PutP(wild type)] and a steady-state level of proline accumulation of  $24 \pm 3$  nmol/mg [100% of PutP(wild type)].

Initial analyses of rates and steady-state levels of proline accumulation newly identified G328, S332, Q345, and L346 as important for PutP function (Fig. 3). The most severe defect was detected for PutP( $\Delta$ Cys)-S332C [2.6% and 15.8% of the initial rate and steady-state level of proline accumulation of PutP( $\Delta$ Cys)]. Intermediate inhibitory effects [30–40% of the initial rate and 70–100% of steady-state level of proline accumulation of PutP( $\Delta$ Cys)] were observed for cells containing PutP( $\Delta$ Cys)-G328C, -Q345C, or -L346C. In contrast, cells with PutP( $\Delta$ Cys)-A337C or -C344 exhibited about twofold stimulated initial rates and unaltered steady-state levels of proline accumulation compared to PutP( $\Delta$ Cys). It should be noted that placement of Cys at position 344 [Ser in PutP( $\Delta$ Cys)] restored a native Cys residue. All remaining substitutions had only little or no impact on transport kinetics (Fig. 3).

### Effect of Cys replacements in TM IX of PutP(wild type) on transport kinetics

Substitutions in PutP( $\Delta$ Cys) causing alterations of transport were also analyzed in the wild-type background. Cys in place of G328, S332, Q345, and L346 reduced the initial rate of transport to 30%, 6%, 17%, and 28%, respectively, of the wild-type value and, in the case of the three latter substitutions, also led to reduced maximum levels of proline accumulation (19–56% of the wild-type value). In contrast, replacement of A337 increased the initial rate of transport by a factor of 1.8 with no significant effect on the steady-state level of accumulation (data not further illustrated). These results confirmed the observations made in the PutP( $\Delta$ Cys) background.

A more detailed kinetic analysis of the functional consequences of the Cys substitutions revealed diverse effects on Michaelis–Menten parameters (Table 1). Replacement of G328 by Cys

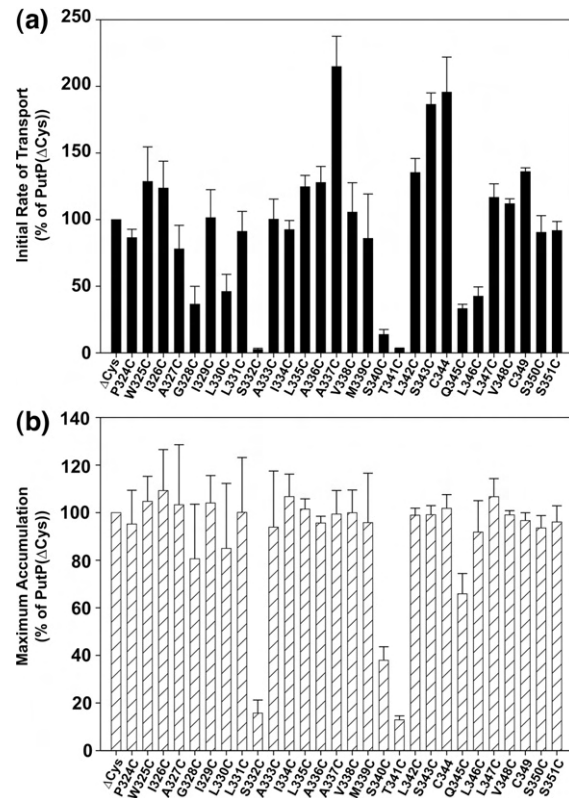


**Fig. 3.** Influence of amino acid replacements in TM IX on Na<sup>+</sup>-coupled proline uptake. Transport of L-[U-<sup>14</sup>C] proline (10  $\mu$ M final concentration) into cells of *E. coli* WG170 was assayed in the presence of 50 mM NaCl and 20 mM D-lactate (Na<sup>+</sup> salt) as electron donor at 25 °C under aerobic conditions using a rapid filtration method. (a) Initial rates of proline uptake. (b) Steady-state levels of proline accumulation. All values are expressed as percentage of the corresponding value of PutP( $\Delta$ Cys) (initial rate,  $23 \pm 5$  nmol/min·mg; steady-state level of proline accumulation,  $24 \pm 3$  nmol/mg). Standard deviations were calculated from a minimum of three independent experiments.

affected  $V_{\max}$  (3-fold decreased) and left  $K_{m(\text{pro})}$  and  $K_{0.5(\text{Na}^+)}$  almost unaltered compared to PutP(wild type). PutP-S332C and -L346C exhibited decreased  $K_{m(\text{pro})}$  (3- and 21-fold, respectively) and  $V_{\max}$  values (22- and 8-fold, respectively). While  $K_{0.5(\text{Na}^+)}$  of PutP-L346C was only slightly altered, the value could not be reliably determined for PutP-S332C due to the low transport activity (signal-to-noise ratio) in intact cells. Therefore, the analysis was performed with proteoliposomes containing the purified transporter in an inside–out orientation. Under these

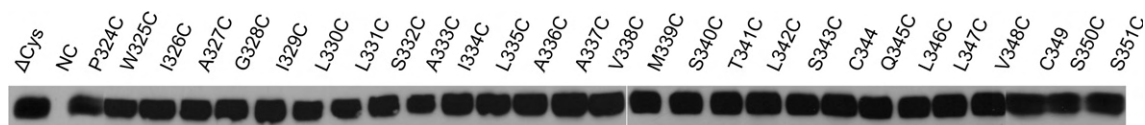


**Fig. 2.** Immunological detection of PutP containing replacements of amino acids in TM IX. Twenty-five micrograms of total membrane protein of each mutant was separated by 10% SDS-PAGE. Proteins were transferred onto a nitrocellulose membrane (0.45  $\mu$ m pore size) and probed with mouse anti-FLAG M2 monoclonal antibody linked to horseradish peroxidase. Detection was performed according to the enhanced chemiluminescence method. Cells transformed with plasmid pT7-5 without *putP* served as negative control (NC).

**Table 1.** Proline uptake kinetics of PutP bearing replacements of given amino acid residues

PutP	$K_{m(\text{pro})}$ ( $\mu\text{M}$ )	$V_{\text{max}}$ (nmol/min·mg of protein)	$K_{0.5(\text{Na}^+)}$ (mM)
Wild type	1.3±0.2	44.6±1.6	0.038±0.007 (0.7±0.09) <sup>a</sup>
G328C	1.5±0.5	16.7±1.0	0.018±0.004
S332C	0.4±0.3	2.1±0.2	n.s. <sup>b</sup> (0.055±0.014) <sup>b</sup>
A337C	1.7±0.5	72.5±3.8	0.117±0.025
Q345C	49.3±1.0	23.0±1.8	0.705±0.088
L346C	0.063±0.016	5.8±0.3	0.071±0.011

To determine  $K_{m(\text{pro})}$  and  $V_{\text{max}}$ , we measured initial rates of L-[U-<sup>14</sup>C]proline uptake by *E. coli* WG170 producing either PutP (wild type) or PutP with given replacements in the wild-type background in the presence of 50 mM NaCl and 20 mM D-lactate (Na<sup>+</sup> salt) at proline concentrations from 0.2 to 500  $\mu\text{M}$ . For determination of the ion-specific parameters [ $K_{0.5(\text{Na}^+)}$ ], transport of 10  $\mu\text{M}$  L-[U-<sup>14</sup>C]proline was measured in the presence of 0.005 to 250 mM NaCl at 25 °C. The resulting data were plotted according to Eadie-Hofstee.

<sup>a</sup> Values in parentheses were obtained with proteoliposomes containing the purified PutP variants.

<sup>b</sup> n.s., no stimulation of proline uptake into intact cells by increasing concentrations of Na<sup>+</sup>.

conditions, S332C exhibited a  $K_{0.5(\text{Na}^+)}$ , which was 13-fold reduced compared to the wild type in proteoliposomes (Table 1). In contrast to PutP-S332C and -L346C, placement of Cys at the position of Q345 increased  $K_{m(\text{pro})}$  and  $K_{0.5(\text{Na}^+)}$  38- and 19-fold, respectively, compared to PutP(wild type).  $V_{\text{max}}$  was about 2-fold reduced (Table 1). The latter results fit to previous analyses of substitutions for Ser340 and Thr341, albeit the impact of alterations at the latter positions on  $K_{m(\text{pro})}$  and  $K_{0.5(\text{Na}^+)}$  was even stronger than that of the Gln345 replacement.<sup>14</sup> Finally, placement of Cys at the position of A337, which was shown to stimulate proline uptake in the initial analyses, slightly increased  $K_{0.5(\text{Na}^+)}$  and  $V_{\text{max}}$  (3- and 1.6-fold) and left  $K_{m(\text{pro})}$  unaltered (Table 1).

### Influence of Cys modification on transport activity

Site-directed sulfhydryl modification of single Cys proteins *in situ* has been particularly useful for studying both static and dynamic features of transporters.<sup>18–20</sup> Here, we used the method to probe a potential participation of TM IX of PutP in the formation of a hydrophilic cavity in the transporter. In a first approach, accessibility of Cys placed throughout TM IX to membrane-permeant *N*-ethylmaleimide (MalNET) and membrane-impermeant methanethiosulfonate ethyltrimethylammonium (MTSET) was analyzed via the impact of the reagents on proline uptake into intact cells. Only freshly prepared cells were used for transport and additional energization by D-lactate was omitted to minimize indirect inhibitory effects (e.g., caused by reaction of MalNET or MTSET with components of the respiratory chain). In this way, MalNET- or MTSET-treated cells containing PutP( $\Delta\text{Cys}$ ) maintained a minimum of 80% and 96%, respectively, of

the activity of untreated cells. PutP( $\Delta\text{Cys}$ ) was not chemically modified as demonstrated below and elsewhere.<sup>14</sup>

MalNET avidly reacted with Cys at distinct positions in the cytoplasmic half of TM IX (C344, L347C, and S351C) as indicated by the highly reduced activities of the respective MalNET-treated cells (8% or less remaining activity compared to untreated cells) (Figs. 4a and 5). Intermediate inhibitory effects of MalNET were observed with cells containing PutP( $\Delta\text{Cys}$ )-T341C or -V348C (40% and 48% remaining activity, respectively). The activity of all other single Cys PutP variants was not or only slightly altered by MalNET treatment. Here, either Cys was not accessible to MalNET or labeling had only a minor impact on transport activity. Since alkylation reagents are known to react with sulfhydryl groups in polar but not in apolar environments,<sup>21,22</sup> the observed MalNET inhibition pattern suggested that T341, C344, L347, V348, and S351 are in contact with a polar (hydrophilic) environment.

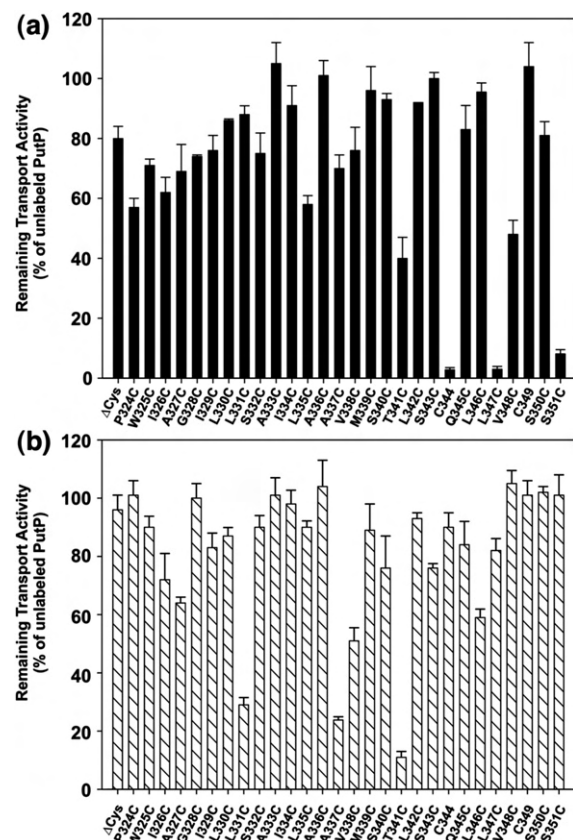
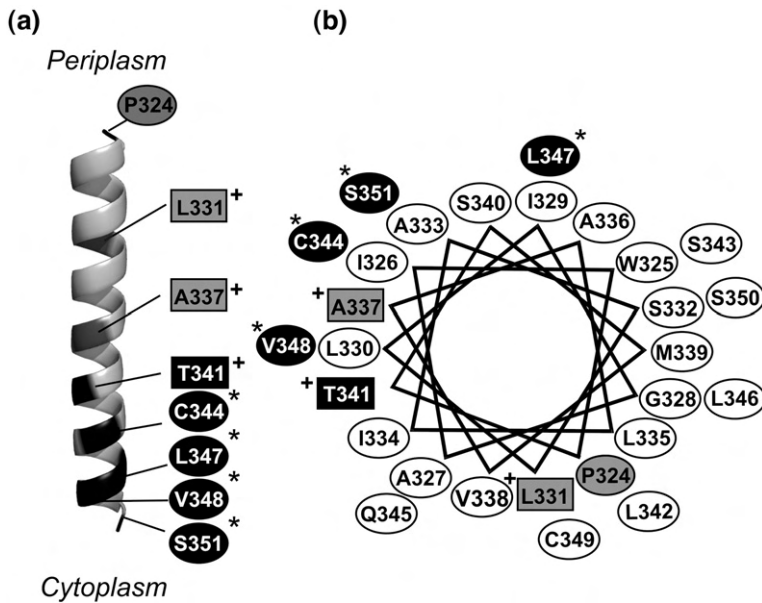


**Fig. 4.** Influence of sulfhydryl reagents on proline uptake into cells containing single Cys PutP variants of TM IX. Cells were incubated with 2 mM sulfhydryl reagent (MalNET and MTSET) at room temperature for 15 min. The reaction was stopped by dilution with 100 mM Tris/Mes buffer, pH 6.0, containing 0.1% BSA. Cells were washed and resuspended in the same buffer without BSA, and transport was analyzed as described in the legend to Fig. 3. Activities of MalNET-treated (a) or MTSET-treated (b) cells are presented as percentage of the activity of the respective unlabeled PutP variant. Standard deviations were calculated from a minimum of three measurements.

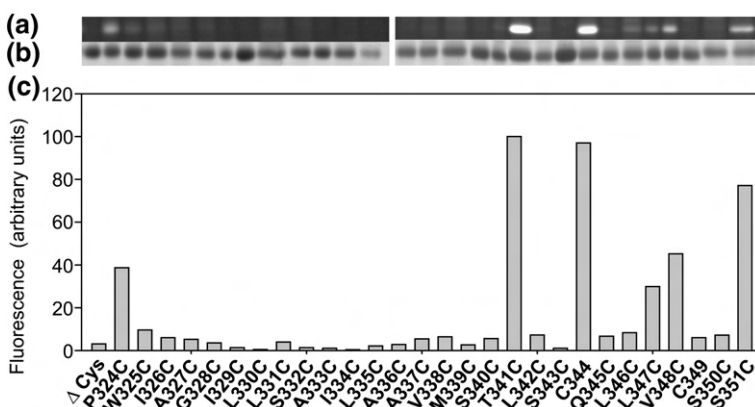


The inhibition pattern of membrane-impermeant, positively charged MTSET differed significantly from the MalNet inhibition pattern (Figs. 4b and 5). MTSET inhibited transport of single Cys PutP variants when Cys was placed in the periplasmic half (L331C, 29% remaining activity) or the middle of TM IX (A337C, 23%; T341C, 11% remaining activity). Also, PutP( $\Delta$ Cys)-A327C and -V338C were inhibited by MTSET albeit to a significantly lesser extent (64% and 51% remaining activity, respectively). Contrary to MalNet, MTSET did not inhibit single Cys PutP activity when Cys was placed into the cytoplasmic half of the domain (Figs. 4b and 5). These results suggested that the transporter contained a narrow cavity (funnel), allowing the positively charged MTSET with a width similar to the

diameter of hydrated  $\text{Na}^+$  to reach amino acids in the middle of TM IX from the periplasmic side of the membrane. The more rigid and, as compared to MTS reagents, chemically less reactive MalNet presumably could not efficiently enter this cavity or the transporter variants were insensitive to Cys modification by the neutral reagent.

#### Accessibility of Cys to fluorescein-5-maleimide

Since the analysis of transport inhibition did not allow discrimination between unlabeled and labeled but functionally unaffected proteins, Cys modification was directly determined by analyzing fluorescence of single Cys PutP variants incubated with membrane-permeant fluorescein-5-maleimide (FM).



zation with 1.5% (w/v) *n*-dodecyl- $\beta$ -D-maltoside and purification via  $\text{Ni}^{2+}$ -NTA affinity chromatography, 5  $\mu\text{g}$  protein was loaded onto 10% SDS-PAGE and separated. Fluorescent bands were detected using a MultiImager<sup>TM</sup> (BioRad). Afterwards, the same gel was stained with Coomassie Blue. Fluorescence intensities detected by MultiImager were corrected for background fluorescence and quantitatively analyzed using software ImageQuant 5.0 and plotted. (a) Fluorescent protein bands. (b) Coomassie Blue-stained protein. (c) Relative fluorescence intensities normalized to the amount of protein. PutP( $\Delta$ Cys)-T341C showed the highest fluorescence intensity, and the respective value was arbitrarily set to 100. Relative fluorescence intensity (rel. fl.) is expressed in arbitrary units (AU).

**Fig. 5.** Schematic presentation of Cys accessibility in TM IX. The figure summarizes the Cys accessibility data shown in Figs. 4, 6–8. (a) Side view of TM IX. (b) Helical wheel projection of TM IX. The helix was visualized by PyMOL. Black ellipses indicate single Cys PutP variants inhibited by FM; gray ellipses denote single Cys PutP variants not inhibited by MalNet but modified by FM; white ellipses represent single Cys PutP variants not or only marginally inhibited or modified by MalNet and FM; gray rectangles indicate single Cys PutP variants inhibited by MTSET; black rectangles denote single Cys PutP variant inhibited by MalNet and MTSET and modified by FM. \*Cys protected by proline; <sup>+</sup>Cys partially protected by  $\text{Na}^+$ . The accessibility of the remaining residues was not affected by  $\text{Na}^+$  or proline.

**Fig. 6.** Accessibility of Cys individually introduced throughout TM IX to FM. Randomly oriented membrane vesicles containing the indicated PutP derivative were prepared as described in Experimental Procedures. One hundred fifty microliters of a suspension of membranes of *E. coli* WG170 containing given PutP derivatives (10 mg of total membrane protein/mL) were incubated with 200  $\mu\text{M}$  FM for 10 min. Labeling reactions were stopped by addition of 5 mM  $\beta$ -mercaptoethanol. After solubilization

Labeling was performed with randomly oriented membrane vesicles; labeled PutP derivatives were solubilized from the membranes, purified by Ni<sup>2+</sup>-NTA affinity chromatography, and subjected to SDS-PAGE. Fluorescence was detected by UV excitation and normalized to the protein amount. The normalized fluorescence intensity of PutP( $\Delta$ Cys)-T341C was arbitrarily set to 100. Unspecific labeling was estimated with PutP( $\Delta$ Cys) as negative control and corresponded to 3 arbitrary units (AU) or less (Fig. 6).

FM reacted essentially with all single Cys PutP variants inhibited by MalNEt [PutP( $\Delta$ Cys)-T341C, -C344, -L347C, -V348C, and -S351C; fluorescence intensities between 30 and 100 AU] (Figs. 4–6). In addition, PutP( $\Delta$ Cys)-P324C was modified by FM (fluorescence intensity, 40 AU). P324 is located at the periplasmic border of TM IX. Following TM IX from the periplasmic side, accessibility decreased abruptly, and Cys at positions 325 to 340 was not significantly accessible to the sulfhydryl reagent (relative labeling yields between 0.4% and 7%) including positions at which Cys was modified by MTSET (Figs. 5 and 6). The only single Cys PutP variant modified by all three sulfhydryl reagents was PutP( $\Delta$ Cys)-T341C. As alkylation by maleimide-based reagents requires the sulfhydryl group to be in the deprotonated form,<sup>21,22</sup> the high accessibility and reactivity of Cys placed into the middle or cytoplasmic half of TM IX suggest that the respective residues are exposed to a hydrophilic environment as already deduced above from the MalNEt inhibition pattern.

### Influence of ligand on Cys accessibility

The accessibility analyses described above suggest that various residues of TM IX are exposed to a hydrophilic environment as they originate, for example, from hydrophilic cavities or funnels formed by the transport protein. To explore the physiological significance of the putative cavities, the influence of ligands (Na<sup>+</sup>, proline) on Cys accessibility was tested throughout TM IX. For this purpose, FM labeling of randomly oriented membrane vesicles containing individual single Cys PutP variants was performed in the absence and presence of ligand(s). Subsequently, PutP was isolated and FM fluorescence was detected as described above.

FM labeling of Cys at positions 324 and 341 was not significantly influenced by ligands (Fig. 7). However, labeling of the accessible positions 344, 347, 348, and 351 was inhibited by proline in the presence of Na<sup>+</sup>, while Na<sup>+</sup> alone had no effect (Fig. 7). Also, proline alone inhibited Cys modification at all four positions albeit somewhat less efficient than upon addition of Na<sup>+</sup> (data not shown). Finally, neither Na<sup>+</sup> nor proline stimulated reaction of FM with Cys at all remaining positions reported inaccessible in the absence of ligands (data not shown).

The effect of ligands on MTSET labeling of PutP( $\Delta$ Cys)-L331C, -A337C, and -T341C was investigated. For this purpose, freshly prepared cells containing the respective single Cys PutP derivatives

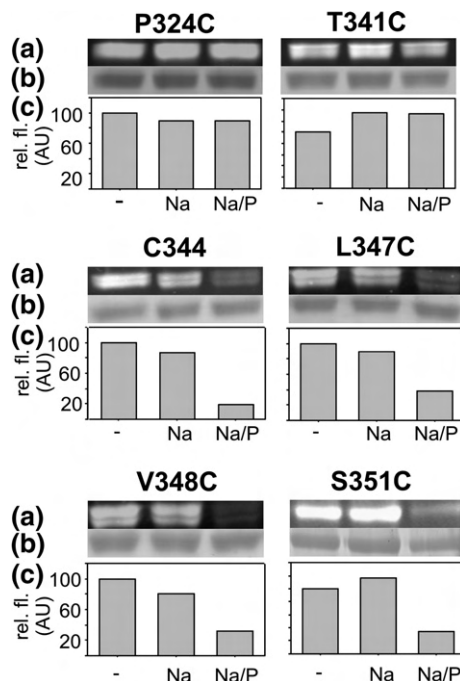


**Fig. 7.** Influence of ligands on Cys accessibility to FM. Membrane vesicles containing the indicated PutP derivatives were prepared as described in the legend to Fig. 5. Aliquots (150  $\mu$ L) of a suspension of membranes of *E. coli* WG170 containing given PutP( $\Delta$ Cys) derivatives (10 mg of total membrane protein/mL) were preincubated in the absence (-) or presence of 30 mM NaCl (Na) and 30 mM NaCl/10 mM proline (Na/P) at 25  $^{\circ}$ C for 10 min. Subsequently, labeling of the samples with 200  $\mu$ M FM was performed for 10 min. The reaction was stopped by addition of 5 mM  $\beta$ -mercaptoethanol. Labeled PutP was isolated and analyzed as described in the legend to Fig. 4. (a) Fluorescent protein bands. (b) Coomassie Blue-stained protein. (c) Relative fluorescence intensities (rel. fl.) in arbitrary units (AU) normalized to the amount of protein.

were labeled with MTSET in the presence and absence of ligands, and proline uptake was analyzed after cell washing. The effect of ligand on MTSET labeling is expressed as the ratio of the activities measured after MTSET labeling in the presence and absence of ligand to better compare protective effects between the respective proteins (Fig. 8). In contrast to the protective effect of proline on Cys in the cytoplasmic half of TM IX described above, the substrate alone did not significantly inhibit labeling of Cys placed into the periplasmic half or middle of TM IX (position 331, 337, or 341) with MTSET (Fig. 8). Instead, the results of the activity assay suggested a partial protective effect of Na<sup>+</sup>. In fact, MTSET labeling of cells containing PutP( $\Delta$ Cys)-L331C, -A337C, or -T341C in the presence of Na<sup>+</sup> led to proline uptake rates that were 1.4-, 1.7-, or 1.4-fold higher, respectively, than that of cells labeled in the absence of Na<sup>+</sup> (Fig. 8). The protective effect was somewhat strengthened than when both Na<sup>+</sup> and proline were present during the labeling reaction. However, it should be noted that protection of Cys at position 341 was not very efficient as even under

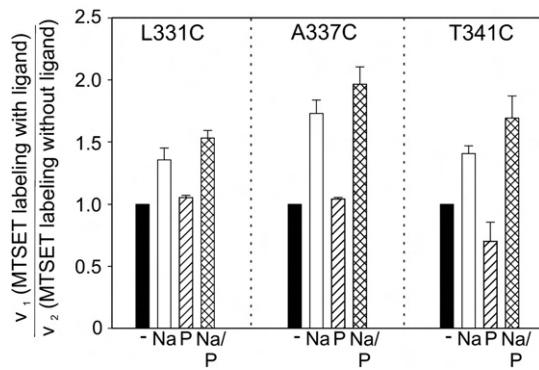


**Fig. 8.** Influence of ligands on Cys accessibility to MTSET. Cells containing the respective single Cys variant were preincubated in the absence (–) or presence of 30 mM NaCl (Na), 10 mM proline, or 30 mM NaCl/10 mM proline (Na/P) at 25 °C for 10 min. Subsequently, 2 mM MTSET was added and incubation was continued for 10 min. The reaction was stopped, cells were washed, and transport was analyzed as described in the legend to Fig. 4. The effect of ligand is shown as the ratio of the activities measured after MTSET labeling in the presence ( $v_1$ ) and absence ( $v_2$ ) of ligand. Ratios  $>1$  indicate inhibition, whereas ratios  $<1$  denote stimulation of MTSET labeling.

conditions of maximum protection, uptake activities of MTSET-treated cells were reduced to 30% of the value of unlabeled cells. Cells containing PutP ( $\Delta$ Cys)-L331C or -A337C showed a maximum of 60–70% of the activity of unlabeled cells if labeling was performed in the presence of  $\text{Na}^+$  and proline.

## Discussion

S340 and T341 in TM IX of PutP have previously been suggested to play key roles in ligand binding and transport; thereby, the side chain of T341 may directly participate in  $\text{Na}^+$  binding.<sup>14</sup> The current analysis of structure–function relationships in PutP newly identified G328, S332, Q345, and L346 of the same domain as important for  $\text{Na}^+$ -coupled proline uptake. In addition, the Cys accessibility pattern of TM IX suggests the existence of hydrophilic cavities in the transporter that are affected by ligand binding.

What are the roles of the newly identified structural and/or functional important residues? While none of the four residues appears to be crucial for membrane insertion and stability of PutP, functional analyses of the effect of Cys replacements reveal significant alterations of kinetic parameters of transport.  $K_{m(\text{pro})}$  is most severely affected (more than 1 order of magnitude) upon replacement of Q345 or L346. Although the effects at both positions are diametrical, the data suggest that ligand binding is highly sensitive to alterations in this part of the protein. In particular, the properties of PutP-Q345C [increased  $K_{m(\text{pro})}$  and  $K_{0.5(\text{Na}^+)}$ , comparatively small changes of  $V_{\text{max}}$ ] are, to some extent, reminiscent of the results obtained upon replacement of S340 or T341.<sup>14</sup> These observations further support the idea that these polar residues of TM IX are located at or

close to a ligand binding site of PutP. Furthermore, as both  $K_{m(\text{pro})}$  and  $K_{0.5(\text{Na}^+)}$  are highly affected upon replacement of S340, T341, or Q345, the idea that binding of coupling ion and substrate occurs in close proximity is supported. Furthermore, the reduced  $V_{\text{max}}$  values observed with PutP-G328C, -S332C, and -L346C hint at defects in the transport cycle subsequent to ligand binding, for example, inhibition of conformational alterations or a hampered release of ligands. The latter idea is, in principle, supported by the decreased Michaelis–Menten parameters found for PutP-S332C [ $K_{m(\text{pro})}$  and  $K_{0.5(\text{Na}^+)}$ ] and PutP-Q346C [ $K_{m(\text{pro})}$ ] (Table 1).

If, in fact, residues of TM IX are located at or close to a ligand binding site, they might be accessible from one side and/or from the other side of membrane. First evidence for the existence of an outwardly oriented cavity (funnel) in PutP comes from labeling of PutP-S340C and -T341C in right-side-out membrane vesicles with various methane thiosulfonate compounds.<sup>14</sup> Here, we present new evidence for the existence of a funnel that may connect T341 with the periplasmic surface of PutP. This evidence comes from the observation that  $\text{Na}^+$ -coupled proline uptake into intact cells containing PutP( $\Delta$ Cys)-L331C, -A337C, or -T341C is efficiently inhibited by MTSET.  $\text{Na}^+$  but not proline inhibits the labeling reaction, although it cannot completely protect the respective Cys residues from modification possibly due to the dynamics of the system. Considering the  $\text{Na}^+$ -sensitive accessibility of these residues to positively charged MTSET with a width similar to the diameter of hydrated  $\text{Na}^+$ , as well as the previously reported particular significance of T341 for  $\text{Na}^+$  binding,<sup>14</sup> it is tempting to speculate that the proposed funnel is used by  $\text{Na}^+$  as an entrance to a  $\text{Na}^+$  binding site in about the middle of the membrane (Fig. 9). Clearly, inhibition of MTSET labeling of the reported residues could also be achieved by

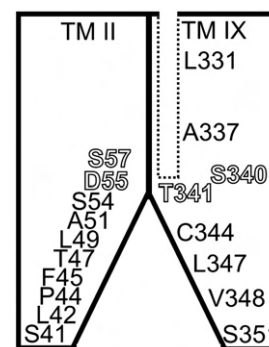


**Fig. 9.** Model showing the participation of TMs II and IX in the formation of hydrophilic cavities in PutP. The model is based on the current analysis as well as on previous investigations.<sup>11–15</sup> Amino acids of TMs II and IX supposed to line a hydrophilic cavity (funnel) are indicated. Residues shown to be important for ligand binding and/or translocation are represented as open characters. There is no evidence so far that the periplasmic half of TM II participates in the formation of the outwardly oriented funnel (drawn as dotted box) suggested to be lined by residues of TM IX.

conformational alterations induced by Na<sup>+</sup> binding elsewhere.

Unlike the periplasmic half of TM IX, Cys placed at positions in the cytoplasmic half of the domain (C344, L347C, V348C, and S351C) is highly accessible to MalNEt and FM but not to MTSET (if MTSET is added from the periplasmic side of the membrane). The labeling pattern suggests the existence of an inwardly oriented hydrophilic cavity (Fig. 9). Cavities open to the cytoplasm have also been seen, for example, by Cys accessibility analyses and X-ray crystallography of lactose permease and glycerol-3-phosphate transporter (both members of the major facilitator family), and are suggested for members of the neurotransmitter/sodium symporter family (TC 2A.22, SLC6).<sup>19,23–27</sup> In the case of PutP, proline but not Na<sup>+</sup> effectively blocks modification of Cys at the respective positions. Cys protection may be achieved by direct steric hindering or closure of the cavity due to either movement of neighboring TMs relative to each other or a gating mechanism. The latter mechanism has recently been suggested for NIS and members of the neurotransmitter/sodium symporter family and is supposed to involve amino acids of adjoining loops that participate in salt bridge formation.<sup>17,28,29</sup> For lactose permease, site-directed spin labeling and EPR spectroscopy revealed a substrate-induced closure of an inwardly oriented cytoplasmic cavity.<sup>30</sup> Cavities of this kind are frequently thought to participate in the release of ligands from the transporter into the cytoplasm.

T341 is the only position at which Cys is highly accessible to all three sulfhydryl reagents (MTSET, MalNEt, and FM). In this context, it appears interesting to note that a recent backbone model of TM IX generated based on intrahelical distance measurements by EPR spectroscopy shows a pronounced kink near T341, which is associated with a short loop-like structure.<sup>31</sup> While these results agree, in principle, with the idea of T341 being located at the interface between periplasmic and cytoplasmic cavities, a direct involvement in the transition of ligands between these cavities remains elusive.

Alternatively to the cavity model, the accessibility of Cys to sulfhydryl reagents could be taken as a hint at a location of respective positions in a cytoplasmic or periplasmic loop rather than in a TM. The following arguments are contrary to this interpretation: (i) the in silico predicted location and orientation of TM IX of PutP is confirmed by *phoA* and *lacZ* gene fusion analyses and site-specific proteolysis;<sup>9</sup> (ii) the FM labeling pattern of the periplasmic half of TM IX agrees perfectly with the current topology model of PutP (Figs. 1, 5, and 6); (iii) the FM labeling pattern of the cytoplasmic half of TM IX hints at an  $\alpha$ -helical arrangement of this part of the domain (Figs. 5 and 6); (iv) intrahelical distances determined by site-directed spin labeling and EPR spectroscopy are in full agreement with a kinked  $\alpha$ -helical backbone structure of TM IX within the borders indicated in the current topology model;<sup>31</sup> (v) the membrane topography of TM II is confirmed by site-directed spin labeling and EPR spectro-

scopy,<sup>10</sup> and Cys cross-linking<sup>14</sup> aligns TMs II and IX within the borders of the current topology model; and (vi) our current model is in agreement with topological analyses of other tSSSF members.<sup>32,33</sup>

Finally, it should be noted that a Cys accessibility pattern very similar to the cytoplasmic half of TM IX was previously observed for TM II (Fig. 1).<sup>15</sup> Proline blocked modification of Cys at respective positions in TM II as detected here for TM IX. Since pairs of Cys residues placed in both domains can efficiently be cross-linked even by the “zero length” cross-linker Cu(1,10-phenanthroline)<sub>3</sub>,<sup>14</sup> we suggest that TM IX is joint by TM II in forming an inwardly oriented cavity (Fig. 9).

Taken together, the results indicate that G328, S332, Q345, and L346 in TM IX of PutP are important for ligand binding and/or translocation in addition to the previously identified S340 and T341. Furthermore, it is suggested that distinct residues of the domain participate in the formation of an outwardly oriented funnel (L331, A337, and T341) and a larger inwardly directed cavity (T341, C344, L347, V348, and S351).

## Experimental Procedures

### Bacterial strains and plasmids

*E. coli* JM109 [*endA1 recA1 gyrA96 thi hsdR17 supE44 relA1 Δ(lac-proAB) (F' traΔ36pro AB<sup>+</sup> lacI<sup>q</sup>ZΔM15)*]<sup>34</sup> and *E. coli* DH5 $\alpha$  [F<sup>-</sup>  $\phi$ 80d *lacZ*  $\Delta$ M15  $\Delta$ (*lacZYA-argF*) U169 *deoR recA1 endA1 hsd R17*(r<sub>k</sub><sup>-</sup>,m<sub>k</sub><sup>+</sup>) *phoA supE44*  $\lambda$ <sup>-</sup> *thi-1 gyrA96 relA1*] were used as carriers for the plasmids generated in this study. *E. coli* WG170 [F<sup>-</sup> *trp lacZ rpsL thi Δ(putPA)101 proP219*],<sup>35</sup> harboring the given plasmids, was used for overexpression of the *putP* gene and transport assays. The following plasmids, derivatives of pT7-5,<sup>36</sup> containing the *lac* promoter/operator for expression of the *putP* gene were used for all gene manipulations: pT7-5/*putP* and pT7-5/*putP*( $\Delta$ Cys), each of which harbors a cassette version of the *putP* gene encoding PutP-wild-type and an engineered transporter devoid of all five native Cys residues [PutP( $\Delta$ Cys)], respectively, and a C-terminal-attached amino acid sequence resembling the FLAG epitope and a 6His tag.<sup>9,10</sup>

### Site-directed mutagenesis

Every amino acid of TM IX was individually replaced by Cys by site-directed mutagenesis using plasmid pT7-5/*putP*( $\Delta$ Cys) as a template and synthetic mutagenic oligonucleotides in a one- or two-step PCR reaction with *Taq*-DNA polymerase. PCR fragments were digested with PstI and SpeI and ligated with similarly treated plasmid pT7-5/*putP*( $\Delta$ Cys) additionally incubated with alkaline phosphatase. Constructs were verified by sequencing the resulting plasmid DNA. For overexpression, the mutated *putP* gene was cut out with restriction endonucleases NcoI and HindIII and ligated to the similarly treated vector pTrc99a additionally incubated with alkaline phosphatase.

### Purification and reconstitution of PutP

PutP was purified by Ni<sup>2+</sup>-NTA affinity chromatography and reconstituted into proteoliposomes prepared

from *E. coli* polar lipid extracts (Avanti Polar Lipids, Inc., Alabaster, AL) at a lipid-to-protein ratio of 100:1 (w/w) as described before.<sup>37</sup>

### Proline transport assays

Transport was measured in *E. coli* WG170 transformed with plasmid pT7-5/*putP*( $\Delta$ Cys) or pT7-5/*putP* harboring the given mutations. Cells were grown and prepared as previously described.<sup>12</sup> Smf-driven proline uptake was assayed under standard conditions with 10  $\mu$ M L-[U-<sup>14</sup>C] proline (26 Ci/mol) in the presence of 20 mM D-lactate (Na<sup>+</sup> salt) and 50 mM NaCl using the rapid filtration method as described previously.<sup>38</sup> Initial rates of transport were calculated from the initial linear portion of the time course. Steady-state levels of proline accumulation were determined from time points after leveling out of the uptake curve. Kinetic parameters were determined by plotting initial rates and substrate concentrations according to Eadie-Hofstee. The resulting  $K_{m(\text{pro})}$ ,  $K_{0.5(\text{Na}^+)}$ , and  $V_{\text{max}}$  values of pT7-5/*putP*-encoded PutP(wild type) closely match the parameters of the native, fully induced, chromosome-encoded PutP in the absence of PutA<sup>39,40</sup> suggesting that deviations of kinetic parameters are solely due to the site-specifically introduced amino acid replacements and not to overexpression artifacts.

For transport inhibition analyses, cells containing the respective single Cys variant were incubated with 2 mM sulfhydryl reagent (MalNEt or MTSET) at room temperature for 15 min. The reaction was stopped by two-fold dilution of the reaction mixture with 100 mM Tris/4-morpholineethanesulfonic acid (Mes) buffer, pH 6.0, containing 0.1% bovine serum albumin (BSA). Cells were washed and resuspended in the same buffer without BSA, and transport was analyzed as described above.

For analysis of the effect of ligand on MTSET labeling, cells containing the respective single Cys variant were washed four times in sodium-free 100 mM Tris/Mes buffer, pH 6.0, and preincubated in the absence or presence of 30 mM NaCl, 10 mM proline, or 30 mM NaCl/10 mM proline at 25 °C for 10 min. Subsequently, 2 mM MTSET was added and incubation was continued for 10 min. The reaction was stopped by twofold dilution of the reaction mixture with 100 mM Tris/Mes buffer, pH 6.0, containing 0.1% BSA, and washed two times with the same buffer without BSA. The transport was analyzed as described above.

Smf-driven proline uptake into proteoliposomes was analyzed as described before.<sup>37</sup>

### Cys accessibility to FM

*E. coli* WG170 transformed with pTrc99a/*putP*( $\Delta$ Cys) were grown, disrupted by sonification, and randomly oriented membrane vesicles were prepared as previously described.<sup>15</sup> For accessibility analyses, 150- $\mu$ L aliquots of the membrane suspension containing 10 mg/mL total protein were incubated without or with Na<sup>+</sup>, K<sup>+</sup>, and/or L-proline at given concentrations at 25 °C for 10 min. Subsequently, 200  $\mu$ M FM was added, and incubation was continued at 25 °C for an additional 10 min. Reactions were stopped by addition of 5 mM  $\beta$ -mercaptoethanol. After labeling, PutP was solubilized with 1.5% (w/v) *n*-dodecyl- $\beta$ -D-maltoside under stirring at 4 °C for 30 min. Then, samples were purified via Ni<sup>2+</sup>-NTA spin columns and eluted with 200 mM imidazole as described before.<sup>13</sup> After protein determination, equal amounts of protein were subjected to 10% SDS-PAGE. Fluorescent bands of PutP

were visualized using the MultiImager™ device (BioRad, Munich) and quantified using the software ImageQuant 5.0. After analysis of fluorescent PutP bands, the gel was stained with Coomassie Blue to detect total amounts of protein.

### Western blot analysis

Relative amounts of PutP with given amino acid replacements in membranes of *E. coli* WG170 were estimated by Western blot analysis with horseradish peroxidase-linked mouse anti-FLAG immunoglobulin G directed against the FLAG epitope at the C terminus of each PutP variant as described before.<sup>12</sup>

### Protein determination

Determination of protein was performed according to Bradford<sup>41</sup> for purified protein and a modified Lowry method<sup>42</sup> for total membrane protein with BSA as standard.

## Acknowledgements

We thank Maret Böhm for generating PutP-S332C. This work was financially supported by the Deutsche Forschungsgemeinschaft (Ju333/3-2, Ju333/4-2, and Exc114-1).

## References

- Jung, H. (2002). The sodium/substrate symporter family: structural and functional features. *FEBS Lett.* **529**, 73–77.
- Wright, E. M. & Turk, E. (2004). The sodium/glucose cotransport family SLC5. *Pflugers Arch.* **447**, 510–518.
- Reizer, J., Reizer, A. & Saier, M. H., Jr (1994). A functional superfamily of sodium/solute symporters. *Biochim. Biophys. Acta*, **1197**, 133–166.
- Jung, H. (2001). Towards the molecular mechanism of Na<sup>+</sup>/solute symport in prokaryotes. *Biochim. Biophys. Acta*, **1505**, 131–143.
- Jackowski, S. & Alix, J. H. (1990). Cloning, sequence, and expression of the pantothenate permease (panF) gene of *Escherichia coli*. *J. Bacteriol.* **172**, 3842–3848.
- Dohan, O., De la Vieja, A. & Carrasco, N. (2006). Hydrocortisone and purinergic signaling stimulate sodium/iodide symporter (NIS)-mediated iodide transport in breast cancer cells. *Mol. Endocrinol.* **20**, 1121–1137.
- Wright, E. M., Hirayama, B. A. & Loo, D. F. (2007). Active sugar transport in health and disease. *J. Intern. Med.* **261**, 32–43.
- Kojima, S., Bohner, A., Gassert, B., Yuan, L. & von Wiren, N. (2007). AtDUR3 represents the major transporter for high-affinity urea transport across the plasma membrane of nitrogen-deficient *Arabidopsis* roots. *Plant J.* **52**, 30–40.
- Jung, H., Rübénhagen, R., Tebbe, S., Leifker, K., Tholema, N., Quick, M. & Schmid, R. (1998). Topology of the Na<sup>+</sup>/proline transporter of *Escherichia coli*. *J. Biol. Chem.* **273**, 26400–26407.
- Wegener, C., Tebbe, S., Steinhoff, H. J. & Jung, H. (2000). Spin labeling analysis of structure and

- dynamics of the Na<sup>+</sup>/proline transporter of *Escherichia coli*. *Biochemistry*, **39**, 4831–4837.
11. Quick, M. & Jung, H. (1997). Aspartate 55 in the Na<sup>+</sup>/proline permease of *Escherichia coli* is essential for Na<sup>+</sup>-coupled proline uptake. *Biochemistry*, **36**, 4631–4636.
  12. Quick, M., Tebbe, S. & Jung, H. (1996). Ser57 in the Na<sup>+</sup>/proline permease of *Escherichia coli* is critical for high-affinity proline uptake. *Eur. J. Biochem.* **239**, 732–736.
  13. Pirch, T., Quick, M., Nietschke, M., Langkamp, M. & Jung, H. (2002). Sites important for Na<sup>+</sup> and substrate binding in the Na<sup>+</sup>/proline transporter of *Escherichia coli*, a member of the Na<sup>+</sup>/solute symporter family. *J. Biol. Chem.* **277**, 8790–8796.
  14. Hilger, D., Böhm, M., Hackmann, A. & Jung, H. (2008). Role of Ser-340 and Thr-341 in transmembrane domain IX of the Na<sup>+</sup>/proline transporter PutP of *Escherichia coli* in ligand binding and transport. *J. Biol. Chem.* **283**, 4921–4929.
  15. Pirch, T., Landmeier, S. & Jung, H. (2003). Transmembrane domain II of the Na<sup>+</sup>/proline transporter PutP of *Escherichia coli* forms part of a conformationally flexible, cytoplasmic exposed aqueous cavity within the membrane. *J. Biol. Chem.* **278**, 42942–42949.
  16. Yamato, I. & Anraku, Y. (1993). Na<sup>+</sup>/substrate symport on prokaryotes. In *Alkali Cation Transport Systems in Prokaryotes* (Bakker, E. P., ed), pp. 53–76, CRC Press, Boca Raton, FL.
  17. De la Vieja, A., Reed, M. D., Ginter, C. S. & Carrasco, N. (2007). Amino acid residues in transmembrane segment IX of the Na<sup>+</sup>/I<sup>-</sup> symporter play a role in its Na<sup>+</sup> dependence and are critical for transport activity. *J. Biol. Chem.* **282**, 25290–25298.
  18. Guan, L. & Kaback, H. R. (2007). Site-directed alkylation of cysteine to test solvent accessibility of membrane proteins. *Nat. Protoc.* **2**, 2012–2017.
  19. Kaback, H. R., Dunten, R., Frillingos, S., Venkatesan, P., Kwaw, I., Zhang, W. & Ermolova, N. (2007). Site-directed alkylation and the alternating access model for LacY. *Proc. Natl Acad. Sci. USA*, **104**, 491–494.
  20. Karlin, A. & Akabas, M. H. (1998). Substituted-cysteine accessibility method. *Methods Enzymol.* **293**, 123–145.
  21. Zhou, J., Fazzio, R. T. & Blair, D. F. (1995). Membrane topology of the MotA protein of *Escherichia coli*. *J. Mol. Biol.* **251**, 237–242.
  22. Poelarends, G. & Konings, W. N. (2002). The transmembrane domains of the ABC multidrug transporter LmrA form a cytoplasmic exposed, aqueous chamber within the membrane. *J. Biol. Chem.* **277**, 42891–42898.
  23. Abramson, J., Smirnova, I., Kasho, V., Verner, G., Kaback, H. R. & Iwata, S. (2003). Structure and mechanism of the lactose permease of *Escherichia coli*. *Science*, **301**, 610–615.
  24. Huang, Y., Lemieux, M. J., Song, J., Auer, M. & Wang, D. N. (2003). Structure and mechanism of the glycerol-3-phosphate transporter from *Escherichia coli*. *Science*, **301**, 616–620.
  25. Guan, L., Mirza, O., Verner, G., Iwata, S. & Kaback, H. R. (2007). Structural determination of wild-type lactose permease. *Proc. Natl Acad. Sci. USA*, **104**, 15294–15298.
  26. Quick, M., Yano, H., Goldberg, N. R., Duan, L., Beuming, T., Shi, L. *et al.* (2006). State-dependent con-  
formations of the translocation pathway in the tyrosine transporter Tyt1, a novel neurotransmitter: sodium symporter from *Fusobacterium nucleatum*. *J. Biol. Chem.* **281**, 26444–26454.
  27. Zhang, Y. W. & Rudnick, G. (2006). The cytoplasmic substrate permeation pathway of serotonin transporter. *J. Biol. Chem.* **281**, 36213–36220.
  28. Yamashita, A., Singh, S. K., Kawate, T., Jin, Y. & Gouaux, E. (2005). Crystal structure of a bacterial homologue of Na<sup>+</sup>/Cl<sup>-</sup> dependent neurotransmitter transporters. *Nature*, **437**, 215–223.
  29. Loland, C. J., Granas, C., Javitch, J. A. & Gether, U. (2004). Identification of intracellular residues in the dopamine transporter critical for regulation of transporter conformation and cocaine binding. *J. Biol. Chem.* **279**, 3228–3238.
  30. Smirnova, I., Kasho, V., Choe, J. Y., Altenbach, C., Hubbell, W. L. & Kaback, H. R. (2007). Sugar binding induces an outward facing conformation of LacY. *Proc. Natl Acad. Sci. USA*, **104**, 16504–16509.
  31. Hilger, D., Polyhach, Y., Jung, H. & Jeschke, G. (2008). Backbone structure of transmembrane domain IX of the Na<sup>+</sup>/proline transporter PutP of *Escherichia coli*. *Biophys. J.* submitted.
  32. Turk, E., Kerner, C. J., Lostao, M. P. & Wright, E. M. (1996). Membrane topology of the human Na<sup>+</sup>/glucose cotransporter SGLT1. *J. Biol. Chem.* **271**, 1925–1934.
  33. Levy, O., De la Vieja, A., Ginter, C. S., Riedel, C., Dai, G. & Carrasco, N. (1998). N-linked glycosylation of the thyroid Na<sup>+</sup>/I<sup>-</sup> symporter (NIS). Implications for its secondary structure model. *J. Biol. Chem.* **273**, 22657–22663.
  34. Yanisch-Perron, C., Vieira, J. & Messing, J. (1985). Improved M13 phage cloning vectors and host strains: nucleotide sequences of the M13mp18 and pUC19 vectors. *Gene*, **33**, 103–119.
  35. Stalmach, M. E., Grothe, S. & Wood, J. M. (1983). Two proline porters in *Escherichia coli* K-12. *J. Bacteriol.* **156**, 481–486.
  36. Tabor, S. & Richardson, C. C. (1985). A bacteriophage T7 RNA polymerase/promoter system for controlled exclusive expression of specific genes. *Proc. Natl Acad. Sci. USA*, **82**, 1074–1078.
  37. Jung, H., Tebbe, S., Schmid, R. & Jung, K. (1998). Unidirectional reconstitution and characterization of purified Na<sup>+</sup>/proline transporter of *Escherichia coli*. *Biochemistry*, **37**, 11083–11088.
  38. Chen, C. C., Tsuchiya, T., Yamane, Y., Wood, J. M. & Wilson, T. H. (1985). Na<sup>+</sup> (Li<sup>+</sup>)-proline cotransport in *Escherichia coli*. *J. Membr. Biol.* **84**, 157–164.
  39. Wood, J. M. & Zadworny, D. (1979). Characterization of an inducible porter required for L-proline catabolism by *Escherichia coli* K12. *Can. J. Biochem.* **57**, 1191–1199.
  40. Chen, C. C., Tsuchiya, T., Yamane, Y., Wood, J. M. & Wilson, T. H. (1985). Na<sup>+</sup> (Li<sup>+</sup>)-proline cotransport in *Escherichia coli*. *J. Membr. Biol.* **84**, 157–164.
  41. Bradford, M. M. (1976). A rapid and sensitive method for the quantitation of microgram quantities of protein utilizing the principle of protein-dye binding. *Anal. Biochem.* **72**, 248–254.
  42. Peterson, G. L. (1977). A simplification of the protein assay method of Lowry *et al.* which is more generally applicable. *Anal. Biochem.* **83**, 346–356.

**3 HOMOLOGY MODEL OF THE  $\text{Na}^+$ /PROLINE TRANSPORTER  
PUTP OF *ESCHERICHIA COLI* AND ITS FUNCTIONAL  
IMPLICATIONS**



# Homology Model of the Na<sup>+</sup>/Proline Transporter PutP of *Escherichia coli* and Its Functional Implications

Elena Olkhova<sup>1\*†</sup>, Michael Raba<sup>2†</sup>, Susanne Bracher<sup>2</sup>,  
Daniel Hilger<sup>2</sup> and Heinrich Jung<sup>2\*</sup>

<sup>1</sup>Department of Molecular Membrane Biology, Max Planck Institute of Biophysics, Max-von-Laue Str. 3, D-60438 Frankfurt am Main, Germany

<sup>2</sup>Mikrobiologie, Biozentrum der LMU München, Großhaderner Strasse 2-4, 82152 Martinsried, Germany

Received 7 July 2010;  
received in revised form  
19 November 2010;  
accepted 22 November 2010  
Available online  
3 December 2010

Edited by J. Bowie

## Keywords:

secondary transport;  
PutP;  
sodium/solute symport;  
molecular modeling;  
docking

Na<sup>+</sup>/solute symporters are essential membrane integrated proteins that couple the flow of Na<sup>+</sup> ions driven by electrochemical Na<sup>+</sup> gradients to the transport of solutes across biological membranes. Here, we used a combination of molecular modeling techniques and evolutionary conservation analysis to construct and validate a first model of the Na<sup>+</sup>/proline symporter PutP of *Escherichia coli* based on the crystal structure of the bacterial Na<sup>+</sup>/galactose symporter vSGLT. Ligand docking experiments were employed to gain information about residues involved in proline binding. The proposed model is consistent with the available experimental data and was further validated by amino acid substitutions and kinetic and protein chemical analyses. Combination of the results of molecular modeling and functional studies predicts the location and organization of the Na<sup>+</sup> and proline binding sites. Remarkably, as proposed computationally and discovered here experimentally, residues Y140, W244, and Y248 of transmembrane segments 4 and 7 are found to be particularly important for PutP function and suggested to participate in proline binding and/or gating.

© 2010 Elsevier Ltd. All rights reserved.

## Introduction

Sodium solute symporters (SSS) form a large family of membrane transport proteins (TC 2A.21, SLC5) that co-transport Na<sup>+</sup> with sugars, amino acids, inorganic ions, and some vitamins.<sup>1–3</sup> Members of this family are important in human physi-

ology. The function of several family members has been well characterized, including the mammalian glucose (SGLTs), the iodide (NIS), the *Vibrio parahaemolyticus* galactose/glucose (vSGLT), and the *Escherichia coli* proline (PutP) symporters. Like other secondary transporters, the SSS proteins are thought to accomplish transport via alternating access of the substrate binding site to either side of the membrane.<sup>4,5</sup> Experimental evidence for this mechanism comes from numerous biochemical analyses and more recently from X-ray crystallographic data (e.g., Refs. 6,7).

The Na<sup>+</sup>/proline transporter PutP of *E. coli* is a biochemically well-characterized prokaryotic member of the SSS family.<sup>8,9</sup> It catalyzes the coupled translocation of Na<sup>+</sup> and proline with a stoichiometry of 1:1. Kinetic analyses of Na<sup>+</sup>/solute symport catalyzed by different members of the SSS family

\*Corresponding authors. E-mail addresses:

[Elena.Olkhova@biophys.mpg.de](mailto:Elena.Olkhova@biophys.mpg.de); [hjung@lmu.de](mailto:hjung@lmu.de).

† E.O. and M.R. contributed equally to this work.

Abbreviations used: FM, fluorescein-5-maleimide; MTSET, methanethiosulfonate ethyltrimethylammonium; NEM, N-ethylmaleimide; PutP(ΔCys), engineered transporter devoid of all five native cysteine residues; SSS family, Na<sup>+</sup>/solute symporter family (TC 2A.21, SLC5); TMS, putative transmembrane segment.

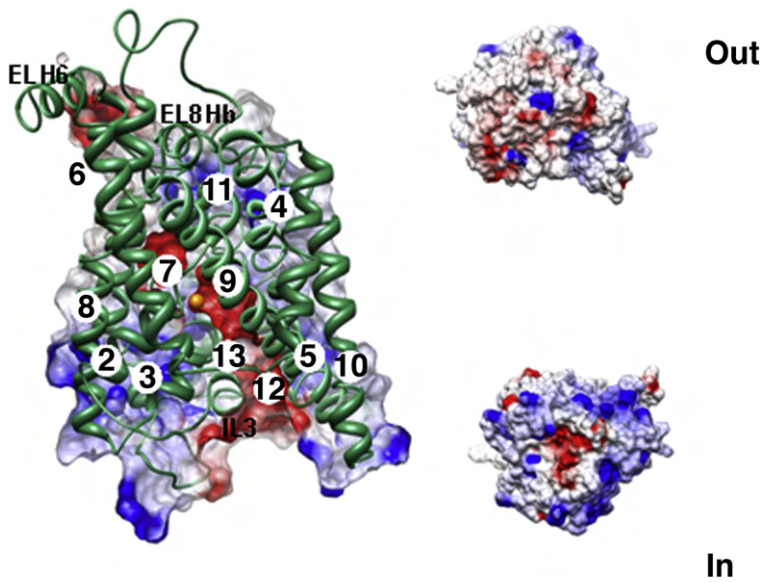


**Fig. 1.** Overall architecture and electrostatic surface potential of the PutP homology model in the inward-facing conformation viewed parallel with the membrane (left), from the outside (top right) and from the inside (bottom right). TMSs are shown as green ribbons and numbered in circles; the  $\text{Na}^+$  ion is shown in orange. The electrostatic potential was calculated using GRASP software; positive and negative areas are indicated in blue or red, respectively.

including PutP suggest that transport occurs according to an ordered binding mechanism.<sup>10–12</sup> In this scheme,  $\text{Na}^+$  binds to the empty transporter first, thereby inducing a conformational change, which increases the affinity of the transporter for the solute. The formation of the ternary complex induces another structural change that exposes  $\text{Na}^+$  and the solute to the opposite side of the membrane. The transport cycle is completed by the release of  $\text{Na}^+$  and proline and the reorientation of the empty transporter in the membrane, allowing the cycle to start again.

However, an understanding of the mechanism of action of PutP requires detailed structural information. Despite intensive attempts, very little is known about the three-dimensional structure of PutP and the location and structure of the proline binding site. Biochemical data indicate that the transporter contains 13 transmembrane segments (TMSs), a motif supposed to be present in all SSS family transporters.<sup>13</sup> Recently, the three-dimensional structure of vSGLT has been determined by X-ray crystallography at 2.7-Å resolution (PDB: 3DH4).<sup>14</sup> The vSGLT structure represents an occluded inward-facing conformation, as indicated by a large internal hydrophilic cavity open to the cytoplasmic side. The structure contains 14 TMSs with a core structure of 10 TMSs arranged in two repeating units (TMSs 2 to 6 and TMSs 7 to 11). The substrate galactose is bound in the centre of the core, occluded from the outside solution by hydrophobic residues.<sup>14</sup>

The availability of the structural information offers an opportunity to build and test a reliable homology model of PutP using the X-ray structure of vSGLT as a template and to perform ligand docking calculations in order to identify possible

ligand binding site(s). In parallel, we applied biochemical and kinetic approaches to test the computational results and to reveal how the structural organization of the transporter is related to function and ligand recognition (binding).

## Results

### Homology model of PutP and ligand docking calculations

#### *Overall architecture of the PutP model*

The homology model of PutP from *E. coli* was constructed by using the Prime module in Maestro (Prime, 1.6; Schrödinger, Portland, OR). The backbone coordinates for the core of the homology model were built based on the crystal structure of vSGLT (PDB: 3DH4). The homology model of PutP represents a conformation of the transporter open to the cytoplasmic side of the membrane. It comprises 443 residues (38–481), which are arranged in 12 TMSs (TMSs 2–13), the connecting loops, and the termini (Fig. 1). TMS 1 was not modeled because the homologous segment is not resolved in the vSGLT structure. The model contains an inverted structural symmetry motif, a common feature in known structures of  $\alpha$ -helical membrane transporters and channels. It comprises 10 TMSs, organized in two repeating units (TMSs 2–6, residues 38–220; and TMSs 7–11, residues 221–434), connected by an external loop helix (ELH6) and followed by the two additional TMSs 12 and 13. The helical secondary structure of TMSs 2 and 7 is interrupted by extended chains, leading to the formation of the periplasmic and cytoplasmic helical TMS fragments 2E, 2I, 7E,

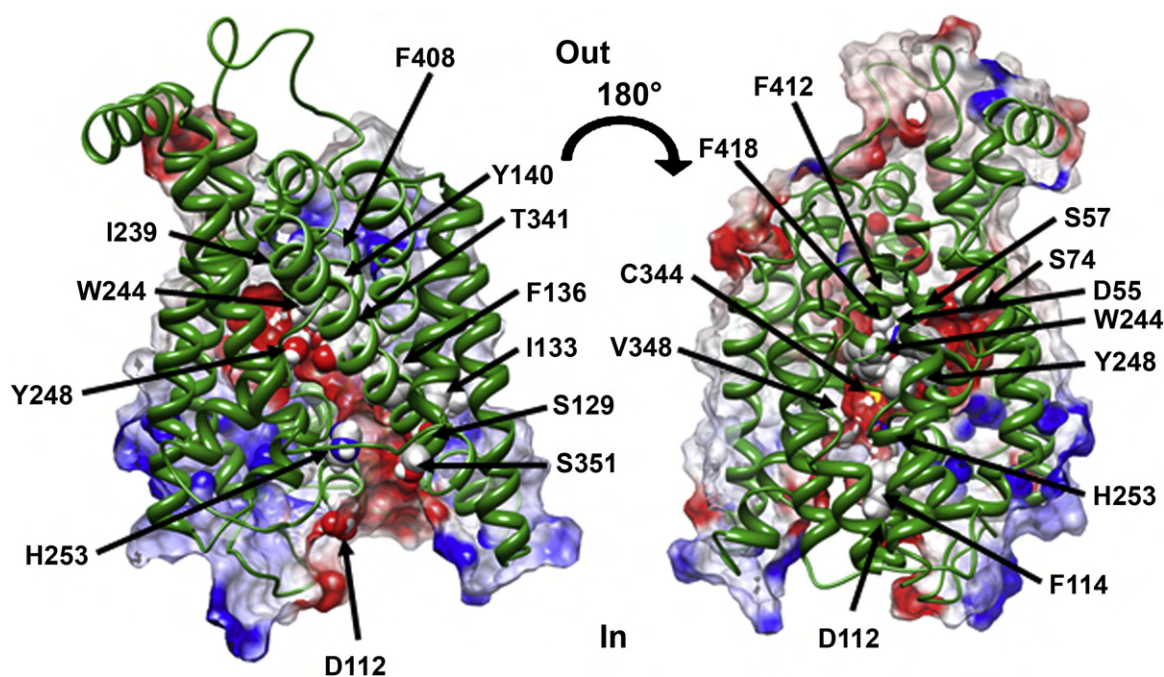


**Fig. 2.** Surface representation of the PutP model, sliced along the membrane normal to show the inward-facing cavity, which connects the cytoplasm with the transmembrane area. A second, small negatively charged cavity is located above the large cavity. Surface coloring represents the electrostatic potential, calculated by GRASP; positive and negative areas are indicated in blue or red, respectively. The location of residues lining the cavities is indicated.

and 7I. This structural fold has first been observed for LeuT from *Aquifex aeolicus* (LeuT<sub>Aa</sub>).<sup>15</sup> The same fold has been found also for the ApcT transporter,<sup>16</sup> although PutP, vSGLT, LeuT<sub>Aa</sub> and ApcT belong to different transporter families and do not share significant sequence identity.

An electrostatic potential surface map of the PutP model reveals a belt of hydrophobic residues corresponding to the transmembrane area. The electrostatic potential surface map viewed from the cytoplasm demonstrates that the cytoplasmic surface is positively charged (Fig. 1, right, In) whereas the periplasmic surface is negatively charged, in line with the positive-inside rule (Fig. 1, right, Out).<sup>17</sup>

The PutP model reveals a large negatively charged inward-facing cavity, which extends from the middle of the transmembrane zone to the cytoplasm. The cavity is lined by amino acids of TMS 2 (S57), internal loop 3 (D112, F114), TMS 4 (S129, I133, F136, and Y140), TMS 7 (W244, Y248, and H253), TMS 9 (T341, C344, V348, and S351), and TMS 11 (F412, F418) (Fig. 2). These results are in agreement with previous experimental findings which demonstrated that residues S41, L42, P44, T47, L49, A51, S54, and S57 of TMS 2 and residues T341, C344, L347, V348, and S351 of TMS 9 participate in the formation of a ligand-sensitive hydrophilic cavity connecting the substrate binding site and the cytoplasm.<sup>18,19</sup> In addition, a small negatively charged cavity is predicted, which

includes residues D55, E75, and I239 (Fig. 2). These two cavities point to each other and are separated by the large hydrophobic residue W244. New Cys accessibility analyses are described below in the experimental part of Results and also confirm the existence of the predicted cavity.

#### Computational validation of the PutP model

The refined PutP homology model was subjected to a series of validation analyses for its consistency and reliability. The overall sequence identity between PutP and vSGLT is 19% and the sequence similarity is 41%. The stereochemical quality of the model was analyzed using the MolProbity web server. Further protein structure checks of the homology model were conducted using the ProSa web server (see Materials and Methods for details). The homology model is, of course, not comparable to a structural model obtained by X-ray crystallography. It might be considered as a low-resolution model with some unavoidable inaccuracies. Therefore, the model has to be carefully validated and subjected to experimental testing.

The ConSurf algorithm<sup>‡</sup> has been applied to determine the level of conservation of each residue

<sup>‡</sup> <http://consurf.tau.ac.il>

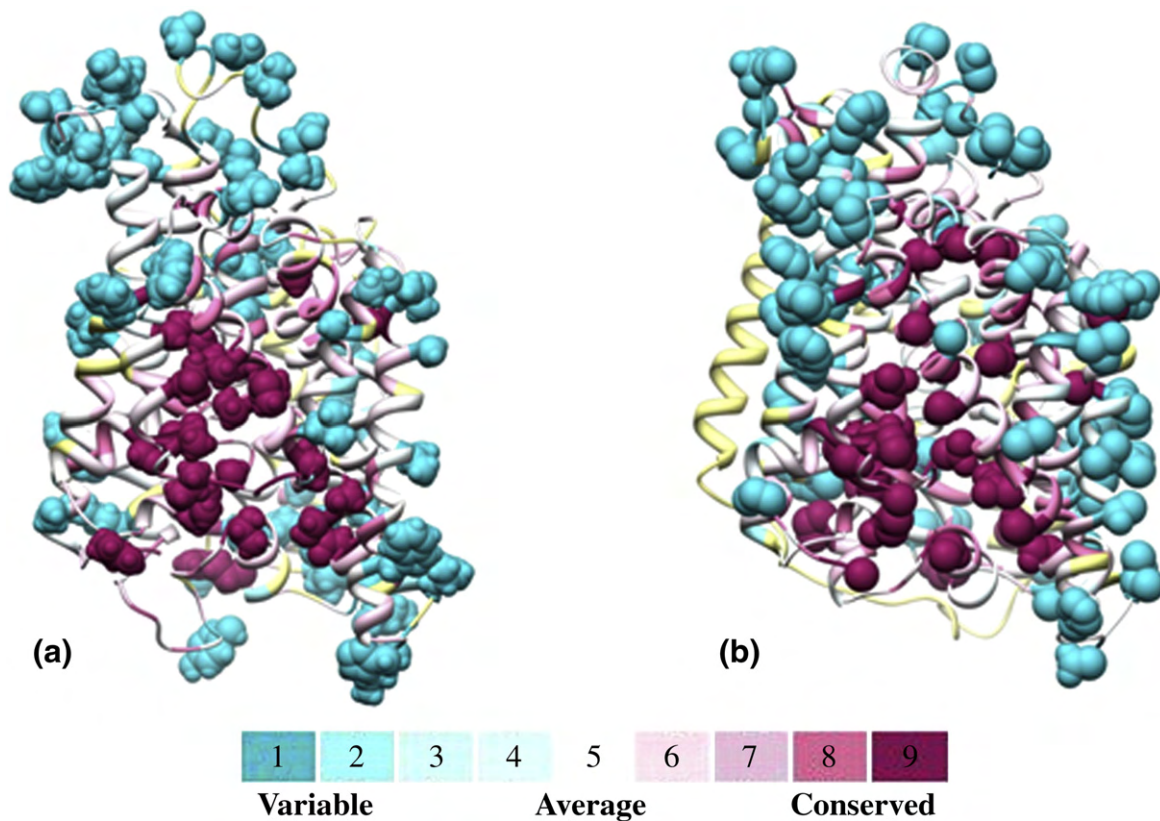


**Fig. 3.** Evolutionary conservation profiles of PutP (a) and vSGLT (b), calculated by the ConSurf web server. Conservation scores were calculated individually for vSGLT and PutP by using two different sets of homologues (50 homologues for each). The PutP homology model and crystal structure of vSGLT are colored according to their conservation scores. The color-coding bar shows the coloring scheme. The most conserved (in magenta) and most variable (in blue) positions of each transporter are shown. The depicted residues of the PutP homology model and the crystallographic structure of vSGLT are colored according to their conservation scores.

in the PutP model.<sup>20</sup> Conservation scores were calculated individually for vSGLT and PutP by using two different sets of homologues. For the PutP model, the protein core was found to be highly conserved within the PutP subfamily, while residues located at the protein–lipid and protein–water interfaces are variable (Fig. 3a). The vSGLT structure demonstrates a similar distribution of the conservative and variable regions (Fig. 3b). The observation that the conserved residues are seen in the cores whereas the variable residues are located on the surface of the proteins provides additional support for the overall correctness of the PutP model.

#### The Na<sup>+</sup> binding site

In our study, the X-ray structure of vSGLT<sup>14</sup> serves as the template for the homology modeling of PutP. However, the Na<sup>+</sup> binding site in vSGLT was not identified crystallographically, but was predicted based on a comparison with the LeuT<sub>Aa</sub> structure, conservation of amino acid residues in the SSS family, and mutational analysis.<sup>14,15</sup>

In the LeuT<sub>Aa</sub> crystal structure, two distinct Na<sup>+</sup> binding sites, Na1 and Na2, were identified. For the vSGLT structure, only one Na<sup>+</sup> binding site has been proposed based on the different Na<sup>+</sup>/substrate stoichiometry. This binding site corresponds to the Na2 site of LeuT<sub>Aa</sub> and appears to be important for substrate translocation. In LeuT<sub>Aa</sub>, the Na2 binding site comprises residues G20 and V23 in TMS 1 and A351, T354, and S355 in TMS 8, which correspond to A53 and M56 in TMS 2 and A337, S340, and T341 in TMS 9 of PutP. Residue A53 of PutP is conserved within the subfamily of putative Na<sup>+</sup>/proline transporters and shown to be crucial for function.<sup>18</sup> Substitution of M56 and A337 by Cys led to a 20-fold and 3-fold increase of the Na<sup>+</sup> concentration required for half-maximum stimulation of transport [ $K_{0.5(\text{Na}^+)}$ ], respectively.<sup>18,19</sup> Previous functional and site-directed mutagenesis studies on PutP indicated that residue S340 is located in a potential ligand translocation pathway and that residue T341 directly participates in Na<sup>+</sup> binding.<sup>21</sup>

Based on these observations and experimental results, the Na<sup>+</sup> ion was placed in PutP in the

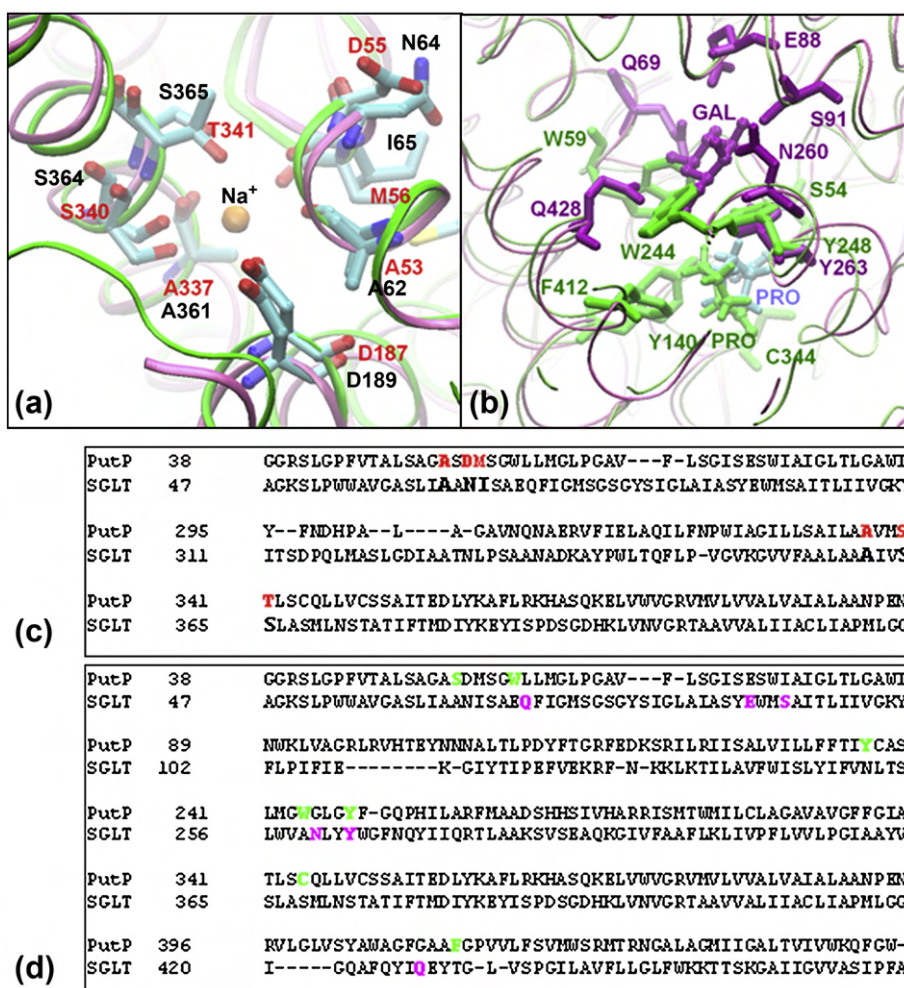


**Fig. 4.** Overlay of the  $\text{Na}^+$  binding sites (a) and ligand binding sites (b) of the PutP model and the vSGLT structure and corresponding local sequence alignments (c, d). PutP backbones are shown in green; vSGLT backbones are shown in pink. (a) The residues of PutP are labeled in red, and those of vSGLT in black. (b) The residues of PutP are shown and numbered in green, and those of vSGLT in pink. The substrates proline and galactose are shown in blue and pink, respectively.

vicinity of residues A53, M56, A337, S340, and T341 (Figs. 4a,c and 5a). This prediction is further supported by the fact that replacement of S365 in vSGLT, which is equivalent to T341 of PutP, completely abrogates  $\text{Na}^+$ -dependent transport.<sup>14</sup> Analysis of the evolutionary conservation scores of the PutP model reveals that all residues that take part in  $\text{Na}^+$  binding are highly conserved (Fig. 4a,c). In our model, the distance between  $\text{Na}^+$  and oxygen atoms of A337 and T341 is 2.8 Å, compared to distances of 3.2 Å and 3.7 Å between  $\text{Na}^+$  and the corresponding residues A361 and S365 in vSGLT (Fig. 5).<sup>14</sup> The oxygen atoms of A53, M56, and S340 are located in distances of 3.2 Å, 2.8 Å, and 2.9 Å from the  $\text{Na}^+$  ion, compared to distances of 3.6 Å, 3.3 Å, and 3.1 Å between  $\text{Na}^+$  and the corresponding residues A62, I65, and S364 in vSGLT. The large  $\text{Na}^+$ -oxygen distances in vSGLT may be due to the

fact that the vSGLT structure was probably observed in an ion-releasing state as proposed recently.<sup>22</sup> It should be noted that the  $\text{Na}^+$ -oxygen distances given for PutP are not experimentally verified. It remains unclear whether the differences of these distances between the PutP model and the vSGLT structure represent different  $\text{Na}^+$  binding states.

#### Key residues responsible for proline binding

The potential proline binding site(s) was (were) predicted using modified fragment-based Glide XP ligand docking calculations employing the constructed PutP homology model. To verify the accuracy of the Glide XP docking procedures, we used the Glide XP protocol to observe bound conformations of the galactose-vSGLT complex and compared the results to the original crystal

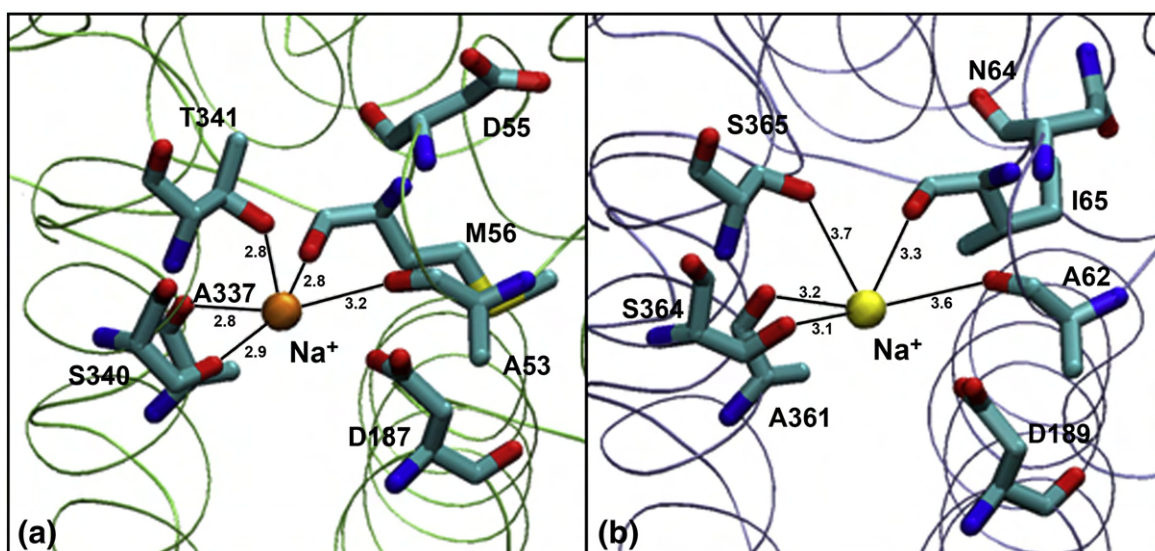


**Fig. 5.** Na<sup>+</sup> binding site organization in PutP (a) and vSGLT (b). The TMSs are drawn as green ribbons for PutP and as pink ribbons for vSGLT; Na<sup>+</sup> is colored orange. The PutP Na<sup>+</sup> binding site is composed of residues A53, M56, A337, S340, and T341 with distances of 3.2 Å, 2.8 Å, 2.8 Å, 2.9 Å, and 2.8 Å between the Na<sup>+</sup> ion and the corresponding residue. The vSGLT Na<sup>+</sup> binding site is composed of residues A62, I65, A361, S364, and S365 with distances of 3.6 Å, 3.3 Å, 3.2 Å, 3.1 Å, and 3.7 Å between the Na<sup>+</sup> ion and the corresponding residue. D55 and D187 of PutP are not within the liganding distance of a Na<sup>+</sup> at this position.

structure (data not shown). Like the galactose binding site in vSGLT, the PutP ligand binding site is located at the tip of the negatively charged inward-facing cavity at the approximate midpoint of the lipid bilayer and is accessible from the cytoplasmic side. However, it is shifted towards the cytoplasmic side by ~6 Å, and different residues not predictable by sequence alignments are involved in ligand binding (Fig. 4b).

The ligand binding site lies within a mainly hydrophobic pocket approximately halfway across the membrane, and it is lined by residues of TMSs 2, 4, 7, 9, and 11. The two ligand binding modes with the lowest energy have been used for the evaluation of the binding site (Table 1). In the first binding

mode, the proline pyrrolidine ring lies almost parallel with the membrane, forming hydrogen bonds with the hydroxyl groups of Y140 (TMS 4) and Y248 (TMS 7) (Fig. 6a). Binding is further stabilized by a hydrogen bond between the carboxyl group of proline and the S54 side chain (TMS 2).

In the second binding mode, the pyrrolidine ring of proline has a slightly different orientation and is no longer parallel with the membrane. In contrast to the first binding mode, the carboxyl group of the ligand does not form a hydrogen bond with S54, whereas the pyrrolidine ring of proline forms a hydrogen bond with the hydroxyl group of Y140. Furthermore, potential  $\pi$ -cation interactions have been observed between the ligand pyrrolidine ring

**Table 1.** Docking results for proline docked against the inward-facing PutP model using a fragment-based Glide XP docking approach

Mode	Gscore	Emodel	E	Hbond	Hbond ligand	Hbond protein	Hbond dist, Å	$\pi$ -cation inter	$\pi$ -cation inter	Protein residues located ~10 Å from the ligand molecule
1	-3.02	-27.14	-19.83	-0.70	HN	Tyr140:OH	1.9	0		Gln251, Pro252, Tyr248, Phe418, His253, Ile254, Val348, Phe136, Phe408, Trp59, Ser54, Thr341, Cys344, Gln345, Leu135, Val132, Phe418
					HN	Tyr248:OH	2.0			
					O	Tyr140:H	1.8			
					O	Ser54:H	1.8			
2	-3.10	-20.47	-16.10	0	HN	Tyr140:OH	2.1	-0.33	Trp59, Tyr140, Tyr248	Val348, His253, Ile254, Cys344, Gln345, Ser54, Pro252, Thr341, Asp55, Gln251, Tyr248, Val132, Phe136, Leu135, Phe418, Phe408, Trp59, Trp244

Gscore, total Glide scoring function; Emodel, model energy scoring function; E-modified Coulomb, van der Waals interaction energy; Hbond, hydrogen-bonding term;  $\pi$ -cation inter, reward for  $\pi$ -cation interaction.

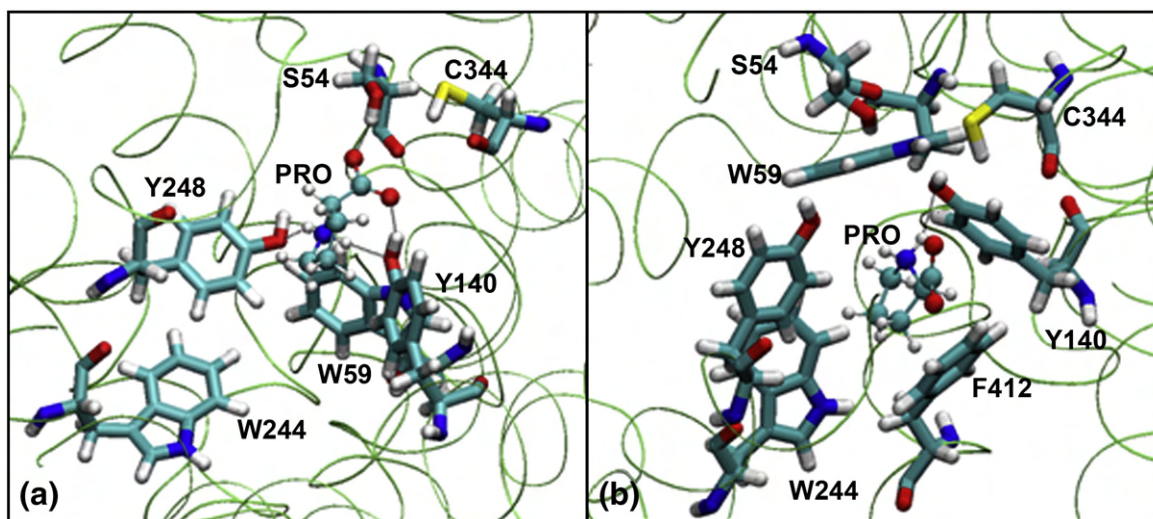


**Fig. 6.** The ligand binding site is located halfway across the membrane in the cytoplasmic cavity (a). It is lined by residues W59, Y140, W244, and Y248. (b) The second binding mode with a different orientation of the proline ligand in the binding pocket. Proline ligand is indicated in ball and stick; hydrogen bonds are shown as dot lines.

and the aromatic rings of residues W59, Y140, and Y248 (Fig. 6b). In both binding modes, the hydroxyl group of Y248 forms a hydrogen bond with the carboxyl oxygen of D55, a residue that influences  $\text{Na}^+$  binding.<sup>23,24</sup>

Besides that, residues W244 (TMS 7), C344 (TMS 9), and F412 (TMS 11), which are located in close proximity to the bound proline, give an additional contribution to the formation of the binding pocket via hydrophobic contacts. Residue W244 is highly conserved and separates the proline binding pocket from the small negatively charged cavity located nearby (Figs. 2 and 6). The native Cys residue at position 344 was previously shown to be important for proline binding and transport activity.<sup>19,25</sup>

## Experimental validation of the PutP model

### Functional significance of residues predicted to be involved in proline binding

In order to validate the model structure experimentally and to analyze the significance of the amino acids predicted to be involved in proline binding, residues W59, Y140, W244, Y248, and F412 were individually replaced with Cys and other more structurally related amino acids. Except F412, all these amino acids proved to be of particular functional significance (Fig. 7; Table 2). Most deleterious effects on transport under standard test conditions (70 mM NaCl, 10  $\mu\text{M}$  proline) were observed upon replacement of Y140, W244, or Y248

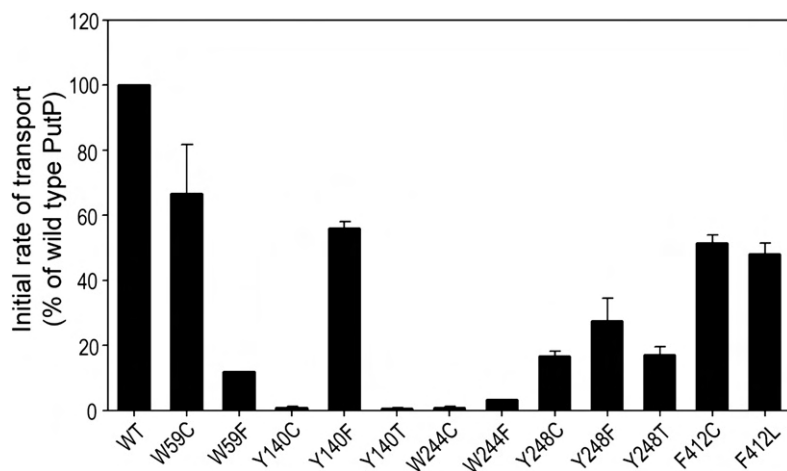


**Fig. 7.** Influence of the replacement of amino acids predicted to be involved in proline binding on  $\text{Na}^+$ -coupled proline uptake. The transport of  $\text{L-}^{14}\text{C}$ -proline (10  $\mu\text{M}$  final concentration) into cells of *E. coli* WG170 was assayed in the presence of 50 mM NaCl and 20 mM D-lactate ( $\text{Na}^+$ -salt) as electron donor at 25°C under aerobic conditions using a rapid filtration method. Initial rates of proline uptake are presented as percentage of the wild-type value ( $56 \pm 5$  nmol/min mg). Standard deviations were calculated from a minimum of three independent experiments.

**Table 2.** Proline uptake kinetics of PutP bearing replacements of given amino acid residues

PutP	$K_{m(\text{pro})}$ [ $\mu\text{M}$ ]	$K_{0.5(\text{Na}^+)}$ [ $\mu\text{M}$ ]	$V_{\text{max}}$ [nmol/min mg of protein]
Wild type	2.1±0.2	38±7	82.4±3.9
W59C	3.7±1.2 (2×↗) <sup>a</sup>	513±48 (14×↑)	44.2±3.1 (2×↘)
W59F	2.7±0.7 (1×→)	147±28 (4×↗)	9.9±0.5 (8×↓)
Y140C	24.3±9.0 (12×↑)	n.d. <sup>b</sup>	0.5±0.06 (165×↓)
Y140F	14.9±1.4 (7×↑)	91±16 (2×↗)	98.2±4.3 (1×→)
W244C	915±196 (436×↑)	33±5 (1×→)	7.8±0.6 (11×↓)
W244F	241±52 (115×↑)	30±6 (1×→)	25.9±3.3 (3×↘)
Y248C	3.9±0.8 (2×↗)	963±283 (26×↑)	23.0±3.2 (4×↘)
Y248T	6.3±1.3 (3×↗)	1,040±410 (27×↑)	22.0±4.6 (4×↘)
Y248F	51.7±1.9 (25×↑)	2,041±100 (54×↑)	130.2±8.5 (1.5×↗)
F412C	5.0±1.1 (2×↗)	40±10 (1×→)	27.9±1.4 (3×↘)
F412L	4.2±0.49 (2×↗)	29±1 (1×→)	43.9±1.1 (2×↘)

$L$ - $^{14}\text{C}$ -proline uptake by *E. coli* WG170 producing either PutP-wild-type or PutP with given replacements was measured in the presence of 50 mM NaCl and 20 mM D-lactate ( $\text{Na}^+$  salt) at proline concentrations from 0.2 to 500  $\mu\text{M}$  (in the case of PutP-W244C, up to 5000  $\mu\text{M}$ ). For determination of the ion-specific parameters [ $K_{0.5(\text{Na}^+)}$ ,  $K_{0.5(\text{Li}^+)}$ ], transport of 10  $\mu\text{M}$   $L$ - $^{14}\text{C}$ -proline was measured in the presence of 0.005 to 250 mM NaCl at 25 °C. The resulting data were plotted according to Lineweaver–Burk and Eadie–Hofstee using the kinetic module of the SigmaPlot software.

<sup>a</sup> The value in parentheses represents the dimension of deviation from the respective wild-type value, and the arrow indicates the direction of deviation.

<sup>b</sup> n.d.,  $K_{0.5(\text{Na}^+)}$  could not reliably be determined, since the extended washing procedure necessary to adjust the  $\text{Na}^+$  concentration of the cell suspension to values lower than 5  $\mu\text{M}$  reduced the proline uptake rate below the detection limit.

by a nonaromatic amino acid (initial rates of 1–16% of the wild-type value), while respective substitutions for W59 or F412 were comparatively well tolerated (initial rates of 65% and 50% of the wild-type value) (Fig. 7). The activity of PutP-Y140C was not influenced by the presence or absence of the native Cys at the neighboring position 141 (data not shown). Out of the substitutions tested for Y140 or Y248, Phe yielded the highest but still reduced activities (initial rates of 60% and 35% of the wild-type value), suggesting that both aromatic ring and hydroxyl group at these positions were crucial for function (Fig. 7). Transport activity remained low or was even further decreased upon substitution of W59 or W244 with Phe. Western blot analyses indicated that the reduced proline uptake rates were not or only to a minor extent due to changes of the amount of protein in the membrane. Only the reduced transport rates observed upon substitution of F412 were explained by reduced amounts of transporter molecules in the membrane (Fig. 8).

A more detailed kinetic analysis of transport revealed an increase of the apparent  $K_m$  for proline [ $K_{m(\text{pro})}$ ] by 1 order (Y140C, Y140F, Y248F) or 2 orders of magnitude (W244C, W244F) and minor alterations for the other substitutions (Table 2).

Changes of  $K_{m(\text{pro})}$  might arise from changes of the proline affinity and/or the rate of translocation following binding. Since for PutP the rate of proline binding was estimated to be >50-fold higher than the rate of translocation,<sup>12</sup> changes of the rate of translocation were expected to have only a low impact on  $K_{m(\text{pro})}$ . Instead, it was suggested that the elevated  $K_{m(\text{pro})}$  values observed upon substitution of Y140, W244, or Y248 arose, at least in part, from a decrease of the proline affinity. In particular, the elevated  $K_{m(\text{pro})}$  values together with the only slightly affected maximum rates of proline uptake ( $V_{\text{max}}$ ) of PutP-Y140F and PutP-Y248F supported the docking analysis-based prediction of a participation of the hydroxyl groups of the Tyr residues in proline binding either by direct interaction with the substrate or indirectly by stabilizing the substrate binding pocket. The other substitutions (Y140C; W244C,F; Y248C,T) altered  $V_{\text{max}}$  significantly (0.5–30% of the wild-type value), suggesting that the nature of the amino acid side chains at these positions was crucial not only for binding but also for a subsequent step in the transport cycle (Table 2). Replacement of W59 also reduced  $V_{\text{max}}$  but had little impact on  $K_{m(\text{pro})}$ . However,  $K_{0.5(\text{Na}^+)}$  was significantly increased upon substitution of the latter

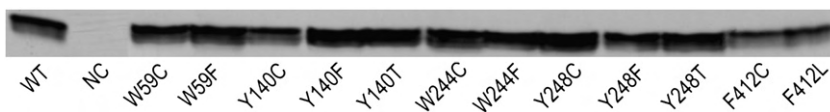


**Fig. 8.** Immunological detection of PutP containing given amino acid replacements. Total membrane protein (25  $\mu\text{g}$ ) of each mutant was separated by 12.5% SDS-PAGE.

Proteins were transferred onto a nitrocellulose membrane (0.45  $\mu\text{m}$  pore size) and probed with mouse anti-FLAG M2 monoclonal antibody linked to horseradish peroxidase. Detection was performed according to the enhanced chemiluminescence method. Cells transformed with plasmid pT7-5 without *putP* served as a negative control (NC).

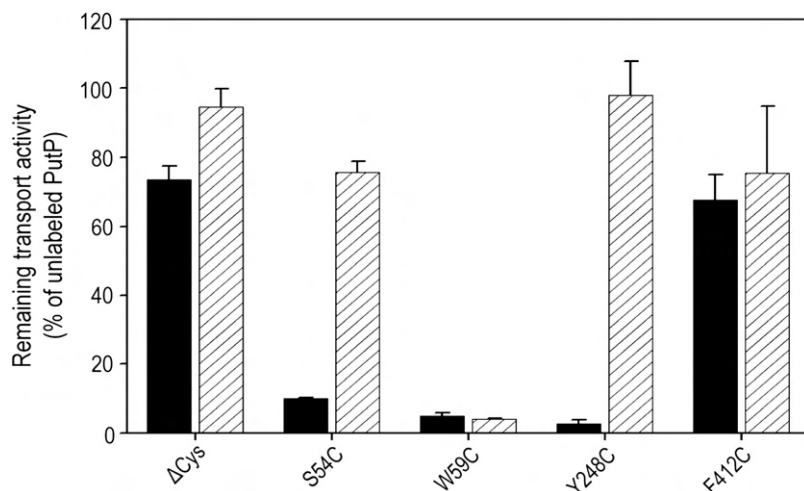


**Fig. 9.** Influence of sulfhydryl reagents on proline uptake into cells containing given PutP( $\Delta$ C) variants. Cells were incubated with 2 mM sulfhydryl reagent (NEM, MTSET) at room temperature for 15 min. The reaction was stopped by dilution with 100 mM Tris/Mes buffer (pH 6.0) containing 0.1% BSA. Cells were washed and resuspended in the same buffer without BSA, and transport was analyzed as described in the legend to Fig. 6. Activities of NEM (black columns) or MTSET-treated cells (striped columns) are presented as percentage of

activity of the respective unlabeled PutP( $\Delta$ C) variant. Standard deviations were calculated from a minimum of three measurements.

residue. In addition,  $K_{0.5(\text{Na}^+)}$  was elevated by more than 1 order of magnitude after replacement of Y248 (Table 2). The altered  $K_{0.5(\text{Na}^+)}$  might be due to defects in  $\text{Na}^+$  binding or a disturbed cooperativity between the sites of  $\text{Na}^+$  and proline binding. The reduced  $V_{\text{max}}$  values of the F412 substitutions were explained by the reduced amounts of PutP in the membrane.

Taken together, the kinetic analyses confirm the predicted functional significance of W59, Y140, W244, and Y248 and support the idea of a direct participation of Y140 and W244 in proline coordination and/or the gating mechanism. W59 and Y248 may be involved in coupling  $\text{Na}^+$  and proline binding. Contrary to the model-based prediction, the side chains of S54 and F412 are dispensable for function.

#### Cys accessibility analyses

Cys modification analyses were performed to probe the existence of hydrophilic cavities within the protein and to analyze the potential effects of ligands on the cavities. For this purpose, all Cys substitutions (S54C, W59C, Y140C, W244C, Y248, F412C) were placed into a Cys-free background [PutP( $\Delta$ C)]. PutP( $\Delta$ C) possessed about 50% of the wild-type activity,<sup>13</sup> and the resulting mutants exhibited an activity pattern that was similar to that of the mutants in the wild-type background (data not shown). Cys modification was assessed indirectly by probing the impact of sulfhydryl reagents [*N*-ethylmaleimide (NEM), membrane permeable; methanethiosulfonate ethyltrimethylammonium (MTSET), membrane impermeable] on the transport activity of intact cells, and directly by using fluorescein-5-maleimide (FM) for labeling and detection of Cys modification by fluorescence

measurements. FM labeling was performed with membrane vesicles, and fluorescence was detected after protein purification. The previously characterized PutP( $\Delta$ C)-D55C was included in the FM labeling analyses for comparison. The mutant was transport inactive, Cys was readily modified by sulfhydryl reagents, and modification was not influenced by ligands.<sup>18</sup>

NEM inhibited proline uptake by intact cells almost completely when Cys was placed at the position of S54, W59, or Y248 (Fig. 9). The activity of PutP( $\Delta$ C)-F412C was only slightly affected by NEM. MTSET blocked proline uptake by PutP( $\Delta$ C)-W59C, but had only little or no influence on the other mutants. The activities of PutP( $\Delta$ C)-Y140C and PutP( $\Delta$ C)-W244C were within the detection limit and did not allow a reliable detection of inhibitory effects. NEM modification of the native Cys at position 344 was previously demonstrated to inhibit transport in intact cells, while MTSET had no effect under these conditions.<sup>19</sup> FM readily modified Cys in place of S54 and D55 (Fig. 10). Under the same conditions, Cys at the position of Y140, W244, Y248, or F412 showed significantly lower labeling rates and was inaccessible to FM when placed at the position of W59. Since alkylating reagents are known to react with sulfhydryl groups in polar, but not in apolar, environments,<sup>26,27</sup> the observed NEM and FM labeling patterns suggested that S54, D55, and W59 are in contact with a polar (hydrophilic) environment. Furthermore, modification of Cys in place of W59 by NEM and MTSET in intact cells proposed a location of the residue in a hydrophilic cavity accessible from the outside, which was too narrow for the larger FM. Y140, W244, Y248, and F412 appeared to be located at more buried positions or in apolar environment under the test conditions (i.e., in the absence of ligands). Since the

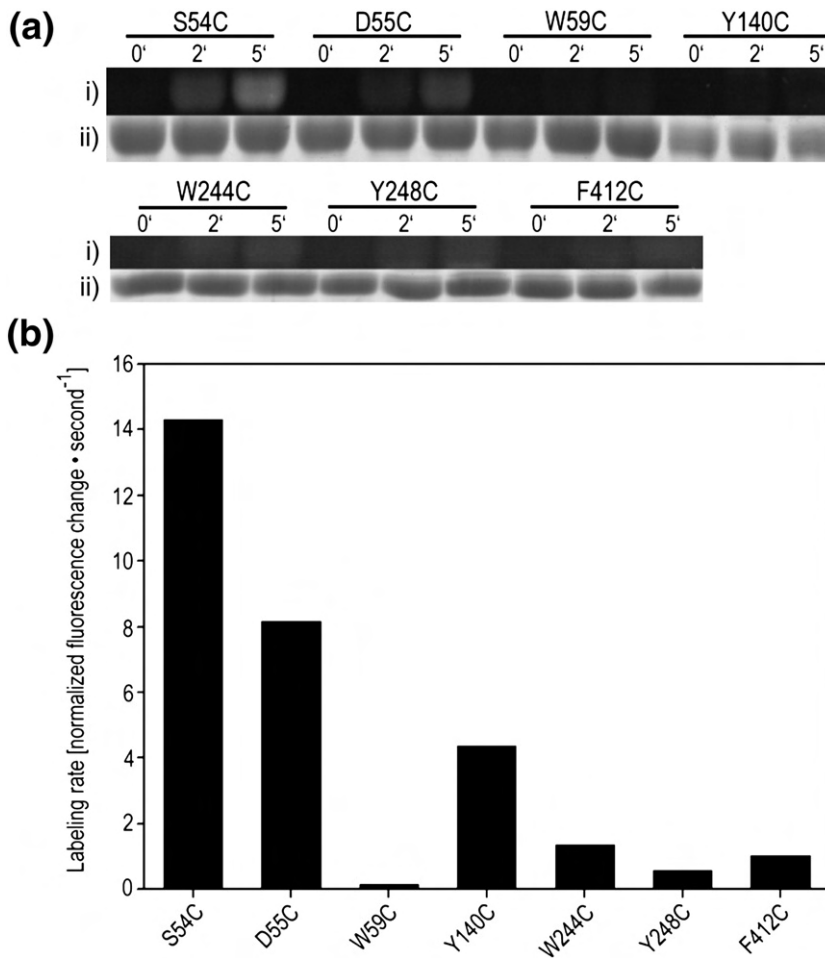


**Fig. 10.** Accessibility of Cys individually introduced into PutP( $\Delta$ C) to FM. One hundred microliters of a suspension of membranes of *E. coli* WG170 containing given PutP derivatives (10 mg of total membrane protein/mL) was incubated with 200  $\mu$ M FM for 0, 2, and 5 min. Labeling reactions were stopped by addition of 5 mM  $\beta$ -mercaptoethanol. After solubilization with 1.5% (w/v) *n*-dodecyl- $\beta$ -D-maltoside and purification via  $\text{Ni}^{2+}$ -NTA affinity chromatography, equal amounts of protein were loaded onto a 12.5% SDS-PAGE and separated. Fluorescent bands were detected using the gel documentation system N-08 of Peqlab. Afterwards, the same gel was stained with Coomassie Blue. The fluorescence intensities were corrected for background fluorescence and quantitatively analyzed using software ImageQuant 5.0 and plotted. (a-i) Fluorescent protein bands. (a-ii) Coomassie Blue-stained protein. (b) Rates of fluorescence labeling normalized to the amount of protein.

latter residues were proposed to line the large hydrophilic cavity (Fig. 2), the latter observation challenged our homology model.

However, the accessibility analyses described thus far were done in the absence of ligands, and our model does not necessarily show the structure of the empty transporter. Therefore, we analyzed the impact of  $\text{Na}^+$  and proline on Cys modification by FM. Ligand effects were analyzed under standard conditions by pre-equilibration of membranes with 30 mM NaCl (or KCl) and/or 10 mM proline prior to FM labeling (Fig. 11).  $\text{Na}^+$  stimulated the labeling rate of Cys placed at the position of Y140 about 5-fold compared to  $\text{Na}^+$ -free conditions. In addition, reaction of PutP( $\Delta$ C)-W244C with FM was stimulated by  $\text{Na}^+$  albeit to a significantly lesser extent (1.6-fold). These results suggested a direct participation of these positions in  $\text{Na}^+$ -induced conformational alterations and/or the opening of a cavity within the protein providing access to these positions. All other labeling reactions were not significantly influenced by  $\text{Na}^+$ .  $\text{K}^+$  was used in control experiments and affected the rate of Cys labeling only when used at concentrations higher than 250 mM (Figs. 11 and 12). Furthermore, proline

alone had no or only little effect on FM labeling. However, in the presence of  $\text{Na}^+$ , proline inhibited the rate of FM labeling of PutP( $\Delta$ C)-S54C (2-fold) and reversed the stimulatory  $\text{Na}^+$  effect on the labeling rate of PutP( $\Delta$ C)-Y140C (Fig. 11). These effects were not observed when  $\text{Na}^+$  was replaced by  $\text{K}^+$  (Fig. 11). In addition, proline at concentrations higher than 100 mM inhibited the labeling rate of PutP( $\Delta$ C)-W244C (Fig. 12). In these experiments, glycine was used as a negative control and did not influence FM labeling (Fig. 12). Finally, labeling of PutP( $\Delta$ C)-D55C, PutP( $\Delta$ C)-Y248C, and PutP( $\Delta$ C)-F412C was not influenced by  $\text{Na}^+$  or proline or a combination of both (data not shown).

The accessibilities of S54, D55, Y140, and W244 strongly supported a location of the residues at the boarder of a hydrophilic cavity as suggested by the PutP homology model. Thereby, the latter two positions required  $\text{Na}^+$  to improve contact with the cavity. On the contrary, the side chains of Y248 and F412 did not appear to be exposed to the cavity. Furthermore, the significant differences of the accessibilities of D55 and Y248 are in conflict with the model according to which the side chains are in hydrogen-bond distance. The possibility that the

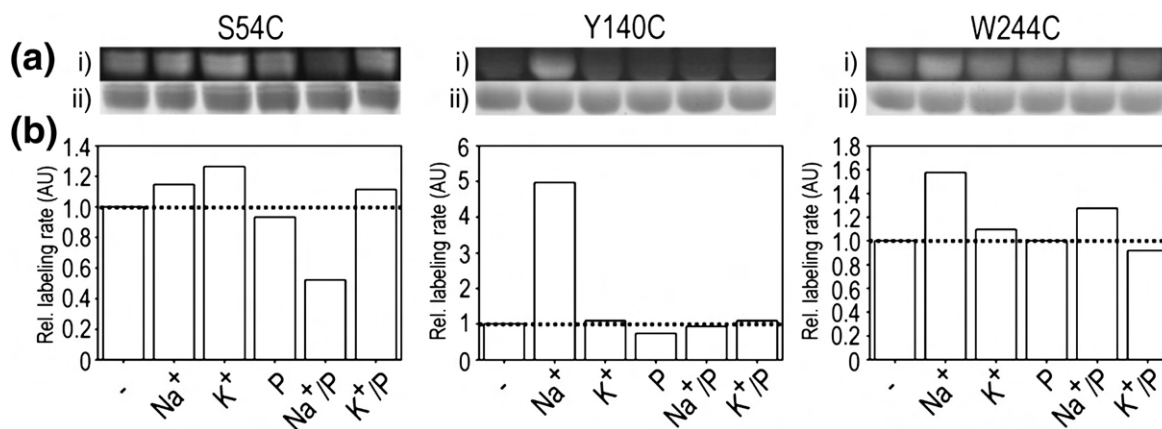


**Fig. 11.** Influence of ligands on the rate of Cys labeling with fluorescein-5-maleimide. Aliquots (100  $\mu$ L) of a suspension of membranes of *E. coli* WG170 containing given PutP( $\Delta$ C) derivatives (10 mg of total membrane protein/ml) were preincubated in the absence (-) or presence of 30 mM NaCl (Na<sup>+</sup>) or KCl (K<sup>+</sup>), 30 mM NaCl/10 mM proline (Na<sup>+</sup>/P), or 30 mM KCl/10 mM proline (K<sup>+</sup>/P) at 25°C for 10 min. Subsequently, labeling of the samples with 200  $\mu$ M FM was performed and protein was isolated as described in the legend to Fig. 6. (a-i) Fluorescent protein bands. (a-ii) Coomassie Blue-stained protein. (b) Relative rates of fluorescence labeling normalized to the amount of protein. The labeling rate in the absence of ligand was set to 1.0 for each PutP( $\Delta$ C) variant.

necessary Cys substitutions stabilize different conformational states cannot be excluded and may account for the differences. Clearly, we will also further test and improve the model.

## Discussion

In this study, we present a homology model of PutP from *E. coli* based on the crystal structure of

vSGLT. The model shows PutP (amino acids 38–481) with a LeuT-type structural motif in an inward-facing conformation. It is consistent with the available Cys accessibility, cross-linking, and electron paramagnetic resonance distance data as well as the 13 TMS motif of the previously proposed secondary-structure model of PutP, except that TMS 1 is omitted from the model.<sup>13,21,28</sup>

The Na<sup>+</sup> ion is placed at the intersection of TMS 2 (A53, M56) and TMS 9 (A337, S340, T341), which

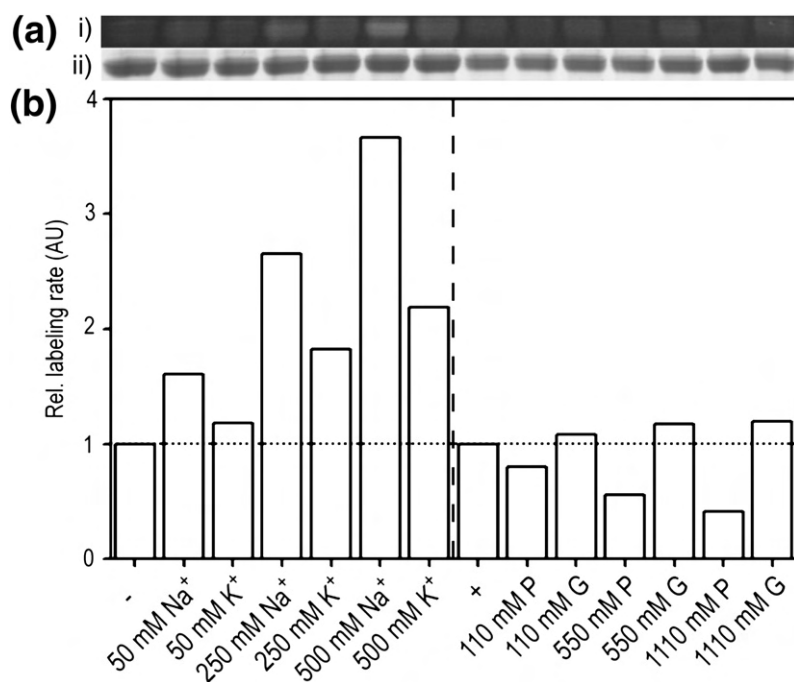


**Fig. 12.** Influence of ligands on the rate of FM labeling of PutP( $\Delta$ C)-W244C. Aliquots (100  $\mu$ L) of a suspension of membranes of *E. coli* WG170 containing PutP( $\Delta$ C)-W244C (10 mg of total membrane protein/ml) were preincubated in the absence (-) or presence of given concentrations of NaCl (Na<sup>+</sup>) and KCl (K<sup>+</sup>) (left half of graph) or in the presence of 30 mM NaCl (+) and given concentrations of proline (P) or glycine (G) (right half of graph) at 25°C for 10 min. Subsequently, labeling of the samples with 200  $\mu$ M FM was performed, and protein was isolated as described in the legend to Fig. 6. (a-i) Fluorescent protein bands. (a-ii) Coomassie Blue-stained protein. (b) Relative rates of fluorescence labeling normalized to the amount of protein. The labeling rate in the absence of ligand (-) was arbitrarily set to 1.0.

corresponds to the predicted Na<sup>+</sup> binding site in the homologous vSGLT and resembles the Na<sub>2</sub> binding site of LeuT.<sup>14,15</sup> With shorter Na<sup>+</sup>-oxygen distances compared to vSGLT, our model confirms and extends predictions of Na<sup>+</sup> coordinating residues in PutP from primary sequence alignments and experimental analyses.<sup>14,18,21</sup> Because of fundamental differences in substrate specificity, the sites of proline binding cannot be predicted by a simple primary sequence alignment of PutP and vSGLT. Also, a primary sequence alignment with amino acid transporters of the LeuT-type structural family does not yield helpful information due to low sequence identity (e.g., 13% with LeuT). Therefore, we used the PutP homology model for proline docking. The results suggest a proline binding site located at the inner end of the inward-facing cavity and formed by amino acids of TMS 2 (S54, W59), TMS 4 (Y140), TMS 7 (W244, Y248), TMS 9 (C344), and TMS 11 (F412). Substitution of the amino acids led in fact to the identification of four residues of particular significance for proline uptake (W59 in TMS 2, Y140 in TMS 4, W244 and Y248 in TMS 7), demonstrating the validity of our model as a guide for experimental analyses. C344 was already previously suggested to be close to the binding site, while the side chains of S54 and F412 do not seem to be of particular functional significance (Refs. 24, 25 and this study).

Do the above residues indeed participate in the formation of the proline binding pocket, or do they play different roles in the transport cycle? The following results support the idea of a direct interaction of Y140 and W244 with proline: (i) the residues are conserved within eubacterial (W244) and archaeal members (Y140) of the SSS family with experimentally demonstrated or predicted proline specificity, but are replaced by other amino acids in SSS members of different specificity (e.g., PanF, vSGLT, SGLT1); (ii) our docking analysis places proline close to both residues allowing hydrogen-bond formation,  $\pi$ -cation interaction, and/or hydrophobic contacts; (iii) substitution of Y140 or W244 dramatically alters transport kinetics including  $K_{m(\text{pro})}$ ; and (iv) Na<sup>+</sup> apparently stimulates accessibility of both residues via a hydrophilic cavity, while proline protects both positions. The latter behavior is consistent with an ordered binding mechanism of both ligands. In addition, it should be noted that tyrosine at a position corresponding to that of Y140 (middle of TMS 3 of the 10 TMS core) is part of the amino acid binding pockets of nonhomologous LeuT (Y108) and ApcT (Y97).<sup>15,16</sup> Furthermore, superimposition of the PutP homology model on the vSGLT structure places W244 adjacent to N260 of the sugar transporter. In vSGLT, N260 interacts with the sugar substrate.<sup>14</sup> Together with further comparisons with the crystal structures of LeuT, BetP, and Mhp1, our results lend further

support to the idea of a common location of the substrate binding site in transporters with a five-plus-five TMS inverted repeat core.<sup>14,15,29,30</sup> Substitution of key amino acids in this region seems to ensure substrate specificity.<sup>31</sup>

Contrary to Y140 and W244, substitution of W59 and Y248 in PutP affects  $K_{0.5(\text{Na}^+)}$  rather than  $K_{m(\text{pro})}$ . Also, the accessibility patterns differ significantly (e.g., Na<sup>+</sup> does not stimulate accessibility of the latter two positions). Based on their location between the sites of Na<sup>+</sup> and proline binding in our model, the residues may play a role in coupling Na<sup>+</sup> and proline transport and/or participate in forming a periplasmic gate. The latter idea is supported by the fact that superimposition of the PutP model with the vSGLT crystal structure places Y248 close to Y263 of vSGLT. Y263 participates in the formation of an inner hydrophobic gate that blocks the sugar binding site on the cytoplasmic side of vSGLT.<sup>14</sup> In addition, recent molecular dynamic simulations of vSGLT demonstrate that the release of sugar requires the rotation of the Y263 side chain without a significant change in vSGLT backbone conformation.<sup>32</sup> For PutP, it should also be noted that the hydroxyl group of Y248 forms a hydrogen bond with the carboxyl group of D55 in our model. D55 is essential for proline transport and was previously implicated in Na<sup>+</sup> binding.<sup>23</sup> Our new data suggest that D55 and Y248 play a role in the energy coupling mechanism instead of ligand coordination. Regarding the participation of S54 and F412 in proline binding proposed by our model, the lack of significant functional effects of side-chain alterations still leaves the possibility that substrate interacts with main-chain atoms at these sites, or proline binds elsewhere. Previous amino acid substitution analyses implicate S57 in proline coordination.<sup>18,33</sup> Like S54, the residue is part of the unwound region of TMS 2. In the current PutP model, S57 localizes between the sites of Na<sup>+</sup> and proline binding and may rather be involved in transmitting interactions between the two sites instead of making direct contact with one of the ligands. Clearly, further analyses are necessary to identify the complete network of proline coordinating sites. Here, the model will serve as a guide. In addition, a potential contribution of the hitherto omitted TMS 1 to ligand binding needs to be considered. Thus far, we have not identified amino acids in TMS 1 contributing to ligand binding in our experiments. However, this possibility also cannot be excluded.

In addition to the information on putative sites of ligand binding, the homology model allows a re-evaluation of the role residue D187 in transport. The residue is highly conserved within the SSS family and required for optimum PutP function.<sup>33</sup> Its substitution by a neutral residue makes proline uptake apparently independent from the presence of

Na<sup>+</sup>.<sup>33</sup> In our homology model, the residue is moved from a previously predicted cytoplasmic loop position into TMS 6 and is now located in a distance of 4.4 Å from the Na<sup>+</sup> ion (Fig. 5a). This location further supports our previous assumption that Asp187 is located close to the pathway of the coupling ion through the membrane and involved in the release of Na<sup>+</sup> on the cytoplasmic side of the membrane.<sup>33</sup> Similar observations have been made for the corresponding residue, D189, in human SGLT1.<sup>31,34</sup> Substitution of D189 in SGLT1 generates a glucose-gated H<sup>+</sup> channel.<sup>34</sup> Computational studies demonstrate that the amino acid side chain exhibits strong electrostatic interaction with the Na<sup>+</sup> ion, suggesting that D189 facilitates the diffusion of the ion toward the cytoplasm.<sup>31,32</sup>

Clearly, higher-resolution structural data will likely be needed to unambiguously interpret functional data on the mechanism of the Na<sup>+</sup>/proline symport. Nonetheless, in the absence of a crystal structure, the low-resolution model of PutP provides valuable first insights into the structural basis of the Na<sup>+</sup>/proline symport. The good agreement of the model with the results of the model-guided experimental studies demonstrates the relevance of the model as a structural framework for further studies on the transporter. For example, more data are needed to precisely locate a presumed outwardly facing cavity of PutP and to test whether outwardly and inwardly facing cavities open and close in a reciprocal manner as demanded by the alternating access mechanism. Also for this purpose, the homology model will serve as a guide.

## Materials and Methods

### Homology modeling

Homology modeling was performed by using the Prime module in Maestro (Prime, 1.6; Schrödinger, Portland, OR). The backbone coordinates for the core of the homology model were built based on the crystal structure of the inward-facing galactose/glucose vSGLT transporter from *V. parahaemolyticus* (PDB: 3DH4) as template. For the template structure, the bound ligand was kept. During the building of the homology model, the backbones were kept rigid for those cases in which the backbone does not need to be reconstructed due to gaps in the alignment. A Na<sup>+</sup> atom was placed into the PutP model using the corresponding LeuT<sub>Aa</sub> and vSGLT coordinates. The side chain of residue S340 was manually oriented to point towards the Na<sup>+</sup> ion and then minimized together with the side chains of the neighboring residues using a standard minimization procedure implemented in Prime (Schrödinger, Inc).

The sequence of PutP from *E. coli* was taken from the NCBI web site§ (ID: NP\_415535.1). Initial secondary-

structure prediction was done using the PSIPRED Protein Structure Prediction Server|| and Prime module in Maestro (Prime, 1.6; Schrödinger, Inc.). The HHpred web server¶ identified the Na<sup>+</sup>/galactose transporter vSGLT<sup>14</sup> and the Na<sup>+</sup>-independent amino acid transporter ApcT<sup>16</sup> as the closest relatives of known structures with *E*-values of 1.5e-37 and 1.3e-7 and HHSearch scores of 284.3 and 96.7, respectively. The Mhp1 transporter,<sup>29</sup> the glycine/betaine transporter BetP,<sup>30</sup> and the Na<sup>+</sup>/neurotransmitter symporter LeuT<sub>Aa</sub><sup>15</sup> were found as next possible hits. Therefore, the backbone coordinates for the core of the homology model were built based on the crystal structure of the inward-facing galactose/glucose vSGLT transporter from *V. parahaemolyticus* (PDB: 3DH4) as a template. The vSGLT structure possesses a gap in the loop region between residues I178 and V185, corresponding to positions T175–V183 of *E. coli* PutP. We used the sequence of vSGLT as an intermediate to build the gap and, thus, were able to use all residues of vSGLT.

### Homology model validation

The refined PutP homology model was subjected to a series of validation analyses for its consistency and reliability. The overall sequence identity between PutP and vSGLT is 19%, and the sequence similarity is 41%. The stereochemical quality of the model was analyzed using the MolProbity web server. It provides an all-atom contact analysis identifying any steric problems within the molecule and uses high-accuracy Ramachandran and rotamer distributions to check main chains and side chains for conformational outliers. In general, the PutP model scores were similar to those of the crystallographic structure of vSGLT. The distribution of the Ψ/Φ angles was well within the allowed regions. The majority (90.1%) of all residues was found in the favored regions of the plot, and almost all (98.1%) residues were found in the allowed regions. The corresponding percentages for the vSGLT template structure were 89.2 and 98.0. Several steric clashes and rotamers outliers were identified and fixed. Only 8 out of 357 residues of the subsequent PutP model were located in the disallowed regions, with four outliers being glycines (G58, G413, G451, and G465). Four more residues (S122, A182, K231, and Q251) were found in the loop regions near the surface of the model. Manual alteration of problematic Ψ/Φ angles along the entire protein backbone was performed during the refinement phase of the model construction. Comparing this result with similar ones for template crystal structures, we confirmed that the backbone conformations of the model structure are, by this criterion, as reliable as those of the template structure.

A validation check of the energetic properties of the homology model was performed using the ProSa web server. ProSa analysis of the PutP homology model revealed a *z*-score of -5.93 compared to the value of -6.22 for the vSGLT template, and it is in the range of native conformations of the template.

Next, we examined the locations of amphipathic aromatic residues (Trp and Tyr) and basic side chains

§ <http://www.ncbi.nlm.nih.gov/protein>

|| <http://bioinf.cs.ucl.ac.uk/psipred/>

¶ <http://toolkit.tuebingen.mpg.de>

(Lys and Arg) on the surface of the model. It has been found that rings of residues Y103, Y160, Y295, Y358, W373, Y403, and Y491 mark the potential interface in the PutP model, and residues R40, R91, R96, R98, R117, K121, R123, K482, R483, and R498 are clustered near the intracellular membrane-solvent interface. Therefore, the initial PutP homology model demonstrates a reliable surface side-chain distribution for a membrane protein.

The ConSurf algorithm<sup>a</sup> was applied to determine the level of conservation of each residue in the model.<sup>20</sup>

Finally, the model validation was followed by a comparison with the experimental results. It has been observed that the initial homology model was consistent with the experimental constraints available from the previous functional biochemical and electron paramagnetic resonance studies.<sup>13,18,19,21,28,35</sup>

## Docking

The structure of the proline ligand was taken from the PubChem Substance database<sup>b</sup> (compound ID: 145742) as sdf file and prepared for docking using the LigPrep utility (Schrödinger, Portland, OR) with Epik (Schrödinger, Portland, OR) to define protonation and tautomeric states at pH 7.0±2.0. The PutP model structure was prepared using the Protein Preparation Wizard utilities (Schrödinger, Portland, OR) in Maestro with the default options to assign the charge states of ionizable residues and add hydrogens. This procedure optimizes the protein's hydrogen bond network by means of a systematic, cluster-based approach and performs a restrained minimization that allows hydrogen atoms to be freely minimized while allowing for sufficient heavy-atom movement to relax strained bonds, angles, and clashes. Flexible docking calculations were performed with Glide XP 5.0 (Grid-based Ligand Docking from Energetics)<sup>36,37</sup> (Schrödinger, Portland, OR) following the fragment-based procedure in order to increase the number of energetically favorable poses to the value of 1000.<sup>38</sup> The scoring function Gscore was employed to rank all poses. The final choice of the best-docked structure for each ligand was made using a model energy score (Emodel) that combines the energy grid score, the binding affinity predicted by Glide score, and the internal strain energy for the model potential used to direct the conformational-search algorithm. After docking, the best poses were minimized within the protein model. This minimization was performed using conjugate gradient minimization (0.05 convergence criteria), the OPLS-AA force field, and the GB/SA continuum water model. Protein residues that fell within 10 Å of the binding sites were allowed to optimize during minimization.

## Validation of the docking procedure

To verify the accuracy of the Glide XP docking procedures, we re-docked the galactose to the crystal structure of vSGLT and compared the results to the original crystal structure. First, we moved the ligand galactose out of the active site and then docked it back to

the corresponding vSGLT crystal structure after a minimization of the galactose-free structure. The best docked poses closely match the crystallographic ligand position. This result is in good agreement with the crystal structure of vSGLT, where the galactose binding pocket is formed by residues Q69, E88, S91, N260, Y263, K294, and Q428.<sup>14</sup> Our calculations show that the docked galactose molecule was bound in a similar orientation and conformation to the active site of vSGLT. Therefore, the docking results clearly show that the Glide XP docking algorithm and scoring function are able to consistently produce top-scoring poses that are in close agreement with the crystal structure pose.

## Bacterial strains and plasmids

*E. coli* JM109 [*endA1 recA1 gyrA96 thi hsdR17 supE44 relA1 Δ(lac-proAB) (F' traΔ36pro AB+ lacIq ZΔM15)*] and *E. coli* DH5α [*F' φ80d lacZ ΔM15 Δ(lacZYA-argF) U169 deoR recA1 endA1 hsd R17(rk<sup>-</sup>,mk<sup>+</sup>) phoA supE44 λ<sup>-</sup> thi-1 gyrA96 relA1*] were used as carriers for the plasmids generated in this study. *E. coli* WG170 [*F' trp lacZ rpsL thi Δ(putPA)101 proP219*]<sup>39</sup> harboring given plasmids was used for overexpression of the *putP* gene and transport assays. The following plasmids, derivatives of pT7-5,<sup>40</sup> containing the *lac* promoter/operator for expression of the *putP* gene, were used for all gene manipulations: pT7-5/*putP* and pT7-5/*putP*(ΔC), each of which harboring a cassette version of the *putP* gene encoding PutP-wild-type and an engineered transporter devoid of all five native Cys residues [PutP(ΔC)], respectively, and a C-terminal attached amino acid sequence resembling the FLAG epitope and a 6His tag.<sup>13</sup> Vector pTrc99a<sup>41</sup> was used for overexpression.

## Site-directed mutagenesis

Desired nucleotide substitutions in *putP* were generated by PCR with *Taq*-DNA polymerase using plasmid pT7-5/*putP* as a template and synthetic mutagenic oligonucleotides. Altered sequences were cloned into plasmid pT7-5/*putP* or pT7-5/*putP*(ΔC). Resulting plasmid DNA was verified by sequencing using an ABI 3730 device.

## Transport assay

Active transport was measured in *E. coli* WG170 (PutP<sup>-A</sup>) harboring derivatives of plasmids pT7-5/*putP* or pT7-5/*putP*(ΔC) encoding PutP with given amino acid replacements. The cells were grown aerobically in LB medium<sup>42</sup> containing 100 μg/mL ampicillin at 37 °C. Overnight cultures were diluted 25-fold and were allowed to grow to an optical density at 420 nm (OD<sub>420</sub>) of 1.0, followed by induction with 0.5 mM IPTG for 2 h. Cells were harvested by centrifugation at 13,200g for 10 min and washed up to six times with 100 mM Tris/Mes (pH 6.0) at 4 °C to reduce the Na<sup>+</sup> contamination below 5 μM. For transport assays, cells were resuspended in the same buffer and adjusted to a total protein concentration of 0.35 mg/mL. Transport of 10 μM L-<sup>14</sup>C-proline (26 Ci/mol) (if not otherwise indicated) was assayed under standard test conditions in the presence of 20 mM D-lactate (Na<sup>+</sup> salt)

<sup>a</sup> <http://consurf.tau.ac.il>

<sup>b</sup> <http://www.ncbi.nlm.gov/sites/entrez>

and 50 mM NaCl. Transport assays were terminated at various time points (0, 0.17, 0.5, 1, 2, 5, 10, 30 min) using the rapid filtration method as described.<sup>23</sup> Initial rates of transport were calculated from the initial linear portion of the time course. Standard deviations were determined from at least three independent experiments. For transport inhibition analyses, cells containing the respective single Cys variant were incubated with 2 mM sulfhydryl reagent (NEM or MTSET) at room temperature for 15 min. The reaction was stopped by 5-fold dilution of the reaction mixture with 100 mM Tris/Mes buffer (pH 6.0) containing 0.1% bovine serum albumin (BSA). Cells were washed and resuspended in the same buffer without BSA, and transport was analyzed as described above.

### Immunological analysis

Relative amounts of PutP with given amino acid replacements in membranes of *E. coli* WG170 were estimated by Western blot analysis with HRP-linked mouse anti-FLAG IgG directed against the FLAG epitope at the C terminus of each PutP variant as described before.<sup>23</sup>

### Cys accessibility to fluorescein-5-maleimide

*E. coli* WG170 transformed with pTrc99a/*putP*( $\Delta$ C) were grown and disrupted by sonification, and randomly oriented membrane vesicles were prepared as described.<sup>18</sup> For accessibility analyses, 100- $\mu$ L aliquots of the membrane suspension containing 10 mg/mL total protein were incubated without or with Na<sup>+</sup>, K<sup>+</sup>, and/or L-proline at given concentrations at 25 °C for 10 min. Subsequently, 200  $\mu$ M FM was added and incubation was continued at 25 °C for additional 0, 2, and 5 min. Reactions were stopped by addition of 5 mM  $\beta$ -mercaptoethanol. After labeling, PutP was solubilized with 1.5% (w/v) *n*-dodecyl- $\beta$ -D-maltoside under stirring at 4 °C for 30 min. Then, samples were purified via Ni<sup>2+</sup>-NTA spin columns and eluted with 200 mM imidazole as described before.<sup>19</sup> After protein determination, equal amounts of protein were subjected to a 12.5% SDS-PAGE. Fluorescent bands of PutP were visualized using the gel documentation system N-08 of Peqlab and quantified using the software ImageQuant 5.0. After analysis of fluorescent PutP bands, the gel was stained with Coomassie Blue to detect total amounts of protein.

### Determination of Na<sup>+</sup>

Na<sup>+</sup> concentrations in buffers used for transport assays and Cys accessibility analyses were determined with a VARIAN AA240 atomic absorption spectrometer.

### Protein determination

Determination of protein was performed according to a modified Lowry method<sup>27</sup> for total membrane protein, according to Bradford<sup>43</sup> for detergent solubilized protein, and by the amido black method<sup>44</sup> for protein in proteoliposomes.

## Acknowledgements

This work was financially supported by the Deutsche Forschungsgemeinschaft (Ju333/3-2, Ju333/4-2 and Exc114-1) and the Max-Planck-Gesellschaft. M.R. is a fellow of the Elite Network of Bavaria. We thank Prof. E. Padan (Hebrew University of Jerusalem) and Prof. H. Michel (Max Planck Institute of Biophysics) for critical reading of the manuscript.

## Supplementary Data

Supplementary data associated with this article can be found, in the online version, at [doi:10.1016/j.jmb.2010.11.045](https://doi.org/10.1016/j.jmb.2010.11.045)

## References

- Jung, H. (2002). The sodium/substrate symporter family: structural and functional features. *FEBS Lett.* **529**, 73–77.
- Wright, E. M. & Turk, E. (2004). The sodium/glucose cotransport family SLC5. *Pflugers Arch.* **447**, 510–518.
- Reizer, J., Reizer, A. & Saier, M. H., Jr (1994). A functional superfamily of sodium/solute symporters. *Biochim. Biophys. Acta*, **1197**, 133–166.
- Jardetzky, O. (1966). Simple allosteric model for membrane pumps. *Nature*, **211**, 969–970.
- West, I. C. (1997). Ligand conduction and the gated-pore mechanism of transmembrane transport. *Bioch. Biophys. Acta*, **1331**, 213–234.
- Smirnova, I., Kasho, V., Sugihara, J. & Kaback, H. R. (2009). Probing of the rates of alternating access in LacY with Trp fluorescence. *Proc. Natl Acad. Sci. USA*, **106**, 21561–21566.
- Shimamura, T., Weyand, S., Beckstein, O., Rutherford, N. G., Hadden, J. M., Sharples, D. *et al.* (2010). Molecular basis of alternating access membrane transport by the sodium-hydantoin transporter Mhp1. *Science*, **328**, 470–473.
- Yamato, I. & Anraku, Y. (1993). Na<sup>+</sup>/substrate symport on prokaryotes. In (Bakker, E. P., ed.), pp. 53–76, CRC-Press, Boca Raton.
- Jung, H., Pirch, T. & Hilger, D. (2006). Secondary transport of amino acids in prokaryotes. *J. Membr. Biol.* **213**, 119–133.
- Eskandari, S., Loo, D. D., Dai, G., Levy, O., Wright, E. M. & Carrasco, N. (1997). Thyroid Na<sup>+</sup>/I<sup>-</sup> symporter. Mechanism, stoichiometry, and specificity. *J. Biol. Chem.* **272**, 27230–27238.
- Wright, E. M., Loo, D. D., Panayotova-Heiermann, M., Hirayama, B. A., Turk, E., Eskandari, S. & Lam, J. T. (1998). Structure and function of the Na<sup>+</sup>/glucose cotransporter. *Acta Physiol. Scand. Suppl.* **643**, 257–264.
- Zhou, A., Wozniak, A., Meyer-Lipp, K., Nietschke, M., Jung, H. & Fendler, K. (2004). Charge translocation during cosubstrate binding in the Na<sup>+</sup>/proline transporter of *E. coli*. *J. Mol. Biol.* **343**, 931–942.
- Jung, H., Rübenthal, R., Tebbe, S., Leifker, K., Tholema, N., Quick, M. & Schmid, R. (1998). Topology

- of the Na<sup>+</sup>/proline transporter of *Escherichia coli*. *J. Biol. Chem.* **273**, 26400–26407.
14. Faham, S., Watanabe, A., Besserer, G. M., Cascio, D., Specht, A., Hirayama, B. A. *et al.* (2008). The crystal structure of a sodium galactose transporter reveals mechanistic insights into Na<sup>+</sup>/sugar symport. *Science*, **321**, 810–814.
  15. Yamashita, A., Singh, S. K., Kawate, T., Jin, Y. & Gouaux, E. (2005). Crystal structure of a bacterial homologue of Na<sup>+</sup>/Cl<sup>-</sup> dependent neurotransmitter transporters. *Nature*, **437**, 215–223.
  16. Shaffer, P. L., Goehring, A., Shankaranarayanan, A. & Gouaux, E. (2009). Structure and mechanism of a Na<sup>+</sup>-independent amino acid transporter. *Science*, **325**, 1010–1014.
  17. Gavel, Y., Nilsson, L. & von Heijne, G. (1988). Mitochondrial targeting sequences. Why 'non-amphiphilic' peptides may still be amphiphilic. *FEBS Lett.* **235**, 173–177.
  18. Pirch, T., Landmeier, S. & Jung, H. (2003). Transmembrane domain II of the Na<sup>+</sup>/proline transporter PutP of *Escherichia coli* forms part of a conformationally flexible, cytoplasmic exposed aqueous cavity within the membrane. *J. Biol. Chem.* **278**, 42942–42949.
  19. Raba, M., Baumgartner, T., Hilger, D., Klempahn, K., Härtel, T., Jung, K. & Jung, H. (2008). Function of transmembrane domain IX in the Na<sup>+</sup>/proline transporter PutP. *J. Mol. Biol.* **382**, 884–893.
  20. Landau, M., Mayrose, I., Rosenberg, Y., Glaser, F., Martz, E., Pupko, T. & Ben-Tal, N. (2005). ConSurf 2005: the projection of evolutionary conservation scores of residues on protein structures. *Nucleic Acids Res.* **33**, W299–302.
  21. Hilger, D., Böhm, M., Hackmann, A. & Jung, H. (2008). Role of Ser-340 and Thr-341 in transmembrane domain IX of the Na<sup>+</sup>/proline transporter PutP of *Escherichia coli* in ligand binding and transport. *J. Biol. Chem.* **283**, 4921–4929.
  22. Li, J. & Tajkhorshid, E. (2009). Ion-releasing state of a secondary membrane transporter. *Biophys. J.* **97**, L29–L31.
  23. Quick, M. & Jung, H. (1997). Aspartate 55 in the Na<sup>+</sup>/proline permease of *Escherichia coli* is essential for Na<sup>+</sup>-coupled proline uptake. *Biochemistry*, **36**, 4631–4636.
  24. Pirch, T., Quick, M., Nietschke, M., Langkamp, M. & Jung, H. (2002). Sites important for Na<sup>+</sup> and substrate binding in the Na<sup>+</sup>/proline transporter of *Escherichia coli*, a member of the Na<sup>+</sup>/solute symporter family. *J. Biol. Chem.* **277**, 8790–8796.
  25. Hanada, K., Yoshida, T., Yamato, I. & Anraku, Y. (1992). Sodium ion and proline binding sites in the Na<sup>+</sup>/proline symport carrier of *Escherichia coli*. *Biochim. Biophys. Acta*, **1105**, 61–66.
  26. Poelarends, G. & Konings, W. N. (2002). The transmembrane domains of the ABC multidrug transporter LmrA form a cytoplasmic exposed, aqueous chamber within the membrane. *J. Biol. Chem.* **277**, 42891–42898.
  27. Guan, L. & Kaback, H. R. (2007). Site-directed alkylation of cysteine to test solvent accessibility of membrane proteins. *Nat. Protoc.* **2**, 2012–2017.
  28. Wegener, C., Tebbe, S., Steinhoff, H. J. & Jung, H. (2000). Spin labeling analysis of structure and dynamics of the Na<sup>+</sup>/proline transporter of *Escherichia coli*. *Biochemistry*, **39**, 4831–4837.
  29. Weyand, S., Shimamura, T., Yajima, S., Suzuki, S. i., Mirza, O., Krusong, K. *et al.* (2008). Structure and molecular mechanism of a nucleobase-cation-symport-1 family transporter. *Science*, **322**, 709–713.
  30. Ressler, S., Terwisscha van Scheltinga, A. C., Vonnrhein, C., Ott, V. & Ziegler, C. (2009). Molecular basis of transport and regulation in the Na<sup>+</sup>/betaine symporter BetP. *Nature*, **458**, 47–52.
  31. Abramson, J. & Wright, E. M. (2009). Structure and function of Na<sup>+</sup>-symporters with inverted repeats. *Curr. Opin. Struct. Biol.* **19**, 425–432.
  32. Zomot, E. & Bahar, I. (2010). The sodium/galactose symporter crystal structure is a dynamic, not so occluded state. *Mol. Biosyst.* **6**, 1040–1046.
  33. Quick, M., Tebbe, S. & Jung, H. (1996). Ser57 in the Na<sup>+</sup>/proline permease of *Escherichia coli* is critical for high-affinity proline uptake. *Eur. J. Biochem.* **239**, 732–736.
  34. Quick, M., Loo, D. D. & Wright, E. M. (2001). Neutralization of a conserved amino acid residue in the human Na<sup>+</sup>/glucose transporter (hSGLT1) generates a glucose-gated H<sup>+</sup> channel. *J. Biol. Chem.* **276**, 1728–1734.
  35. Jeschke, G., Wegener, C., Nietschke, M., Jung, H. & Steinhoff, H. J. (2004). Interresidual distance determination by four-pulse double electron–electron resonance in an integral membrane protein: the Na<sup>+</sup>/proline transporter PutP of *Escherichia coli*. *Biophys. J.* **86**, 2551–2557.
  36. Friesner, R. A., Banks, J. L., Murphy, R. B., Halgren, T. A., Klicic, J. J., Mainz, D. T. *et al.* (2004). Glide: a new approach for rapid, accurate docking and scoring. 1. Method and assessment of docking accuracy. *J. Med. Chem.* **47**, 1739–1749.
  37. Friesner, R. A., Murphy, R. B., Repasky, M. P., Frye, L. L., Greenwood, J. R., Halgren, T. A. *et al.* (2006). Extra precision glide: docking and scoring incorporating a model of hydrophobic enclosure for protein–ligand complexes. *J. Med. Chem.* **49**, 6177–6196.
  38. Loving, K., Salam, N. & Sherman, W. (2009). Energetic analysis of fragment docking and application to structure-based pharmacophore hypothesis generation. *J. Comput. Aided Mol. Des.* **23**, 541–554.
  39. Stalmach, M. E., Grothe, S. & Wood, J. M. (1983). Two proline porters in *Escherichia coli* K-12. *J. Bacteriol.* **156**, 481–486.
  40. Tabor, S. & Richardson, C. C. (1985). A bacteriophage T7 RNA polymerase/promoter system for controlled exclusive expression of specific genes. *Proc. Natl Acad. Sci. USA*, **82**, 1074–1078.
  41. Amann, E., Ochs, B. & Abel, K. J. (1988). Tightly regulated *tac* promoter vectors useful for the expression of unfused and fused proteins in *Escherichia coli*. *Gene*, **69**, 301–315.
  42. Miller, J. H. (1992). *A short course in bacterial genetics. A laboratory manual and handbook for Escherichia coli and related bacteria*. Cold Spring Harbor Laboratory Press, Cold Spring Harbor, New York.
  43. Bradford, M. M. (1976). A rapid and sensitive method for the quantitation of microgram quantities of protein utilizing the principle of protein–dye binding. *Anal. Biochem.* **72**, 248–254.
  44. Peterson, G. L. (1977). A simplification of the protein assay method of Lowry *et al.* which is more generally applicable. *Anal. Biochem.* **83**, 346–356.

## 4 LIGAND-DEPENDENT STRUCTURAL DYNAMICS OF EXTRACELLULAR LOOP 4 OF PUTP, A MEMBER OF THE LEUT STRUCTURAL FAMILY

### 4.1 Abstract

The structural class of LeuT-like transporters comprises a diverse group of permeases that is important for the uptake of a broad range of substrates such as amino acids, ions, sugars, or neurotransmitters. Representatives of this structural family are involved in a variety of human diseases and play a role in bacterial pathogenicity and are therefore targets for therapeutical approaches. Despite the rapidly increasing number of available crystal structures little is known about protein dynamics during the transport cycle. Deduced from the available crystal structures, several slightly different transport mechanisms were proposed, focusing mainly on movements of transmembrane helices. Within this work the Na<sup>+</sup>/proline symporter PutP of *Escherichia coli* was used to examine the mechanistic role of extracellular loop 4 during the transport process. To analyze the functional importance of this domain a Cys scanning mutagenesis was performed in combination with subsequent spin-labeling, reconstitution, and electron paramagnetic resonance spectroscopic analyses. Overall conformational rearrangements in PutP were tracked by double electron-electron resonance measurements of distances. The data obtained provided first insights into the secondary structure of eL4 and ligand dependent motions of this domain. The results are in good agreement with the proposed alternating access mechanism of secondary transporters and suggest an involvement of eL4 in the gating mechanism.

### 4.2 Introduction

The sodium/solute symporter family (SSSF; TC 2.A.21; SLC5) comprises several hundred representatives, which can be found in all three kingdoms of life (Jung *et al.*, 2012). Members of this group of transporters use a preexisting Na<sup>+</sup> gradient to drive the uphill transport of various solutes such as amino acids, vitamins, or ions across the membrane (Jung, 2002). The human Na<sup>+</sup>/I<sup>-</sup> symporter (NIS) and the Na<sup>+</sup>/glucose transporter (SGLT1) were shown to be involved in diseases such as iodide transport defect (Reed-Tsur *et al.*, 2008) or glucose-galactose malabsorption (Wright *et al.*, 2007). Moreover, PutP-mediated proline uptake in bacteria plays an important role in human infectious diseases. In *Staphylococcus aureus*, the proline permease contributes to the survival of the pathogen in the host organism (Bayer *et al.*, 1999). Furthermore, a knock out of the homologous gene in

*Helicobacter pylori* abolished its ability to colonize the stomach of model organisms (Kavermann *et al.*, 2003).

To understand the molecular principles of Na<sup>+</sup>-coupled transport the Na<sup>+</sup>-dependent proline permease PutP of *Escherichia coli* was used, the functionally best-characterized member of the SSSF. Kinetic analysis suggested that this symporter functions according to an ordered binding mechanism (Yamato & Anraku, 1990, Yamato, 1992). The Na<sup>+</sup>-coupled proline uptake is mediated with a stoichiometry of 1:1 (Yamato, 1992, Yamato & Anraku, 1990). For PutP a topology model comprising 13 TMs was proposed with the N-terminus facing the periplasm and the C-terminus found in the cytoplasm (Suppl. Fig. 4.2) (Wegener *et al.*, 2000, Jung *et al.*, 1998a). With the successful crystallization of vSGLT of *Vibrio parahaemolyticus*, first insights into the architecture of SSSF transporters were gained at atomic resolution (Faham *et al.*, 2008). The three dimensional structure revealed that the SSSF shares the same fold with the LeuT structural family, a group of unrelated transporter gene families that turned out to have a 10 TM core domain in common (Abramson *et al.*, 2003, Yernool *et al.*, 2004, Schulze *et al.*, 2010, Faham *et al.*, 2008, Weyand *et al.*, 2008, Murakami *et al.*, 2002, Ressler *et al.*, 2009, Yamashita *et al.*, 2005). The available structural information on vSGLT was used to generate a homology model of PutP (Olkhova *et al.*, 2010). Using a combination of docking calculations and functional analyses, Na<sup>+</sup> and proline binding residues were identified.

Despite the increasing number of available transporter crystal structures with LeuT-like core architecture, detailed information on the protein dynamics during the translocation cycle is rather low. Based on the available structural information on LeuT, a molecular mechanism of function was proposed (Forrest *et al.*, 2008, Forrest & Rudnick, 2009). According to this model the reciprocal opening and closing of an outward- and an inward-facing cavity is achieved by a 'rocking bundle' motion of two domains formed by topologically inverted repeats. Movements of TMs 1, 2, 6, and 7 with respect to the remaining protein 'scaffold' were predicted. The importance of these helices for transport was supported by LeuT structures in the outward- and inward facing conformation (Krishnamurthy & Gouaux, 2012). Major conformational alterations were shown for TMs 1, 2, 5, 6, and 7. A similar mechanism was suggested for the Na<sup>+</sup>/L-5-benzyl-hydantoin symporter Mhp1 of *Microbacterium liquefaciens* based on crystal structures of different conformations (Shimamura *et al.*, 2010). In this symporter, the so-called 'hash' motif, a protein domain comprising TMs 3, 4, 8, and 9, moves relative to the rest of the protein during the transport cycle. These rigid body motions are proposed to be the basis for the alternating access to the substrate binding site from either side of the membrane. Since crystal structures just provide static snapshots of proteins and transitions between different conformational states are just

extrapolated, biochemical and biophysical studies are indispensable to directly address transporter dynamics.

Available high-resolution structures were used as a starting point to guide electron paramagnetic resonance (EPR) spectroscopic and single molecule fluorescence energy resonance transfer (smFRET) measurements in LeuT and other members of the structural family. For LeuT, it was shown that TM1a is involved in the transition between the outward-facing and the inward-facing conformation (Zhao *et al.*, 2010, Zhao *et al.*, 2011). EPR spectroscopic analysis of TM 1' of PutP suggests that this helix plays a similar role in the transport cycle as in LeuT. Binding of proline in the presence of Na<sup>+</sup> induced conformational alterations in the respective helix and the preceding loop (Wegener *et al.*, 2000). Moreover, a Cys scanning mutagenesis in combination with Cys accessibility analyses supported these findings (Pirch *et al.*, 2003). The data suggest that the cytoplasmic half of TM 1' is involved in the formation of a water-filled inwardly oriented cavity that is occluded upon Na<sup>+</sup> and proline binding.

Interestingly, it was shown that closing of the outward-facing cavity is not exclusively achieved by movements of transmembrane helices. In Mhp1 an  $\alpha$ -helical domain in extracellular loop 4 (eL4), connecting TMs 7 and 8, contributes to the formation of a 'thick' gate that occludes the substrate binding site (Shimamura *et al.*, 2010). The general importance of this loop structure for the molecular mechanism of function of LeuT-like transporters was also supported by biophysical measurements on LeuT (Claxton *et al.*, 2010). EPR spectroscopic analyses could demonstrate that eL4 regulates access from the extracellular milieu to the ion and substrate binding sites in a Na<sup>+</sup> and leucine dependent manner. These data were supported by the comparison of crystal structures of LeuT in an outward-open and an inward-open conformation (Krishnamurthy & Gouaux, 2012). The transition of an outward-facing open to an inward-facing open conformation comes along with a substrate dependent movement of eL4 into the outward-facing cavity thereby occluding the binding site from the extracellular space. The functional role of eL4 is also described for eukaryotic representatives of this structural family. Cys accessibility analyses of SERT supports the idea that eL4 undergoes conformational alterations during the transport cycle (Mitchell *et al.*, 2004). As observed for LeuT and Mhp1, a direct participation of any residue of eL4 in substrate binding could not be shown. A similar mechanistic role was also observed in the  $\gamma$ -aminobutyric acid transporter GAT-1 (Zomot & Kanner, 2003). The authors also proposed that at least parts of eL4 are involved in structural rearrangements during transport. But in contrast to SERT, in GAT-1 direct or indirect participation of residues located in eL4 in GABA binding was suggested.

In order to provide first experimental information on the dynamics and functional role of the homologous loop (eL4) in members of the sodium/solute symporter family (SSSF), a

Cys scanning mutagenesis of the respective domain in PutP was performed, followed by site-directed spin labeling and EPR spectroscopic analyses. EPR is a suitable technique to determine structures of subdomains and ligand-dependent rearrangements within membrane proteins under physiological conditions (Hilger *et al.*, 2009, Wegener *et al.*, 2000, Hubbell *et al.*, 2000). For the EPR spectroscopic characterization of PutP three different parameters were determined: the mobility of the nitroxide spin label, the polarity of the microenvironment surrounding the spin label, and intramolecular inter spin distances by double electron-electron resonance (DEER). In the course of this work three major tasks were addressed: First, the secondary structure of eL4 was analyzed based on the EPR data. Second, ligand induced local dynamics of eL4 were monitored by a combination of mobility and polarity measurements in the presence or absence of Na<sup>+</sup> and/or proline. Third, to correlate the ligand dependent transitions of eL4 with the global conformations of PutP during the transport cycle, interspin distances in specifically selected double-Cys PutP constructs were measured.

### 4.3 Materials and Methods

#### 4.3.1 *In vivo proline transport assay*

In order to determine the influence of the amino acid substitutions on PutP activity an *in vivo* proline uptake assay was performed. Transport was measured in *E. coli* WG170 transformed with the plasmid pTrc99a/*putP*( $\Delta$ Cys) harboring the given mutations. Over night cultures were diluted 1:50 in Luria-Bertani (LB) medium (Miller, 1992) containing 100  $\mu$ g/mL ampicillin. The cells were grown under oxic conditions at 37°C up to an optical density measured at 420 nm ( $A_{420}$ ) of 1.0, followed by induction with 0.5 mM isopropyl 1-thio- $\beta$ -D-galactopyranoside for 1 h. Cells were harvested, washed with 100 mM Tris/MES pH 6.0 and resuspended to an  $A_{420}$  of 5.0. PutP mediated proline transport was assayed under standard conditions with 10  $\mu$ M L-[U-<sup>14</sup>C] proline (26 Ci/mol) in the presence of 20 mM D-lactate (Na<sup>+</sup> salt) and 50 mM NaCl using a rapid filtration method as described previously (Chen *et al.*, 1985). The initial rate of transport was calculated from the initial linear portion of the time course. Under these conditions PutP $\Delta$ Cys exhibits 50% initial rate of transport of wild type PutP.

#### 4.3.2 *Scintillation proximity assay (SPA)*

To test the impact of the amino acid substitutions and spin-labeling on the proline binding properties of PutP, a scintillation proximity assay was performed. The PutP derivatives were purified and spin-labeled as described in the following section. The Cu<sup>2+</sup> chelate YSi scintillation SPA beads (PerkinElmer) were diluted in 150 mM Tris/MES, pH 7.5, 50 mM NaCl, 10% glycerol, and 0.1% DDM to a concentration of 2.5 mg/mL. One hundred

microliter of the suspension were supplemented with 1  $\mu\text{M}$   $^3\text{H}$ -proline (4.2 Ci/mmol) and 50 ng of the respective PutP $\Delta\text{Cys}$  derivative. The samples were incubated for one hour on a vibrating platform at 4°C in a 96-well white-wall clear bottom plate and measured in a photomultiplier (1450 LSC & Luminescence Counter, WALLAC Micro Beta TriLux, PerkinElmer) in SPA cpm mode. To compare the proline affinities of labeled and unlabeled protein, the samples were measured with and without the addition of 5 mM DTT. For background correction 800 mM imidazole was added. Total radioactivity was determined by addition of 200  $\mu\text{l}$  Optiphase Supermix (PerkinElmer) and after 3 h incubation the plate was again measured in normal cpm mode. Binding properties of PutP $\Delta\text{Cys}$  and the respective single- and double-Cys variants were calculated relative to unlabeled PutP wild type.

#### **4.3.3 Determination of $\text{Na}^+$**

$\text{Na}^+$  concentrations in buffers used for incubation of proteoliposomes and subsequent ligand dependent EPR measurements were determined with a VARIAN AA240 atomic absorption spectrometer.

#### **4.3.4 Site-directed spin labeling**

The *putP* alleles encoding single- and double-Cys PutP molecules used in this study were generated by site-directed mutagenesis using plasmid pT7-5/*putP*( $\Delta\text{Cys}$ ) as a template and synthetic mutagenic oligonucleotides in one- or two-step PCR reactions using *Taq*-DNA polymerase. Plasmid pT7-5/*putP*( $\Delta\text{Cys}$ ) is a derivative of pT7-5 (Tabor & Richardson, 1985) and contains the *lac* promoter/operator for expression of *putP* and an engineered cassette version of this gene that is devoid of all five native Cys coding codons. PCR fragments were digested with appropriate restriction endonucleases and ligated with similarly treated plasmid pT7-5/*putP*( $\Delta\text{Cys}$ ). For overexpression, the *putP* alleles were cloned into plasmid pTrc99a (Amann *et al.*, 1988) using restriction endonucleases *Nco*I and *Hind*III. The resulting plasmids were transformed into *E. coli* WG170 [*F*<sup>-</sup> *trp lacZ rpsL thi*  $\Delta$ (*putPA*)101 *proP219*] (Stalmach *et al.*, 1983). Cells were grown, membranes were prepared, and PutP was solubilized and purified by Ni-nitrilotriacetic acid affinity chromatography as previously described (Jung *et al.*, 1998a). The single- or double-Cys PutP variants were labeled with (1-oxyl-2,2,5,5-tetramethylpyrroline-3-methyl)-methanethiosulfonate (MTSSL; Toronto Research Chemicals, Toronto, Canada) on the column. For this purpose, 1 mM MTSSL in buffer W (50 mM  $\text{KPi}$ , pH 8.0, 300 mM KCl, 10 mM imidazole, 10% glycerol (v/v), 0.04%  $\beta$ -D-dodecylmaltoside (w/v)) was applied to the column and incubated for 3 h at 4°C. The unbound label was removed by washing the column with buffer W, and the labeled protein was eluted with 200 mM imidazole in buffer W. After elution, the protein was reconstituted under non-reducing conditions into liposomes composed of *E. coli* lipids (67% phosphatidylethanolamine, 23.2% phosphatidylglycerol, and 9.8% cardiolipin; Avanti Polar

Lipids, Alabaster, AL) at a lipid/protein ratio of 20:1 (single-Cys PutP derivatives) or 40:1 (double-Cys PutP derivatives) (w/w) as previously described (Jung *et al.*, 1998b). Finally, the proteoliposomes were washed twice with 50 mM Tris/HCl, pH 7.5 and stored in liquid nitrogen until use. To determine the influence of ligands on the EPR spectra, after thawing the respective proteoliposomes were supplemented with 50 mM NaCl or 50 mM NaCl and 10 mM proline, incubated at 4°C over night, centrifuged and resuspended in the appropriate buffer to yield a PutP concentration of 100 – 250  $\mu$ M. As negative control, measurements were also performed in the presence of 50 mM KCl or 50 mM KCl and 10 mM proline.

The following spin-labeled single- and double-Cys PutP molecules were prepared: single spin-labeled derivatives: A294R1, Y295R1, F296R1, N297R1, D298R1, H299R1, P300R1, A301R1, L302R1, A303R1, G304R1, A305R1, V306R1, N307R1, Q308R1, N309R1, A310R1, E311R1, R312R1, V313R1, F314R1, I315R1, E316R1, L317R1, A318R1, Q319R1, I320R1, L321R1, F322R1, N323R1, and P324R1.

double spin-labeled derivatives: S50R1/G304R1, K91R1/L371R1, A149R1/L450R1, A294R1/Y403R1, and D298R1/Q446R1.

#### **4.3.5 Continuous-wave EPR (cw EPR) measurements**

Spin label mobility and ligand dependent changes in the EPR spectra were determined by cw EPR measurements using a Miniscope MS200 X-band spectrometer (microwave frequency  $\approx$  9.4 GHz) equipped with a rectangular TE102 resonator (Magnettech GmbH). The experiments were performed at a stable temperature of 298 K adjusted by a temperature control unit TC H02 (Magnettech GmbH). The microwave power was set to 10 mW and the B-field modulation amplitude was individually adjusted for every sample ( $\frac{1}{3}$  of the linewidth measured at 500 mG). The minima and maxima of the experimental cw EPR spectra were fitted by fifth-order polynomials with the MATLAB (The MathWorks, Natick, MA)-based program DynAnalysis. The line widths of the spectra were extracted and the reciprocal line width  $\Delta H_0^{-1}$  was used as a measure for the spin label mobility.

The polarity of spin label environment was determined at 160 K using a homemade X-band EPR spectrometer equipped with an AEG H103 rectangular cavity. The microwave power was set to 0.2 mW and the B-field modulation amplitude adjusted to 0.25 mT. A B-N 12 B-field meter (Bruker) and a continuous flow cryostat Oxford ESR 900 allowed measurement of the magnetic field and stabilization of the sample temperature. Proteoliposomes in the absence of Na<sup>+</sup> and proline or supplemented with the respective ligands were measured in quartz capillaries (3 mm inner diameter) at a concentration of 15-20 mg/mL. As a measure for the polarity  $A_{zz}$  was determined.

### 4.3.6 DEER measurements

Four-pulse DEER measurements were performed at Q-band frequency (34-35 GHz) on a homemade spectrometer equipped with a homemade 3 mm rectangular resonator at a temperature of 50 K. Before insertion into the probe head, the samples were shock-frozen in liquid nitrogen to avoid crystallization of water. The four-pulse DEER sequence  $(\pi/2)_{\nu_1} - \tau_1 - (\pi)_{\nu_1} - t' - (\pi)_{\nu_2} - \tau_1 + \tau_2 - t' - (\pi)_{\nu_1} - \tau_2 - \text{echo}$  was used (Pannier *et al.*, 2000). All pulses were set to 12 ns. The long interpulse delay  $\tau_2$ , defining the dipolar evolution time was typically 3000-3600 ns, depending on the relaxation properties of the sample and on distance. Deuterium nuclear modulations were averaged by increasing the first interpulse delay by 16 ns for 8 steps. A phase cycle  $[(+x), -(-x)]$  was applied to the first pulse. The pump frequency  $\nu_2$  was set at the maximum of the echo detected field swept spectrum, 80 MHz higher than the observer frequency  $\nu_1$ . Accumulation times for the data sets varied between 6 and 14 h. Data were analyzed for dipolar evolution times  $t = t' - \tau_1 \geq 0$ . Analysis of the data in terms of distance distributions and mean distances was performed with the program DeerAnalysis2011 (Jeschke *et al.*, 2006).

## 4.4 Results

### 4.4.1 Activity and binding properties of spin-labeled PutPΔCys derivatives

For the elucidation of the functional role of eL4 of PutP in the transport cycle, an EPR-based approach was chosen. To be able to site-specifically introduce nitroxide spin labels into this extracellular domain, a Cys scanning mutagenesis from position 294 to 324 was performed. In addition, a set of double-Cys variants was constructed to correlate the dynamics of eL4 with the alternating access mechanism by tracking intramolecular, ligand dependent distance changes. For this purpose positions on the periplasmic and the cytoplasmic side were chosen that are, according to the proposed transport mechanism of LeuT-like transporters, involved in conformational rearrangements. To test the influence of these substitutions on the transporter activity, the initial rate of transport was determined *in vivo* (Fig. 4.1 A) by a proline uptake assay. Furthermore, the proline binding properties of purified MTSSL-labeled and unlabeled protein were determined (Fig. 4.1 B). A Western Blot analysis showed that all constructs and PutPΔCys were produced in comparable amounts (data not shown). Therefore, variation in the expression level of the *putP* mutants could be excluded as reason for the differences in the initial rate of transport.

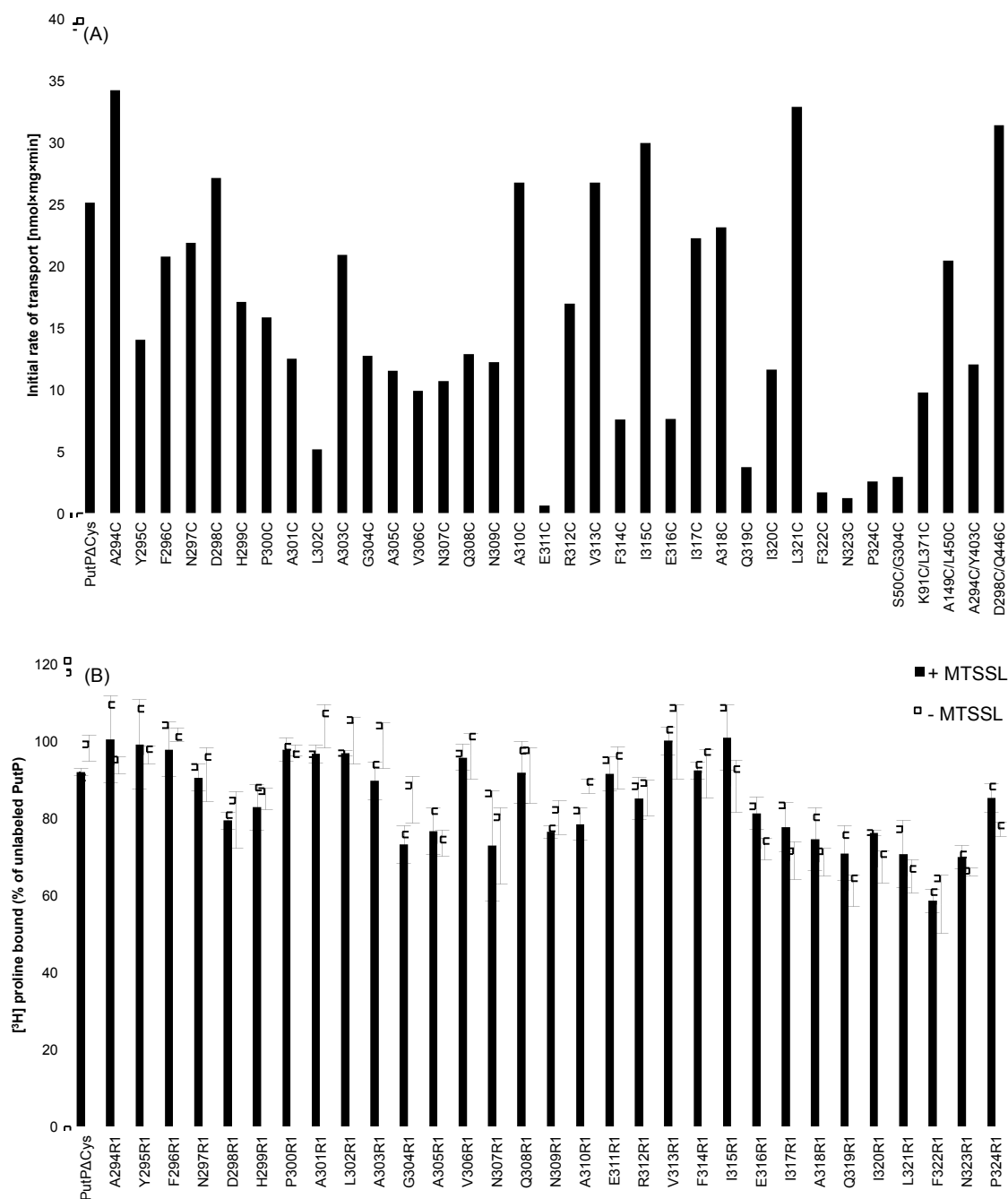


**Fig. 4.1 Influence of single- and double-Cys substitutions and spin labeling on PutPΔCys activity.** (A) Initial rate of transport of L-[U-<sup>14</sup>C]-proline (10 μM final concentration) into *E. coli* WG170 was assayed in the presence of 50 mM NaCl and 20 mM D-lactate (Na<sup>+</sup> salt) as electron donor at 25°C under aerobic conditions using a rapid filtration method (Chen et al., 1985). The diagramed initial rates are the result of two independent experiments. (B) The proline binding properties of the constructed PutPΔCys-derivatives and the influence of spin labeling was determined by means of the scintillation proximity assay. Measurements were either performed with purified and spin labeled protein or with unlabeled protein (MTSSL was removed by addition of 5 mM DTT). Data are shown as the mean ± S.E.M. (standard error of the mean) and relative to unlabeled PutP wild type. Standard deviations were calculated from a minimum of three independent experiments.

*In vivo* proline uptake assays showed that the majority of the single- and double-Cys derivatives exhibited transport activities similar to PutPΔCys (differences ≤50%). Only at a small number of positions, the replacement of the native amino acids by Cys led to a drastically reduced initial rate of transport (E311, F322, N323, P324). In order to test the influence of the respective amino acid substitutions and spin-labeling on proline binding, a

SPA was performed. Kinetic analysis of wild type PutP and PutP $\Delta$ Cys revealed a  $K_{d(\text{pro})}$  of 2  $\mu\text{M}$  (data not shown). This is in good agreement with the previously determined proline affinity of PutP (Yamato & Anraku, 1993). For all generated PutP derivatives proline binding was detected. Compared to unlabeled wild type PutP, PutP $\Delta$ Cys supplemented with 5 mM DTT ('unlabeled') resulted in 98% and without DTT ('labeled') in 92% substrate binding activity. For none of the PutP derivatives a severe impact of the nitroxide spin label on the proline binding capacity was observed: all PutP derivatives showed significant binding activities. The biggest impact on the substrate affinity was observed upon substitution of F322. From the combination of *in vivo* uptake experiments and *in vitro* binding assays, it can be concluded that the reduction in the initial rate of transport of variants such as L302C, E311C, Q319C, F322C, N323C and P324C results rather from an affected transport cycle than from reduced binding activities.

#### **4.4.2 Analysis of the mobility of spin labels attached to Cys placed in eL4 of PutP**

In order to get first insights into the architecture of eL4, the spin label mobility was determined. The local protein environment influences the reorientation motion of the nitroxide side chain (Steinhoff *et al.*, 2000). While tertiary interactions, van der Waals interactions, backbone atoms or other amino acid side chains confine the side chain mobility, spin labels on helix surfaces or in loop regions exhibit only slightly reduced motional dynamics. In recent studies it was shown that cw EPR data are suitable to analyze and predict secondary structures (Dalmás *et al.*, 2010, Bordignon *et al.*, 2005). Therefore, X-band EPR spectra of the modified transporter variants were determined at room temperature in the absence of ligands (Fig. 4.2). As measure for the mobility of the spin probe attached to the respective thiol group, the reciprocal line width ( $\Delta H_0^{-1}$ ) of the central resonance line was determined. In most of the nitroxide spectra a composite spectral shape was observed. This can be a result of inhomogeneous structural constraints in the microenvironment of the spin label, as reported previously or might hint on different stable spin label conformations (Hubbell *et al.*, 1996, Langen *et al.*, 2000). According to the spectral line widths, eL4 can be divided into two subdomains (Fig. 4.3, black line): a region in the N-terminal half (298-308) with weak to moderate interactions and a region in the C-terminal (309-324) half that is involved in tertiary interactions.

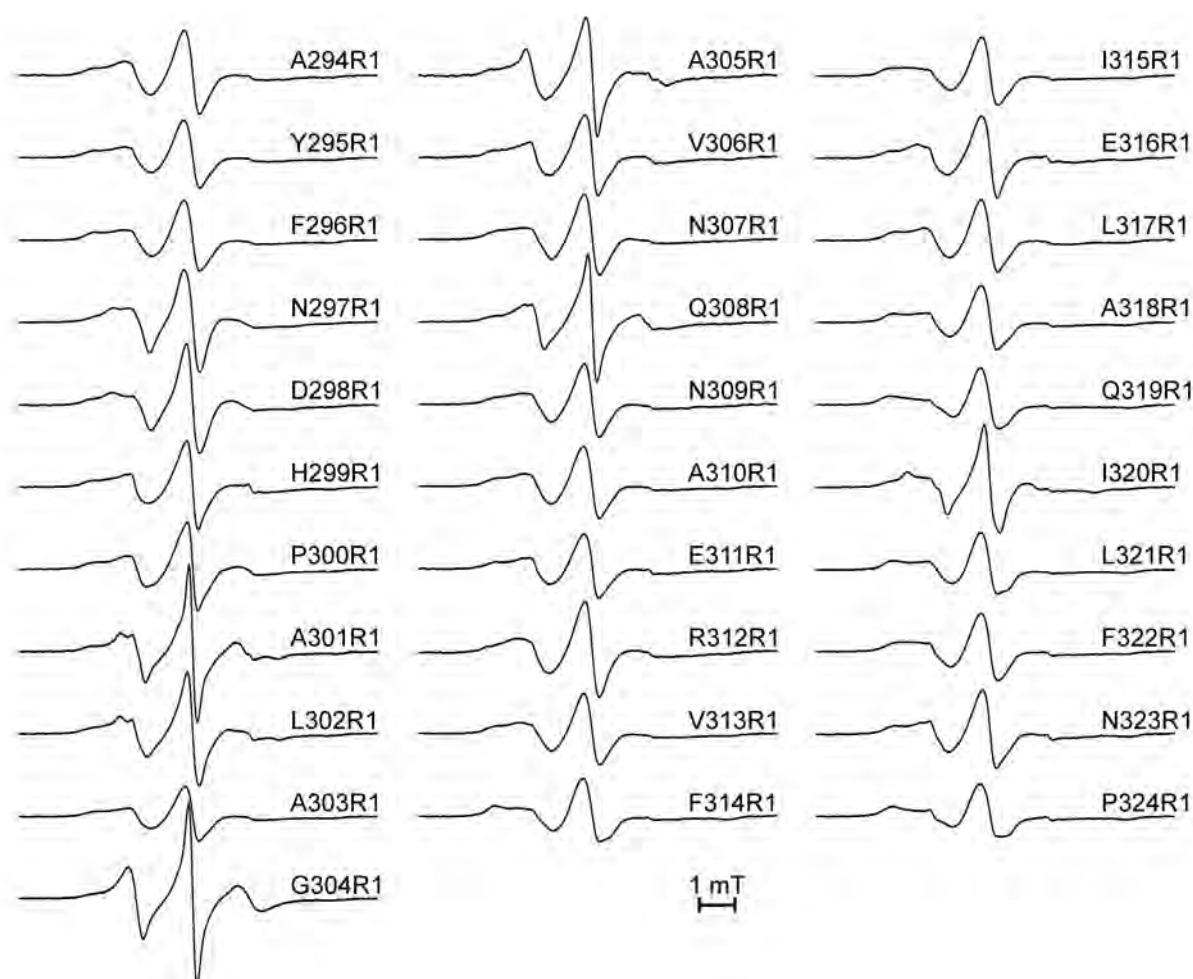


**Fig. 4.2 Room temperature cw X-band EPR spectra of singly spin-labeled PutP derivatives in the membrane environment.** The spectra were recorded at 298 K in the absence of ligands using a Miniscope HS200 X-band spectrometer. The PutP variants were purified, labeled with MTSSL and subsequently reconstituted into *E. coli* lipids with a protein to lipid ratio of 1:20 (w/w). The native amino acids at the respective positions are shown as single letter code. R1: MTSSL side chain linked to site specifically introduced Cys residues by disulfide bridges.

Moving from the periplasmic side of TM 7 into eL4 leads to a steady increase of the spin label mobility (Fig. 4.3, black line), starting from a  $\Delta H_0^{-1}$  of  $\sim 2 \text{ mT}^{-1}$ , a characteristic value for side chains participating in tertiary interactions (Bordignon & Steinhoff, 2007). The increase in the reciprocal line width leads to the first maximum that is reached at position 301, followed by two other highly dynamic nitroxide side chains attached to positions 304 and 308. For these three positions a  $\Delta H_0^{-1}$  of  $\sim 4 \text{ mT}^{-1}$  was determined, a typical value for spin labels involved in weak or no interactions as detected for positions in loop regions of soluble and membrane proteins (McHaourab *et al.*, 1996). Between positions 309 to 324, moderate to strong interactions of the nitroxide side chain with the protein were detected ( $\Delta H_0^{-1}$  values between  $1.7$  and  $2.6 \text{ mT}^{-1}$ ). Interestingly, the mobility profile of the  $\Delta H_0^{-1}$  values revealed a clear periodic pattern at the N-terminal half of eL4 between residues D298 and Q308. The corresponding minima and maxima are shifted by three to four positions, suggesting that this N-terminal region forms a secondary structure in which attached spin labels with minor restraints on the mobility cluster on one side of a putative  $\alpha$ -helix. In the C-terminal half of

eL4 a second periodic pattern, resembling a second putative  $\alpha$ -helix was observed in the mobility profile, starting from position 310 and ending at position 317. An  $\alpha$ -helical domain in this part of eL4 was already proposed in a vSGLT based homology model, but the predicted secondary structure was predicted between residues 313 to 317 (Olkhova et al., 2010).

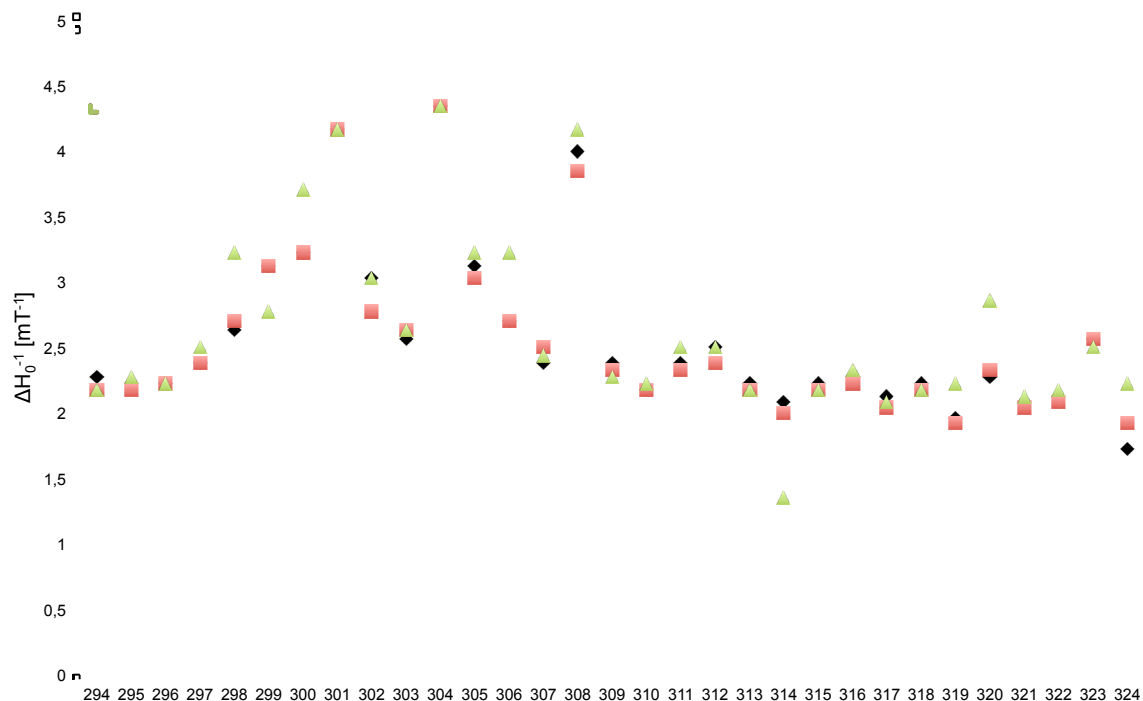


**Fig. 4.3 Ligand dependent changes in the spin label mobility parameter  $\Delta H_0^{-1}$  in eL4.** The purified Put $\Delta$ Cys single-Cys derivatives were spin labeled and reconstituted at a protein to lipid ratio of 1:20 (w/w). The cw EPR spectra were collected at 298 K using a Miniscope HS200 X-band spectrometer. In order to investigate the influence of the coupling ion and the substrate on the spin label mobility measurements were performed in the absence of ligands (black) or in the presence of 50 mM NaCl (red) or 50 mM NaCl and 10 mM proline (green).

#### 4.4.3 Analysis of the polarity of the microenvironment of nitroxide spin labels attached to single-Cys derivatives

To gain a more detailed view on the microenvironment of the attached spin label, the polarity of the surrounding milieu was determined. For that low temperature cw EPR spectra of the singly spin-labeled PutP derivatives were measured. As a measure for the chemical nature of the surrounding milieu, the hyperfine tensor element  $A_{zz}$  was determined. In an apolar surrounding attached spin labels are described by low and in polar microenvironments by high  $A_{zz}$  values (Bordignon & Steinhoff, 2007). Major determinants for the polarity of the microenvironment are neighboring amino acid side chains, aqueous solvent or the membrane bilayer (polar headgroups/apolar aliphatic tail).

The obtained polarity profile (Fig. 4.4) of eL4 revealed significant differences in the chemical nature of the environment of spin labels attached to positions under investigation. The resulting  $A_{zz}$  values range from 3.64 mT at position 298 corresponding to a highly polar environment to 3.40 mT at position 310 corresponding to a highly apolar environment. In addition to 298, maxima ( $\sim 3.55$  or higher) in the  $A_{zz}$  profile were observed at positions 304,

305, 312, 315, and 319. Minima ( $\sim 3.45$  or lower) in the profile were detected at positions 299, 307, 310, 311, 314, 318, and 322.

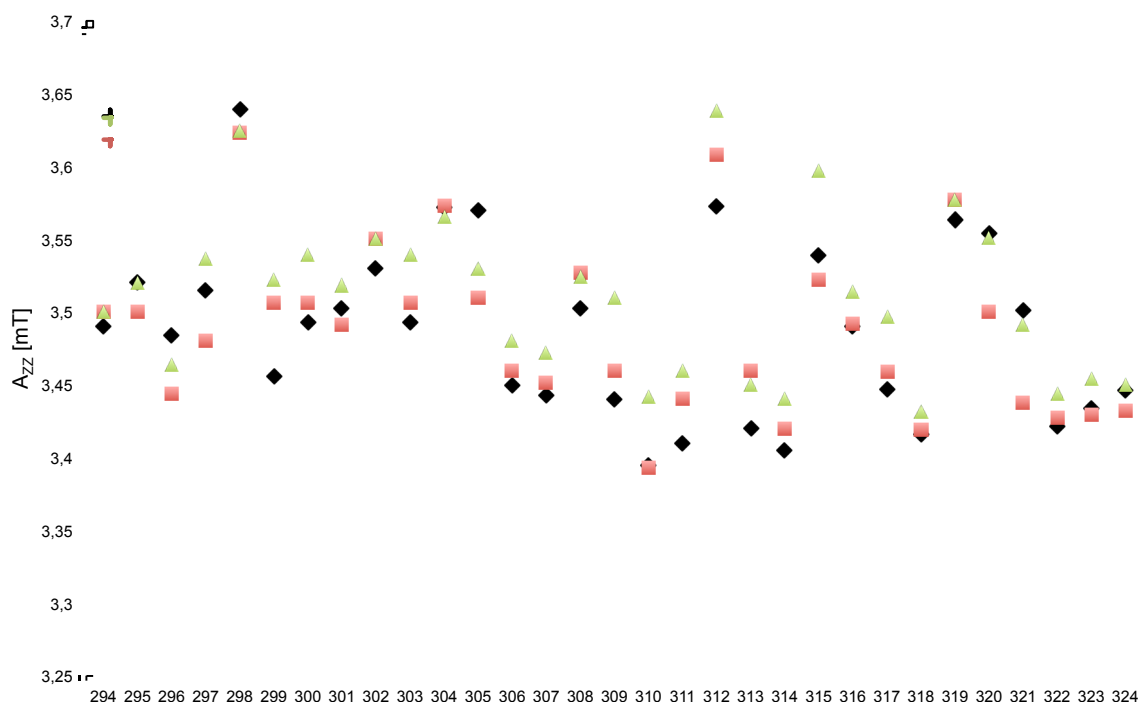


**Fig. 4.4 Ligand dependent changes in the polarity of the microenvironment of spin labels attached to positions in eL4 of PutP.** The purified PutP single-Cys derivatives were spin labeled and reconstituted at a protein to lipid ratio of 1:20 (w/w). The EPR spectra were measured at 160 K. To elucidate the influence of both ligands on the microenvironment of the MTSSL side chain either no ligands (black) or 50 mM NaCl (red) or 50 mM NaCl and 10 mM proline (green) were added.

As already seen in the mobility measurements, a periodic pattern in the recorded polarity profile became evident. Starting from position 310, periods of approximately 3.6 between the respective minima or maxima were detected, hinting at an  $\alpha$ -helical secondary structure in the C-terminal part of eL4 ending at position 318. This is in good agreement with spin label mobility data. In the N-terminal region, the periodicity was not as pronounced as in the succeeding part. In combination with the  $\Delta H_0^{-1}$  profile, an  $\alpha$ -helix ranging from 298 to 308 was predicted. A periodic pattern is also visible in the polarity profile in this region with maxima at positions 298, 304 and, 308. A disturbed putative fourth maximum at position 301 might be explained by the influence of neighboring side chains, which in addition to the solvent determine the microenvironment. The minima in the N-terminal region (294-309) of eL4, harboring the first  $\alpha$ -helical domain are exposed to a more polar environment compared to the minima in the C-terminal region (310-324). An explanation could be that the rear part of this loop is more protected from the water phase, or the surrounding protein bulk is more hydrophobic.

If residues were fully exposed to water or the periplasm respectively,  $A_{zz}$  values between 3.6 and 3.7 would be expected. Since only a small number of positions under investigation were found in this range, it can be assumed that major parts of eL4 are involved

in the formation of secondary structures, tertiary contacts or in the interaction with the membrane.

#### **4.4.4 Ligand influence on spin label mobility and on the microenvironment**

PutP of *E. coli* is suggested to work according to an ordered binding mechanism (Yamato, 1992). To track the dynamics of eL4 during the transport cycle, the influence of Na<sup>+</sup> or Na<sup>+</sup> and proline on the spin label mobility and on the polarity of the surrounding milieu was tested. Therefore the  $\Delta H_0^{-1}$  and the  $A_{ZZ}$  values were determined in the presence of 50 mM NaCl or 50 mM NaCl and 10 mM proline and compared with the values obtained in the absence of ligands. To determine the specificity of the changes in the EPR spectra, for selected positions measurements were performed in the presence of 50 mM KCl or 50 mM KCl and 10 mM proline. Measurements without ligands or if Na<sup>+</sup> was replaced by K<sup>+</sup> were performed in the virtual absence of Na<sup>+</sup> (~10  $\mu$ M).

*Spin label mobility* – In comparison to the EPR spectra obtained in the absence of ligands, at positions 298, 299, 300, 302, 306, 314, 319, 320, and 324 a pronounced change in  $\Delta H_0^{-1}$  was measured upon addition of Na<sup>+</sup> or Na<sup>+</sup> and proline. The impact of Na<sup>+</sup> alone on the line width was less pronounced than the influence of proline in the presence of Na<sup>+</sup>. At positions 302, adding the coupling ion resulted in a decreased mobility of the MTSSL side chain, at position 324 the contrary effect was detected. Strikingly a slight but systematic decrease of the  $\Delta H_0^{-1}$  values in the C-terminal region of eL4 (311-319) was observed (Fig. 4.3, red line). Compared to Na<sup>+</sup>, proline in the presence of Na<sup>+</sup> had a bigger impact on the mobility profile. The addition of both ligands increased the reciprocal line width at positions 298, 300, 302, 306, 319, 320, and 324 (Fig. 4.3, green line). The mobility of the MTSSL side chain was more restricted at positions 299 and 314. Since the reciprocal line width is strongly biased by the mobile component of the spectrum, for a more subtle interpretation of the spin label dynamics the low field peaks were considered (Suppl. Fig 4.3 A). The respective changes revealed that the presence of Na<sup>+</sup> induced a decrease of the mobile component in the spectra of positions 294, 296, 302, 305, 307, 309, 312, 317, 318, and 321. Upon addition of both ligands, for residues 295-297, 299, 305, 309, 312-315, and 317 a decrease in the mobile component was detected. The opposite effect was measured for 298, 300, 302, 308, 316, 319, 320, and 324. In order to test the specificity of the observed effects measurements in the presence of 50 mM KCl and/or 10 mM proline were performed (Suppl. Fig. 4.3 B; Supp. Table 4.1). As described above Na<sup>+</sup> induced changes in  $\Delta H_0^{-1}$  at positions 302 and 324. If K<sup>+</sup> was added to PutP-L302R1 instead of Na<sup>+</sup>, the decrease of the spin label mobility is less pronounced, indicating a Na<sup>+</sup>-specific effect. In contrast, at position 324 both ions had a similar impact on the EPR spectra, hinting on an unspecific ionic effect. Proline effects on the spin label mobility observed for D298R1, P300R1, F314R1, and Q319R1 proved to be dependent on Na<sup>+</sup>. If K<sup>+</sup> and proline were added the effects were less pronounced, compared

to the results obtained upon addition of Na<sup>+</sup> and proline. At position 319 no significant difference in the shift of  $\Delta H_0^{-1}$  between Na<sup>+</sup> and proline or K<sup>+</sup> and proline was detected.

**Polarity measurements** – To describe the putative conformational flexibility of eL4 in more detail, ligand-induced changes in the microenvironment of the spin label were measured. At the transition zones between the periplasmic loop and the adjoining TMs 7' and 8', the presence of the coupling ion shifted  $A_{zz}$  to values corresponding to a more apolar environment (295, 296, 297, 320, 321, and 324) (Fig. 4.4, red line). Within eL4 only for positions 301, 305, and 315 a decrease in the polarity was observed upon Na<sup>+</sup> binding. In contrast, MTSSL side chains at positions 299, 300, 302, 308, 309, 311, 312, 313, and 314 were shown to move into a more polar environment in a Na<sup>+</sup>-dependent manner. If both ligands are added to the labeled PutP derivatives, a systematic pattern in the polarity profile was detected (Fig. 4.4, green line). Except for 298, 302, 304, 308, and 313, all other residues were shifted to a more polar environment.

Even though the addition of Na<sup>+</sup> or Na<sup>+</sup> and proline led to changes in the mobility as well as the polarity profile, no structural rearrangements in the putative  $\alpha$ -helical structures could be shown. The data rather suggest ligand-induced movements of the loop as a rigid body.

#### **4.4.5 Intramolecular distances and ligand influence on the distance distribution**

A characteristic feature of the alternating access mechanism is the reciprocal opening and closing of two water-filled hemichannels. These polar permeation pathways mediate access to the substrate and ion binding site, either from the periplasm or the cytoplasm. In order to integrate the local dynamics of eL4 into the context of global conformational alterations during the transport cycle, DEER measurements were performed. A PutP homology model, based on the crystal structure of vSGLT of *V. parahaemolyticus* (Olkhova et al., 2010), was used to select for double-Cys derivatives appropriate to track putative ligand induced changes in the transporter conformation (Fig. 4.5). Even though the oligomeric state of PutP still remains to be elucidated, in previous EPR studies no evidence for PutP oligomerization was observed (Jeschke et al., 2006). Therefore spin-spin dipolar coupling effects most probably result from MTSSL side chains attached to the respective thiol groups in the constructed PutP double-Cys variants.

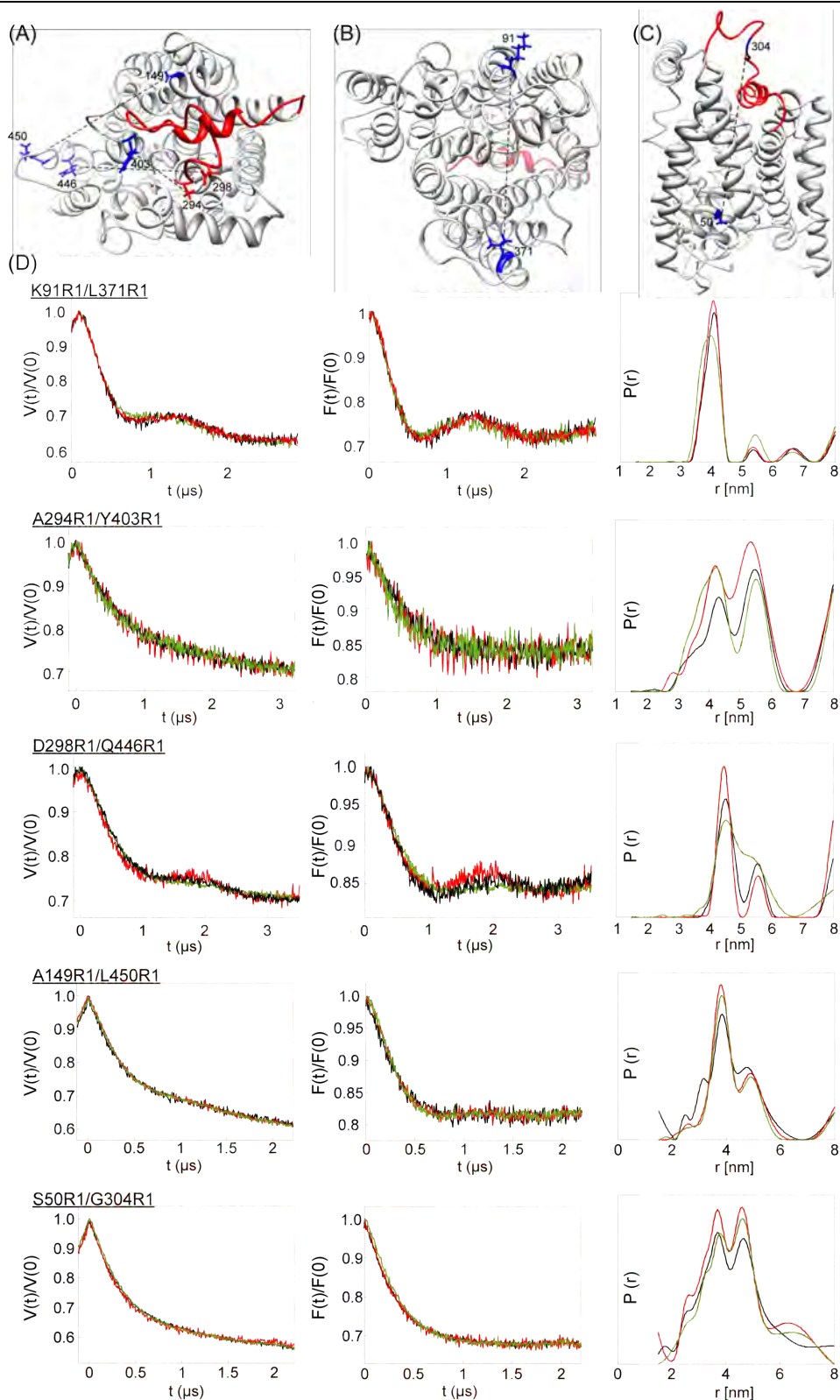


**Fig. 4.5 Intramolecular distance measurements of spin-labeled double-Cys PutP derivatives in the absence or presence of ligands.** Positions substituted by Cys and subsequently labeled by MTSSL are shown as blue sticks. Utilized double-Cys variants on the periplasmic side viewed from the periplasm (A), on the cytoplasmic side viewed from the cytoplasm (B), and derivatives used to analyze motions of eL4 relative to the proline binding site, viewed from the plane of the membrane (C). A PutP homology model based on the vSGLT (3DH4) crystal structure was used to guide the selection of the PutP double-Cys derivatives (Oikhova et al., 2010). The PutP variants were overproduced, purified, spin labeled, and reconstituted. Samples were measured at 50 K in the absence or presence of ligands. To improve phase memory time of electron spins 10% glycerol-d8 was added. (D) Results of the inter-spin distance determination for each variant under investigation. The graphs show from left to right the normalized experimental data  $V(t)/V(0)$ , the background-corrected normalized form factor  $F(t)/F(0)$  and distance distribution  $P(r)$  obtained by Tikhonov regularization using a regulation parameter of 100. To test the influence of ligands on  $P(r)$ , measurements were performed in the absence of ligands (black) or in the presence of 50 mM NaCl (red) or 50 mM NaCl and 10 mM proline (green).

On the periplasmic half of PutP, the distance distributions ( $P(r)$ ) between D298R1 (eL4) and Q446R1 (non-core TM 11'), A294R1 (eL4) and Y403R1 (TM 10'), and A149R1 (TM 3') and L450R1 (TM 12') were determined. On the cytoplasmic side the pair K91R1 (TM 2') - L371R1 (TM 9') was investigated. To determine putative movements of eL4 relative to the proline binding site, the pair S50R1 (TM 1') - G304R1 (eL4) was chosen. The value  $P(r)$  describes the probability that two introduced spin labels, each harboring an unpaired electron, are located within a distinct distance.

The most pronounced effects of  $\text{Na}^+$  or  $\text{Na}^+$  and proline on the distance distribution were observed for PutP-D298R1/Q446R1. In the absence of ligands, two peaks were detected at 4.5 and 5.5 nm respectively. These two populations could indicate an equilibrium of two conformational states of PutP or different spin label conformations. A mean distance of 4.82 nm ( $\sigma = 0.53$  nm) was calculated. Upon addition of 50 mM NaCl, the distance distribution was shifted to shorter distances (4.70 nm;  $\sigma = 0.49$  nm). If 10 mM proline in the presence of 50 mM NaCl was added, the distance distribution was shifted to longer distances (4.93 nm;  $\sigma = 0.61$ ). The shifts in the mean distance are mainly caused by changes in the equilibrium between the two major peaks. In fact, additional measurements of this variant in micelles revealed that the peak at 5.5 nm results from aggregated PutP molecules or concentrative effects in liposomes. This peak vanishes in micelles while the other peak stays put and narrows. In micelles, no change whatsoever in the distance between D298R1 and Q446R1 upon addition of  $\text{Na}^+$ /proline was observed. Also for the labeled double-Cys derivatives A149R1/L450R1 and A294R1/Y403R1 no significant changes in the mean distance were detected upon ligand binding. In the case of PutP-A149R1/L450R1, neither in the absence nor in presence of ligands (absence of ligands: 4.10 nm ( $\sigma = 0.61$ );  $\text{Na}^+$ : 4.13 nm;  $\sigma = 0.75$ ;  $\text{Na}^+$  and proline: 4.12;  $\sigma = 0.71$ ) changes in the mean distance were observed. For PutP-A294R1/Y403R1 a shift to shorter distances (absence of ligands: 4.84,  $\sigma = 0.83$ ;  $\text{Na}^+$ : 4.85,  $\sigma = 0.77$ ;  $\text{Na}^+$  and proline: 4.59,  $\sigma = 0.83$ ) was detected in the presence of  $\text{Na}^+$  and proline, compared to samples without ligands or supplemented with  $\text{Na}^+$ . However due to the low signal to noise ratio of the primary data, the significance of these changes cannot clearly be evaluated.

To address the conformational alterations on the cytoplasmic side, the derivative PutP-K91R1/L371R1 was chosen. Position 91 is found in TM 2', which is part of the four-helix bundle. Position 371 is located in TM 9' that contributes to the formation of the 'hash' motif. Comparing the inward- and the outward-facing conformation of Mhp1, these two domains undergo pronounced conformational alterations during reciprocal opening and closing of extra- and intracellular vestibule (Shimamura et al., 2010). If PutP and Mhp1 share the same mechanism of transport, changes in the interspin distance should be expected. The determined distance distributions again showed only subtle differences between samples

measured without ligands (3.98 nm;  $\sigma = 0.23$ ) and samples containing 50 mM NaCl (3.97 nm;  $\sigma = 0.24$ ) or 50 mM NaCl and 10 mM proline (3.89;  $\sigma = 0.27$ ).

To describe the role of eL4 as a putative gate in the transport mechanism interspin distances between positions 50 and 304 were analyzed. According to the PutP homology model, S50 is located in TM 1' below the proline binding site. Therefore changes in the distance distribution would hint at movements of the loop domain relative to the binding pocket. Shorter distances would further support the idea that eL4 might be involved in regulating access to the binding site from the periplasm. The recorded spectra showed a very broad distance distribution and no significant changes in the mean distance (absence of ligands: 4.08 nm,  $\sigma = 0.90$ ; Na<sup>+</sup>: 4.04,  $\sigma = 0.87$ ; Na<sup>+</sup> and proline: 4.11,  $\sigma = 0.86$ ).

Considering all determined intramolecular distance measurements in PutP, compared to DEER analysis in LeuT (Claxton et al., 2010), on the periplasmic- as well as on the cytoplasmic side of PutP only negligible changes in the mean distance were observed upon ligand binding implicating that in a reconstituted system, in the absence of a membrane potential at 50 K no transition between an inward- and an outward facing conformation can be observed.

## 4.5 Discussion

Starting with the crystallization of the bacterial multi-drug efflux pump AcrB (Murakami et al., 2002), the progress in structure determination of secondary transporters is accelerating rapidly. The high-resolution X-ray structure of the Na<sup>+</sup>/leucine symporter LeuT (Yamashita et al., 2005) gave rise to the LeuT structural family, a group of phylogenetically unrelated transporter gene families, sharing the same core architecture. By the crystal structure of vSGLT it was shown that amongst others also the SSSF belongs to this structural class. Despite the wealth of structural information, X-ray structures only represent a static snapshot and deduced transport mechanisms differ between the individual LeuT-like transporters (Krishnamurthy & Gouaux, 2012, Shimamura et al., 2010). In this study new insights were gained into the conformational dynamics underlying the translocation cycle of transporters belonging to the SSSF, emphasizing the functional significance of eL4 in the Na<sup>+</sup>/proline symporter PutP.

*In vivo* proline uptake assays gave first evidence for the importance of the investigated loop domain. Substituting E311 by Cys abolished transport almost completely (Fig. 4.1 A). Interestingly, anionic amino acid side chains are highly conserved among prokaryotic and eukaryotic members of the SSSF at this position (Suppl. Fig. 4.1). Since the proline binding properties were almost unaffected, the amino acid substitution rather impairs the translocation cycle subsequent to ligand binding than substrate binding itself. For LeuT it was shown that charged amino acids can be involved in the gating mechanism by salt bridge

formation (Yamashita et al., 2005, Shi et al., 2008). Using the PutP homology model, putative cationic interaction partners close to E311 were predicted. In order to experimentally confirm these *in silico* analysis, a site-directed mutagenesis study was performed and the transport activity of the respective variants were tested. However, Coulombic interactions of the negatively charged side chain with adjacent positively charged amino acids (R150, R312 and R396) could not be shown (Bracher and Jung, unpublished data). Nevertheless ionic interactions of E311 with cationic amino acids cannot be excluded since water molecules are known to mediate interactions between side chains that are actually not within interaction range (Sabarinathan et al., 2011). Replacement of F322, N323 and P324 also resulted in reduced initial rates of transport. P324 is highly conserved and it was shown to be located at the N-terminal end of the functionally important TM 8' at the water/membrane interface (Raba et al., 2008). Pro was shown to be of general structural importance (MacArthur & Thornton, 1991). It is frequently found as first amino acid of  $\alpha$ -helices, but it can also disrupt or kink helices. Hence the reduction in the transport activity might be explained by the structural distortion of the following functionally important TM 8'. In contrast, amino acid residues at position 322 and 323 are not conserved and in order to investigate their mechanistic role, more detailed functional analyses are required. Functionally important residues in homologous loop domains of LeuT like transporters were identified. In SERT replacement of native amino acids by Cys led to a decreased transporter activity while no direct involvement in serotonin binding was observed (Mitchell et al., 2004, Smicun et al., 1999). First direct structural evidence for the functional importance of eL4 was gained by the X-ray crystal structures of LeuT in complex with transporter-inhibiting tricyclic antidepressants. It was shown that residues located at the helix turn between eL4a and eL4b are involved in inhibitor binding (Zhou et al., 2007, Singh et al., 2007). Subsequent steered molecular dynamics simulations in combination with docking analysis predicted a second substrate binding site (S2) at a similar position in the periplasmic vestibule of LeuT, in which A319 and F320 of eL4 are involved in leucine coordination (Shi et al., 2008). The antidepressant binding site and S2 are formed by a similar set of residues. Binding of the second substrate is supposed to allosterically trigger  $\text{Na}^+$  and leucine release from the primary binding site, halfway across the membrane, into the cytoplasm. As a remark, there is still a vivid discussion in the field concerning the importance of S2. Since leucine was never directly observed in X-ray crystal structures, it is alternatively proposed that the substrate only transiently occupies S2 on its way from the periplasm to S1 and that S2 does not have a regulatory function at all. To date there is no experimental evidence for the presence of a second proline binding site, but a more detailed analysis of the PutP stoichiometry needs to be performed.

Since no high resolution information on the tertiary structure of PutP is available, biochemical, biophysical, and bioinformatic approaches were chosen to gain structural

insights into the Na<sup>+</sup>/proline symporter (Jung et al., 2012). The results of this work can be used to extend and refine the available three-dimensional model of PutP and the proposed molecular mechanism of function. EPR spectroscopic analysis of the Apo-state of PutP revealed periodic patterns in the spin label mobility as well as in the polarity profile. Periods of 3.6 between the respective  $\Delta H_0^{-1}$  (Fig. 4.3) or  $A_{zz}$  (Fig. 4.4) maxima indicate two  $\alpha$ -helices comprising residues D298 to Q308 as well as A310 to A318. A recently computed homology model of PutP predicted only one  $\alpha$ -helical domain from V313 to G319 (Oikhova et al., 2010). In vSGLT two  $\alpha$ -helices (EL8a and EL8b) in the homologous loop domain were identified (Faham et al., 2008, Watanabe *et al.*, 2010). The proposed secondary structure of the PutP model aligns with EL8b in the C-terminal part of the extracellular loop of vSGLT. Most probably a second  $\alpha$ -helix in PutP, following TM 7', could not be identified because of the low sequence identity and similarity in this region. Available crystal structures of members of the LeuT structural family showed that two  $\alpha$ -helices are a common feature in the corresponding loop domains, except for Mhp1 and BetP, in which only one secondary structural element was observed. Also biochemical studies on the homologous loop in SERT identified two  $\alpha$ -helical domains, connected by a hinge (Mitchell et al., 2004).

In the course of the X-ray structure based proposed transport cycle of LeuT (Krishnamurthy & Gouaux, 2012) and Mhp1 (Shimamura et al., 2010) no structural rearrangements within the secondary structures of eL4 were observed. This is in good agreement with the recorded mobility and polarity profiles of PutP upon Na<sup>+</sup> and/or proline binding. Again no clear shifts in the periodicity patterns (Fig. 4.3 and 4.4) were observed. Nevertheless the spectroscopic measurements revealed changes in the spin label mobility as well as in the polarity of the spin label microenvironment (Fig. 4.6 A). Addition of Na<sup>+</sup> had minor effects on the MTSSL mobility. Only the flexibility of spin labels attached to the C-terminal half of eL4 was slightly reduced. The polarity profile of eL4 at the water/membrane transition zone was shifted in the presence of Na<sup>+</sup> to a more apolar environment. At positions in the hinge region connecting the two  $\alpha$ -helical domains, approximately in the middle of eL4, a clear shift to a more polar environment was observed (Fig. 4.6 B). This shift in the polarity might either be explained by the presence of polar solvent or by a closer proximity to hydrophilic protein bulk. A concomitant decrease of the spin label mobility and an increase in the polarity of the microenvironment rather supports the latter idea. This assumption is supported by the fact that spin labels attached to Cys at the water/membrane interface (295, 296, 297, 322, and 324) are shifted to a more apolar environment upon Na<sup>+</sup> binding. This might be explained by movements of the respective residues deeper into the membrane or the extracellular vestibule. To sum up the data suggest that during the transition from the Apo- to the Na<sup>+</sup>-bound state eL4 is dipping deeper into a putative periplasmic cavity. A crevice that might be lined by predominantly hydrophilic residues, as it was also observed

e.g. in LeuT, ApcT, vSGLT, and LacY (Yamashita et al., 2005, Shaffer *et al.*, 2009, Faham et al., 2008). The resulting closer interaction with polar residues could explain the observed decrease of the mobility and the concomitant increase in the polarity of the surrounding of the spin label. Ligand induced movements of homologous loop domains were also described for other representatives of the LeuT structural family (Shimamura et al., 2010, Krishnamurthy & Gouaux, 2012, Claxton et al., 2010).

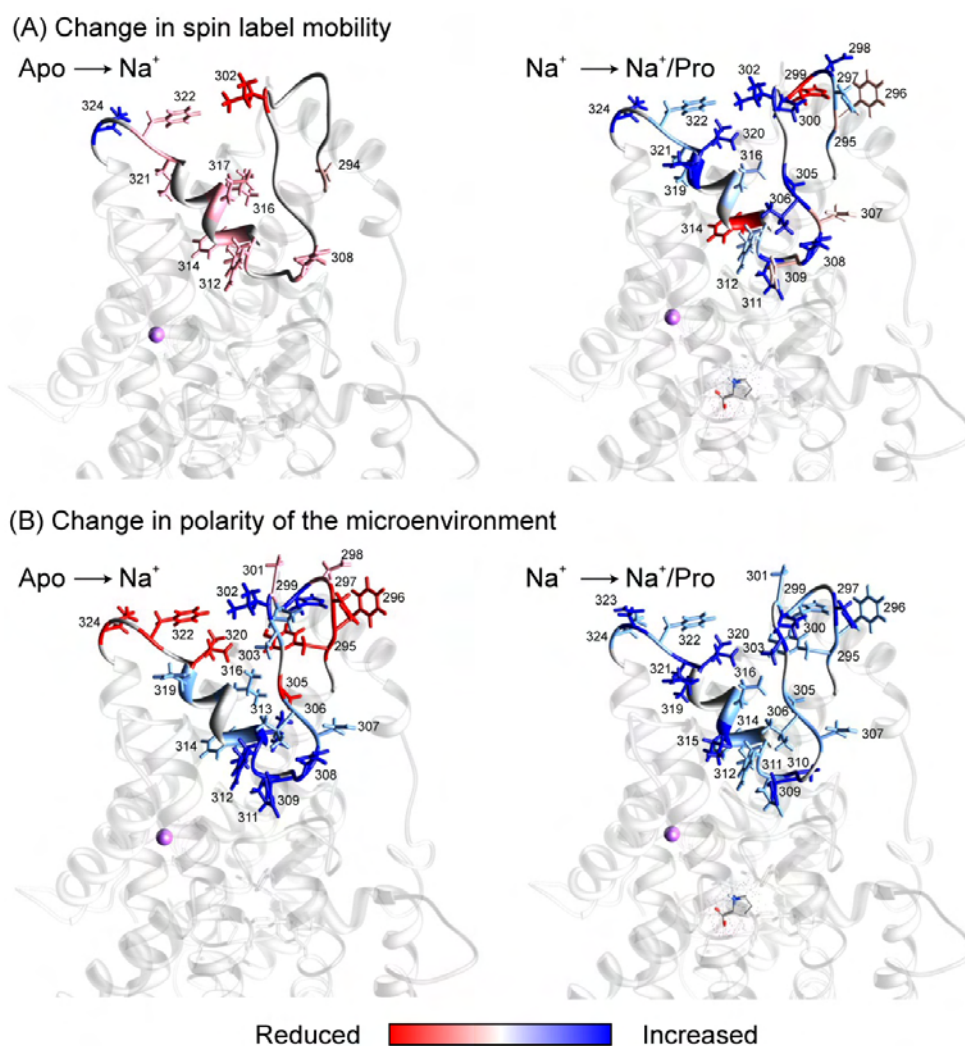


**Fig. 4.6 The presence of Na<sup>+</sup> and/or proline induces changes in the spin label mobility and polarity.** Residue specific mapping of changes in  $\Delta H_0^{-1}$  (A) and the  $A_{zz}$  (B) upon Na<sup>+</sup> binding relative to the Apo-state or upon proline binding relative to the Na<sup>+</sup> bound state onto the PutP homology model (Oikhova et al., 2010). Residues exhibiting an increase in  $\Delta H_0^{-1}$  or  $A_{zz}$  are shown as sticks and are colored in blue. Residues with decreased  $\Delta H_0^{-1}$  or  $A_{zz}$  are shown as sticks and are highlighted in red. Na<sup>+</sup> is depicted as purple sphere, proline is shown as stick model.

When Na<sup>+</sup> and proline were added and the formation of the ternary complex was induced, the effects on the spin label mobility were reversed with respect to the Na<sup>+</sup> bound state. The overall mobility is increased even though at some positions a slight decrease in the spin label flexibility was observed (296, 299, 306, 307, and 314). In parallel, for almost all positions in the loop domain an increase in the polarity of the microenvironment was detected. Combining these observations suggests that interactions of eL4 with other protein domains are weakened upon addition of Na<sup>+</sup> and proline, compared to the Na<sup>+</sup>-bound state.

This could be explained by looser packing of eL4 into a periplasmic cavity that is followed by water influx. But it also needs to be discussed whether the loop itself is moving or if surrounding helices, comprising a putative periplasmic cavity, move farther apart.

In order to describe the impact of ligands on the transporter conformation intramolecular distance changes triggered by Na<sup>+</sup> or Na<sup>+</sup> and proline were determined. These results might help to put the dynamics of eL4 into the global context of the alternating access mechanism. The observed ligand induced changes in spin label mobility and polarity of the microenvironment supported the idea that Na<sup>+</sup> induces stronger interactions of eL4 with other domains of PutP. Subsequent addition of proline reversed this effect (increased spin label mobility and polarity even compared to the Apo-state). If eL4 adopts a similar plug-like function in PutP as the homologous domain in LeuT, these findings could suggest that the decreased tertiary interactions hint on an opening of a periplasmic cavity.

For all tested PutP double-Cys derivatives neither on the periplasmic nor on the cytoplasmic side significant ligand-induced changes in the mean distance were detected. In proteoliposomes harboring PutP-D298R1/Q446R1 indeed an equilibrium between two distances (4.5 nm and 5.5 nm) was detected. Two distance peaks might hint on two conformational states of the protein or of the spin-label. However subsequent measurements in micelles showed that the latter peak could be attributed to a fraction of aggregated PutP in the reconstituted sample and not to a reciprocal opening and closing of cavities. Interestingly, for the corresponding positions in LeuT (Claxton et al., 2010), in the presence Na<sup>+</sup> and the substrate leucine significant shifts in the distance distribution were observed. If PutP works according to the proposed mechanism of function of LeuT and Mhp1, also on the cytoplasmic side, between K91 (TM 2') and L371 (TM 9'), significant distance changes would have been expected. For both proteins, a relative movement of the four-helix bundle (TMs 1, 2, 6, and 7) relative to the 'hash' motif (TM 3, 4, 8, and 9) is the proposed molecular basis for the alternating access of the ligand binding sites via a periplasmic or a cytoplasmic vestibule (Shimamura et al., 2010, Krishnamurthy & Gouaux, 2012). But again only subtle changes in the mean distance were detected. For the double-Cys constructs 50/304 and 149/450 also no changes in the mean distance were observed. Interestingly, in both samples broad distance distributions were determined indicating a highly dynamic system. These dynamics could derive from spin label flexibility or from structural rearrangements within the protein (Polyhach *et al.*, 2011, Fleissner *et al.*, 2011). In fact, the broad distance distribution most probably results from a combination of both, dynamics of the protein and the spin-label. In summary, under the experimental conditions the addition of ligands did not trigger global conformational alterations in PutP between an inward- and an outward-facing conformation as they were expected according to the alternating access mechanism (Jardetzky, 1966) and as they were already described for LeuT under similar conditions (Zhao et al., 2010, Claxton

et al., 2010). Since the binding properties of spin-labeled PutP were not affected (Fig. 4.1 B) and the results of the DEER measurements in PutP and LeuT showed significant discrepancies, this study suggests that despite their structural similarity, the transport mechanism of both proteins might differ considerably. These findings raise the question at which stage the mechanistic differences become obvious? Previously it was shown that PutP function is not only dependent on a  $\text{Na}^+$ -gradient, but also on the membrane potential (Chen & Wilson, 1986, Jung *et al.*, 1998b). For LeuT, a  $\text{Na}^+$ -gradient proved to be the driving force for leucine uptake. Until now, the role of the membrane potential was not investigated in detail. In the absence of a membrane potential LeuT is found predominately in an outward-facing conformation (Zhao *et al.*, 2010, Wang *et al.*, 2012), whereas PutP was shown to be in an inward-facing conformation (Pirch *et al.*, 2003). For SGLT1, another member of the SSSF a similar orientation was shown and a transition to an outward-facing conformation was triggered only in the presence of a membrane potential (Loo *et al.*, 1998). Since the EPR measurements were performed in non-energized proteoliposomes, it might be possible that the energy source required for the transition between an inwardly-oriented and an outwardly-oriented conformation was missing. The observed subtle distance changes might also be explained by the cryogenic conditions (50 K) during the DEER measurements since low temperatures may trap proteins in distinct conformations (Xu & Gunner, 2001). Due to the observed changes in the polarity profile and previously described distance changes in PutP (Jeschke *et al.*, 2004), LacY (Smirnova *et al.*, 2007), and LeuT (Claxton *et al.*, 2010), the latter possibility seems to be rather unlikely.

How do these observations fit into the proposed transport mechanism of PutP? Since PutP functions as a  $\text{Na}^+$ /proline symporter, catalyzing the accumulation of proline in the bacterial cell, the results of this investigation on the first glimpse contradict this accepted fact. Binding of  $\text{Na}^+$  seems to result in stronger tertiary interactions of eL4 with other PutP domains on the periplasmic side. Subsequent binding of proline more than reverses this effect, possibly explained by opening of an outward-facing cavity. For an importer one would expect opposite effects. An explanation for this phenomenon might be that depending on the orientation of the electrochemical  $\text{Na}^+$  gradient, PutP (Jung *et al.*, 1998b) and other members of the SSSF e.g. the  $\text{Na}^+$ /glucose symporter (Wright *et al.*, 1994) were shown to work in either one direction or the other. To interpret the results of this work it needs to be clarified which conformation PutP adopts in the Apo-state. Cys accessibility studies suggested that in the absence of ligands, in non-energized membrane vesicles, PutP is predominantly found in an inward-facing conformation (Raba *et al.*, 2008, Pirch *et al.*, 2003). Interestingly, as already mentioned above, it was also shown that in the absence of a membrane potential SGLT1 is not accessible from the extracellular phase by membrane impermeant compounds, if no ligands are present (Loo *et al.*, 1998). If the membrane was energized, the transporter

became accessible from the outside reminiscent with the opening of an outwardly-oriented vestibule. Since the EPR measurements on eL4 of PutP were performed in non-energized proteoliposomes, it can be assumed that reconstituted PutP adopts a similar orientation. In summary, it can be supposed that the inward-facing conformation of PutP is harboring the lowest free energy and that this state is the starting point for conformational alterations under the experimental conditions (Fig. 4.7).

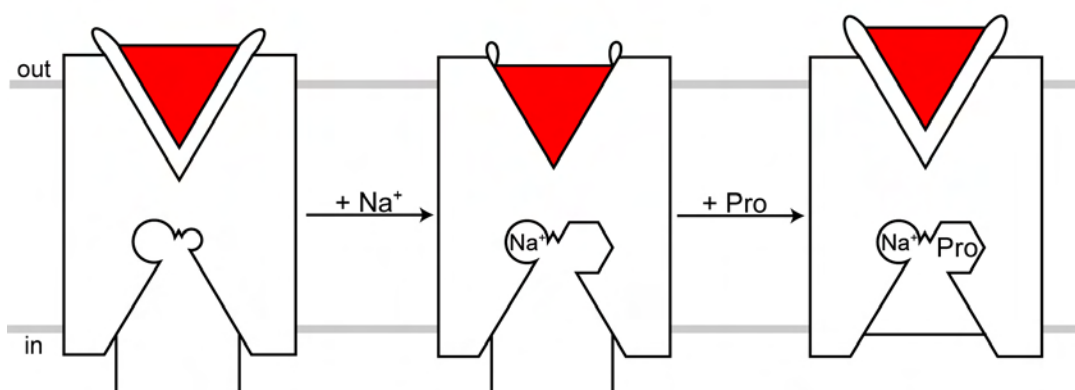


**Fig. 4.7 Predicted schematic of the ligand induced dynamics of eL4 in the transport cycle of PutP.** Under the experimental conditions, PutP is proposed to adopt an inward-facing open conformation in the Apo-state. The presence of  $\text{Na}^+$  induced tighter packing of eL4 into the periplasmic cavity, while the cytoplasmic cavity was stabilized. According to the ordered binding mechanism, the affinity for the actual substrate proline is increased subsequent to  $\text{Na}^+$  binding. If both ligands were added, a decrease of tertiary interactions of eL4 and an increase in the polarity of the surrounding was observed, supporting the idea of an improved accessibility of the substrate binding sites. The fact that no distance changes on the cytoplasmic side were detected, but previous Cys accessibility analyses showed that the presence of both ligands led to a reduced accessibility of residues lining the intracellular cavity, might hint at a inward-facing occluded conformation (red triangle: eL4; Pro: proline; out:periplasm; in cytoplasm).

For this reason added  $\text{Na}^+$  accesses the ion binding site via an intracellular cavity. In this study, upon ion binding neither on the periplasmic, nor on the cytoplasmic side significant distance changes were observed. However, previously a  $\text{Na}^+$  dependent increase of the distance between spin labels attached to positions 37 (iL1) and D187 (TM 5') was observed (Jeschke et al., 2004). For this reason it might be speculated that  $\text{Na}^+$  stabilizes the inward facing conformation. In addition, in Cys accessibility analyses of TM 1' and 8'  $\text{Na}^+$  did not alter the labeling pattern of residues lining the intracellular vestibule (Pirch et al., 2003, Raba et al., 2008). In contrast, proline in the presence of  $\text{Na}^+$  had more pronounced effects on the mobility and polarity profile of eL4 compared to  $\text{Na}^+$  alone, suggesting that interactions between eL4 and other protein domains were weakened. The fact that  $\text{Na}^+$  and proline together did not lead to changes in the distance distributions suggests that no global alterations such as reciprocal opening and closing of cavities were induced in PutP. Although closure of an intracellular cavity could not be shown using DEER, previous Cys accessibility analyses on TM 1' and 8' gave evidence for conformational alterations on the cytoplasmic side (Pirch *et al.*, 2002, Pirch et al., 2003, Raba et al., 2008). The addition of  $\text{Na}^+$  and proline, reduced the labeling efficiency by fluorescein-5-maleimide (FM) on the intracellular side drastically. Due to the presented DEER data these observations might rather be explained by

closing intracellular gates that occlude a water-filled cavity than a complete closure of the vestibule reminiscent to the situation in the occluded state of BetP (Ressl et al., 2009). In the X-ray crystal structure an evolving inward-cavity was visible that is occluded by residues located in TMs 1', 5', and 8' right before the translocation pathway opens out into the cytoplasm.

In conclusion, the results of this work showed that Na<sup>+</sup> and proline induce conformational alterations within PutP that are to some extent in accordance with the alternating access mechanism. EL4 presumably adopts a similar functional role as key element in regulating access to the substrate binding site from the periplasmic space, as it was described for other members of the LeuT structural family. Differences in the observed conformational rearrangements and the fact that no transitions between an inward- and an outward-facing conformation were detected might be explained by the energetic properties of LeuT-like transporters. In contrast to LeuT, in PutP the membrane potential is pivotal for transporter function. According to the results of this work, the energetic state of the membrane is essential to swap the transporter from an inward- to an outward-facing state. To test this hypothesis additional central questions have to be addressed in the near future. How does the membrane potential influence ligand induced distance changes? Under energized conditions, do Na<sup>+</sup> and/or proline trigger conformational alterations in a physiological direction? How does PutP 'sense' the membrane potential and how is an outward facing conformation triggered? Challenges for these follow up experiments will be the generation of a membrane potential and a Na<sup>+</sup>-gradient, and a concerted start of these bulk experiments under the experimental conditions. These obstacles might be overcome by co-reconstitution of PutP with light inducible ion-pumps such as channelrhodopsin-1 and 2 (Nagel *et al.*, 2005). Thus, a joint start of the transporter activity could be achieved by using directed light pulses. An alternative would be a caged substrate, an inert precursor that can directly be transformed to a biologically active compound by photolysis.

## 4.6 References

- Abramson, J., I. Smirnova, V. Kasho, G. Verner, H. R. Kaback & S. Iwata, (2003) Structure and mechanism of the lactose permease of *Escherichia coli*. *Science* 301: 610-615.
- Amann, E., B. Ochs & K. J. Abel, (1988) Tightly regulated tac promoter vectors useful for the expression of unfused and fused proteins in *Escherichia coli*. *Gene* 69: 301-315.
- Bayer, A. S., S. N. Coulter, C. K. Stover & W. R. Schwan, (1999) Impact of the high-affinity proline permease gene (*putP*) on the virulence of *Staphylococcus aureus* in experimental endocarditis. *Infect Immun* 67: 740-744.
- Bordignon, E., J. P. Klare, M. Doebber, A. A. Wegener, S. Martell, M. Engelhard & H. J. Steinhoff, (2005) Structural analysis of a HAMP domain: the linker region of the

- phototransducer in complex with sensory rhodopsin II. *The Journal of biological chemistry* 280: 38767-38775.
- Bordignon, E. & H. J. Steinhoff, (2007) Membrane protein structure and dynamics studied by site-directed spin labeling ESR. In: ESR Spectroscopy in Membrane Biophysics. . M. A. Hemminga & L. J. Berliner (eds). New York: Springer US, pp. 129-164.
- Chen, C. C., T. Tsuchiya, Y. Yamane, J. M. Wood & T. H. Wilson, (1985) Na<sup>+</sup> (Li<sup>+</sup>)-proline cotransport in *Escherichia coli*. *The Journal of membrane biology* 84: 157-164.
- Chen, C. C. & T. H. Wilson, (1986) Solubilization and functional reconstitution of the proline transport system of *Escherichia coli*. *The Journal of biological chemistry* 261: 2599-2604.
- Claxton, D. P., M. Quick, L. Shi, F. D. de Carvalho, H. Weinstein, J. A. Javitch & H. S. McHaourab, (2010) Ion/substrate-dependent conformational dynamics of a bacterial homolog of neurotransmitter:sodium symporters. *Nat Struct Mol Biol* 17: 822-829.
- Dalmas, O., L. G. Cuello, V. Jogini, D. M. Cortes, B. Roux & E. Perozo, (2010) Structural dynamics of the magnesium-bound conformation of CorA in a lipid bilayer. *Structure* 18: 868-878.
- Faham, S., A. Watanabe, G. M. Besserer, D. Cascio, A. Specht, B. A. Hirayama, E. M. Wright & J. Abramson, (2008) The crystal structure of a sodium galactose transporter reveals mechanistic insights into Na<sup>+</sup>/sugar symport. *Science* 321: 810-814.
- Fleissner, M. R., M. D. Bridges, E. K. Brooks, D. Cascio, T. Kalai, K. Hideg & W. L. Hubbell, (2011) Structure and dynamics of a conformationally constrained nitroxide side chain and applications in EPR spectroscopy. *Proceedings of the National Academy of Sciences of the United States of America* 108: 16241-16246.
- Forrest, L. R. & G. Rudnick, (2009) The rocking bundle: a mechanism for ion-coupled solute flux by symmetrical transporters. *Physiology (Bethesda)* 24: 377-386.
- Forrest, L. R., Y. W. Zhang, M. T. Jacobs, J. Gesmonde, L. Xie, B. H. Honig & G. Rudnick, (2008) Mechanism for alternating access in neurotransmitter transporters. *Proceedings of the National Academy of Sciences of the United States of America* 105: 10338-10343.
- Hilger, D., (2010) Electron paramagnetic resonance spectroscopic analysis of membrane transport proteins. In: Department of Biology - Microbiology. Munich: Ludwig-Maximilians-Universität München, pp. 252.
- Hilger, D., Y. Polyhach, H. Jung & G. Jeschke, (2009) Backbone structure of transmembrane domain IX of the Na<sup>+</sup>/proline transporter PutP of *Escherichia coli*. *Biophys J* 96: 217-225.
- Hubbell, W. L., D. S. Cafiso & C. Altenbach, (2000) Identifying conformational changes with site-directed spin labeling. *Nat Struct Biol* 7: 735-739.
- Hubbell, W. L., H. S. Mchaourab, C. Altenbach & M. A. Lietzow, (1996) Watching proteins move using site-directed spin labeling. *Structure* 4: 779-783.
- Jardetzky, O., (1966) Simple allosteric model for membrane pumps. *Nature* 211: 969-970.

- Jeschke, G., V. Chechik, P. Ionita, A. Godt, H. Zimmermann, J. Banham, C. R. Timmel, D. Hilger & H. Jung, (2006) DeerAnalysis2006 - a comprehensive software package for analyzing pulsed ELDOR data. *Appl Magn Reson* 30: 473-498.
- Jeschke, G., C. Wegener, M. Nietschke, H. Jung & H. J. Steinhoff, (2004) Interresidual distance determination by four-pulse double electron-electron resonance in an integral membrane protein: the Na<sup>+</sup>/proline transporter PutP of *Escherichia coli*. *Biophys J* 86: 2551-2557.
- Jung, H., (2002) The sodium/substrate symporter family: structural and functional features. *FEBS letters* 529: 73-77.
- Jung, H., D. Hilger & M. Raba, (2012) The Na<sup>+</sup>/L-proline transporter PutP. *Front Biosci* 17: 745-759.
- Jung, H., R. Rubenhagen, S. Tebbe, K. Leifker, N. Tholema, M. Quick & R. Schmid, (1998a) Topology of the Na<sup>+</sup>/proline transporter of *Escherichia coli*. *J Biol Chem* 273: 26400-26407.
- Jung, H., S. Tebbe, R. Schmid & K. Jung, (1998b) Unidirectional reconstitution and characterization of purified Na<sup>+</sup>/proline transporter of *Escherichia coli*. *Biochemistry* 37: 11083-11088.
- Kavermann, H., B. P. Burns, K. Angermuller, S. Odenbreit, W. Fischer, K. Melchers & R. Haas, (2003) Identification and characterization of *Helicobacter pylori* genes essential for gastric colonization. *J Exp Med* 197: 813-822.
- Krishnamurthy, H. & E. Gouaux, (2012) X-ray structures of LeuT in substrate-free outward-open and apo inward-open states. *Nature*.
- Langen, R., K. J. Oh, D. Cascio & W. L. Hubbell, (2000) Crystal structures of spin labeled T4 lysozyme mutants: implications for the interpretation of EPR spectra in terms of structure. *Biochemistry* 39: 8396-8405.
- Loo, D. D., B. A. Hirayama, E. M. Gallardo, J. T. Lam, E. Turk & E. M. Wright, (1998) Conformational changes couple Na<sup>+</sup> and glucose transport. *Proceedings of the National Academy of Sciences of the United States of America* 95: 7789-7794.
- MacArthur, M. W. & J. M. Thornton, (1991) Influence of proline residues on protein conformation. *Journal of molecular biology* 218: 397-412.
- McHaourab, H. S., M. A. Lietzow, K. Hideg & W. L. Hubbell, (1996) Motion of spin-labeled side chains in T4 lysozyme. Correlation with protein structure and dynamics. *Biochemistry* 35: 7692-7704.
- Miller, J. H., (1992) *A Short Course in Bacterial Genetics: A Laboratory Manual and Handbook for Escherichia coli and Related Bacteria*, p. 456. CSHL Press.
- Mitchell, S. M., E. Lee, M. L. Garcia & M. M. Stephan, (2004) Structure and function of extracellular loop 4 of the serotonin transporter as revealed by cysteine-scanning mutagenesis. *J Biol Chem* 279: 24089-24099.
- Murakami, S., R. Nakashima, E. Yamashita & A. Yamaguchi, (2002) Crystal structure of bacterial multidrug efflux transporter AcrB. *Nature* 419: 587-593.

- Nagel, G., T. Szellas, S. Kateriya, N. Adeishvili, P. Hegemann & E. Bamberg, (2005) Channelrhodopsins: directly light-gated cation channels. *Biochemical Society transactions* 33: 863-866.
- Olkhova, E., M. Raba, S. Bracher, D. Hilger & H. Jung, (2010) Homology Model of the Na(+)/Proline Transporter PutP of Escherichia coli and Its Functional Implications. *J Mol Biol.*
- Pannier, M., S. Veit, A. Godt, G. Jeschke & H. W. Spiess, (2000) Dead-time free measurement of dipole-dipole interactions between electron spins. *J Magn Reson* 142: 331-340.
- Pearson, W. R., (1990) Rapid and sensitive sequence comparison with FASTP and FASTA. *Methods Enzymol* 183: 63-98.
- Pearson, W. R. & D. J. Lipman, (1988) Improved tools for biological sequence comparison. *Proceedings of the National Academy of Sciences of the United States of America* 85: 2444-2448.
- Pirch, T., S. Landmeier & H. Jung, (2003) Transmembrane domain II of the Na+/proline transporter PutP of Escherichia coli forms part of a conformationally flexible, cytoplasmic exposed aqueous cavity within the membrane. *J Biol Chem* 278: 42942-42949.
- Pirch, T., M. Quick, M. Nietschke, M. Langkamp & H. Jung, (2002) Sites important for Na+ and substrate binding in the Na+/proline transporter of Escherichia coli, a member of the Na+/solute symporter family. *J Biol Chem* 277: 8790-8796.
- Polyhach, Y., E. Bordignon & G. Jeschke, (2011) Rotamer libraries of spin labelled cysteines for protein studies. *Phys Chem Chem Phys* 13: 2356-2366.
- Raba, M., T. Baumgartner, D. Hilger, K. Klempahn, T. Hartel, K. Jung & H. Jung, (2008) Function of transmembrane domain IX in the Na+/proline transporter PutP. *J Mol Biol* 382: 884-893.
- Reed-Tsur, M. D., A. De la Vieja, C. S. Ginter & N. Carrasco, (2008) Molecular characterization of V59E NIS, a Na+/- symporter mutant that causes congenital I-transport defect. *Endocrinology* 149: 3077-3084.
- Ressl, S., A. C. Terwisscha van Scheltinga, C. Vonrhein, V. Ott & C. Ziegler, (2009) Molecular basis of transport and regulation in the Na(+)/betaine symporter BetP. *Nature* 458: 47-52.
- Sabarinathan, R., K. Aishwarya, R. Sarani, M. K. Vaishnavi & K. Sekar, (2011) Water-mediated ionic interactions in protein structures. *J Biosci* 36: 253-263.
- Schulze, S., S. Koster, U. Geldmacher, A. C. Terwisscha van Scheltinga & W. Kuhlbrandt, (2010) Structural basis of Na(+)-independent and cooperative substrate/product antiport in CaiT. *Nature* 467: 233-236.
- Shaffer, P. L., A. Goehring, A. Shankaranarayanan & E. Gouaux, (2009) Structure and mechanism of a Na+-independent amino acid transporter. *Science* 325: 1010-1014.
- Shi, L., M. Quick, Y. Zhao, H. Weinstein & J. A. Javitch, (2008) The mechanism of a neurotransmitter:sodium symporter--inward release of Na+ and substrate is triggered by substrate in a second binding site. *Mol Cell* 30: 667-677.

- Shimamura, T., S. Weyand, O. Beckstein, N. G. Rutherford, J. M. Hadden, D. Sharples, M. S. Sansom, S. Iwata, P. J. Henderson & A. D. Cameron, (2010) Molecular basis of alternating access membrane transport by the sodium-hydantoin transporter Mhp1. *Science* 328: 470-473.
- Singh, S. K., A. Yamashita & E. Gouaux, (2007) Antidepressant binding site in a bacterial homologue of neurotransmitter transporters. *Nature* 448: 952-956.
- Smicun, Y., S. D. Campbell, M. A. Chen, H. Gu & G. Rudnick, (1999) The role of external loop regions in serotonin transport. Loop scanning mutagenesis of the serotonin transporter external domain. *The Journal of biological chemistry* 274: 36058-36064.
- Smirnova, I., V. Kasho, J. Y. Choe, C. Altenbach, W. L. Hubbell & H. R. Kaback, (2007) Sugar binding induces an outward facing conformation of LacY. *Proceedings of the National Academy of Sciences of the United States of America* 104: 16504-16509.
- Stalmach, M. E., S. Grothe & J. M. Wood, (1983) Two proline porters in *Escherichia coli* K-12. *Journal of bacteriology* 156: 481-486.
- Steinhoff, H., A. Savitsky, C. Wegener, M. Pfeiffer, M. Plato & K. Mobius, (2000) High-field EPR studies of the structure and conformational changes of site-directed spin labeled bacteriorhodopsin. *Biochimica et biophysica acta* 1457: 253-262.
- Tabor, S. & C. C. Richardson, (1985) A bacteriophage T7 RNA polymerase/promoter system for controlled exclusive expression of specific genes. *Proceedings of the National Academy of Sciences of the United States of America* 82: 1074-1078.
- Wang, H., J. Elferich & E. Gouaux, (2012) Structures of LeuT in bicelles define conformation and substrate binding in a membrane-like context. *Nature structural & molecular biology*.
- Watanabe, A., S. Choe, V. Chaptal, J. M. Rosenberg, E. M. Wright, M. Grabe & J. Abramson, (2010) The mechanism of sodium and substrate release from the binding pocket of vSGLT. *Nature* 468: 988-991.
- Wegener, C., S. Tebbe, H. J. Steinhoff & H. Jung, (2000) Spin labeling analysis of structure and dynamics of the Na<sup>(+)</sup>/proline transporter of *Escherichia coli*. *Biochemistry* 39: 4831-4837.
- Weyand, S., T. Shimamura, S. Yajima, S. Suzuki, O. Mirza, K. Krusong, E. P. Carpenter, N. G. Rutherford, J. M. Hadden, J. O'Reilly, P. Ma, M. Saidijam, S. G. Patching, R. J. Hope, H. T. Norbertczak, P. C. Roach, S. Iwata, P. J. Henderson & A. D. Cameron, (2008) Structure and molecular mechanism of a nucleobase-cation-symport-1 family transporter. *Science* 322: 709-713.
- Wright, E. M., B. A. Hirayama & D. F. Loo, (2007) Active sugar transport in health and disease. *J Intern Med* 261: 32-43.
- Wright, E. M., D. D. Loo, M. Panayotova-Heiermann, M. P. Lostao, B. H. Hirayama, B. Mackenzie, K. Boorer & G. Zampighi, (1994) 'Active' sugar transport in eukaryotes. *J Exp Biol* 196: 197-212.
- Xu, Q. & M. R. Gunner, (2001) Trapping conformational intermediate states in the reaction center protein from photosynthetic bacteria. *Biochemistry* 40: 3232-3241.

- Yamashita, A., S. K. Singh, T. Kawate, Y. Jin & E. Gouaux, (2005) Crystal structure of a bacterial homologue of Na<sup>+</sup>/Cl<sup>-</sup>-dependent neurotransmitter transporters. *Nature* 437: 215-223.
- Yamato, I., (1992) Ordered binding model as a general mechanistic mechanism for secondary active transport systems. *FEBS letters* 298: 1-5.
- Yamato, I. & Y. Anraku, (1990) Mechanism of Na<sup>+</sup>/proline symport in *Escherichia coli*: reappraisal of the effect of cation binding to the Na<sup>+</sup>/proline symport carrier. *The Journal of membrane biology* 114: 143-151.
- Yamato, I. & Y. Anraku, (1993) Alkali Cation Transport Systems in Prokaryotes. In: Alkali Cation Transport Systems in Prokaryotes. E. P. Bakker (ed). Boca Raton, FL: CRC-Press, pp. 464.
- Yernool, D., O. Boudker, Y. Jin & E. Gouaux, (2004) Structure of a glutamate transporter homologue from *Pyrococcus horikoshii*. *Nature* 431: 811-818.
- Zhao, Y., D. Terry, L. Shi, H. Weinstein, S. C. Blanchard & J. A. Javitch, (2010) Single-molecule dynamics of gating in a neurotransmitter transporter homologue. *Nature* 465: 188-193.
- Zhao, Y., D. S. Terry, L. Shi, M. Quick, H. Weinstein, S. C. Blanchard & J. A. Javitch, (2011) Substrate-modulated gating dynamics in a Na<sup>+</sup>-coupled neurotransmitter transporter homologue. *Nature* 474: 109-113.
- Zhou, Z., J. Zhen, N. K. Karpowich, R. M. Goetz, C. J. Law, M. E. Reith & D. N. Wang, (2007) LeuT-desipramine structure reveals how antidepressants block neurotransmitter reuptake. *Science* 317: 1390-1393.
- Zomot, E. & B. I. Kanner, (2003) The interaction of the gamma-aminobutyric acid transporter GAT-1 with the neurotransmitter is selectively impaired by sulfhydryl modification of a conformationally sensitive cysteine residue engineered into extracellular loop IV. *The Journal of biological chemistry* 278: 42950-42958.

## 4.7 Supplementary Material

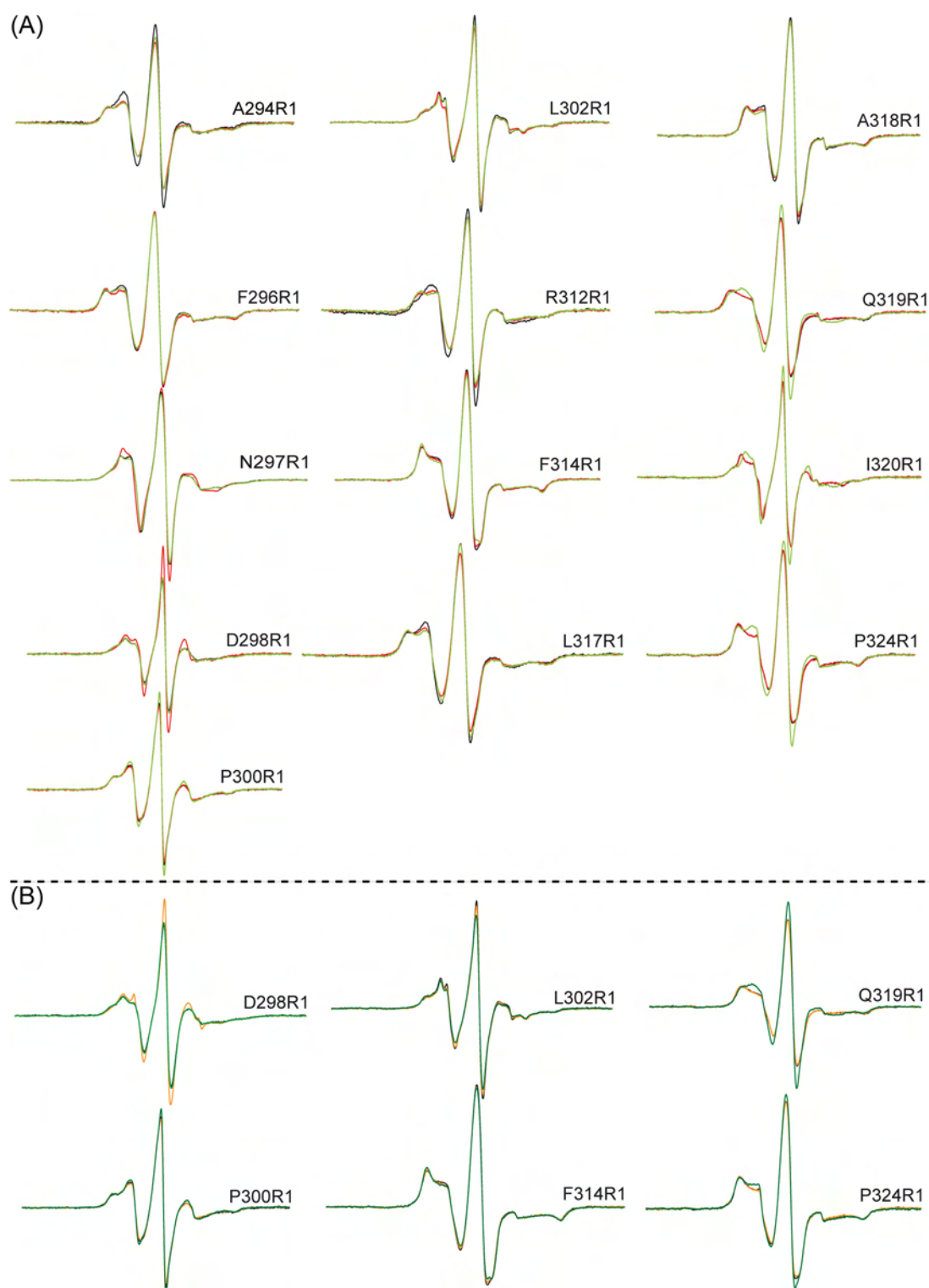
```

          300                               310                               320
sp_P07117_PUTP_ECOLI AYFNDHPALAG.....AVNQNAERVFVFIELAQILFN..P
sp_P10502_PUTP_SALTY AYFNNNPALAG.....AVNQNSERVFVFIELAQILFN..P
tr_Q7CI08_PUTP_YERPE AYFENNPEQAG.....NVSQNGERVFVFIELAKLLFN..P
tr_Q915F5_PUTP_PSEAE AYFQAHPEQAG.....AVSENPERVFVFIELAKILFN..P
tr_Q7DDQ5_PUTP_NEIMB AYFGANPKVVS.....SMSGNHERRIFVFIELSTLLFN..P
tr_Q9CN55_PUTP_PASMU AYFFANPQVAD.....TVNANHEQVFVFIELAKLLFN..P
tr_O24896_PUTP_HELPY AYVHKFDLS.....LEDPEKIFVFIELVMSQLLFN..P
tr_A3GXV9_PUTP_VIBCH IFVTQSGTIG.....LDDGEKIFVFIELVNSLFLH..P
sp_Q2FWY7_PUTP_STAA8 AFVPAYHIK.....LEDPEKIFVFIELVMSQVLFH..P
sp_O06493_OPUE_BACSU AYAHKFGVA.....VKDPEMIFVFIELVMSQVLFH..P
tr_Q79VH1_PUTP_CORGL VFFAQNPDANI.....TDTRAYESIFVFIELVMSQVLFH..P
tr_O59086_PUTP_PYRHO ALAINGSIK.....IDDPKIFVFIELVMSQVLFH..P
tr_Q9V2P3_PUTP_PYRAB AIVPDVSQLPG.....KNAEMIFVFIELVMSQVLFH..P
sp_P16256_PANF_ECOLI AVIPDLTVP.....DLVFIPIELVMSQVLFH..P
tr_Q8D1P2_PANF_YERPE AVLPLDKIP.....DQVFIPIELVMSQVLFH..P
sp_P44963_PANF_HAEIN AVIPNLTVS.....DQVFIPIELVMSQVLFH..P
sp_P13866_SGLT1_HUMAN ILYTEKIACVV.....PSECEKYCGTKVGCTNIAYPTLVVLELMP..N
sp_Q9NY91_SGLT3_HUMAN ILYTDMVACVV.....PSECVKHCQVGVGCTNIAYPTLVVLELMP..Q
sp_P31639_SGLT2_HUMAN ILYPDEVACVV.....PEVCRRCVCGTEVGCNIAYPTLVVLELMP..N
sp_Q9Y289_SL56_HUMAN AYYQEYPMISIQQ.....AQAAPDQFVLYFVMDLLKGLP
sp_Q92911_NIS_HUMAN VFYTDQDPLLLG.....RISAPDQYMPPLVLDIFEDLP
sp_P96169_SGLT_VIBPA VITSDPQLMAS.....LGDIAATNLPSAANADKAYPWL.T.QFLP..V
tr_O27884_PUTP_METTH VYFFRKMGMIA.....VQAAG.....GNADKIIPIFFIKSAMP..E
tr_Q9HP63_PANF_HALSA GVGLPLPDG.....ENIVPILLSEYTP..G
tr_O29293_PUTP_ARCFU LMIETGPMGGEGANAVKILQSYMAQYGVGGWTDYSMIAAVEALQN..P
tr_O29063_PANF_ARCFU ATPEFAELG.....AKTATPAMIVSVLP..T
sp_P33413_DUR3_YEAST AVETSPNFPTYP.....DP...LTSFQANSGLVLPAAAIAMG..K

```

**Suppl. Fig. 4.1 Multiple sequence alignment of pro- and eukaryotic members of the SSSF (Hilger, 2010).** A multiple alignment was generated using ClustalX (2.0.10) with sequences (FASTA) obtained from a blastp search ([www.ncbi.nlm.nih.gov/BLAST](http://www.ncbi.nlm.nih.gov/BLAST)) against PutP of *E. coli* K12 (swiss-prot entry P07117) at the EBI [www-server](http://www.ebi.ac.uk/clustalw/) ([www.ebi.ac.uk/clustalw/](http://www.ebi.ac.uk/clustalw/)) (Pearson, 1990, Pearson & Lipman, 1988). The chosen matrix was Gonnet series, penalties were 10 (gap opening), 0.2 (gap extension) and 4 (gap separation distance). The resulting alignment was optically improved by ESPrpt.cgi Version 3.06 CGI 3.05 (<http://esprpt.ibcp.fr/ESPrpt/cgi-bin/ESPrpt.cgi>). Strictly conserved residues (100% identical to consensus) are in red blocks and highly homologous residues (>60% similar to consensus) are in red type inserted in blue boxes. The term PutP refers to the homology with PutP of *E. coli*, experimental evidence for Na<sup>+</sup>/proline transporter activity exists only for *Salmonella typhimurium* (SALTY), *Staphylococcus aureus* (STAAS), and OpuE of *Bacillus subtilis* (BACSU). Arabic numbers indicate the position in the primary sequence and refer to the first amino acid of PutP of *E. coli* of the alignment. Black bars on the top mark the position of the transmembrane domains (numbered with Roman numerals) in PutP of *E. coli*, according to Jung *et al.* (1998).





**Suppl. Fig. 4.3 Ligand dependent cw EPR spectra of spin labeled single-Cys PutP derivatives.** (A) EPR spectra of singly-labeled PutP derivatives in which changes in the low- and high field peaks were observed upon ligand binding. PutP constructs were expressed, purified, spin-labeled, and reconstituted in a protein to lipid ratio of 1:20 (w/w). EPR measurements were performed at 298 K in the absence of ligands (black line) or in the presence of 50 mM NaCl (red line) or 50 mM NaCl and 10 mM proline (green line). (B) As negative control samples were measured in the presence of KCl instead of NaCl. black line: EPR spectrum in the absence of ligands; orange line: EPR spectrum in the presence of 50 mM KCl; dark green line: EPR spectrum in the presence of 50 mM KCl/10 mM proline; R1: MTSSL side chain linked to site specifically introduced Cys residues by disulfide bridges. Native amino acids at the respective positions are shown as one letter code.

**Suppl. Table 4.1 Ligand dependent changes in  $\Delta H_0^{-1}$  of spin labeled single-Cys PutP derivatives.** To test the significance of the observed changes in the reciprocal line width, in addition to samples supplemented with NaCl or NaCl and proline samples containing KCl or KCl and proline were also analyzed.

	$\Delta H_0^{-1}$ [mT <sup>-1</sup> ]					
	D298R1	P300R1	L302R1	F314R1	Q319R1	P324R1
<b>Apo</b>	2,70	3,33	3,03	1,92	1,96	1,92
<b>50 mM NaCl</b>	2,70	3,23	2,78	1,92	2,00	1,85
<b>50 mM KCl</b>	2,70	3,23	2,94	1,89	1,96	1,85
<b>50 mM NaCl/10 mM proline</b>	3,33	3,70	3,03	1,32	2,22	2,22
<b>50 mM KCl/10 mM proline</b>	3,33	3,57	2,86	1,92	2,17	2,08

## **5 THE $\text{Na}^+$ /L-PROLINE TRANSPORTER PUTP**

## The Na<sup>+</sup>/L-proline transporter PutP

Heinrich Jung<sup>1</sup>, Daniel Hilger<sup>1</sup>, Michael Raba<sup>1</sup>

<sup>1</sup>LMU Munich, Biocentre, Microbiology, Grosshaderner Strasse 2-4, Martinsried, D-82152, Germany

### TABLE OF CONTENTS

1. Abstract
2. Introduction
3. PutP – a member of the Na<sup>+</sup>/solute symporter family
4. Physiological significance of PutP
  - 4.1. PutP in L-proline catabolism and osmoprotection
  - 4.2. Role of PutP in bacteria host interactions
5. PutP and the LeuT-type structural fold
6. Structure-function relationships in PutP
  - 6.1. The Na<sup>+</sup> binding site
  - 6.2. The L-proline binding site
7. Molecular mechanism of Na<sup>+</sup>/solute symport
  - 7.1. Transport via alternating access
  - 7.2. Impact of Na<sup>+</sup> on the outward-facing cavity and substrate binding
  - 7.3. The outer thin gate and substrate binding
  - 7.4. Transition between outward- and inward-facing conformations
  - 7.5. The inner thin gate and substrate release into the cytoplasm
8. Conclusions and perspectives
9. Acknowledgements
10. References

## 1. ABSTRACT

The Na<sup>+</sup>/L-proline transporter PutP is a member of the Na<sup>+</sup>/solute symporter family (TC 2A.21, SLC5), which contains several hundred proteins of pro- and eukaryotic origin. Within the family, the capability of L-proline uptake is restricted to proteins of prokaryotes. PutP contributes to the use of L-proline as a nutrient. In addition, the transporter may supply cells with compatible solute during adaptation to osmotic stress. Based on these and other functions, PutP is of significance for various bacteria-host interactions including the virulence of human pathogens. A homology model of *Escherichia coli* PutP was generated based on the crystal structure of the *Vibrio parahaemolyticus* Na<sup>+</sup>/galactose symporter. According to the model, PutP has a core structure of five plus five transmembrane domains forming an inverted repeat similar as originally revealed by the crystal structure of the Na<sup>+</sup>/leucine transporter LeuT. The homology model is experimentally verified by Cys cross-linking and site-directed spin labeling in combination with electron paramagnetic resonance spectroscopy. The putative sites of Na<sup>+</sup> and L-proline binding are described, and a putative transport mechanism is discussed.

## 2. INTRODUCTION

L-Proline is an amino acid of particular significance. It is the only proteinogenic amino acid in which the nitrogen attached to C<sub>alpha</sub> forms a secondary amine with an aliphatic side chain. In proteins, the resulting rigid ring system has a specific impact on structure and may serve, for example, as alpha-helix breaker (1). Also free L-proline carries out important functions in cells of all branches of life. It may serve as i) source of carbon, nitrogen and energy (2-4); ii) compatible solute during adaptation to conditions of high osmolality (5, 6); iii) regulator of cell metabolism (7); iv) scavenger of reactive oxygen species (8, 9); and v) modulator of the intracellular redox environment (10). The free amino acid does not only occur intracellularly, but is also found on inner and outer surfaces of higher eukaryotes, for example, in the gastric juice, urine, the gut of mammals and nematodes, the insect fat body, and plant exudates in concentrations ranging from micromolar to millimolar (11-15). In view of the abundance and different functions of L-proline, it is not surprising that bacteria employ various L-proline-specific transport systems and enzymes allowing utilization of external L-proline. These systems play important roles in

## Putp

adaptation of single cell organisms to steadily changing environmental conditions as they occur in soil, water and during interactions with eukaryotic hosts. For example, enteric bacteria like *Escherichia coli* contain three L-proline transport systems (PutP, ProP, ProU) which differ in substrate specificity, mechanism of energy coupling, and physiological role. PutP is a high affinity transporter specific for L-proline and involved in L-proline catabolism (16-18). ProP is less specific and catalyzes the uptake of L-proline and betaines with low affinity. It functions both as an osmosensor and transporter (19-21). ProU (ProWXV) transports L-proline and betaines, and is like ProP involved in cell adaption to osmotic stress (5, 22). PutP and ProP are secondary transporters, while ProU is an ABC-type transporter. The transport and enzymatic functions of these proteins are conserved among different bacteria and archaea, whereas the genetic organization and regulatory mechanisms are diverse, and the physiological significance varies. This review focuses on the properties and physiological roles of PutP in bacteria, and summarizes the current state of knowledge of the transporter structure and molecular mechanism of function. Since PutP and other Na<sup>+</sup>/solute transporters are assumed to share a structural fold originally described for the bacterial Na<sup>+</sup>/leucine transporter LeuT (23), known structure-function relationships of PutP are discussed in relation to the information obtained from crystal structures of LeuT and structurally similar proteins.

### 3. PUTP – A MEMBER OF THE NA<sup>+</sup>/SOLUTE SYMPORTER FAMILY

The Na<sup>+</sup>/L-proline transporter PutP is a member of the Na<sup>+</sup>/solute symporter (SSS) family (TC 2A.21, SLC5), which contains several hundred proteins of pro- and eukaryotic origin (4, 24, 25). These proteins have the capability to couple an electrochemical Na<sup>+</sup> gradient with the transport of solutes like glucose, nucleosides, L-proline, pantothenate, or iodide. Within the SSS family, the capability of L-proline uptake is restricted to proteins of bacteria and archaea.

PutP of *E. coli* is the best characterized bacterial L-proline transporter of the SSS family. It catalyzes the symport of Na<sup>+</sup> and L-proline with a stoichiometry of 1:1 (17). Na<sup>+</sup> can be substituted by Li<sup>+</sup>, however despite earlier assumptions H<sup>+</sup>-driven L-proline uptake by PutP could not be demonstrated (17, 26, 27). Kinetic and ligand binding analyses identify PutP as a high affinity L-proline transporter with a  $k_{d(Pro)}$  and  $k_{m(Pro)}$  of 2  $\mu$ M (16, 17, 28). Modifications of the pyrrolidine ring or the carboxyl group of proline reduce affinity significantly, an observation which is in agreement with the high specificity of PutP for L-proline. Known competitive inhibitors are 3,4-dehydroproline ( $k_i = 9 \mu$ M), azetidine-2-carboxylate ( $k_i = 125 \mu$ M), and thioproline ( $k_i = 190 \mu$ M) (29). A Na<sup>+</sup> concentration required for half-maximum stimulation of L-proline uptake ( $k_{0.5(Na^+)}$ ) of 30  $\mu$ M suggests a high affinity also for Na<sup>+</sup> (26, 30). However, the  $k_{d(Na^+)}$  of Na<sup>+</sup> binding is with about 10 mM more than two orders of magnitude higher than,  $k_{0.5(Na^+)}$  (30). The discrepancy between kinetic and binding parameters is explained by a functional

asymmetry of the transporter i.e., the Na<sup>+</sup> affinity is high on the periplasmic side and low on the cytoplasmic side of the transporter (17, 30). This idea is supported by a significantly increased  $k_{0.5(Na^+)}$  when uptake is measured with PutP in an inside-out orientation (28). The lower Na<sup>+</sup> affinity on the inside of the transporter may facilitate ligand release into the cytosol under physiological conditions.

Besides transport proteins, the SSS family comprises proteins containing a domain similar to PutP at the primary and secondary structure level, fused to domains typically found in bacterial sensor kinases (4). Proteins exhibiting such a domain composition are found in proteobacteria of the subgroups alpha, gamma, delta (for example the putative proline sensor PrlS of *Aeromonas hydrophila*, CbrA of *Pseudomonas aeruginosa*). CbrA appears to be a global regulator that modulates metabolism, virulence and antibiotic resistance in *P. aeruginosa* (31). The signal(s) sensed by this type of sensor kinases remains to be elucidated. Based on the similarity of the N-terminal domain of CbrA to PutP one may speculate that the domain functions as an amino acid (L-proline) sensor. However, an analysis of the functional properties of CbrA did neither reveal a transport activity for L-proline or other amino acids, nor an influence of these compounds on the autokinase activity (Kerstin Schipper and Heinrich Jung, unpublished information).

### 4. PHYSIOLOGICAL SIGNIFICANCE OF PUTP

#### 4.1. PutP in L-proline catabolism and osmoprotection

In enteric bacteria *putP* is genetically associated with *putA* in the *put* operon (2, 3, 32). The *putA* gene encodes a multifunctional enzyme catalyzing the sequential oxidation of L-proline and delta<sup>1</sup>-pyrroline-5-carboxylate to L-glutamate (3, 33, 34). The *put* operon is responsible for the use of L-proline as source of carbon, nitrogen and energy. Expression of the operon is induced by L-proline and subject to catabolite repression. Induction involves the chemical reduction of PutA, which in its oxidized state functions as a transcriptional repressor of the *put* operon (34, 35). Other bacteria such as *Vibrio*, *Pseudomonas*, and *Helicobacter* species control expression of the *put* operon by separate proteins. In *P. aeruginosa*, the regulator PruR mediates *put* gene expression, while *P. putida* PutA regulates L-proline catabolism similar as enteric bacteria (36). In *Vibrio vulnificus* the regulator PutR and a cAMP binding protein (CRP) coactivate *put* expression (37). Remarkably, oxidation of L-proline to L-glutamate is stimulated under high salt conditions in *V. vulnificans*. The resulting L-glutamate is accumulated as a compatible solute and contributes to osmoprotection (38, 39). However, the *putP* gene and its orthologs are not always genetically linked with *putA*, and the transporter may not be functionally associated with a L-proline degradation pathway. For example OpuE, a PutP ortholog of *Bacillus subtilis*, is involved in cell adaptation to osmotic stress (40). The *opuE* gene is expressed from two osmoregulated promoters: *opuE* P-1 recognized by the vegetative sigma factor A and *opuE* P-2 dependent on the stress-induced transcription factor sigma B (41). Consistent with the temporary pattern of sigma<sup>B</sup> activation after sudden

**Table 1.** Significance of *put* and related genes for bacteria-host interactions

Bacterium	Gene	Encoded Protein	Significance	Reference
<i>Helicobacter pylori</i>	<i>putP</i>	Na <sup>+</sup> /proline symporter*	essential for stomach colonization	(49)
	<i>putA</i>	proline dehydrogenase	essential for bacterial motility and stomach colonization	(50, 53)
<i>Helicobacter hepaticus</i>	<i>putA</i>	proline dehydrogenase	modification of bacterial redox status, impact on host inflammatory response	(52, 53)
<i>Staphylococcus aureus</i>	<i>putP</i>	Na <sup>+</sup> /proline symporter	transcriptional activation by low proline concentrations and osmotic stress, contribution to <i>in vivo</i> survival of <i>S. aureus</i> in various infection models	(45-47)
<i>Vibrio cholerae</i>	<i>putP</i>	Na <sup>+</sup> /proline symporter	important for initial steps in biofilm formation (monolayer formation)	(58, 59)
	<i>sssA</i>	Na <sup>+</sup> /solute symporter*	important for initial steps in biofilm formation (monolayer formation)	(58, 59)
<i>Vibrio vulnificus</i>	<i>putP</i>	Na <sup>+</sup> /proline symporter	adaptation to changing osmolalities during host infection	(39)
<i>Francisella novicida</i>	<i>putP</i>	Na <sup>+</sup> /proline symporter*	required for pulmonary and systematic infection of mice	(56)
<i>Yersinia pestis</i>	<i>putP</i>	Na <sup>+</sup> /proline symporter*	induced upon temperature shift from 26 to 37°C	(57)
<i>Photobacterium luminescens</i>	<i>putP</i>	Na <sup>+</sup> /proline symporter*	regulation of alternative lifestyles during adaptation to nematode and insect hosts	(7)
<i>Pseudomonas putida</i>	<i>putP</i>	Na <sup>+</sup> /proline symporter	facilitation of the colonization of plant rhizosphere	(12)
	<i>putA</i>	proline dehydrogenase	facilitation of the colonization of plant rhizosphere	(12)
<i>Escherichia coli</i>	<i>putP</i>	Na <sup>+</sup> /proline symporter	expressed in clinical isolates, performs housekeeping functions important for survival of <i>E. coli</i> in different environments including the human host	(108)

\*Protein function not experimentally verified

environmental challenges, activity of the sigma<sup>B</sup>-dependent *opuE* P-2 promoter rises transiently upon osmotic upshock. The promoter allows the input of other typical sigma<sup>B</sup>-inducing stimuli such as heat and ethanol stress into the genetic control of *opuE*. In contrast, transcription initiating from the sigma<sup>A</sup>-dependent *opuE* P-1 promoter increases in proportion to the external osmolarity and is maintained at high levels (41). Differing from other uptake systems for osmoprotectants such as ProP or BetP, OpuE activity is not controlled at the protein level (19, 41, 42). *B. subtilis* contains another PutP ortholog, YcgO, as well as genes predicted to encode proline oxidizing enzymes. Whether or not the gene products are involved in L-proline catabolism remains to be experimentally tested.

#### 4.2. Role of PutP in bacteria host interactions

In addition to ensuring bacterial survival and growth in soil and aqueous environments, PutP and its substrate L-proline play a role in various bacteria host interactions (Table 1). Most extensive investigations have been performed for *Staphylococcus aureus* infections. The L-proline transporter PutP does specifically contribute to *in vivo* survival of *S. aureus* in various animal models, for example, murine abscess, urinary tract and systemic infection models (43-45). Here, PutP supports adaptation of the bacterium to high osmolarity. Similar to *opuE* of *B. subtilis*, the *putP* gene of *S. aureus* is not genetically linked with a gene coding for a L-proline oxidizing enzyme. Furthermore, the *putP* gene is transcriptionally activated by low-proline and high osmotic environments both in growth media and in murine or human clinical specimens (44, 46, 47). However, in high-proline and high osmotic environments, *putP* expression is down-regulated. Under these conditions, proline uptake is likely to be taken over by the osmoresponsive, low affinity proline and betaine transporter ProP which is also present in *S. aureus*. Down-regulation of *putP* expression depends on sigma<sup>B</sup> which acts here as a transcriptional repressor (46). PutP activity of *S. aureus* is not known to be regulated at the protein level.

L-proline transport and metabolism is also important for interactions between Gram-negative bacterial

pathogens and hosts. Growth of *Helicobacter pylori*, the causative agent of type B gastritis, peptic ulcer and a risk factor for the development of gastric carcinoma and mucosa associated lymphoma in humans, is reported to be enhanced by amino acids released by gastric epithelial cells (48). A genome-wide screen for genes involved in the virulence of *H. pylori* identified the *putP* gene as essential for colonization of the stomach in the Mongolian gerbil infection model (49). *H. pylori putP* forms together with the L-proline dehydrogenase gene *putA* the *put* operon. Remarkably, a *putA* mutant does neither accumulate L-proline, show motility in response to amino acids, nor display swarming activity. Flagella seem to exist but full length sheathed flagella are rarely observed. Finally, the *putA* mutant proves incapable to colonize the stomach of mice (50). The precise role of *putP* and *putA* in *H. pylori* metabolism and virulence is not known. The respective proteins may be required to utilize L-proline as a nutrient ensuring, for example, the supply of energy for transmembrane transport processes and bacterial cell motility. In fact, L-proline is suggested to be the predominant amino acid in the gastric juice of humans infected with *H. pylori* reaching concentration of up to 10 mg per g gastric juice (11, 50, 51). In addition, L-proline is shown to function as respiratory substrate in *H. pylori* (11, 52). But it cannot be excluded that the PutP-catalyzed accumulation of L-proline contributes also to the resistance of *H. pylori* against osmotic or oxidative stress. In fact, L-proline appears to be the most abundant free amino acid in *H. pylori* cells (accumulation to up to 600 nmol/g wet weight of cells during growth on Brucella agar plates (50). While L-proline accumulation may protect the bacterium from oxidative stress in the host, there is also the potential that L-proline oxidation via PutA affects the redox status of the bacterium by the transfer of electrons from reduced flavin to molecular oxygen leading to the generation of reactive oxygen species (52, 53). Clearly, further investigations are necessary to fully understand the significance of PutP and PutA in *H. pylori*. Finally, it is not known whether PutP is solely responsible for L-proline accumulation in *H. pylori*. The genome analysis predicts

## Putp

the existence of minimum two additional transporters potentially catalyzing L-proline accumulation: ProP and ProU (ProV/ProWX) (54). Since L-proline is not an essential amino acid for *H. pylori* (55), L-proline biosynthesis may also contribute to intracellular L-proline accumulation. The significance of the latter transporters and of L-proline biosynthesis for *H. pylori* is not known.

Similar to *H. pylori*, a recent genome-wide screen in *Francisella novicida*, a Gram-negative facultative intracellular bacterium and a causative agent of the potentially life-threatening disease tularemia in a large number of mammals, identified *putP* as one of the genes required for pulmonary and systemic infection of mice (56). The molecular basis of the effect of the *putP* deletion is not known. Furthermore, in *Yersinia pestis*, eleven genes required for efficient catabolism of amino acids are rapidly induced upon temperature shift from 26 to 37 °C, including those encoding the L-proline transporter PutP and the proline dehydrogenase PutA. It is speculated that these and other regulatory events allow a profligate catabolism of numerous metabolites available in the mammalian host (57). In *Vibrio cholerae*, a halophilic bacterium found in estuarine and coastal waters and an infectious agent of the diarrheal disease cholera, utilizes PutP and the ABC-type transporter OpuD for accumulation of L-proline and betaine under osmotic stress conditions. In this context it is hypothesized that these transport processes support the association of *V. cholerae* with the surfaces of algae, phytoplankton, and zooplankton, which in turn may lead to cholera outbreaks during plankton blooms (58). In addition, PutP and its homolog SssA are shown to play a role in the transition from transient to permanent attachment of *V. cholerae* to surfaces (59). L-proline is also involved in regulating alternative lifestyles in entomopathogenic bacteria (7, 60). Bacteria of the genera *Photorhabdus* and *Xenorhabdus* participate in trilateral interactions in which they enable their nematode hosts to parasitize insect larvae. Differential metabolomic profiling in *Photorhabdus luminescens* and *Xenorhabdus nematophila* revealed that L-proline in the insect's hemolymph initiates a metabolic shift leading to adaptation of the bacterial metabolism to the host environment. Thereby, PutP, PutA, and the ProU system are proposed to regulate the metabolic shift and to maintain the bacterial proton motive force that ultimately regulates the downstream bacterial pathways affecting virulence and antibiotic production (7).

L-Proline uptake and metabolism may also support symbiotic interactions between bacteria and plants. Almost all of the twenty proteinogenic amino acids can be detected in plant exudates, with L-proline being one of the most abundant (12, 13). For root colonizing *Pseudomonas* species it is assumed that the PutP and PutA-dependent L-proline catabolism supports interactions of the soil bacteria with the plant rhizosphere (12). In *Sinorhizobium meliloti*, L-proline catabolism contributes to root colonization as well as to the establishment of symbiotic interactions with roots (61, 62). However, the latter strain does not contain a PutP homolog, and the role and mechanism of proline transport in the strain remains to be elucidated.

## 5. PUTP AND THE LEUT-TYPE STRUCTURAL FOLD

In view of the significance of PutP for bacterial physiology and interorganismic interactions, the molecular mechanism of Na<sup>+</sup>/solute symport catalyzed by the transporter is investigated. Clearly, information of the three dimensional structure of the protein is a prerequisite for understanding of this mechanism. However, despite the growing number of available crystal structures of secondary transporters (23, 63-72), a high resolution structure of PutP or any other L-proline transporting integral membrane protein is not available yet. A first insight into the fold of a member of the SSS family was gained by the crystallization of the Na<sup>+</sup>-dependent galactose symporter vSGLT of *Vibrio parahaemolyticus* (65). It turned out that vSGLT shares a characteristic core architecture with genetically unrelated gene families which are integrated in a structural family of LeuT-like transporters (23, 65, 67, 68, 70-72). The common core architecture is in good agreement with former hydropathy profile alignments (73). The core contains ten transmembrane domains (TMs) in which TMs 1-5 are related to TMs 6-10 by a pseudo-two-fold axis located in the plane of the membrane. This finding suggests that these two domains arose by gene duplication and evolved from an ancestral transporter whose functional unit consisted of multiple identical domains (74). With the increasing number of high resolution structures of LeuT-like proteins it became obvious that the ten TM core can be divided into two subdomains. TMs 3, 4, 8, and 9 form a so called hash motif, and a four helix bundle is built up by TMs 1, 2, 6, and 7 (67). These two domains do not only built up substrate and ion binding sites. They are also involved in structural rearrangements which allow sequential opening and closing of extra- and intracellular cavities during the transport cycle. Beside this unexpected internal structural repeat, the first TMs of both repeats (TMs 1 and 6) adopt an “alpha-helix – extended peptide - alpha-helix” motif. As a consequence of these breaks in the alpha-helical structures approximately in the middle of the membrane, main chain carbonyl oxygen and nitrogen atoms are exposed and serve as hydrogen bonding partners for ions and substrates. This interruption of the secondary structure is accompanied by the exposition of positive and negative partial charges of helix dipoles in a low dielectric environment in the middle of the membrane which can be saturated either by tertiary contacts or by interaction with ions or substrates. The antiparallel oriented TMs 1 and 6 which are in close proximity in LeuT-like proteins are not only major determinants for the formation of polar microenvironments of binding pockets but also for transporter dynamics with the unwound regions used as a hinge (65, 75).

Based on the crystal structure of vSGLT, a homology model of PutP was generated which contains amino acids 38–481 (76) (Figure 1). In the model the core of PutP exhibits the characteristics described above for a core of LeuT-like proteins. The 3D model does not contain the N-terminal extension of the core (TM -1) which is also missing in the vSGLT structure. Two additional TMs are

## Putp

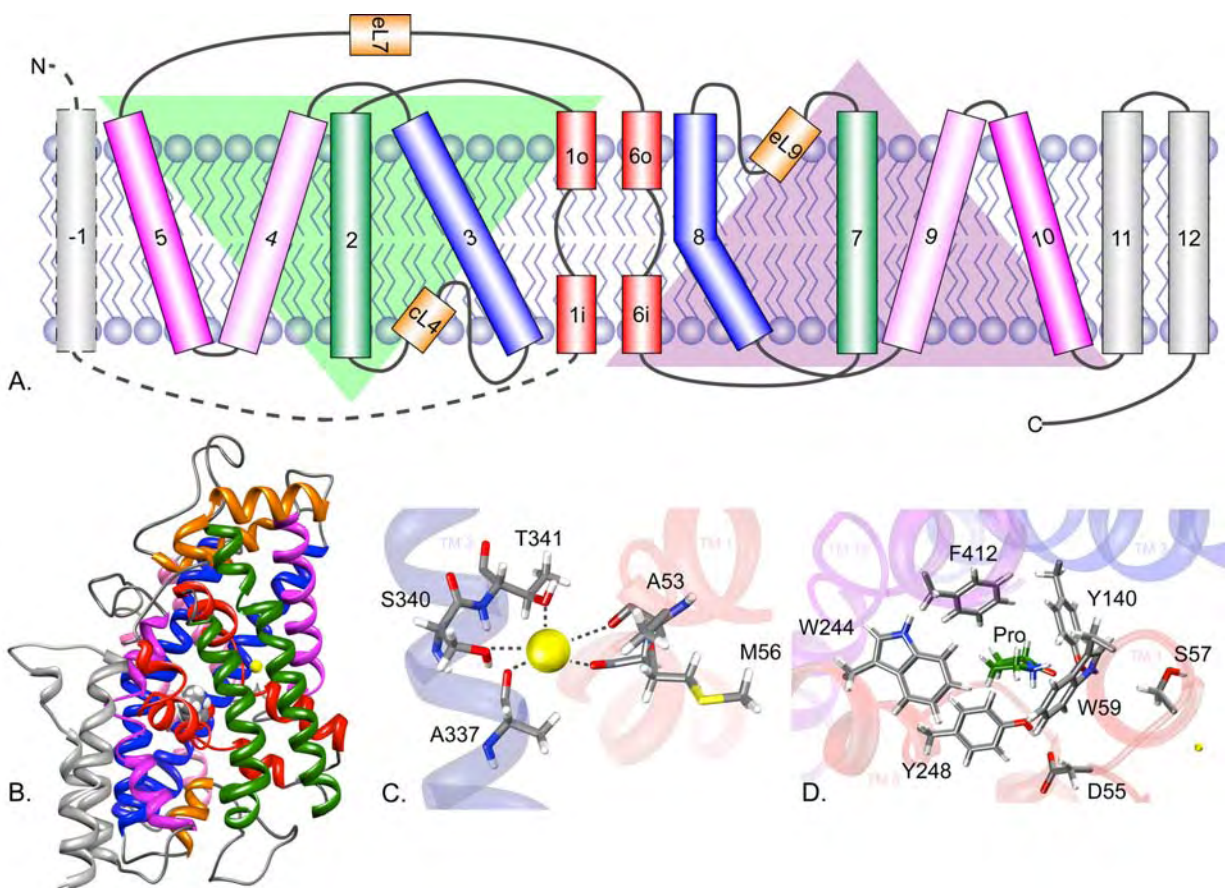


**Figure 1.** Architecture of the  $\text{Na}^+$ /proline symporter PutP of *E. coli*. A. Topology model of PutP. To avoid confusion the 10 TM core is numbered as in LeuT. TM 2 of PutP corresponds to TM 1 in LeuT. Additional peripheral TMs (N-terminal: -1; C-terminal: 12 and 13) are colored in grey. The five TM repeats related by a pseudo-two-fold symmetry axis are overlapped by a green and purple triangle respectively. TMs corresponding in the two repeats are highlighted in the same color. B. Homology model of PutP based on the crystal structure of vSGLT. The structure represents PutP in an inward-facing, occluded conformation. TMs are colored as in A. L-Proline (shown as spheres) is located in the center of the 10 TM core domain approximately in the middle of the membrane.  $\text{Na}^+$  (yellow sphere) is placed in a binding site corresponding to  $\text{Na}_2$  of LeuT  $\sim 11$  Angstrom away from the substrate. C. Close up view on the  $\text{Na}^+$  binding site. Residues in TM 1 and 8 involved in ion coordination are displayed as sticks colored by atom type. D. Close up view on the L-proline binding site. Residues in TMs 1, 3, 6, and 10 predicted to be close to or part of the L-proline binding pocket are depicted as sticks colored by atom type. L-Proline is highlighted in green. The figure was prepared with the program UCSF Chimera (109).

located C-terminal to the ten TMs core (Figure 1AB). The model shows PutP in an inward-facing occluded conformation ( $\text{C}_i\text{S}$ ). In this conformation PutP contains a large negatively charged cavity extending from approximately the middle of the membrane to the cytoplasmic space. It is built by TMs 1, 3, 6, 8, 10, and the internal loop cL4 (76). Direct access from the cytoplasm to the putative sites of  $\text{Na}^+$  and L-proline binding located at the apex of the cavity is blocked by an intramolecular gate.

Is the homology model of PutP supported by experimental data? Topological analyses of PutP by hydrophathy profile analysis, Cys-accessibility, LacZ/PhoA-fusions and electron paramagnetic resonance (EPR) spectroscopy revealed a thirteen TM motif with the N-terminus facing the periplasm and the C-terminus facing the cytoplasm (28, 77, 78). This motif is in good agreement

with the homology model except that borders of some TMs had to be shifted. Furthermore, biochemical and biophysical approaches support the tertiary structure of PutP. Previous Cys scanning mutagenesis of TMs 1 and 8 suggested already a close proximity of both TMs and an involvement in the formation of a cytoplasmic cavity which spans approximately from the middle of the membrane to the cytoplasm (79-81). A more detailed view on TM 8 was gained by a combination of site-directed spin labeling and double electron electron resonance (DEER) measurements of distances and subsequent modeling of the membrane spanning domain. The results suggest that TM 8 exhibits a pronounced kink near residue T341 which is important for  $\text{Na}^+$  binding (79-82). Breaking up interhelical H-bonds in this region of the protein exposes backbone oxygen atoms which may allow complexing of the cation. Also A337 which is located near this non-helical interruption is

## Putp

supposed to be involved in the formation of the Na<sup>+</sup> binding site (76, 81). Taken together, the currently available experimental data strongly support the PutP homology model.

## 6. STRUCTURE-FUNCTION RELATIONSHIPS IN PUTP

### 6.1. The Na<sup>+</sup> binding site

Despite the increasing number of available transporter structures with the LeuT-type structural fold, only the LeuT diffraction data provide direct information of Na<sup>+</sup> coordinating amino acids. In LeuT two binding sites, Na<sub>1</sub> and Na<sub>2</sub>, were identified (23). The Na<sup>+</sup> binding sites of structurally related Na<sup>+</sup> dependent transporters were assigned only indirectly by sequence and structure alignments with LeuT and inclusion of functional analyses.

For PutP, site-directed mutagenesis studies and biochemical characterization identified various residues important for Na<sup>+</sup> binding (79-81, 83, 84). Combining these data with the vSGLT-based homology model and LeuT led to the proposal of a Na<sup>+</sup> binding site corresponding to Na<sub>2</sub> of LeuT (23, 65, 76). Accordingly, Na<sup>+</sup> is coordinated by A53 and M56 of TM 1, and A337, S340 and T341 of TM 8 in a trigonal bi-pyramidal manner (Figure 1C). Since A53 and M56 are located in the unwound region of TM 1 and A337 at the kinked part of TM 8 the residues are able to bind Na<sup>+</sup> by main chain carbonyl oxygen atoms. In contrast, S340 and T341 are coordinating Na<sup>+</sup> by hydroxyl oxygens (76). Interestingly this cation binding site can be found in all crystallized symporters within the LeuT structural family up to now. A fascinating aspect is the observation, that even in Na<sup>+</sup>-independent transporters a positive charge at the according positions seems to be essential. In the H<sup>+</sup>-coupled amino acid transporter ApcT, Na<sup>+</sup> is replaced by K158 and in the L-carnitine/ $\gamma$ -butyrobetaine antiporter CaiT by R262 (70, 85).

What is the functional role of the bound coupling ion? It was postulated that Na<sup>+</sup> bound to the Na<sub>2</sub>-site stabilizes unwound TM 1, thereby increasing the substrate binding affinity of the transporter (86, 87). In vSGLT, N64 is part of the unwound region of TM 1 near the Na<sub>2</sub> site and thought to mediate crosstalk between the sites of Na<sup>+</sup> and substrate binding and an intracellular gate formed by Y263. The first structure showed vSGLT in an inward-facing, occluded conformation (65). Here a loosely coordinating Na<sup>+</sup> binding site is described which is readily releasing the ion to the intracellular space (65, 88, 89). A follow up structure shows vSGLT in an inward-facing, open conformation. The release of Na<sup>+</sup> leads to a reorientation of gating residue Y263 and minor helical movements, which open the substrate binding site towards the cytoplasm and allows dissociation of galactose (90).

### 6.2. The L-proline binding site

Putative L-proline coordinating sites in PutP were identified by ligand docking experiments with the PutP homology model and experimental analyses (76) (Figure 1D). The L-proline binding pocket is located at the apex of the inward-facing cavity, approximately in the middle of

the membrane bilayer. This is in good agreement with the location of substrate binding sites observed in crystal structures of other transporters with a LeuT-like structural fold. Residues located in TMs 1, 3, 6, 8, and 10 of PutP are involved in L-proline coordination. The interrupted helices of TMs 1 and 6 play an important role in the formation of the L-proline binding pocket. Main chain hydrogen bonding partners are exposed in the unwound stretch of the respective TMs and in addition helix dipoles contribute to a polar environment that allows substrate coordination. These polar features of the binding site may be important for recognition of the imino and carbonyl groups. However, the role of the helix dipoles of TMs 1 and 6 and of backbone carbonyl H-bonding partners remains elusive since these are difficult to track. Also a hydrophobic pocket seems to be involved in L-proline binding (29). Recently the two conserved amino acids Y140 (TM 3) and W244 (TM 6) were shown to be crucial for PutP function and are proposed to play a role in L-proline coordination. Substitution of the residues led to a decrease of the apparent L-proline affinity by two or three orders of magnitude (76). For Y140, both the apolar benzene side chain and the hydroxyl group are required for optimum L-proline binding. Y140 of PutP aligns with Y108 of LeuT which builds together with other residues of TMs 6 and 8 a hydrophobic pocket allowing accommodation of the aliphatic tail of the LeuT substrate leucine. In PutP, Y140 and W244 may not only be involved in L-proline binding but may also fulfill a gating function. Further discussions of the subject can be found below (paragraph 7.3).

Kinetic analysis suggested either a direct involvement of S57 in substrate binding or at least close proximity to the binding site (91). In the homology model, S57 is localized within the unwound stretch of TM 1 but does not seem to directly participate in L-proline coordination. It is shown for other LeuT-like transporters that residues localized in this discontinuous segment are involved in substrate binding (68). The exact localization of S57 between the Na<sup>+</sup> and the proline binding site rather suggests an involvement in coupling Na<sup>+</sup> and L-proline binding.

## 7. MOLECULAR MECHANISM OF NA<sup>+</sup>/SOLUTE SYMPORT

### 7.1. Transport via alternating access

Based on available information on membrane topology, structure, conformational alterations, and kinetics, PutP and other secondary transporters are thought to operate via an alternating access mechanism (92-94). According to this mechanism, the transporter can adopt two major alternating conformations in which the opening of the translocation pathway is outward- (Co) or inward-facing (Ci) (Figure 2). Transitions between these two conformational states expose the substrate-binding site alternately to the *cis* or *trans* side of the lipid bilayer, and thereby allow the translocation of substrates across the membrane without formation of a continuous transmembrane pore. By comparison of the currently available X-ray crystal structures of members of the LeuT

## Putp

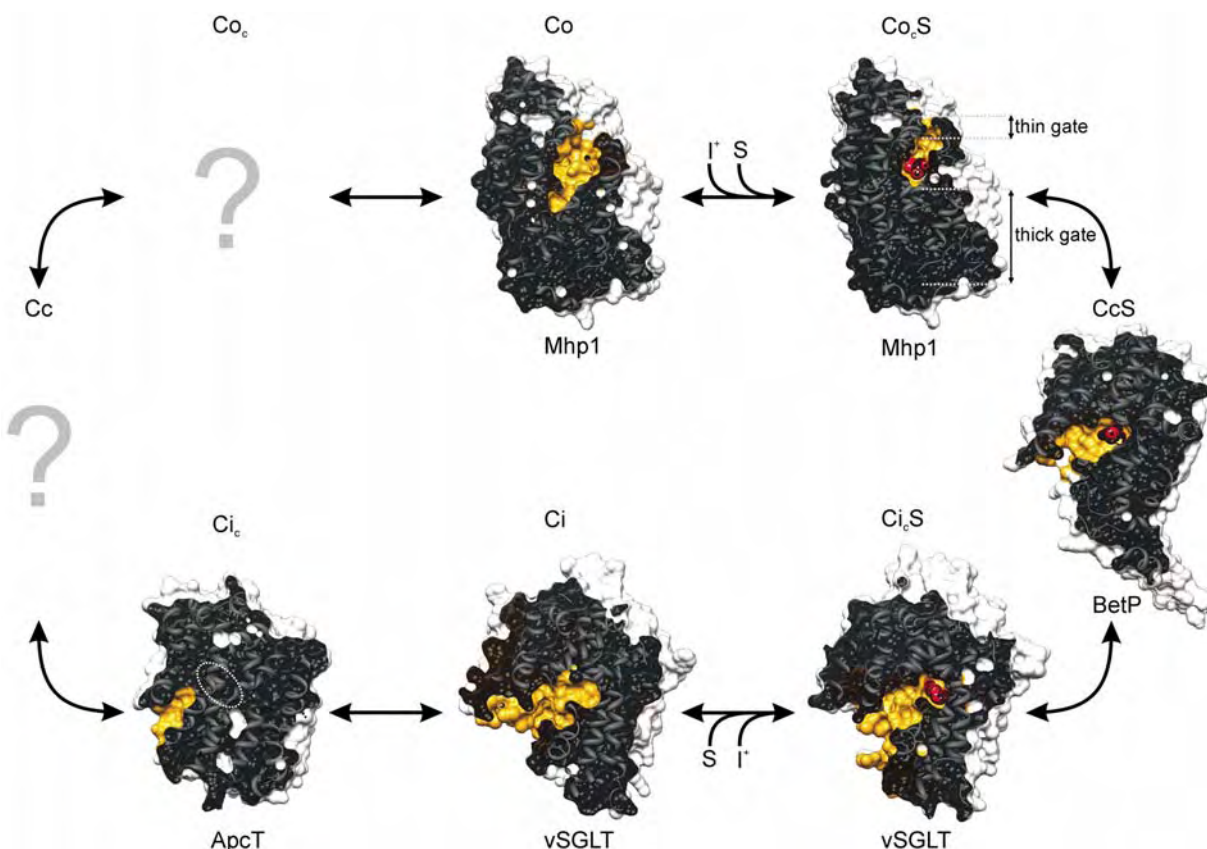


**Figure 2.** Alternating access mechanism for symport. The individual conformational states appearing throughout the transport cycle are shown based on currently available crystal structures of secondary transporters of the LeuT structural family. Shown are slices through surface-models of the transporters, viewed approximately parallel to the membrane with the extracellular side at the top. The surface of residues lining the cavities and substrate binding sites is colored in yellow. Respective bound substrates are shown as van der Waals spheres, highlighted in red and the backbone of the proteins is illustrated as ribbon models colored in dark grey. The position of the thin and thick gates is exemplarily shown for Mhp1 in the Co<sub>e</sub>S state by grey dashed lines. For ApcT, the position of the putative ligand-binding site is highlighted by a white dashed ellipse. Predicted transport intermediates for which no crystal structure is available yet are represented by grey question marks. S, substrate; I<sup>+</sup>, coupling ion; Co, open, outward-facing; Co<sub>e</sub>, occluded, outward-facing; Cc, occluded, inward-facing; Ci, open, inward-facing. The figure was prepared with the program UCSF Chimera (109).

structural family, the alternating access mode of transport can be extended to at least eight different conformational states that emerge throughout the transport cycle (23, 65, 67, 68, 70, 71, 90, 95, 96) (Figure 2). Since PutP shares the same overall fold of the ten-helix core domain with the LeuT structural family, it is suggested to show similar conformational states during substrate transport. In the following, the individual steps of the alternating access mechanism are described in detail based on the structures of Mhp1, AdiC, LeuT, BetP, vSGLT, CaiT, and ApcT, that all share the LeuT structural fold.

In the first state of the transport cycle, the protein adopts an open, outward-facing conformation (Co), as represented by the substrate-free structures of Mhp1 (PDB: 2JLN) and AdiC (PDB: 3HQK, 3LRB). This state exposes a water-filled cavity to the extracellular aqueous solution and allows access to the ligand binding sites from the outside of the membrane. Subsequently, the translocation pathway

becomes partly occluded due to small conformational alterations induced by solute binding. Such an occluded, outward-facing conformation (Co<sub>e</sub>S) can be found in the substrate-bound structures of Mhp1 (PDB: 2JLO), LeuT (PDB: 2A65), and AdiC (PDB: 3L1L). Here, the binding pocket is shielded from the extracellular, aqueous bulk by relatively small structural elements that build up a thin gate, while the access to the intracellular solvent in the Co and the Co<sub>e</sub>S state is blocked by around 20 Angstrom of tightly packed protein residues, known as a thick gate (Figure 2). The transporter then converts from the outward- to the inward-facing state via an intermediate, occluded conformation (CcS) that is suggested to be represented by the BetP structure (PDB: 2WIT). In this state, the ligand-binding site is protected from the extracellular aqueous bulk by a thick gate, but an initial stage of an evolving intracellular cavity is observed. However, it can be clearly distinguished from the next, inward-facing, occluded state (Ci<sub>e</sub>S) by the fact that opening of the cytoplasmic cavity

## Putp

will require considerable conformational changes of the protein backbone. An additional argument for the correct assignment of the BetP structure as a CcS state is given by the structural symmetry of the two 5 TM repeats that was observed to be significantly higher than in the inward- and outward-facing conformations (71). The already mentioned Ci<sub>c</sub>S state can be described by the structure of vSGLT (PDB: 3DH4) in its substrate-bound form. This conformation exposes an intracellular cavity to the inner aqueous bulk. Similar to the Co<sub>c</sub>S state, the substrate resides in the binding pocket at the apex of the cavity, and is separated from the translocation pathway by a thin gate, whereas the accessibility from the extracellular environment is blocked by a thick gate. Interestingly, MD simulations of this Ci<sub>c</sub>S state of vSGLT indicates that this structure already represents an ion-releasing state facilitating the diffusion of Na<sup>+</sup> towards the cytoplasm (88-90). The transporter then proceeds through the cycle by opening the small gate to connect the substrate binding site with the water-filled cavity. This open, inward-facing conformation (Ci), which is shown in the ligand-free structures of vSGLT (PDB: 2XQ2), CaiT (PDB: 2WSX, 2WSW), and Mhp1 (2X79), allows dissociation of the substrate to the intracellular solvent and thus completes the translocation process. However, to enable several rounds of substrate translocation, the empty transporter has to switch back to the Co state to restart the transport cycle. Such a reorientation of the protein may occur through three additional substrate-free conformations: an occluded, inward-facing (Ci<sub>c</sub>), occluded (Cc), and occluded, outward-facing (Co<sub>c</sub>) state. While there is no crystal structure available yet for the Cc and Co<sub>c</sub> conformations, the apo state of ApcT (PDB: 3GIA) is proposed to represent the Ci<sub>c</sub> state, appearing after substrate release and closure of the intracellular thin gate that shields the binding pocket from the intracellular oriented cavity.

For PutP, no direct evidence for one of the eight conformations is available due to missing three-dimensional structural information. Nevertheless, analyses of changes in Cys accessibility, spectroscopic properties of site-specifically attached fluorescent or paramagnetic groups and intramolecular distances have led to the identification of an inward-facing, polar cavity (76, 80, 81, 83, 97, 98). This finding is in good agreement with the homology model of PutP, representing an inward-facing conformation (76). In addition to topological analyses, it is shown that binding of Na<sup>+</sup> and/or L-proline to the transporter decreases the accessibility to Cys-specific labels and the mobility of paramagnetic groups attached to positions located in the identified crevice. From these findings, it is concluded that binding of ligands induces conformational alterations of PutP that may lead to a closure of the intracellular permeation pathway and thus to an occluded state of the transporter. Alternatively, it can be envisaged that the conformational changes switch the protein from an inward-facing to an outward-facing conformation. Although the latter idea remains highly speculative, it is supported by a Na<sup>+</sup>-induced increase in the accessibility to thiol-specific ligands observed at positions located above the putative L-proline-binding site on the periplasmic side of the protein (76, 80, 83). Still, whether

these accessibility changes are really due to opening of an outer cavity remains to be demonstrated.

### 7.2. Impact of Na<sup>+</sup> on the outward-facing cavity and substrate binding

During the transport process, the transitions between different conformational states must be tightly regulated to avoid uncoupling of ion and substrate transport. In the case of PutP and other symporters, such a regulation has to prevent interconversion of the outward- and inward-facing state from occurring when only one of the ligands is bound. Otherwise, each solute could traverse the membrane independently, and coupling would be abolished. Furthermore, the opening and closure of the extracellular and intracellular gates has to be strictly regulated to assure that only one gate is open at a time in order to prevent the formation of a continuous membrane-spanning pore. To understand the molecular principles of solute transport including the coupling and gating mechanism, the sequence of ligand binding, the translocation pathway of the solutes and conformational changes have to be considered. For PutP kinetic and electrophysiological measurements show that transport at low L-proline concentrations occurs according to an ordered binding mechanism (30, 99). In this scheme, Na<sup>+</sup> binds to the empty transporter first, thereby inducing a conformational change, which increases the affinity of the transporter for L-proline. At high L-proline concentrations, binding of Na<sup>+</sup> and L-proline is random (99). Evidence for the Na<sup>+</sup>-induced conformational change of PutP comes from analyses of Cys-accessibility to thiol-specific reagents in the presence or absence of Na<sup>+</sup> (76, 79-81). In particular, the accessibility of positions in the periplasmic halves of TMs 1, 3, and 6 was shown to increase in the presence of Na<sup>+</sup>, while positions in the middle and periplasmic half of TM 8 was partially protected by Na<sup>+</sup> binding to the protein. As mentioned above these findings can be interpreted as a Na<sup>+</sup>-induced conformational change that opens an extracellular cavity, which is formed minimum by TMs 1, 3, 6, and 8 of the core structure of PutP. Notably, similar observations have been made by site-directed spin labeling in combination with EPR measurements and MD simulations on LeuT (100). The latter study provides evidence for a Na<sup>+</sup>-dependent opening of the extracellular permeation pathway of LeuT that is lined by TM 1a, TM 3, TM6b, TM8, and TM 10, in full agreement with the results obtained for PutP. The conformational alteration leading to this open conformation of LeuT is based on a movement of eL4 (eL9 in PutP) out of the extracellular crevice. The movement of eL4 allows the entrance of substrate to the binding pocket and thus facilitates solute binding. Furthermore, MD and free energy perturbation simulations on LeuT suggest that Na<sub>2</sub> is important for structural stabilization of the substrate binding pocket leading to a slight increase in binding affinity (86). Although it is not clear whether general conclusions can be drawn from these observations for other members of the structural family, they provide the opportunity to speculate that the ion-based opening of the outer cavity and stabilization of the substrate binding pocket permit cooperativeness of ion and substrate binding.

### 7.3. The outer thin gate and substrate binding

As described before, substrate binding from the periplasmic site of the membrane induces closure of the outer thin gate and switches the transporter to a  $\text{Co}_c\text{S}$  configuration (Figure 2). The importance of this gate in preventing substrate diffusion back to the extracellular aqueous milieu raises the question how these structural elements open and close. In PutP, accessibility measurements provide evidence that the positions in TMs 1, 3, and 6, which are exposed to the periplasmic cavity in the presence of  $\text{Na}^+$ , are protected upon addition of L-proline (76, 80, 83). Since the putative gating residues Y140 and W244 of PutP are located in two of these helices (TM 3 and TM 6), and found to be accessible in the  $\text{Na}^+$ -but not in the  $\text{Na}^+/\text{L-proline}$  bound state, it is tempting to speculate that these residues build up a thin gate that closes due to movement of TMs 3 and 6 towards each other. Notably, both residues are also predicted to be involved in substrate binding, so that closure of this aromatic lid may simultaneously allow improvement of substrate binding. Although these ideas of PutP function are speculative, they parallel results obtained from crystallization, EPR spectroscopy, MD simulations, and accessibility measurements of other transporters of the LeuT family (68, 72, 100, 101). For AdiC, structural alignment of the two available X-ray structures in the Co and  $\text{Co}_c\text{S}$  state revealed a pronounced structural rearrangement in TM 6 and, to a lesser extent, in TMs 2 and 10 (72). Due to the movement of TM 6, the gating residue W202 (W244 in PutP) is positioned directly above the bound substrate, blocking its diffusion back to the extracellular solution. With Mhp1, in comparing the Co and  $\text{Co}_c\text{S}$  state, the most substantial conformational change was observed in the N-terminal part of TM 10 (68). This structural element moves into the outward-facing cavity and occludes the substrate-binding site. Thereby, the side-chain of the corresponding residue W220 in TM 6 is repositioned to interact with the bound substrate, akin to W202 of AdiC. Similar conformational changes are proposed based on accessibility measurements of TM 10 of human SGLT1 (101). For LeuT, EPR measurements and MD simulations show that binding of the substrate leucine alters the conformation of eL4, TM 6 and TM 10 (100). In agreement with the observed changes of the orientation of aromatic residues in other transporters, Y108 and F253 (Y140 and W244 in PutP), engage different rotamer states in the presence of substrate that lead to shielding of the binding pocket from the extracellular vestibule. Besides the aromatic lid, LeuT also exhibits a salt bridge formed by residues R30 and D404 (23). As this salt bridge is proposed to close and open depending on ligand binding, the salt bridge is believed to be part of the extracellular thin gate together with Y108 and F253 (87, 102). Taken together, the ligand-induced conformational changes occurring during closure of the extracellular thin gate are relatively small. Although the general principles of gating, for example, the structural elements that undergo conformational changes, seem to be conserved, the extent and the direction of the conformational alteration varies between the individual transporters of the LeuT structural family. Therefore, further experimental studies are required to understand the movements in PutP that describe the opening or closing of the extracellular gate.

### 7.4. Transition between outward- and inward-facing conformations

In contrast to the relatively small structural rearrangement associated with ligand binding from the extracellular bulk, the transition between the Co and Ci state requires larger-scale conformational alterations that are distributed almost over the entire protein. This is due to the second gating mechanism that includes closing of the outward-facing cavity by a thick extracellular gate and opening of an intracellular thick gate to establish an inward-facing translocation pathway. Evidence for a inwardly-oriented cavity in PutP comes from accessibility analyses at positions in TMs 1 and 8 (80, 81). The results suggest that minimum TMs 1 and 8 participate in the formation of an inner hydrophilic translocation pathway that is closed upon L-proline binding in the presence of  $\text{Na}^+$ . The latter effect of substrate binding on the inner cavity clearly contradicts the presumption that the bound ligand induces an inward-facing conformation of the transporter that allows releasing of the solute to the cytoplasm. One possible reason for this phenomenon could be that the accessibility measurements were performed in random oriented membrane vesicles in the absence of a membrane potential. Since  $\text{Na}^+$ -coupled proline uptake is not detected in the absence of such a potential, inclusion of the effect of a membrane potential in the studies might lead to different results (A. Hackmann, M. Nietschke, and H. Jung, unpublished data). Nevertheless, the identification of the inward-facing conformation suggests that PutP undergoes ligand-induced transitions between outward- and inward-facing conformations.

The only known member of the LeuT family that was crystallized in three states (Ce,  $\text{CecS}$ , and Ci) is Mhp1 (67, 68) (Figure 2). Therefore, comparison between the different conformations of Mhp1 may provide important insights into the conformational alterations involved in transitions between the outward- and inward-facing states. During the conformational switch, the hash motif (TMs 3, 4, 8, and 9) undergoes a rigid-body movement with respect to the four-helix bundle (TMs 1, 2, 6, and 7) to close the outwardly- and to open the inwardly-oriented cavity. During this movement, TMs 5 and 10, which participate in building up the extracellular and intracellular thin gates, bend independently near their helix midpoints. This reorientations lead to closure of the extracellular and opening of the intracellular thin gates, followed by dissociation of the ligands into the cytoplasm. Besides this mechanism, two additional mechanistic models have been proposed (23, 103). In the first one, transitions between the  $\text{Co}_c\text{S}$  and  $\text{Ci}_c\text{S}$  conformations of LeuT are suggested to involve flexing of the discontinuous TMs 1 and 6, together with reorientation of TMs 2 and 7 (23). Although, such bending of the pseudo two-fold related TMs 1 and 6 is in agreement with single-molecule FRET analyses of LeuT and with the conformational alterations seen by comparison of the Co and  $\text{Co}_c\text{S}$  of AdiC, it is still not known whether this reorientation is sufficient to cause a switch between the outward- and inward-facing state (68, 104). The second model involves a rocking movement of the four-helix bundle (TMs 1, 2, 6, and 7) against the scaffold (TMs 3, 4, 5, 8, 9, and 10) of the core structure (103). Similar to the

other two proposed mechanisms, this model allows synchronization of the opening and closure of the extracellular and intracellular gates, respectively, to avoid simultaneous opening of both barriers and the formation of a continuous transmembrane pore.

### 7.5. The inner thin gate and substrate release into the cytoplasm

After adaptation of the inward-facing conformation, the question arises whether release of coupling ion and substrate also occurs in a cooperative manner, as it is proposed for binding. With the recently published vSGLT structure in the Ci state in combination with MD simulations, this appears to be indeed the case (90). In this study, it is proposed that during transition from the Co<sub>c</sub>S to the Ci<sub>c</sub>S (Figure 2), the distance between the Na<sup>+</sup>-binding TMs 1 and 8 increases, resulting in a fast release of the ion from the binding site to the cytoplasm. Upon dissociation, the unwound region of TM 1 undergoes a conformational change that disrupts the H-bonds between the functional important N64 and the gating residue Y263. Subsequently, the side-chain of Y263 becomes reoriented in order to open the cytoplasmic thin gate and to allow dissociation of the substrate. Additionally, the substrate release is facilitated by small rigid-body movements in the hash motif and in the 4-helix bundle that widen the intracellular cavity. As mentioned above, the predicted role of N64 and Y263 in coupling Na<sup>+</sup> and substrate release in vSGLT perfectly fits to the observations made for the corresponding residues, D55 and Y248 in PutP (76, 84). In particular, the carboxylate of D55 proved essential for transport and was previously implicated in Na<sup>+</sup> binding (84). However, in the homology model of PutP, the side-chain of D55 is not found to be part of the Na<sup>+</sup>-binding pocket, but it is involved in H-bonding with the hydroxyl group of Y248 in TM 6, similar to the situation found in vSGLT (76, 90). A substitution analysis implicates Y248 of PutP in coupling Na<sup>+</sup> and proline transport and/or gating. These results are consistent with the idea that Na<sup>+</sup> and L-proline release is coupled in PutP in the same way as it is assumed for vSGLT. This assumption is further supported by the observed role of the highly conserved residue D187 of PutP (D189 in vSGLT) (88-90, 105). In both transporters the aspartate residue is located close to the putative Na<sup>+</sup>-binding site and forms part of the putative pathway of the coupling ion through the membrane. This finding implies that this residue is important for release of Na<sup>+</sup> on the cytoplasmic side of the membrane. Indeed, computational studies demonstrate that D189 of vSGLT facilitates the diffusion of the ion toward the cytoplasm (88-90).

Besides the Na<sup>+</sup>-coupled release of the substrate on the inner side of the membrane, LeuT ligand-binding experiments, MD simulations and steered-molecular-dynamics have identified another mechanism potentially important for coupling of ion and substrate transport (106). This mechanism involves a second binding site (S2) in the extracellular vestibule of LeuT, that triggers Na<sup>+</sup> and substrate release from the primary binding site (S1) upon substrate binding. A S2 site has also been found in the extracellular part of CaiT that triggers binding of co-substrate from the inside of this antiporter (70). Since the

position and function of the allosterical sites in the different transporter significantly varies, it is not clear whether this principle is of general impact for the transport mechanism of LeuT-like proteins. Furthermore, it has to be noted, that the existence of a second binding site in LeuT is still discussed and the data are controversial (107). Moreover, kinetic and binding analyses published for PutP so far have identified only one binding site for L-proline (17).

## 8. CONCLUSIONS AND PERSPECTIVES

Depending on the availability of external L-proline and on environmental conditions, PutP may play important roles for the metabolism and stress response of bacteria and archaea. Clearly, further investigations are necessary to fully understand the molecular basis of the significance of PutP and potentially other L-proline uptake systems. Furthermore, it is expected that L-proline and related transporters and enzymes are crucial for bacteria-host interactions in many more systems than known so far. Because of its physiological significance and as amenable bacterial member of the SSS family, PutP is used as a model system to understand the molecular mechanism of function of SSS family proteins. The described homology model of PutP shows the protein in a LeuT-type structural motif and is in good agreement with the available Cys accessibility, cross-linking, and EPR distance data as well as the previously proposed 13 TMs topology. In addition, the Na<sup>+</sup> and L-proline binding sites are predicted and confirmed based on ligand docking calculations and functional analyses, demonstrating the validity of the model as a guide for further analyses of structure-function relationships. However, it is clear that due to the relatively low sequence identity to the template vSGLT, the homology model has to be considered as a low resolution model and awaits further experimental validation. This can be done by intramolecular distance measurements based on SDSL in combination with DEER spectroscopy. Investigations along this way are currently in progress. Notwithstanding the power of this technique in determining structural data, it does not provide information on side-chain orientation. Therefore, a high-resolution structure obtained, for example by X-ray crystallography, is indispensable for the understanding of molecular interactions and ligand-coordination within the protein. In addition to the structure, information on functional relevant conformational alterations is needed to describe how the ligands are translocated through the protein. Analyses of Cys accessibility and SDSL EPR measurements on PutP in the absence or presence of ligands support a mechanistic model according to which transport follows an alternating access mechanism. With the elucidation of X-ray structures of different LeuT structural family members in different conformations, the mechanistic states and the conformational changes that occur throughout the transport cycle can be predicted. Although the structural alterations observed for PutP fit to this mechanistic model, it is based on structural comparison of transporters with low sequence identity and different substrate specificity. A detailed description of the conformational alterations of an individual transporter, thus require the determination of its structure in each state of the transport cycle. Since the

## Putp

crystallization of secondary transporters is still highly challenging and the structures only represent static pictures, alternating techniques to investigate the dynamic of transporters are required. For PutP, again SDSL EPR spectroscopy provides an efficient means for obtaining information on the nature and the extent of structural changes. This can be done with high time resolution and, in contrast to X-ray crystallography, under native conditions in a lipid bilayer.

## 9. ACKNOWLEDGEMENTS

This work is financially supported by the Deutsche Forschungsgemeinschaft (Ju333/3-2, Ju333/4-2 and Exc114-1). M.R. is a fellow of the Elite Network of Bavaria, Germany.

## 10. REFERENCES

1. T.E. Creighton: Proteins, structure and molecular principles. W.H. Freeman, New York (1992)
2. D.R. Hahn, R.S. Myers, C.R. Kent and S.R. Maloy: Regulation of proline utilization in *Salmonella typhimurium*: molecular characterization of the *put* operon, and DNA sequence of the *put* control region. *Mol Gen Genet* 213, 125-133 (1988)
3. J.M. Wood: Genetics of L-proline utilization in *Escherichia coli*. *J Bacteriol* 146, 895-901 (1981)
4. H. Jung: The sodium/substrate symporter family: structural and functional features. *FEBS Lett* 529, 73-77 (2002)
5. L.N. Csonka and A.D. Hanson: Prokaryotic osmoregulation: genetics and physiology. *Annu Rev Microbiol* 45, 569-606 (1991)
6. J.M. Wood, E. Bremer, L.N. Csonka, R. Kraemer, B. Poolman, T. van der Heide and L.T. Smith: Osmosensing and osmoregulatory compatible solute accumulation by bacteria. *Comp Biochem Physiol A - Mol Integr Physiol* 130, 437-60 (2001)
7. J.M. Crawford, R. Kontnik and J. Clardy: Regulating alternative lifestyles in entomopathogenic bacteria. *Curr Biol* 20, 69-74 (2010)
8. Alia, P. Mohanty and J. Matysik: Effect of proline on the production of singlet oxygen. *Amino Acids* 21, 195-200 (2001)
9. N. Smirnoff and Q.J. Cumbe: Hydroxyl radical scavenging activity of compatible solutes. *Phytochemistry* 28, 1057-1060 (1989)
10. N. Krishnan, M.B. Dickman and D.F. Becker: Proline modulates the intracellular redox environment and protects mammalian cells against oxidative stress. *Free Radic Biol Med* 44, 671-81 (2008)
11. K. Nagata, Y. Nagata, T. Sato, M.A. Fujino, K. Nakajima and T. Tamura: L-Serine, D- and L-proline and alanine as respiratory substrates of *Helicobacter pylori*: correlation between *in vitro* and *in vivo* amino acid levels. *Microbiology* 149, 2023-2030 (2003)
12. S. Vilchez, L. Molina, C. Ramos and J.L. Ramos: Proline catabolism by *Pseudomonas putida*: cloning, characterization, and expression of the *put* genes in the presence of root exudates. *J Bacteriol* 182, 91-99 (2000)
13. E.I. Newman: The rhizosphere; carbon sources and microbial populations. In: *Ecological interactions in soil*. Ed: Fritter A R. Blackwell Scientific Publications Ltd., Boston, Mass (1985)
14. R. Heermann and T. Fuchs: Comparative analysis of the *Photobacterium luminescens* and the *Yersinia enterocolitica* genomes: uncovering candidate genes involved in insect pathogenicity. *BMC Genomics* 9, 40 (2008)
15. H. Inoue, H. Iguchi, A. Kono and Y. Tsuruta: Highly sensitive determination of N-terminal prolyl dipeptides, proline and hydroxyproline in urine by high-performance liquid chromatography using a new fluorescent labelling reagent, 4-(5,6-dimethoxy-2-phthalimidinyl)-2-methoxyphenylsulfonfyl chloride. *J Chromatogr B Biomed Sci Appl* 724, 221-30 (1999)
16. J.M. Wood and D. Zadworny: Characterization of an inducible porter required for L-proline catabolism by *Escherichia coli* K12. *Can J Biochem* 57, 1191-1199 (1979)
17. I. Yamato and Y. Anraku: Na<sup>+</sup>/substrate symport on prokaryotes. In: *Alkali cation transport systems in prokaryotes*. Ed: Bakker E P. CRC-Press, Boca Raton (1993)
18. H. Jung: Sodium/substrate transport. In: *Microbial transport systems*. Ed: Winkelmann G. Wiley-VCH, Weinheim (2001)
19. K.I. Racher, R.T. Voegelé, E.V. Marshall, D.E. Culham, J.M. Wood, H. Jung, M. Bacon, M.T. Cairns, S.M. Ferguson, W.J. Liang, P.J. Henderson, G. White and F.R. Hallett: Purification and reconstitution of an osmosensor: transporter ProP of *Escherichia coli* senses and responds to osmotic shifts. *Biochemistry* 38, 1676-1684 (1999)
20. J.L. Milner, S. Grothe and J.M. Wood: Proline porter II is activated by a hyperosmotic shift in both whole cells and membrane vesicles of *Escherichia coli* K12. *J Biol Chem* 263, 14900-14905 (1988)
21. J.M. Wood: Bacterial osmosensing transporters. In: *Methods Enzymol*. Eds: Häussinger D and Sies H. Academic Press, (2007)
22. J.M. Lucht and E. Bremer: Adaptation of *Escherichia coli* to high osmolarity environments: osmoregulation of

## Putp

the high-affinity glycine betaine transport system ProU. *FEMS Microbiol Rev* 14, 3-20 (1994)

23. A. Yamashita, S.K. Singh, T. Kawate, Y. Jin and E. Gouaux: Crystal structure of a bacterial homologue of Na<sup>+</sup>/Cl<sup>-</sup>-dependent neurotransmitter transporters. *Nature* 437, 215-223 (2005)

24. E.M. Wright and E. Turk: The sodium/glucose cotransport family SLC5. *Pflugers Arch* 447, 510-518 (2004)

25. J. Reizer, A. Reizer and M.H. Saier, Jr.: A functional superfamily of sodium/solute symporters. *Biochim Biophys Acta* 1197, 133-166 (1994)

26. C.C. Chen, T. Tsuchiya, Y. Yamane, J.M. Wood and T.H. Wilson: Na<sup>+</sup> (Li<sup>+</sup>)-proline cotransport in *Escherichia coli*. *J Membr Biol* 84, 157-164 (1985)

27. J. Cairney, C.F. Higgins and I.R. Booth: Proline uptake through the major transport system of *Salmonella typhimurium* is coupled to sodium ions. *J Bacteriol* 160, 22-27 (1984)

28. H. Jung, S. Tebbe, R. Schmid and K. Jung: Unidirectional reconstitution and characterization of purified Na<sup>+</sup>/proline transporter of *Escherichia coli*. *Biochemistry* 37, 11083-11088 (1998)

29. M.K. Liao and S. Maloy: Substrate recognition by proline permease in *Salmonella*. *Amino Acids* 21, 161-174 (2001)

30. I. Yamato: Ordered binding model as a general mechanistic mechanism for secondary active transport systems. *FEBS Lett* 298, 1-5 (1992)

31. A.T. Yeung, M. Bains and R.E. Hancock: The sensor kinase CbrA is a global regulator that modulates metabolism, virulence and antibiotic resistance in *Pseudomonas aeruginosa*. *J Bacteriol* 193, 918-931 (2011)

32. B. Ratzkin and J. Roth: Cluster of genes controlling proline degradation in *Salmonella typhimurium*. *J Bacteriol* 133, 744-754 (1978)

33. S.W. Allen, A. Senti-Willis and S.R. Maloy: DNA sequence of the *putA* gene from *Salmonella typhimurium*: a bifunctional membrane-associated dehydrogenase that binds DNA. *Nucleic Acids Res* 21, 1676 (1993)

34. Y. Zhou, J.D. Larson, C.A. Bottoms, E.C. Arturo, M.T. Henzl, J.L. Jenkins, J.C. Nix, D.F. Becker and J.J. Tanner: Structural basis of the transcriptional regulation of the proline utilization regulon by multifunctional PutA. *J Mol Biol* 381, 174-188 (2008)

35. A.M. Muro-Pastor and S. Maloy: Proline dehydrogenase activity of the transcriptional repressor PutA is required for induction of the *put* operon by proline. *J Biol Chem* 270, 9819-9827 (1995)

36. Y. Nakada, T. Nishijyo and Y. Itoh: Divergent structure and regulatory mechanism of proline catabolic systems: characterization of the *putAP* proline catabolic operon of *Pseudomonas aeruginosa* PAO1 and its regulation by PruR, and AraC/XylS family protein. *J Bacteriol* 184, 5633-5640 (2002)

37. J.H. Lee and S.H. Choi: Coactivation of *Vibrio vulnificus putAP* operon by cAMP receptor protein and PutR through cooperative binding to overlapping sites. *Mol Microbiol* 60, 513-524 (2006)

38. J.H. Lee, N.Y. Park, M.H. Lee and S.H. Choi: Characterization of the *Vibrio vulnificus putAP* operon, encoding proline dehydrogenase and proline permease, and its differential expression in response to osmotic stress. *J Bacteriol* 185, 3842-3852 (2003)

39. H.J. Kim, J.H. Lee, J.E. Rhee, H.S. Jeong, H.K. Choi, H.J. Chung, S. Ryu and S.H. Choi: Identification and functional analysis of the *putAP* genes encoding *Vibrio vulnificus* proline dehydrogenase and proline permease. *J Microbiol Biotechnol* 12, 318-326 (2002)

40. C. von Blohn, B. Kempf, R.M. Kappes and E. Bremer: Osmostress response in *Bacillus subtilis*: characterization of a proline uptake system (OpuE) regulated by high osmolarity and the alternative transcription factor sigma B. *Mol Microbiol* 25, 175-187 (1997)

41. F. Spiegelhalter and E. Bremer: Osmoregulation of the *opuE* proline transport gene from *Bacillus subtilis*: contributions of the sigma A- and sigma B-dependent stress-responsive promoters. *Mol Microbiol* 29, 285-296 (1998)

42. R. Rübenhagen, H. Ronsch, H. Jung, R. Krämer and S. Morbach: Osmosensor and osmoregulator properties of the betaine carrier BetP from *Corynebacterium glutamicum* in proteoliposomes. *J Biol Chem* 275, 735-741 (2000)

43. A.S. Bayer, S.N. Coulter, C.K. Stover and W.R. Schwan: Impact of the high-affinity proline permease gene (*putP*) on the virulence of *Staphylococcus aureus* in experimental endocarditis. *Infect Immun* 67, 740-744 (1999)

44. W.R. Schwan, S.N. Coulter, E.Y. Ng, M.H. Langhorne, H.D. Ritchie, L.L. Brody, S. Westbrook-Wadman, A.S. Bayer, K.R. Folger and C.K. Stover: Identification and characterization of the PutP proline permease that contributes to *in vivo* survival of *Staphylococcus aureus* in animal models. *Infect Immun* 66, 567-572 (1998)

45. P.A. Wengender and K.J. Miller: Identification of a PutP proline permease gene homolog from *Staphylococcus aureus* by expression cloning of the high-affinity proline transport system in *Escherichia coli*. *Appl Environ Microbiol* 61, 252-259 (1995)

46. W.R. Schwan, L. Lehmann and J. McCormick: Transcriptional activation of the *Staphylococcus aureus*

## Putp

*putP* gene by low-proline-high osmotic conditions and during infection of murine and human tissues. *Infect Immun* 74, 399-409 (2006)

47. W.R. Schwan, K.J. Wetzel, T.S. Gomez, M.A. Stiles, B.D. Beitlich and S. Grunwald: Low-proline environments impair growth, proline transport and *in vivo* survival of *Staphylococcus aureus* strain-specific *putP* mutants. *Microbiology* 150, 1055-1061 (2004)

48. K. van Amsterdam and A. van der Ende: Nutrients released by gastric epithelial cells enhance *Helicobacter pylori* growth. *Helicobacter* 9, 614-21 (2004)

49. H. Kavermann, B.P. Burns, K. Angermuller, S. Odenbreit, W. Fischer, K. Melchers and R. Haas: Identification and characterization of *Helicobacter pylori* genes essential for gastric colonization. *J Exp Med* 197, 813-822 (2003)

50. K. Nakajima, S. Inatsu, T. Mizote, Y. Nagata, K. Aoyama, Y. Fukuda and K. Nagata: Possible involvement of *put A* gene in *Helicobacter pylori* colonization in the stomach and motility. *Biomed Res* 29, 9-18 (2008)

51. T. Guszczyn and K. Sobolewski: Deregulation of collagen metabolism in human stomach cancer. *Pathobiology* 71, 308-13 (2004)

52. N. Krishnan, A.R. Doster, G.E. Duhamel and D.F. Becker: Characterization of a *Helicobacter hepaticus putA* mutant strain in host colonization and oxidative stress. *Infect Immun* 76, 3037-3044 (2008)

53. N. Krishnan and D.F. Becker: Oxygen reactivity of PutA from *Helicobacter* species and proline-linked oxidative stress. *J Bacteriol* 188, 1227-1235 (2006)

54. J.F. Tomb, O. White, A.R. Kerlavage, R.A. Clayton, G.G. Sutton, R.D. Fleischmann, K.A. Ketchum, H.P. Klenk, S. Gill, B.A. Dougherty, K. Nelson, J. Quackenbush, L. Zhou, E.F. Kirkness, S. Peterson, B. Loftus, D. Richardson, R. Dodson, H.G. Khalak, A. Glodek, K. McKenney, L.M. Fitzgerald, N. Lee, M.D. Adams, E.K. Hickey, D.E. Berg, J.D. Gocayne, T.R. Utterback, J.D. Peterson, J.M. Kelley, M.D. Cotton, J.M. Weidman, C. Fujii, C. Bowman, L. Watthey, E. Wallin, W.S. Hayes, M. Borodovsky, P.D. Karp, H.O. Smith, C.M. Fraser and J.C. Venter: The complete genome sequence of the gastric pathogen *Helicobacter pylori*. *Nature* 388, 539-47 (1997)

55. D.J. Reynolds and C.W. Penn: Characteristics of *Helicobacter pylori* growth in a defined medium and determination of its amino acid requirements. *Microbiology* 140, 2649-2656 (1994)

56. P.S. Kraemer, A. Mitchell, M.R. Pelletier, L.A. Gallagher, M. Wasnick, L. Rohmer, M.J. Brittnacher, C. Manoil, S.J. Skerrett and N.R. Salama: Genome-wide screen in *Francisella novicida* for genes required for pulmonary

and systemic infection in mice. *Infect Immun* 77, 232-244 (2009)

57. V.L. Motin, A.M. Georgescu, J.P. Fitch, P.P. Gu, D.O. Nelson, S.L. Mabery, J.B. Garnham, B.A. Sokhansanj, L.L. Ott, M.A. Coleman, J.M. Elliott, L.M. Kegelmeyer, A.J. Wyrobek, T.R. Slezak, R.R. Brubaker and E. Garcia: Temporal global changes in gene expression during temperature transition in *Yersinia pestis*. *J Bacteriol* 186, 6298-6305 (2004)

58. D. Kapfhammer, E. Karatan, K.J. Pflughoeft and P.I. Watnick: Role for glycine betaine transport in *Vibrio cholerae* osmoadaptation and biofilm formation within microbial communities. *Appl Environ Microbiol* 71, 3840-3847 (2005)

59. K.L. van Dellen, L. Houot and P.I. Watnick: Genetic analysis of *Vibrio cholerae* monolayer formation reveals a key role for *delta psi* in the transition to permanent attachment. *J Bacteriol* 190, 8185-8196 (2008)

60. N. Waterfield: Host-pathogen interactions: proline gives insect pathogens the green light. *Current Biology* 20, R13-R15 (2010)

61. J.I. Jimenez-Zurdo, F.M. Garcia-Rodriguez and N. Toro: The *Rhizobium meliloti putA* gene: its role in the establishment of the symbiotic interaction with alfalfa. *Mol Microbiol* 23, 85-93 (1997)

62. P. van Dillewijn, P.J. Villadas and N. Toro: Effect of a *Sinorhizobium meliloti* strain with a Modified *putA* gene on the rhizosphere microbial community of alfalfa. *Appl Environ Microbiol* 68, 4201-4208 (2002)

63. J. Abramson, I. Smirnova, V. Kasho, G. Verner, H.R. Kaback and S. Iwata: Structure and mechanism of the lactose permease of *Escherichia coli*. *Science* 301, 610-615 (2003)

64. Y. Huang, M.J. Lemieux, J. Song, M. Auer and D.N. Wang: Structure and mechanism of the glycerol-3-phosphate transporter from *Escherichia coli*. *Science* 301, 616-620 (2003)

65. S. Faham, A. Watanabe, G.M. Besserer, D. Cascio, A. Specht, B.A. Hirayama, E.M. Wright and J. Abramson: The crystal structure of a sodium galactose transporter reveals mechanistic insights into Na<sup>+</sup>/sugar symport. *Science* 321, 810-814 (2008)

66. C. Hunte, E. Screpanti, M. Venturi, A. Rimon, E. Padan and H. Michel: Structure of a Na<sup>+</sup>/H<sup>+</sup> antiporter and insights into mechanism of action and regulation by pH. *Nature* 435, 1197-1202 (2005)

67. T. Shimamura, S. Weyand, O. Beckstein, N.G. Rutherford, J.M. Hadden, D. Sharples, M.S.P. Sansom, S. Iwata, P.J.F. Henderson and A.D. Cameron: Molecular basis of alternating access membrane transport by the

## Putp

sodium-hydantoin transporter Mhp1. *Science* 328, 470-473 (2010)

68. S. Weyand, T. Shimamura, S. Yajima, S.i. Suzuki, O. Mirza, K. Krusong, E.P. Carpenter, N.G. Rutherford, J.M. Hadden, J. O'Reilly, P. Ma, M. Saidijam, S.G. Patching, R.J. Hope, H.T. Norbertczak, P.C.J. Roach, S. Iwata, P.J.F. Henderson and A.D. Cameron: Structure and molecular mechanism of a nucleobase-cation-symport-1 family transporter. *Science* 322, 709-713 (2008)

69. D. Yernool, O. Boudker, Y. Jin and E. Gouaux: Structure of a glutamate transporter homologue from *Pyrococcus horikoshii*. *Nature* 431, 811-818 (2004)

70. S. Schulze, S. Koster, U. Geldmacher, A.C. Terwisscha van Scheltinga and W. Kühlbrandt: Structural basis of Na<sup>+</sup>-independent and cooperative substrate/product antiport in CaiT. *Nature* 467, 233-236 (2010)

71. S. Ressler, A.C. Terwisscha van Scheltinga, C. Vornrhein, V. Ott and C. Ziegler: Molecular basis of transport and regulation in the Na<sup>+</sup>/betaine symporter BetP. *Nature* 458, 47-52 (2009)

72. X. Gao, L. Zhou, X. Jiao, F. Lu, C. Yan, X. Zeng, J. Wang and Y. Shi: Mechanism of substrate recognition and transport by an amino acid antiporter. *Nature* 463, 828-832 (2010)

73. J.S. Lolkema and D.J. Slotboom: Classification of 29 families of secondary transport proteins into a single structural class using hydrophathy profile analysis. *J Mol Biol* 327, 901-909 (2003)

74. K.R. Vinothkumar and R. Henderson: Structures of membrane proteins. *Quart Rev Biophys* 43, 65-158 (2010)

75. E. Screpanti and C. Hunte: Discontinuous membrane helices in transport proteins and their correlation with function. *J Struct Biol* 159, 261-267 (2007)

76. E. Olkhova, M. Raba, S. Bracher, D. Hilger and H. Jung: Homology model of the Na<sup>+</sup>/proline transporter PutP of *Escherichia coli* and its functional implications. *J Mol Biol* 406, 59-74 (2011)

77. H. Jung: Topology and function of the Na<sup>+</sup>/proline transporter of *Escherichia coli*, a member of the Na<sup>+</sup>/solute cotransporter family. *Biochim Biophys Acta* 1365, 60-64 (1998)

78. H. Jung, R. Rübner, S. Tebbe, K. Leifker, N. Tholema, M. Quick and R. Schmid: Topology of the Na<sup>+</sup>/proline transporter of *Escherichia coli*. *J Biol Chem* 273, 26400-26407 (1998)

79. D. Hilger, M. Böhm, A. Hackmann and H. Jung: Role of Ser-340 and Thr-341 in transmembrane domain IX of the Na<sup>+</sup>/proline transporter PutP of *Escherichia coli* in ligand binding and transport. *J Biol Chem* 283, 4921-4929 (2008)

80. T. Pirch, S. Landmeier and H. Jung: Transmembrane domain II of the Na<sup>+</sup>/proline transporter PutP of *Escherichia coli* forms part of a conformationally flexible, cytoplasmic exposed aqueous cavity within the membrane. *J Biol Chem* 278, 42942-42949 (2003)

81. M. Raba, T. Baumgartner, D. Hilger, K. Klempahn, T. Härtel, K. Jung and H. Jung: Function of transmembrane domain IX in the Na<sup>+</sup>/proline transporter PutP. *J Mol Biol* 382, 884-893 (2008)

82. D. Hilger, Y. Polyhach, H. Jung and G. Jeschke: Backbone structure of transmembrane domain IX of the Na<sup>+</sup>/proline transporter PutP of *Escherichia coli*. *Biophys J* 96, 217-225 (2009)

83. T. Pirch, M. Quick, M. Nietschke, M. Langkamp and H. Jung: Sites important for Na<sup>+</sup> and substrate binding in the Na<sup>+</sup>/proline transporter of *Escherichia coli*, a member of the Na<sup>+</sup>/solute symporter family. *J Biol Chem* 277, 8790-8796 (2002)

84. M. Quick and H. Jung: Aspartate 55 in the Na<sup>+</sup>/proline permease of *Escherichia coli* is essential for Na<sup>+</sup>-coupled proline uptake. *Biochemistry* 36, 4631-4636 (1997)

85. P.L. Shaffer, A. Goehring, A. Shankaranarayanan and E. Gouaux: Structure and mechanism of a Na<sup>+</sup>-independent amino acid transporter. *Science* 325, 1010-1014 (2009)

86. D.A. Caplan, J.O. Subbotina and S.Y. Noskov: Molecular mechanism of ion-ion and ion-substrate coupling in the Na<sup>+</sup>-dependent leucine transporter LeuT. *Biophys J* 95, 4613-4621 (2008)

87. L. Celik, B. Schiott and E. Tajkhorshid: Substrate binding and formation of an occluded state in the leucine transporter. *Biophys J* 94, 1600-1612 (2008)

88. J. Li and E. Tajkhorshid: Ion-releasing state of a secondary membrane transporter. *Biophys J* 97, L29-L31 (2009)

89. E. Zomot and I. Bahar: The sodium/galactose symporter crystal structure is a dynamic, not so occluded state. *Mol Biosyst* 6, 1040-1046 (2010)

90. A. Watanabe, S. Choe, V. Chaptal, J.M. Rosenberg, E.M. Wright, M. Grabe and J. Abramson: The mechanism of sodium and substrate release from the binding pocket of vSGLT. *Nature* 468, 988-991 (2010)

91. M. Quick, S. Tebbe and H. Jung: Ser57 in the Na<sup>+</sup>/proline permease of *Escherichia coli* is critical for high-affinity proline uptake. *Eur J Biochem* 239, 732-736 (1996)

92. O. Jardetzky: Simple allosteric model for membrane pumps. *Nature* 211, 969-70 (1966)

93. I.C. West: Ligand conduction and the gated-pore mechanism of transmembrane transport. *Biochim Biophys Acta* 1331, 213-34 (1997)

## Putp

94. P.C. Maloney: Bacterial transporters. *Curr Opin Cell Biol* 6, 571-82 (1994)
95. Y. Fang, H. Jayaram, T. Shane, L. Kolmakova-Partensky, F. Wu, C. Williams, Y. Xiong and C. Miller: Structure of a prokaryotic virtual proton pump at 3.2 Å resolution. *Nature* 460, 1040-1043 (2009)
96. X. Gao, F. Lu, L. Zhou, S. Dang, L. Sun, X. Li, J. Wang and Y. Shi: Structure and mechanism of an amino acid antiporter. *Science* 324, 1565-1568 (2009)
97. G. Jeschke, C. Wegener, M. Nietschke, H. Jung and H.J. Steinhoff: Interresidual distance determination by four-pulse double electron-electron resonance in an integral membrane protein: the Na<sup>+</sup>/proline transporter PutP of *Escherichia coli*. *Biophys J* 86, 2551-2557 (2004)
98. C. Wegener, S. Tebbe, H.J. Steinhoff and H. Jung: Spin labeling analysis of structure and dynamics of the Na<sup>+</sup>/proline transporter of *Escherichia coli*. *Biochemistry* 39, 4831-4837 (2000)
99. A. Zhou, A. Wozniak, K. Meyer-Lipp, M. Nietschke, H. Jung and K. Fendler: Charge translocation during cosubstrate binding in the Na<sup>+</sup>/proline transporter of *E. coli*. *J Mol Biol* 343, 931-942 (2004)
100. D.P. Claxton, M. Quick, L. Shi, F.D. de Carvalho, H. Weinstein, J.A. Javitch and H.S. McHaourab: Ion/substrate-dependent conformational dynamics of a bacterial homolog of neurotransmitter:sodium symporters. *Nat Struct Mol Biol* 17, 822-829 (2010)
101. B.A. Hirayama, D.D. Loo, A. ez-Sampedro, D.W. Leung, A.K. Meinild, M. Lai-Bing, E. Turk and E.M. Wright: Sodium-dependent reorganization of the sugar-binding site of SGLT1. *Biochemistry* 46, 13391-13406 (2007)
102. H. Krishnamurthy, C.L. Piscitelli and E. Gouaux: Unlocking the molecular secrets of sodium-coupled transporters. *Nature* 459, 347-355 (2009)
103. L.R. Forrest, Y.W. Zhang, M.T. Jacobs, J. Gesmonde, L. Xie, B.H. Honig and G. Rudnick: Mechanism for alternating access in neurotransmitter transporters. *Proc Natl Acad Sci USA* 105, 10338-10343 (2008)
104. Y. Zhao, D. Terry, L. Shi, H. Weinstein, S.C. Blanchard and J.A. Javitch: Single-molecule dynamics of gating in a neurotransmitter transporter homologue. *Nature* 465, 188-193 (2010)
105. M. Quick and H. Jung: A conserved aspartate residue, Asp187, is important for Na<sup>+</sup>-dependent proline binding and transport by the Na<sup>+</sup>/proline transporter of *Escherichia coli*. *Biochemistry* 37, 13800-13806 (1998)
106. L. Shi, M. Quick, Y. Zhao, H. Weinstein and J.A. Javitch: The mechanism of a neurotransmitter:sodium symporter-inward release of Na<sup>+</sup> and substrate is triggered by substrate in a second binding site. *Mol Cell* 30, 667-77 (2008)
107. C.L. Piscitelli, H. Krishnamurthy and E. Gouaux: Neurotransmitter/sodium symporter orthologue LeuT has a single high-affinity substrate site. *Nature* 468, 1129-32 (2010)
108. D.E. Culham, K.S. Emmerson, B. Lasby, D. Mamelak, B.A. Steer, C.L. Gyles, M. Villarejo and J.M. Wood: Genes encoding osmoregulatory proline/glycine betaine transporters and the proline catabolic system are present and expressed in diverse clinical *Escherichia coli* isolates. *Can J Microbiol* 40, 397-402 (1994)
109. E.F. Pettersen, T.D. Goddard, C.C. Huang, G.S. Couch, D.M. Greenblatt, E.C. Meng and T.E. Ferrin: UCSF Chimera--a visualization system for exploratory research and analysis. *J Comput Chem* 25, 1605-12 (2004)

**Abbreviations:** DEER spectroscopy, double electron electron resonance spectroscopy; SSS family, Na<sup>+</sup>/solute symporter family; SDSL, site-directed spin labeling; TM, transmembrane domain;

**Key Words:** PutP, Proline, Transport, Sodium/Solute Symport, Review

**Send correspondence to:** Heinrich Jung, Ludwig Maximilians University Munich, Biocentre, Microbiology, Grosshaderner Strasse 2-4, D-82152 Martensried, Germany, Tel: 49089 218074630713-500-2433, Fax: 49089 218074631, E-mail: hjung@lmu.de

## 6 CONCLUDING DISCUSSION

Secondary active transporters are key elements in the physiology of pro- and eukaryotic organisms. These membrane-integrated proteins couple the import or export of a variety of compounds to the energy stored in preexisting solute gradients. We utilized the Na<sup>+</sup>/proline symporter PutP of *E. coli* as a model system to gain general insights into the molecular mechanism of function of the SSSF. For this purpose a combination of biochemical, bioinformatic, and biophysical approaches was chosen. In the course of this work a first three-dimensional model of PutP was proposed. Based on this model the Na<sup>+</sup> and proline binding site were predicted and evaluated. Furthermore the functional properties and the dynamics of TM 8' (numbering according to the 10 TM core of the LeuT structural family) and extracellular loop 4 were analyzed, giving new insights into the molecular mechanism of function of PutP.

### 6.1 A homology model based on vSGLT gives insights into the three-dimensional architecture of PutP

High-resolution structures are an important prerequisite to understand the molecular mechanism of secondary active transporters. Especially due to their hydrophobicity and flexibility, crystallization of membrane proteins is still a challenge and until now a three-dimensional structure of PutP is not available. With the X-ray crystal structure of vSGLT of *V. parahaemolyticus*, a member of the SSSF, an unexpected structural similarity to the LeuT structural family became obvious. Transporters of the SSSF harbor the same 10-helix core domain as LeuT-like transporters (Abramson & Wright, 2009). Within this 10-helix bundle TMs 1-5 can be superimposed on TMs 6-10 along a pseudo two-fold symmetry axis. In vSGLT as well as in PutP TM 1' of the core is preceded by one non-core helix (numbering according to LeuT, PutP core helices are numbered from 1'-10'; additional N-terminal non-core helix: TM -1'; additional C-terminal helices: TM 11' and TM 12'). To obtain a deeper knowledge of the tertiary structure of PutP, a homology model was created using vSGLT as template (Chapter 3, Fig. 1). The model shows PutP (amino acids 38-481) composed of 12 membrane-spanning helices (TM -1' is not resolved in the template structure). This is in good agreement with the previously proposed 13 TM motif of the SSSF (Jung *et al.*, 1998a, Hilger *et al.*, 2008, Wegener *et al.*, 2000), except that borders of some TMs had to be shifted slightly. In the structure, PutP adopts an inward-facing conformation, revealing a large negatively charged cytoplasmic cavity lined by TMs 1', 3', 6', 8', and 10' (Chapter 3, Fig. 2). As in all other members of the LeuT structural family, also in PutP the symmetry related TMs 1' and 6' were predicted to harbor unwound segments approximately halfway across the lipid

bilayer. Discontinuous membrane-integrated helices are known to form a polar surrounding in the membrane environment by providing partially positive and partially negative helix dipoles or backbone carbonyl oxygens for substrate coordination (Screpanti & Hunte, 2007). Since PutP and vSGLT share only a sequence identity of 19% and sequence similarity of 41%, the reliability of the computed model was biochemically validated. Cys accessibility analyses of TMs 1' (Pirch *et al.*, 2003) and 8' (Chapter 2, Fig 6) support the proposed involvement of these helices in the formation of an aqueous cytoplasmic vestibule. Cys put at positions that were predicted to line the cavity were highly accessible to thiol specific compounds from the water phase. The data suggest that in the absence of ligands, the inward-facing state is the most stable conformation of PutP in the absence of a membrane potential. As already proposed by Cys crosslinking studies (Hilger *et al.*, 2008) of TMs 1' and 8', also in the model both TMs are located in close proximity, approximately halfway across the membrane. Taken together, the currently available experimental data strongly support the generated PutP homology model.

Despite the good accordance of the biochemical data with the PutP model, experimental information on the PutP structure is indispensable. In order to determine the secondary structure of functionally important eL4 of PutP, an EPR-based approach was chosen. In the course of this work the mobility and polarity of the microenvironment of spin labels attached throughout the whole loop domain were determined (Chapter 4, Fig. 4.3 and 4.4). In the mobility as well as in the polarity profile periodic patterns were identified reminiscent of two  $\alpha$ -helices, one in the N-terminal half succeeding TM 7' (positions 298 to 308) and one on the C-terminal half preceding TM 8' (positions 310–318). In the homology model one  $\alpha$ -helix between residues V313 and Q319 was predicted. This discrepancy can be explained by the low sequence identity and similarity in the N-terminal region of eL4. A comparison of available structures of members of the LeuT structural family revealed two  $\alpha$ -helical domains in the connecting loop between TMs 7' and 8' as a common feature, except for Mhp1 and BetP (Fig. 6.1).

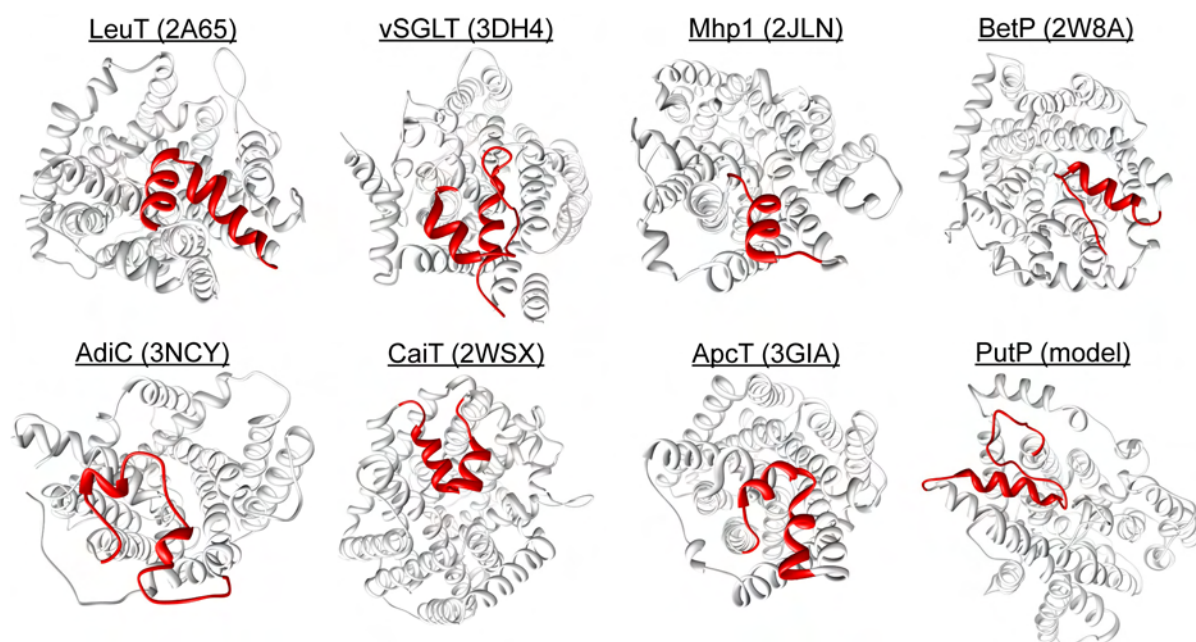


**Fig. 6.1 Homologous loop domains to eL4 of PutP in LeuT-like transporters.** Two  $\alpha$ -helical domains connected by a small unstructured region are a common feature in the LeuT structural family. In BetP and Mhp1 just one secondary structure was detected. In contrast to its template, in the PutP homology model only one  $\alpha$ -helix between positions 313 and 319 was predicted in eL4. The analysis of the spin label mobility and the polarity profile of eL4 revealed two  $\alpha$ -helices (298 to 308; 310 to 318). Differences between the computational and experimental data are most probably due to the low sequence identity and similarity between PutP and vSGLT in the N-terminal half of eL4. eL4 in the respective X-ray crystal structures are colored in red; all structures are viewed from the extracellular side. The figure was prepared with the program UCSF chimera (Pettersen *et al.*, 2004).

## 6.2 Sites of $\text{Na}^+$ and proline binding and release in PutP

*The  $\text{Na}^+$  binding site* - Since the PutP model was consistent with available biochemical and biophysical data it was used to identify the sites of  $\text{Na}^+$  and proline binding. Based on the homology model, the  $\text{Na}^+$  binding site in PutP was identified at the intersection between TMs 1' and 8', composed of the previously identified ion coordinating residues A337, S340, and T341 in TM 8' (Chapter 2; Hilger *et al.*, 2008) and A53 and M56 in TM 1' (Fig. 6.2 A). Even though the latter two amino acid residues were found to be of functional significance previously (Pirch *et al.*, 2003), a direct involvement in ion coordination has so far been unknown. Remarkably, A53 is highly conserved in the SSSF and M56 is conserved in  $\text{Na}^+$ /proline symporters in various organisms even though  $\text{Na}^+$  binding occurs by backbone carbonyl oxygen atoms and not by the amino acid side chains, suggesting that the side chain size at least contributes to the precise binding-site architecture. Corresponding to these observations, A53 and M56 were found close to the unwound region of TM 1' where backbone carbonyl oxygen atoms are exposed. Replacement of the native amino acids by Cys led in both cases to significantly reduced transport activities (Pirch *et al.*, 2003). Also for A337,  $\text{Na}^+$  coordination was proposed to be mediated by the backbone carbonyl oxygen atom (Chapter 2). Taking the backbone structure of TM 8' into account, A337 is found near a kinked region within the TM (Hilger *et al.*, 2009). This interruption in the regular  $\alpha$ -helix

architecture disturbs the intrahelical H-bonding pattern. Hence, the backbone oxygen atom of A337 is available as H-bonding partner for  $\text{Na}^+$  similar as described above for A53 and M56. In a previous study on S340 and T341, a detailed kinetic analysis already suggested a direct participation of these residues in  $\text{Na}^+$  binding (Hilger et al., 2008). While in the case of T341 the side chain hydroxyl group was proposed to coordinate the coupling ion, at position S340 the backbone oxygen atom was suggested to directly bind  $\text{Na}^+$ . Additionally, effects on the proline affinity were observed at both positions, albeit to a lesser extent. This supports the idea of a coupling between the proline and the ion binding site. The described  $\text{Na}^+$  binding site corresponds to the highly conserved  $\text{Na}_2$  site of LeuT, found in all  $\text{Na}^+$ -dependent LeuT-like transporters. Interestingly, in  $\text{Na}^+$ -independent transporters of the LeuT structural family, the missing positive charge of the coupling ion is supplied by cationic amino acid side chains of the protein itself, such as K158 in ApcT (Shaffer et al., 2009) or R262 in CaiT (Schulze et al., 2010). Similar to observations in PutP (Hilger et al., 2008), impairing  $\text{Na}_2$  in ApcT abolishes transport activity. MD simulations on LeuT gave first hints on the functional role of  $\text{Na}_2$ . The bound ion stabilizes the unwound stretch in TM 1, which is involved in leucine binding and in the coordination of a second  $\text{Na}^+$ , thereby increasing the substrate affinity of the transporter (Celik et al., 2008, Caplan et al., 2008).

*Na<sup>+</sup> release into the cytoplasm* - In addition to the identified  $\text{Na}^+$  binding site, the PutP model also shed light on the role of D187, a residue earlier proposed to be involved in  $\text{Na}^+$  release (Quick & Jung, 1998). It is located in the intracellular half of TM 5', 5.6 Å away from bound  $\text{Na}^+$ . This residue is highly conserved throughout the SSSF and particularly crucial for PutP activity. If Asp at this position is replaced by a less polar Cys side chain, a decrease in  $K_{0.5(\text{Na}^+)}$  was observed and  $V_{\text{max}}$  was drastically reduced. These findings can be explained by molecular dynamics simulations on the ion releasing state of vSGLT (Li & Tajkhorshid, 2009, Watanabe et al., 2010). It was shown that after exiting the conserved  $\text{Na}_2$  binding site (corresponding the above described  $\text{Na}^+$  binding site in PutP), the ion is immediately attracted by the negative charge of D189 (corresponds to D187 in PutP) and after transiently interacting with the amino acid side chain, the ion is released into the cytoplasm. By replacing the polar residue Asp with the more unpolar amino acid Cys in PutP (Quick & Jung, 1998), diffusion of  $\text{Na}^+$  from the binding site into the ion-releasing pathway is energetically less favorable, and the probability that  $\text{Na}^+$  remains in the ion binding site increases. This hypothesis would be in good agreement with the observed decrease in  $K_{0.5(\text{Na}^+)}$  and  $V_{\text{max}}$ . If  $\text{Na}^+$  is not readily released, the transporter stays for a longer period of time in the inward-facing  $\text{Na}^+$  and proline bound state, explaining the drastic decrease of the latter parameter. This idea is supported by the fact that substitution of D187 by more polar residues Glu or Asn results in an increase of  $K_{0.5(\text{Na}^+)}$  and  $V_{\text{max}}$  compared to D187C.

*The proline binding site* - To identify putative proline binding sites the PutP homology model was used to perform docking analysis, and the docked proline poses harboring the lowest energy were further evaluated (Chapter 3, Table 1). The predicted substrate binding pocket is found at the apex of the inward-facing cavity at the approximate midpoint of the membrane close to the identified Na<sup>+</sup> binding site (10 Å), similar to the situation in Mhp1 and vSGLT (Krishnamurthy *et al.*, 2009). However compared to the galactose binding site in vSGLT, the proline binding site is shifted by 6 Å towards the cytoplasm. Coordinating residues were predicted in TMs 1', 3', 6', 8', and 10' of PutP (Fig. 6.2 B). Interestingly, in vSGLT instead of TMs 3' and 8', TMs 2' and 7' are supposed to participate in substrate binding. Since vSGLT is catalyzing the uptake of a carbohydrate whereas PutP drives the uphill transport of an amino acid, these differences in the composition of the binding pocket might be explained by the different substrate specificities. However the results of the docking analysis of PutP are in good agreement with crystal structures of LeuT, vSGLT, Mhp1, AdiC, and ApcT (Faham *et al.*, 2008, Yamashita *et al.*, 2005, Weyand *et al.*, 2008, Shaffer *et al.*, 2009, Gao *et al.*, 2009). Structural alignments of LeuT-like transporters revealed a common location of the substrate binding sites in the center of the core domain (Abramson & Wright, 2009). Interestingly, a conserved set of TMs (TMs 1, 3, 6, and 8) is involved in the formation of the substrate binding sites (Fig. 6.2 C). In the case of AdiC and vSGLT, TM 10 complements the binding pocket.

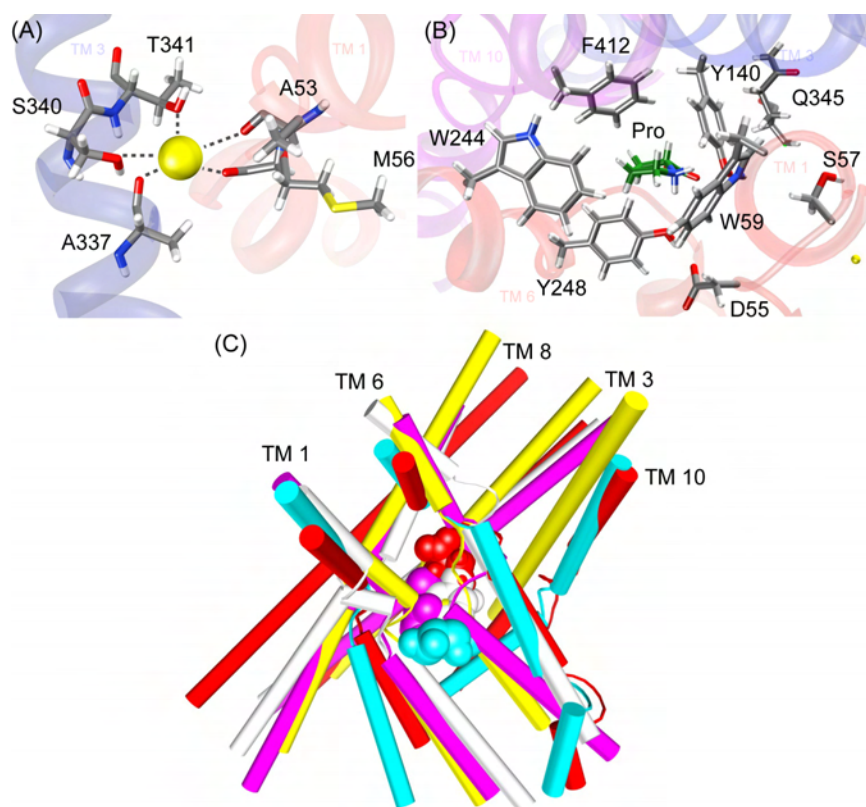


**Fig. 6.2 Architecture of the structurally conserved ion and substrate binding site of PutP** (A) Close up view of the  $\text{Na}^+$  binding site ( $\text{Na}^+$  is shown as yellow sphere). Residues in TM 1' and 8' involved in ion coordination are displayed as sticks coloured by atom type. (B) Close up view of the proline binding site. Residues in TM 1', 3', 6', 8', and 10' predicted to be close to, or part of the L-proline binding pocket are depicted as sticks colored by atom type. Proline is highlighted in green. (C) Superposition of TMs involved in substrate binding and the respective substrates in LeuT(2A65)/leucine (purple), Mhp1(2JLN)/L-5-benzyl-hydantoin (white), vSGLT(3DH4)/galactose (turquoise), AdiC(3L1L)/arginine (yellow), and the PutP homology model/proline (red). The binding sites are located approximately halfway across the membrane in the intersection between TMs 1, 3, 6, 8, and 10 (TMs 1, 2, 6, 7, and 10 for vSGLT). Proteins are viewed from the plane of the membrane and TMs are depicted as pipes. TMs 2 and 7 of vSGLT were omitted for clarity. The periplasmic side is found on the bottom, the cytoplasmic side on the top. The figure was prepared with the program UCSF chimera (Pettersen et al., 2004).

In the course of the biochemical analysis of the predicted binding site, four additional functionally important residues were identified: W59, Y140, W244, and Y248 (Chapter 3). All four residues are highly conserved in proline specific SSSF transporters. Substitution of Y140 or W244 increased  $K_{m(\text{pro})}$  by two to three orders of magnitude, suggesting that both residues are involved in substrate binding (Chapter 3, Table 2). In contrast the  $\text{Na}^+$  affinity remained unaffected. For Y140, the data hint on  $\pi$ -cation interactions between the aromatic ring and proline, also H-bonding between the side chain hydroxyl group and proline could not be excluded. For W244, comparable effects were observed. The kinetic data suggest that similar to Y140, W244 might participate in proline coordination via  $\pi$ -cation interactions or H-bond formation but additional hydrophobic interactions might also play a role. Furthermore, the docking analysis showed that Q345 is located in close proximity to the predicted proline binding site, but a direct participation in substrate coordination could not be detected. However, kinetic analysis of PutP-Q345C revealed a drastic decrease in the proline affinity of the transporter (Chapter 2, Table 1). Even though a direct interaction of Q345 with the

substrate could not be shown bioinformatically, the side chain might be involved in shaping the proline binding pocket.

*Gating and substrate release* - Another striking feature of the kinetic analysis was that beside the proline affinity, also  $V_{\max}$  of PutP-Y140C and PutP-W244C were reduced by two to three orders of magnitude. This result indicates that the aromatic character at the respective positions is not only crucial for proline binding, but also for the progression of the transport cycle after the formation of the ternary complex. Structure based alignments showed that Y140 of PutP corresponds to Y97 in ApcT, Y108 in LeuT, W117 in Mhp1, and M104 in AdiC, residues which were shown to be important for substrate specificity and binding. The well-characterized amino acid Y108 in LeuT is not only involved in leucine binding, but it also regulates access to the substrate binding site from the periplasm together with F253 by the aromatic side chains (small gate) (Yamashita et al., 2005). Remarkably, F253 in LeuT aligns with W244 of PutP. If the indole ring of W244 was replaced by an aliphatic side chain in PutP, a drastic reduction of  $V_{\max}$  was detected. The same was observed for Y140, supporting the idea that Y140 and W244 adopt a similar role as the Y108/F253-gate in LeuT. Furthermore W244 also aligns with W220 in Mhp1, N260 in vSGLT, and W202 in AdiC, residues which were shown to be involved in substrate binding and to some extent also in the gating mechanism. Cys accessibility analyses of the PutP derivatives Y140C and W244C were consistent with the proposed ordered binding mechanism of PutP (Chapter 3, Fig. 11 and 12). Addition of  $\text{Na}^+$  increased FM-labeling efficiency, while proline in the presence of  $\text{Na}^+$  reduced the labeling rates, suggesting that the respective positions move into the binding site in a  $\text{Na}^+$ -dependent manner. Subsequent substrate binding inhibited the labeling reaction at both positions. These proposed rearrangements are reminiscent of ligand-induced movements of W220 in Mhp1 and W202 in AdiC (Weyand et al., 2008, Gao et al., 2010).

In contrast to Y140 and W244, substitution of Y248 rather affected the apparent  $\text{Na}^+$  affinity than  $K_{m(\text{pro})}$ . The proposed involvement of the latter residue in proline binding could not clearly be shown, but nevertheless especially the kinetic data of the analyzed Y248 derivatives gave deeper insights into the coupling between the proline and the  $\text{Na}^+$  binding site (Chapter 3, Table 2). In the PutP homology model, Y248 is in H-bonding distance to D55 in TM 1' (Fig. 6.2 B). The latter residue was shown to be crucial for transport activity (Quick & Jung, 1997). Substitution of D55 led to a significant decrease of the apparent  $\text{Na}^+$  affinity, while the proline affinity remained unaffected. The side chain carboxylate group proved to be essential for function. In structure based alignments the functionally important residues D55 and Y248 align with N64 and Y263 of vSGLT (Faham et al., 2008). Both residues of vSGLT were shown to coordinate the substrate and to interact via H-bonding. N64 is also in H-bonding distance to C2-OH of galactose and Y263 stacks with the pyranose ring and thus

prevents the substrate from being released to the cytoplasm (small gate). If Na<sup>+</sup> is released from the Na<sub>2</sub> site in vSGLT, N64 which is located next to Na<sup>+</sup> binding residues I65 and A62, reorients and the H-bond between N64 and Y263 is disrupted. Subsequently Y263 flips into another conformation and galactose can be released from the binding site into the cytoplasm (Watanabe et al., 2010). The *in vivo* analysis of D55 and Y248 in PutP, combined with the structural comparison with vSGLT suggests that D55 is not directly involved in Na<sup>+</sup> binding as it was previously suggested (Quick & Jung, 1997). It can be speculated whether D55 of PutP adopts a role similar to that of N64 in vSGLT and mediates proline release after Na<sup>+</sup> exits its binding site according to the ordered binding mechanism. Similar to Y248, W59 and S57 are also localized in the intersection between the sites of substrate and ion binding, suggesting that both residues might also be involved in the energy coupling mechanism. Based on a previous amino acid substitution analysis, for the latter residue a direct participation in proline binding was proposed (Quick *et al.*, 1996).

In summary, the PutP homology model guided the identification of the Na<sup>+</sup> and proline binding sites. Residues that are involved in ion and substrate coordination as well as in the gating mechanism were identified. The results support the idea of structurally conserved positions of the Na<sup>+</sup> (lined by residues located in TMs 1' and 8') and substrate binding site (lined by residues located in TMs 1', 3', 6', and 8'). Furthermore, the periplasmic gate, formed by Y140 and W244 in PutP, most likely resembles the situation in LeuT (formed by Y108 and F253). These findings strongly support the idea that members of the LeuT structural family share a common transport mechanism. The good agreement of the structure based predictions and the experimental data underline the relevance of the PutP homology model that can be used as guide for further investigations.

### 6.3 Substrate translocation pathway and structural dynamics of PutP

In 1966 Oleg Jardetzky proposed that secondary active transporter work according to an alternating access mechanism (Jardetzky, 1966). This theory concludes that access to the substrate binding site and release of the transported solutes on the other side is accomplished by reciprocal opening and closing of two hemichannels, implicating major conformational alterations, which transport proteins undergo during the transport cycle.

In contrast to the comparably well-characterized inward-facing vestibule (Chapters 2 and 3), little is known about the periplasmic cavity of PutP that mediates access to the ion and substrate binding sites from the periplasm. *In vivo* Cys accessibility analyses indicated that positions 59, 331, 337, and 341 in TMs 1' and 8' were accessible from the periplasmic space (Chapter 2 and 3). In addition, a previous study in right-side-out membrane vesicles demonstrated that also S340 is accessible from the extracellular space (Hilger et al., 2008). These residues were modified by the small thiol specific compound MTSET (width similar to

the diameter of hydrated  $\text{Na}^+$ ) but not by bigger compounds such as FM. Together these data give first evidence for a periplasmic funnel lined by residues W59 of TM 1' and L331 and A337 of TM 8', that allows  $\text{Na}^+$  to enter the ion binding site, comprised of A53, M56, A337, S340, and T341, which is found approximately halfway across the membrane. In ligand-dependent labeling experiments, it was shown that  $\text{Na}^+$  but not proline inhibited Cys modification at positions 331, 337, and 341 (Chapter 2, Fig. 8), hinting at  $\text{Na}^+$  induced conformational alterations on the periplasmic side of the protein. This would be in good agreement with the proposed ordered binding mechanism of PutP (Zhou *et al.*, 2004, Yamato & Anraku, 1993). In this scenario  $\text{Na}^+$  binds first to the empty transporter, and structural changes lead to an increase of the affinity of PutP for its actual substrate proline. This hypothesis is further supported by the observed  $\text{Na}^+$ -dependent stimulation of the accessibility of Cys put at positions 140 and 244 (Chapter 3, Fig. 11 and 12). Since A337 and T341 were shown to participate in ion binding, direct steric hindrance by  $\text{Na}^+$  could also explain the observed inhibition of the labeling reaction.

$\text{Na}^+$ -induced effects on the accessibility pattern were predominantly observed on the periplasmic side of the transporter. In contrast, proline in the presence of  $\text{Na}^+$  affected labeling reactions on the cytoplasmic side. As described above (cf. 6.1), based on the PutP model and Cys accessibility studies, an inwardly oriented, water-filled vestibule lined by the cytoplasmic halves of TMs 1' and 8', was identified. Proline together with  $\text{Na}^+$  specifically inhibited the labeling reactions (Chapter 2, Fig. 7). Cys protective effects might be explained either by direct steric hindrance or conformational alterations of the protein excluding the thiol group from the aqueous phase. Since Cys substitutions on the respective positions did not affect transporter activity, the latter explanation seems to be more plausible. So far, independent of the method used, large ligand-induced conformational changes (e.g., >0.3 nm) were not observed [Cys crosslinking between TM 1' and 8' (Hilger *et al.*, 2008); intramolecular distance measurements between TM -1' and TM 5' (Jeschke *et al.*, 2004) or TM 2' and TM 9' (Chapter 4)]. Therefore, global structural rearrangements such as a closure of the inward-facing cavity seem to be rather unlikely under the experimental conditions (absence of a membrane potential). However, the reduced accessibility could be attributed to closing gates that occlude the aqueous cavity from the surrounding milieu. Gates can either be formed by a small number of amino acid residues (small gates) or by protein domains such as TMs or loops (thick gates), as seen in vSGLT, LeuT, or Mhp1 (Faham *et al.*, 2008, Yamashita *et al.*, 2005, Krishnamurthy & Gouaux, 2012, Shimamura *et al.*, 2010). To test this hypothesis and to identify gating-domains on the cytoplasmic side of PutP, further analyses needs to be done.

Besides the putative gating residues Y140 and W244 on the periplasmic side (cf. 6.2), eL4 of PutP was shown to be crucial for transporter function, and a pivotal role of this domain

in controlling access to the ion and substrate binding site was proposed. Initial *in vivo* proline uptake assays and SPA revealed E311 as crucial for transporter function. Since the binding properties of the PutP $\Delta$ Cys-E311C were not affected (Chapter 4, Fig. 4.1 A and B), PutP mediated proline uptake is probably inhibited at a step subsequent to proline binding, giving first hint for the importance of eL4 in the transport process. Further kinetic analyses supported these findings. In PutP-E311D  $V_{\max}$  is drastically decreased whereas  $K_{m(\text{Pro})}$  and  $K_{0.5(\text{Na}^+)}$  were only slightly affected, suggesting defects in transporter dynamics and not in ligand binding (Bracher and Jung, unpublished data).

To determine ligand-induced conformational alterations of eL4, EPR measurements were performed in the absence of ligands or in the presence of  $\text{Na}^+$  or  $\text{Na}^+$  and proline. As described above (cf. 6.1), EPR-measurements of the Apo-state of PutP revealed two  $\alpha$ -helices in this loop domain. Changes in the periodic patterns of the mobility and polarity profile were not detected in subsequent ligand-dependent measurements, consequently changes in the secondary structure were not observed. However, the coupling ion and the substrate induced alterations in spin label dynamics and in the polarity of the microenvironment support the idea that eL4 is mechanistically involved in the proposed alternating access mechanism of PutP (Chapter 4, Fig. 4.6). Addition of  $\text{Na}^+$  resulted in a decrease of the spin label mobility, especially in the C-terminal half of eL4 (312, 314, 316, 317, 321, and 322) and an increase of the polarity at the kink preceding the second  $\alpha$ -helical domain. Spin labels attached to positions at the water-membrane interface (295, 296, 297, 320, 322, and 324) moved into a more apolar environment, suggesting that these regions of the loop domain move deeper into the lipid bilayer or are interacting with hydrophobic amino acids of the protein. To conclude,  $\text{Na}^+$  binding stabilizes a conformational state of PutP in which eL4 undergoes stronger tertiary interactions compared to the Apo-state. A movement of eL4 deeper into a putative hydrophilic periplasmic cavity (increase of the polarity) could result in a tighter interaction of eL4 with other domains on the extracellular half of PutP (decrease of spin label mobility). The addition of proline in the presence of  $\text{Na}^+$  reversed the effects detected upon addition of  $\text{Na}^+$ . An overall increase in spin label mobility throughout the whole loop domain was shown, except for positions 299 and 314 where a strong decrease, and at positions 296, 307, and 309 where a slight decrease was observed. In addition, the presence of both ligands induced a shift of the whole loop domain into a more polar environment. Taking both parameters, the spin label mobility and the polarity, into account, the data suggest weaker interactions of eL4 in the ternary complex of PutP, compared to the Apo- and the  $\text{Na}^+$ -bound state. An increase in the polarity of the surrounding of the spin label could either be explained by closer proximity of the spin label to polar protein domains of PutP or by an increased accessibility to water. The concomitant increase of the polarity and the mobility upon  $\text{Na}^+$  and proline binding rather supports the latter idea. In

summary, the cw EPR measurements provided evidence that eL4 is not just a simple connector between TMs 7' and 8', but a functionally important loop domain that is subject to ligand-induced conformational rearrangements. To integrate the dynamics of eL4 into the transport cycle of PutP DEER measurements were performed (Chapter 4, Fig. 4.5). Under the experimental conditions (measurements were performed in proteoliposomes in the absence of a membrane potential), only subtle distance changes on the periplasmic side, as well as on the cytoplasmic side of PutP were detected. In contrast, in the structural homologue LeuT, more distinct intramolecular distance changes between corresponding positions were observed (Claxton *et al.*, 2010), indicating an reciprocal opening and closing of two hemichannels on the extra- and intracellular side. Combining the intramolecular distance measurements with the Cys accessibility analyses of TMs 1' and 8', the data suggest that PutP adopts an inward-facing conformation in the Apo-state, and subsequent addition of Na<sup>+</sup> and proline triggers an inward-facing occluded state. Interestingly and in good agreement with the alternating access mechanism, the accessibility studies and the EPR measurements suggest a coupled movement of the periplasmic- and of the cytoplasmic half of the transporter. The differences between LeuT and PutP might be explained by different energy coupling mechanisms. As it was previously shown, in contrast to LeuT the membrane potential is essential for the transport activity of PutP and other members of the SSSF (Jung *et al.*, 1998b, Loo *et al.*, 1998). For SGLT1, another member of the SSSF, it has been found that an outward-facing conformation could only be triggered in the presence of a membrane potential (Loo *et al.*, 1998). Therefore, more distinct conformational dynamics might be observed if measurements are performed in the presence of a membrane potential.

In summary, the results of this work considerably extended the knowledge of the molecular mechanism of function of the Na<sup>+</sup>/proline symporter PutP of *E. coli*. Based on the results of this work, the following transport cycle can be deduced (Fig. 6.3).

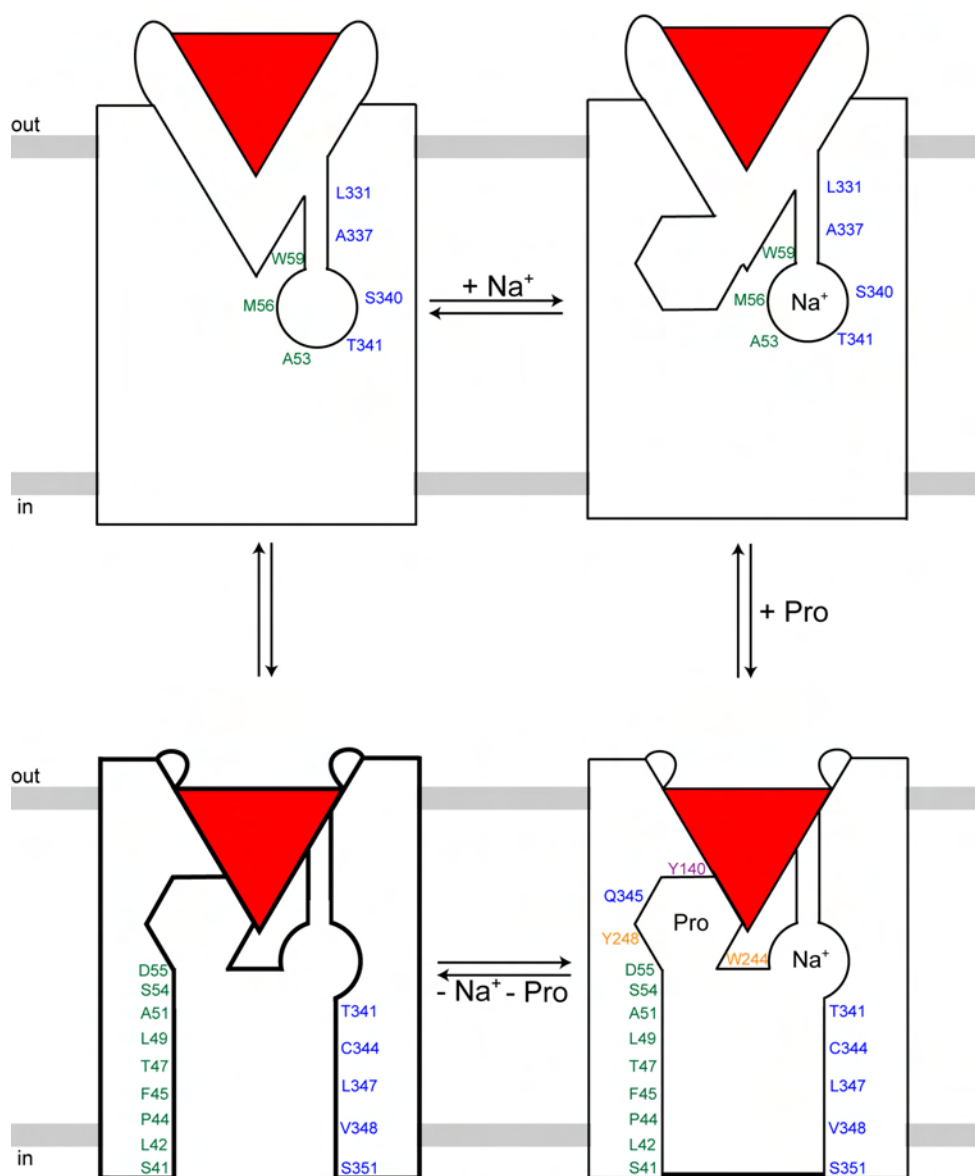


**Fig. 6.3 Hypothetic model of the alternating access mechanism of PutP.** In the Apo-state Na<sup>+</sup> accesses the ion binding site, composed of residues located in TMs 1' and 8' via a small periplasmic funnel (upper left). Bound Na<sup>+</sup> induces conformational alterations in the proline binding site, thereby increasing the substrate affinity of the transporter (upper right). After proline coordination, the substrate binding site is occluded from the periplasmic space by thin gates and eL4. Subsequently, PutP undergoes major structural rearrangements and switches from an outward-facing to an inward-facing occluded conformation (lower right; cytoplasmic gate: thick line). Finally, gates on the cytoplasmic side are opened whereupon both ligands are released into the cytoplasm via an inwardly-oriented aqueous vestibule. The resulting inward-open state is the most stable conformation in the absence of a membrane potential (lower left, thick lines). After reorientation of the empty transporter, the Apo-state again adopts the outward-facing state. Amino acids of structural and functional importance are illustrated as single letter code at the respective positions and are colored according their TM localization (green: TM 1', purple: TM 3', orange: TM 6', blue: TM 8').

In the Apo-state, Na<sup>+</sup> enters the ion binding site via a small funnel lined by residues in TMs 1' and 8'. Na<sup>+</sup> is supposed to be coordinated by carbonyl oxygen atoms of A53 (TM 1'), M56 (TM 1'), A337 (TM 8'), and S340 (TM 8') and the side chain hydroxyl group of T341 (TM 8'). Supporting the idea that PutP works according to an ordered binding mechanism, bound Na<sup>+</sup> was shown to induce conformational alterations on the periplasmic side, and binding residues Y140 (TM 3') and W244 (TM 6') faced an increased water accessibility, implicating

reorientations in the proline binding pocket that might increase the substrate affinity of the transporter. Together with the latter residues, Y248 and Q345 are supposed to shape the substrate binding pocket which is located approximately halfway across the membrane. Furthermore, Y140 and W244 were predicted to build up a thin gate in the ternary complex, which occludes the ion and substrate binding site from the periplasm. In addition to the thin gates, ligand-induced dynamics suggested that eL4 adopts a key role in regulating access from the extracellular space by functioning as a thick gate, similar to the homologous domains in LeuT (Krishnamurthy & Gouaux, 2012) and Mhp1 (Shimamura et al., 2010). According to the ordered binding mechanism, Na<sup>+</sup> was suggested to be released from the ion binding site first and may temporarily interact with D187 before exiting into the cytoplasm. Finally, it is speculated that Na<sup>+</sup> release disrupts the interaction between D55 and Y248 and thus a permeation pathway is opened and proline exits into cytoplasm.

#### 6.4 References

- Abramson, J. & E. M. Wright, (2009) Structure and function of Na(+)-symporters with inverted repeats. *Curr Opin Struct Biol* **19**: 425-432.
- Caplan, D. A., J. O. Subbotina & S. Y. Noskov, (2008) Molecular mechanism of ion-ion and ion-substrate coupling in the Na<sup>+</sup>-dependent leucine transporter LeuT. *Biophys J* **95**: 4613-4621.
- Celik, L., B. Schiott & E. Tajkhorshid, (2008) Substrate binding and formation of an occluded state in the leucine transporter. *Biophys J* **94**: 1600-1612.
- Claxton, D. P., M. Quick, L. Shi, F. D. de Carvalho, H. Weinstein, J. A. Javitch & H. S. McHaourab, (2010) Ion/substrate-dependent conformational dynamics of a bacterial homolog of neurotransmitter:sodium symporters. *Nat Struct Mol Biol* **17**: 822-829.
- Faham, S., A. Watanabe, G. M. Besserer, D. Cascio, A. Specht, B. A. Hirayama, E. M. Wright & J. Abramson, (2008) The crystal structure of a sodium galactose transporter reveals mechanistic insights into Na<sup>+</sup>/sugar symport. *Science* **321**: 810-814.
- Gao, X., F. Lu, L. Zhou, S. Dang, L. Sun, X. Li, J. Wang & Y. Shi, (2009) Structure and mechanism of an amino acid antiporter. *Science* **324**: 1565-1568.
- Gao, X., L. Zhou, X. Jiao, F. Lu, C. Yan, X. Zeng, J. Wang & Y. Shi, (2010) Mechanism of substrate recognition and transport by an amino acid antiporter. *Nature* **463**: 828-832.
- Hilger, D., M. Bohm, A. Hackmann & H. Jung, (2008) Role of Ser-340 and Thr-341 in transmembrane domain IX of the Na<sup>+</sup>/proline transporter PutP of Escherichia coli in ligand binding and transport. *J Biol Chem* **283**: 4921-4929.
- Hilger, D., Y. Polyhach, H. Jung & G. Jeschke, (2009) Backbone structure of transmembrane domain IX of the Na<sup>+</sup>/proline transporter PutP of Escherichia coli. *Biophys J* **96**: 217-225.

- Jardetzky, O., (1966) Simple allosteric model for membrane pumps. *Nature* **211**: 969-970.
- Jeschke, G., C. Wegener, M. Nietschke, H. Jung & H. J. Steinhoff, (2004) Interresidual distance determination by four-pulse double electron-electron resonance in an integral membrane protein: the Na<sup>+</sup>/proline transporter PutP of Escherichia coli. *Biophys J* **86**: 2551-2557.
- Jung, H., R. Rubenhagen, S. Tebbe, K. Leifker, N. Tholema, M. Quick & R. Schmid, (1998a) Topology of the Na<sup>+</sup>/proline transporter of Escherichia coli. *J Biol Chem* **273**: 26400-26407.
- Jung, H., S. Tebbe, R. Schmid & K. Jung, (1998b) Unidirectional reconstitution and characterization of purified Na<sup>+</sup>/proline transporter of Escherichia coli. *Biochemistry* **37**: 11083-11088.
- Krishnamurthy, H. & E. Gouaux, (2012) X-ray structures of LeuT in substrate-free outward-open and apo inward-open states. *Nature*.
- Krishnamurthy, H., C. L. Piscitelli & E. Gouaux, (2009) Unlocking the molecular secrets of sodium-coupled transporters. *Nature* **459**: 347-355.
- Li, J. & E. Tajkhorshid, (2009) Ion-releasing state of a secondary membrane transporter. *Biophys J* **97**: L29-31.
- Loo, D. D., B. A. Hirayama, E. M. Gallardo, J. T. Lam, E. Turk & E. M. Wright, (1998) Conformational changes couple Na<sup>+</sup> and glucose transport. *Proceedings of the National Academy of Sciences of the United States of America* **95**: 7789-7794.
- Pettersen, E. F., T. D. Goddard, C. C. Huang, G. S. Couch, D. M. Greenblatt, E. C. Meng & T. E. Ferrin, (2004) UCSF Chimera--a visualization system for exploratory research and analysis. *J Comput Chem* **25**: 1605-1612.
- Pirch, T., S. Landmeier & H. Jung, (2003) Transmembrane domain II of the Na<sup>+</sup>/proline transporter PutP of Escherichia coli forms part of a conformationally flexible, cytoplasmic exposed aqueous cavity within the membrane. *J Biol Chem* **278**: 42942-42949.
- Quick, M. & H. Jung, (1997) Aspartate 55 in the Na<sup>+</sup>/proline permease of Escherichia coli is essential for Na<sup>+</sup>-coupled proline uptake. *Biochemistry* **36**: 4631-4636.
- Quick, M. & H. Jung, (1998) A conserved aspartate residue, Asp187, is important for Na<sup>+</sup>-dependent proline binding and transport by the Na<sup>+</sup>/proline transporter of Escherichia coli. *Biochemistry* **37**: 13800-13806.
- Quick, M., S. Tebbe & H. Jung, (1996) Ser57 in the Na<sup>+</sup>/proline permease of Escherichia coli is critical for high-affinity proline uptake. *Eur J Biochem* **239**: 732-736.
- Schulze, S., S. Koster, U. Geldmacher, A. C. Terwisscha van Scheltinga & W. Kuhlbrandt, (2010) Structural basis of Na<sup>(+)</sup>-independent and cooperative substrate/product antiport in CaiT. *Nature* **467**: 233-236.

- Screpanti, E. & C. Hunte, (2007) Discontinuous membrane helices in transport proteins and their correlation with function. *J Struct Biol* **159**: 261-267.
- Shaffer, P. L., A. Goehring, A. Shankaranarayanan & E. Gouaux, (2009) Structure and mechanism of a Na<sup>+</sup>-independent amino acid transporter. *Science* **325**: 1010-1014.
- Shimamura, T., S. Weyand, O. Beckstein, N. G. Rutherford, J. M. Hadden, D. Sharples, M. S. Sansom, S. Iwata, P. J. Henderson & A. D. Cameron, (2010) Molecular basis of alternating access membrane transport by the sodium-hydantoin transporter Mhp1. *Science* **328**: 470-473.
- Watanabe, A., S. Choe, V. Chaptal, J. M. Rosenberg, E. M. Wright, M. Grabe & J. Abramson, (2010) The mechanism of sodium and substrate release from the binding pocket of vSGLT. *Nature* **468**: 988-991.
- Wegener, C., S. Tebbe, H. J. Steinhoff & H. Jung, (2000) Spin labeling analysis of structure and dynamics of the Na<sup>(+)</sup>/proline transporter of Escherichia coli. *Biochemistry* **39**: 4831-4837.
- Weyand, S., T. Shimamura, S. Yajima, S. Suzuki, O. Mirza, K. Krusong, E. P. Carpenter, N. G. Rutherford, J. M. Hadden, J. O'Reilly, P. Ma, M. Saidijam, S. G. Patching, R. J. Hope, H. T. Norbertczak, P. C. Roach, S. Iwata, P. J. Henderson & A. D. Cameron, (2008) Structure and molecular mechanism of a nucleobase-cation-symport-1 family transporter. *Science* **322**: 709-713.
- Yamashita, A., S. K. Singh, T. Kawate, Y. Jin & E. Gouaux, (2005) Crystal structure of a bacterial homologue of Na<sup>+</sup>/Cl<sup>-</sup>-dependent neurotransmitter transporters. *Nature* **437**: 215-223.
- Yamato, I. & Y. Anraku, (1993) Alkali Cation Transport Systems in Prokaryotes. In: Alkali Cation Transport Systems in Prokaryotes. E. P. Bakker (ed). Boca Raton, FL: CRC-Press, pp. 464.
- Zhou, A., A. Wozniak, K. Meyer-Lipp, M. Nietschke, H. Jung & K. Fendler, (2004) Charge translocation during cosubstrate binding in the Na<sup>+</sup>/proline transporter of E.coli. *J Mol Biol* **343**: 931-942.

## ACKNOWLEDGEMENTS

First of all I want to express my sincere gratitude to Prof. Dr. Heinrich Jung for introducing me to the fascinating world of membrane proteins and for giving me the freedom to pursue a variety of exciting biological projects and collaborations. I am thankful for his guidance, fruitful discussions and advice, and for his full support throughout the years.

Special thanks go to my thesis committee especially to Prof. Dr. Thorsten Mascher for being the second examiner of this thesis.

With this I would like to thank my collaborators. Without their commitment this work would not have been possible. I would like to thank Dr. Elena Olkhova from the MPI of Biophysics for the homology modeling and the docking analysis. Furthermore, I am grateful to Prof. Heinz-Jürgen Steinhoff, Sabrina Dunkel, and Dr. Johann Klare from the university of Osnabrück for the polarity measurements and their expertise. Many thanks go also to Prof. Gunnar Jeschke, Kamila Lipiszko, and Dr. Yevhen Polyhach from the ETH Zürich for the DEER measurements and the evaluation of the results. Last but not least, I want to express my gratitude to Prof. Dr. Matthias Quick from the Columbia University for introducing me to the SPA technique and for the analyses of the binding properties of the spin labeled variants.

Next, I am also very thankful to the Elite Network of Bavaria for granting me one of their PhD fellowships. It gave me the opportunity to meet leading scientists from around the globe at international conferences and to attend extraordinary soft skill seminars.

I would also like to thank Prof. Dr. Kirsten Jung for her advice, scientific discussions, and her interest in my work.

I am deeply grateful to Dr. Daniel Hilger, an excellent scientist and very dear friend. His passion for science and his precise and analytical view on scientific problems inspired my own work throughout the years. I had a great time with you inside and outside the lab (Käptn's dinner, Paternoster, concerts, discussing life, skiing, FC Bayern curse, bike, beer, and Streifenpullis...). I wish you, Julia, and Leon all the best for your future in San Francisco. Moreover, I want to thank all other members of the H. and K. Jung labs for an interactive and friendly atmosphere. Dr. Torsten Pirch for the initial help with the accessibility studies and the AAS. Thanks to my fellow (former) colleagues Ara, Frank, Günther, Hannah, Ina, Korinna, Nicola, Poldi, Rauschi, Sophie Bu., Sophie Br., Stefan, Susi B., Susi U., and Tobi for all the scientific and non-scientific discussions. The Badminton 'Mitsreiter' Poldi, Sophie, and Stefan for ambitious matches and Daniel, Nicola, Poldi, and Stefan for analyzing the latest soccer results.

Furthermore, I am sincerely grateful for having such good friends who gave me moral support and encouraged me at every stage of this thesis. Torsten, Basti, Käptn, Vroni, Johannes, and Daniel I cannot thank you enough.

Sandi I want to thank you for the wonderful time we had. I do not want to miss a moment.

Zu guter Letzt möchte ich meiner Familie danken, ohne die diese Arbeit nicht möglich gewesen wäre. Vor allem meiner Mutter für ihre uneingeschränkte Unterstützung, dafür dass sie immer an mich geglaubt hat. Meinem Vater und meinem Bruder Max für ihren Rückhalt und ihre stete Hilfsbereitschaft in allen Lebenslagen. Und meinem Opa... mach weiter so!